Oxidative stress homeostasis and longevity in mammals

Natàlia Mota Martorell

Universitat de Lleida

TESI DOCTORAL

Oxidative stress homeostasis and longevity in mammals

Natàlia Mota Martorell

Memòria presentada per optar al grau de Doctor per la Universitat de Lleida

Programa de Doctorat en Salut

Director/a

Dr. Reinald Pamplona Gras

Dra. Mariona Jové Font

Tutor/a

Dr. Reinald Pamplona Gras

2020

ABSTRACT

Long-lived species have evolved by decreasing the rate of endogenous reactive oxygen species production and providing them of oxidation-resistant structures. Hence, species that live longer benefit from metabolically efficient and structurally stable mitochondria. In fact, phenotypic traits of longevity include reduced content of complex I of the electron transport chain and sulphur-containing amino acids. Then, the activity of selected intracellular signalling pathways plays a key role regulating the expression of genes associated to a longevity phenotype.

In this context, this thesis aims to determine i) the modulation of specific complex I subunits associated to longevity; ii) the changes on sulphur amino acids content and its metabolic intermediates in post-mitotic tissues and iii) plasma from long-lived species; iv) the content regulation of the different mTOR complex 1 specific forming elements in terms of longevity; and v) the existence of a metabolic profile associated to human extreme longevity.

The obtained results reveal the existence of metabolic profiles associated to species longevity that, in some cases, differ from those profiles associated to individual longevity. Furthermore, longer lived species have evolved by reducing the content of specific electron complex I subunits that might be responsible for the limited reactive oxygen species production. Otherwise, genetic factors that might determine the basal activity of mTOR complex 1 exist, and that could, at least in part, explain the longevity associated phenotype. Thus, it seems that the achievement of an extended longevity implies a metabolic and structural adaptation.

RESUM

Les espècies més longeves han evolucionat disminuint la producció endògena d'espècies reactives d'oxigen i proveint-se d'estructures resistents a la oxidació. Per tant, aquelles espècies que viuen més gaudeixen de mitocòndries metabòlicament més eficients i estructuralment més estables. De fet, característiques fenotípiques de la longevitat inclouen la reducció del contingut del complex I de la cadena de transport electrònic i dels aminoàcids sulfurats. Aleshores, l'activitat de determinades vies de senyalització intracel·lulars juga un paper clau regulant l'expressió de gens associats a un fenotip longeu.

En aquest context, aquesta tesi pretén determinar i) la modulació de determinades subunitats del complex I associada a la longevitat; ii) els canvis en el contingut dels aminoàcids sulfurats i els seus intermediaris metabòlics en teixits post-mitòtics i iii) plasma d'espècies més longeves; iv) la regulació del contingut dels diferents elements específics del complex 1 de mTOR en termes de longevitat; i v) l'existència un perfil metabòlic associat a humans de longevitat extrema.

Els resultats obtinguts mostren l'existència de perfils metabòlics associats a la longevitat de les espècies que, en alguns casos, són diferents a aquells perfils associats a la longevitat individual. A més, les espècies més longeves han evolucionat disminuint el contingut de determinades subunitats del complex I que podrien ésser responsables de la menor producció d'espècies reactives d'oxigen. Per altra banda, existeixen factors genètics que podrien determinar l'activitat basal del complex 1 de mTOR, i que podrien, almenys en part, explicar el fenotip associat a la longevitat. Per tant, sembla que l'assoliment d'una major longevitat implica una adaptació metabòlica i estructural.

RESUMEN

Las especies más longevas han evolucionado disminuyendo la producción endógena de especies reactivas de oxígeno y proveyéndose de estructuras resistentes a la oxidación. Por lo tanto, aquellas especies que viven más disfrutan de mitocondrias metabólicamente más eficientes y estructuralmente más estables. De hecho, características fenotípicas de la longevidad incluyen la reducción del contenido del complejo I de la cadena de transporte electrónico y de amino ácidos sulfurados. Por lo tanto, la activad de determinadas vías de señalización intracelular juegan un papel clave regulando la expresión de genes asociados a un fenotipo longevo.

En este contexto, esta tesis pretende determinar i) la modulación de determinadas subunidades del complejo I asociada a la longevidad; ii) los cambios en el contenido de amino acido sulfurados y de sus intermediarios metabólicos en tejidos post-mitóticos y iii) plasma de especies más longevas; iv) la regulación del contenido de distintos elementos específicos del complejo 1 de mTOR en términos de longevidad; y v) la existencia de un perfil metabólico asociado a humanos de longevidad extrema.

Los resultados obtenidos muestran la existencia de perfiles metabólicos asociados a la longevidad de las especies que, en algunos casos, son diferentes a aquellos perfiles asociados a la longevidad individual. Además, las especies más longevas han evolucionado disminuyendo el contenido de determinadas subunidades del complejo I que podrían ser responsables de la menor producción de especies reactivas de oxígeno. Por otra parte, existen factores genéticos que podrían determinar la actividad basal del complejo 1 de mTOR, y que podrían, al menos en parte, explicar el fenotipo asociado a la longevidad. Por lo tanto, parece que lograr una mayor longevidad implica una adaptación metabólica y estructural.

TABLE OF CONTENTS

List of figures

LIST OF TABLES

ABBREVIATIONS

5-MTHF: 5-methyl tetrahydrofolate

ACO: Aconitase

ADP: Adenosine diphosphate

Ala: Alanine

Arg: Arginine

Asn: Asparagine

Asp: Aspartate

ATP: Adenosine triphosphate

BCAA: Branched chain amino acids

BCKA: Branched-chain α-ketoacids

Bcl-xl: B-cell lymphoma-extra-large

BHMT: Betaine-homocysteine 5-methyltransferase

BHT: Buthylhydroxytoluene

BLAST: Basic local alignment search tool

BSA: Bovine serum albumin

CARS: Cell aging regulating system

CBS: Cystathionine-β-synthase

cDNA: Complementary DNA

CM: Cristae membranes

CoA: Coenzyme A

CPT: Carnitine palmitoyl transferase

CR: Caloric restriction

CS: Citrate synthase

C_t: Threshold cycle

CTH: Cystathionine-γ-lyase

Cx I: Complex I or NADH:ubiquinone oxidoreductase

Cx II/SDH: Complex II or succinate dehydrogenase

Cx III: Ubiquinone:cytochrome *c* oxidoreductase or cytochrome *c* reductase

Cx IV: Cytochrome *c* oxidase

Cx V: ATP synthase

Cys: Cysteine

CytC: Cytochrome *c*

ddPCR: Droplet digital PCR

Deptor: DEP domain-containing mTOR-interacting protein

DNA: Deoxyribonucleic acid

DR: Dietary restriction

DTPAC: Diethylenetriamine-penta acetic acid

EDTA: Ethylenediaminetetraacetic acid

ESI: Electrospray ionization

ETC: Electron transport chain

FATD: Frap, ATM, TRRAP domain

FeS: Iron-sulfur

FET: Forward electron transfer

FH: Fumarate hydratase or fumarase

FKBP12: FK506 binding protein of 12 kDa

FMN: Flavin mononucleotide

FRBD: FFKBP12-Rapamycin binding domain

Gln: Glutamine

Glu: Glutamate

Gly: Glycine

GSH: Glutathione

GTP: Guanosine triphosphate

H_2O_2: Hydrogen peroxide

H_2S: Hydrogen sulfide

HDMB: Human metabolome database

His: Histidine

$HO^{\bullet}$: Hydroxyl radical

IDH: Isocitrate dehydrogenase

Ile: Isoleucine

IMB: Inner boundary membrane

IMM: Inner mitochondrial membrane

IMS: Intermembrane space

KD: Kinase domain

KGDH: α-Ketoglutarate dehydrogenase

LC: Liquid chromatography

LC-ESI-QqQ-MS: liquid chromatography system coupled to a hybrid mass spectrometer with electrospray ionization and a triple quadrupole mass spectrometer

LC-FA: Long-chain fatty acids

Leu: Leucine

Lys: Lysine

m/z: Mass-to-charge ratio

m: Exact mass

MAT: Methionine adenosyltransferase

MDH: Malate dehydrogenase

Met: Methionine

MetO: Methionine sulfoxide

MetR: Methionine restriction

mLST8: Mammalian lethal with SEC13 protein 8

MOPS: 3-(N-morpholino)propaensulfonic acid

mPTP: Mitochondrial permeability transition pore

MRM: Multiple reaction monitoring

Mrs: Methionine sulfoxide reductase

MS: Methionine synthase

MT: Methyltransferase

mtDNA: Mitochondrial DNA

mTOR: Mechanistic target of rapamycin

mTORC1: mTOR complex 1

NCBI: National Center for Biotechnology Information

nDNA: Nuclear DNA

N-HEAT: N-terminal HEAT

NMR: Naked mole rat

NO: Nitric oxide

$O_2^{\bullet-}$: Superoxide radical

OH^-: Hydroxyl ion

OMM: Outer mitochondrial membrane

$ONOO^-$: Peroxynitrite

OXPHOS: Oxidative phosphorylation

PC: Phosphocholine

PCA: Principal component analysis

PCR: Polymerase chain reaction

PE: Phosphatidylethanolamine

PEMT: Phosphatidylethanolamine methyltransferase

PGLS: Phylogenetic generalised least squares

Phe: Phenylalanine

PI3K: Phosphatidylinositol-3 kinases

PIKK: PI3K-related kinase

PLP: Pyridoxal-5'-phosphate

PLS-DA: Partial least squares-discriminant analyses

PRAS40: Proline-rich AKT1 substrate of 40 kDa

Pro: Proline

PS: Phosphoserine

PUFA: Polyunsaturated fatty acids

PVDF: Polyvinylidene difluoride

Q: Ubiquinone

QH_2: Ubiquinol

qPCR: Real-time PCR

QqQ: Triple quadrupole

Raptor: Regulatory associated protein of TOR

RET: Reverse electron transfer

RNA: Ribonucleic acid

RNAse: Ribonuclease

ROS: Reactive oxygen species

rRNA: Ribosomal RNA

RS: Reactive species

SAH: S-adenosylhomocysteine

SAHH/AHCY: S-adenosylhomocysteine hydrolase

SAM: S-adenosylmethionine

SCS: Succinyl-CoA synthetase

SDS: Sodium dodecyl sulfate

Ser: Serine

SOD: Superoxide dismutase

T_a: Annealing temperature

TCA: Tricarboxylic acid

TEMED: N,N,N',N'-tetramethylethylenediamine

Thr: Threonine

T_m: Melting temperature

Tris: Tris(hydroxymehtyl) aminomethane

Tris-HCl: Tris hydrochlorhydre

Try: Tryptophan

Tyr: Tyrosine

Val: Valine

VDAC: Voltage-dependent anion channel

WHO: World health organisation

$\Delta\psi m$: Membrane potential

Introduction

1.1. LONGEVITY DIVERSITY ACROSS THE TREE OF LIFE

All living beings descent from a common ancestor, the first life on Earth that existed 3.8 billion years ago. From that time, evolution had led to the emergence of an enormous variety of animal species, exhibiting more than 70.000-fold difference maximum longevity ("longevity" from here on out), and up to ~200-fold among mammals (Ma and Gladyshev, 2017) (**Figure 1**). The smallest short-lived mammalian the Etruscan shrew, weighing 2 g and capable to live up to 3.2 years, co-exist with the largest long-lived land and ocean beasts: African elephants, weighing up to 6 tons and living to 70 years, and bowhead whale, which can weight more than 100 tons and are estimated to live 211 years (Tacutu et al., 2013). The fact that even after all living beings evolved from a common cell, they exhibit such an enormous variation in terms of longevity, led the scientific community to meditate *what does make an animal species live longer than others?*

The most straightforward explanation to these huge differences within animal longevity is body size: big animals live longer (Austad and Fischer, 1991; Speakman, 2005). From an ecology point of view, it makes sense that bigger animals live longer since they have no predators. However, exceptionally long-lived species escaping from this rule of thumb, living more than what it is expected from their body size, exist (Szekely et al., 2015). Naked mole rat (NMR) and microbats live 10 times longer than rodents of comparable size (Lewis et al., 2018; Seim et al., 2014). In the same line, birds have an exceptional longevity compared with mammals of similar body size, even after maintaining a high mitochondrial oxygen consumption necessary for flight (Barja, 2019; Barja et al., 1994). In fact, humans are also considered as exceptionally long-lived species since our lifespan is 5 times longer than what is expected for our body size (Ma and Gladyshev, 2017). Besides, the 50-mm shell height bivalve *Arctica islandica* has been documented to live up to 507 years (Butler et al., 2013), refuting the association between longevity and body size.

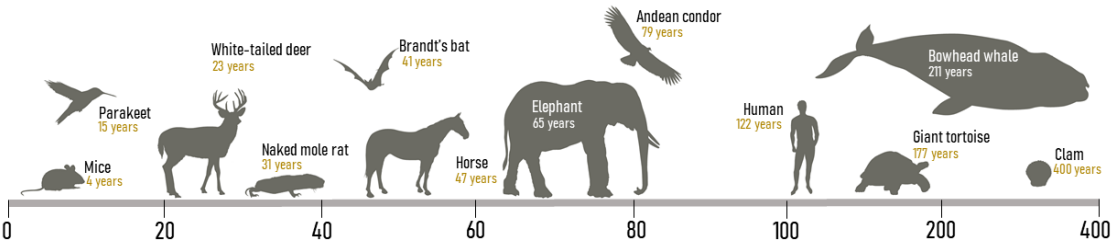

Figure 1. Longevity diversity across the tree of life. Maximum longevity years are reported. Adapted from Deweerdt, 2012.

The evolutionary factors that lead to an extended longevity and longevity diversification across the tree of life are being studied and continuously revised. In fact, tracking structural and molecular changes across animal evolution seem to be the key to firstly determine *how have long-lived animals evolved to slow down the ageing process and achieve such an extreme longevity?* Worldwide population is rapidly ageing, and is expected that between 2015 and 2050, the proportion of the world's population over 60 years will nearly double from 12 to 22% (World Health Organisation, WHO). Although the achievement of a worldwide life expectancy of 74 years can be considered a humankind success due to the medical, technological and social improvements, it is also associated with an increasing co-morbidity and incidence of age-related diseases such as neurodegenerative disease, cardiovascular disease and cancer. In fact, aging is the most significant risk factor for these degenerative diseases (Bulterijs et al., 2015).

Accordingly, it does not come as a surprise that WHO and European commission encourage scientific community to develop research projects targeted to determine the changes that occur throughout the physiological process of ageing. The aim of these studies is not to elucidate how to live longer but to age in good health (henceforth healthspan). Therefore, the study of longevity-associated mechanisms will help to better understand how to slow down the ageing process, and to finally being able to develop methodologies applicable to humans and promote healthspan and healthy ageing.

1.2. ATMOSPHERE OXYGENATION AS A DRIVER OF EVOLUTION

Life evolution is inexorably linked to biosphere oxygenation. Origin of life occurred in a reducing, anoxic and hot environment (Moosmann et al., 2020). The emergence of oxygen in the atmosphere occurred 2.700 billion years ago as a consequence of the metabolic activity of photosynthetic cyanobacteria (Falkowski and Godfrey, 2008a), and raised up from 0 to a 5% levels. Consequently, anaerobic living forms existing at that time adapted, died or were restricted to anoxygenic regions (Pamplona and Barja, 2011). Adaptation of an oxygen-rich atmosphere was feasible due to the acquisition of mitochondria via endosymbiotic processes, leading to the appearance of the first eukaryotes 2.300 and 2.000 billion years ago (Embley and Martin, 2006) (**Figure 2**).

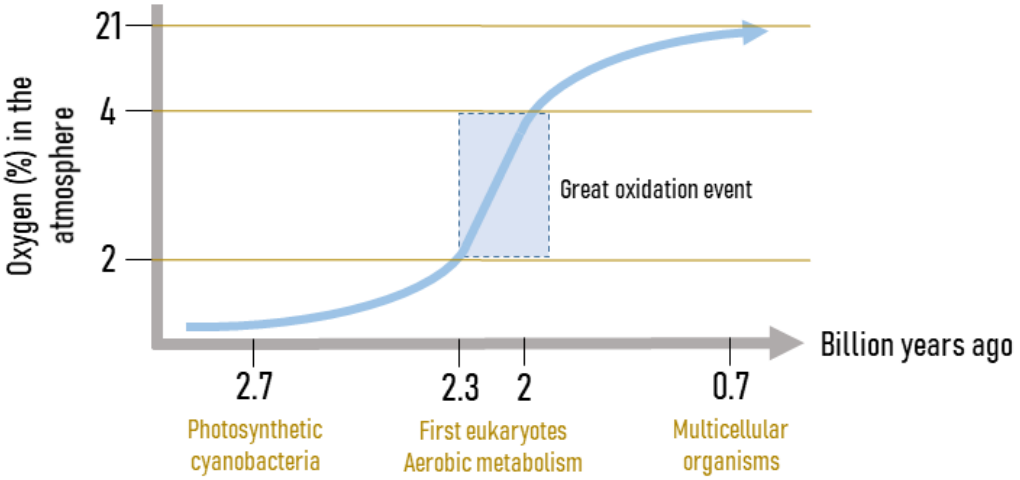

Figure 2. Atmosphere oxygenation triggered life evolution. Adapted from Lyons et al., 2014. Atmosphere composition has been undergoing continuous changes since its anoxic and abiotic composition 4.5 billion years ago. The emergence of alternative metabolic processes such as photosynthesis, followed by the aerobic metabolism, had led to an increased content of oxygen in the atmosphere until the actual composition: 21% of oxygen, 78% of nitrogen and little CO_2 (0.03%), which is optimal for aerobic life.

The shift from a reducing environment to an oxidizing one certainly resulted challenging (McCord, 2000) and demanded metabolic adaptations. Mitochondria from eukaryote cells were able to use oxygen to produce energy more efficiently, leading to the emergence of complex multicellular organisms (Falkowski and Godfrey, 2008b). However, as atmospheric oxygen levels rose, living organisms began to experience its toxicity: as a consequence of normal aerobic metabolism, reactive free radicals and reactive species (RS) were generated, which oxidatively damaged intracellular structures (Halliwell and Gutteridge, 2007). To limit the generation of the RS and prevent or repair oxidation damage, multicellular organisms evolved inducing a huge diversity of antioxidant defence systems (Halliwell, 1999), including both molecules with

antioxidant properties and redox signalling pathways perfectly integrated in cellular metabolism (Pamplona and Barja, 2007, 2011).

1.3. INTRACELLULAR FACTORS LEADING TO AN EXTENDED LONGEVITY

It has been hypothesised that the rate of ageing, and consequently longevity determination, are mainly due to a small number of factors that continuously operate throughout the lifespan. In spite of the existence of antioxidant defences, there is always a steady-state level of RS production under physiological circumstances. Hence, the generation of mitochondrial reactive oxygen species (ROS) in eukaryotic cells as a consequence of an aerobic metabolism, and the detrimental reactions of these ROS with cellular constituents (**Figure 3**), are thought to be the initiators of a series of chemical and biological processes underlying ageing and longevity determination, as stated by the mitochondrial oxidative stress theory of ageing (Harman, 1972; Miquel et al., 1980; Sanz et al., 2006a). Besides, ROS production is species-specific and genetically determined, as is longevity.

The naivest explanation to an extended longevity involves an enhanced antioxidant activity. Accordingly, it would be expected that species that have evolved with an increased longevity are provided of a higher content and activity of antioxidant molecules and systems. Anyway, scientific evidence suggested that antioxidants are not involved in longevity determination. Comparative studies involving animal species with different longevities revealed that long-lived species don't have higher levels of endogenous antioxidants. Unexpectedly, there is a negative correlation between longevity and endogenous antioxidant contents, thus long-lived species have lower content of endogenous antioxidants (Pamplona and Costantini, 2011). Besides, dietary supplementation with antioxidant molecules, as well as pharmacological or genetic induction of tissue antioxidants in animal models doesn't lead to an increased longevity, although it moderately improves mean survival (Barja, 2004; Sanz et al., 2006a). In the same way, inhibition of antioxidant enzymes in animal models lead to the development of health alterations without affecting longevity (Sanz et al., 2006a).

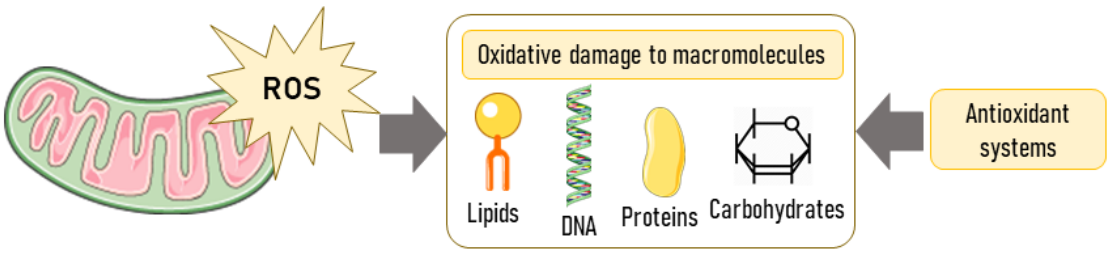

Figure 3. The endogenous generation of ROS alters intracellular structures in spite of the existence of antioxidant systems. Generation of intracellular ROS under physiological circumstances is the price to pay for the acquisition of an optimized aerobic metabolism. These ROS can attack and oxidatively damage intracellular structures, such as lipids, DNA, proteins and carbohydrates. The susceptibility of these structures depend upon its specific composition. However, animals have also evolved with antioxidant systems, that can be induced under stress oxidant conditions to prevent and repair the damage induced by ROS.

The fact that antioxidant defences are not involved in the determination of species longevity suggest that the generation of intracellular ROS demanded different evolutionary metabolic and structural adaptations. In fact, aerobic and long-lived species have evolved by decreasing the rate of intracellular ROS generation, and providing their intracellular structures with oxidation-resistant biomolecules (Pamplona and Barja, 2007) (**Figure 4**). From an energetic point of view,

it makes sense that long-lived species generating less ROS don't need to invest energy to continuously induce and maintain antioxidant defences. Supporting this theory, it has been suggested that although long-lived species have lower content of antioxidant defences, the activity and content of antioxidant regulatory factors are increased (Pamplona and Costantini, 2011). Hence, long-lived species have evolved optimising its intracellular metabolism, transitionally inducing antioxidant systems solely under oxidative stress conditions.

Biomolecules exhibit different susceptibility to oxidative damage according to its chemical structure (Pamplona and Barja, 2007). Thus, in an oxidative stress context is important to remark that lipids are the biomolecules most susceptible to be oxidatively damaged, and its susceptibility exponentially increases with the number of double bounds (Holman, 1954; Hulbert et al., 2007). Therefore, polyunsaturated fatty acids (PUFA) are the most oxidizable biomolecules. On the scale of susceptibility to oxidative injury, deoxyribonucleic acid (DNA) goes after lipids, especially mitochondrial DNA (mtDNA) given its close proximity to the main source of intracellular ROS production (Pamplona, 2011). Besides, guanine is the nucleobase with the lowest oxidation potential and, therefore, the most susceptible to be attacked by ROS (Bjelland, 2003). The content of sulphur-containing amino acids determines protein vulnerability, since methionine (Met) are amongst the amino acids most susceptible to be oxidized by RS (Stadtman et al., 2003). Carbohydrates are the most resistant biomolecules to oxidation, especially those maintaining a ring (hemiacetal or hemiketal) structure, being glucose the most stable and least reactive monosaccharide (Bunn and Higgins, 1981). Given these premises, long-lived species have evolved by decreasing the content of PUFA in biological membranes (Hulbert et al., 2007; Pamplona and Barja, 2006), guanine content in mtDNA (Samuels, 2005) and methionine residues in their proteins (Pamplona et al., 2005; Portero-Otín et al., 2004; Ruiz et al., 2005). Besides, glucose has been positively selected as the universal metabolic fuel and the most abundant monosaccharide in cells (Bunn and Higgins, 1981).

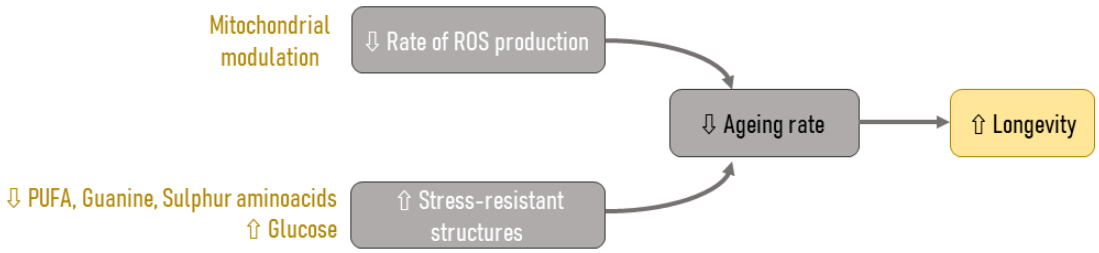

Figure 4. Traits leading to an extended longevity can be grouped into a lowered rate of endogenous damage and increased resistance to it. Adapted from Pamplona and Barja, 2007.

1.4. MITOCHONDRIAL COMPLEX I AS A CENTRAL HUB OF LONGEVITY DETERMINATION

Mitochondria are essential organelles present in all eukaryotic cells (Lane and Martin, 2010) whose main function is to provide cells with adenosine triphosphate (ATP), being critical for proper cell function. However, it is also considered to be the main generator of intracellular ROS, which are derived from physiological electron transport chain (ETC) activity. The achievement of a longevity phenotype is associated with an optimised metabolism. From an energetic and oxidative stress perspective, this occurs through the generation of the maximum amount of energy diminishing production of ROS. Accordingly, long-lived species have evolved by modulating mitochondrial structure and function in a way that they are energetically more

efficiently, decreasing the rate of ROS generation, and resistant to its attack. Nonetheless, it is important to remark that mitochondria are not the only intracellular source of ROS production. For instance, a much higher rate of ROS generation by NADPH oxidase occurs at the outer membrane of immune system cells (Barja, 2019).

1.4.1. MITOCHONDRIAL STRUCTURE

Mitochondria are dynamic cellular organelles, as they are continuously undergoing mitochondrial fusion and fission processes that are responsible for its heterogeneous shape and size (Sharma et al., 2019; Westermann, 2010). Besides, the number and location of mitochondria differs within cell types, and depend on tissue bioenergetics demand (Prasai, 2017). For instance, 35% of the volume of ventricular cardiomyocytes is occupied by mitochondria (Dorn, 2013). Not surprisingly, the number of mitochondria also differ within animal species (Prasai, 2017).

Electron microscope reveals a complex inner mitochondrial morphology, with two membranes, an outer membrane and an inner membrane, leading to the formation of different sub-compartments within the organelle (**Figure 5**). The outer mitochondrial membrane (OMM) encloses the entire organelle and regulates the exchange of a variety of molecules between cellular cytoplasm and mitochondria (van der Laan et al., 2016). Mitochondrial permeability is regulated by the presence of pore-forming proteins such as porins or voltage-dependent anion channels (VDACs), which allow ions and molecules of 5 kDa or less freely diffuse across the OMM (Prasai, 2017). Specific protein and lipid transporters are also embedded in the OMM, as well as enzymes involved in the translocation of fatty acids, amino acids and metabolites across the OMM (Prasai, 2017; Spinelli and Haigis, 2018). Proteins involved in mitochondrial fission and fusion processes, and apoptosis are also present. Thus, OMM regulates both morphology and mitochondrial function.

Unlike the OMM, the inner mitochondrial membrane (IMM) is only permeable to small uncharged molecules of 100-150 Da or less, which rely on specific transporters located in the IMM (Kühlbrandt, 2015; Prasai, 2017). The surface area of the IMM is larger than the OMM (Prasai, 2017), and can be divided into two domains with different functions: the inner boundary membrane (IMB), which is close to the OMM, and the folded cristae membranes (CM), which form invaginations. The IMB, which is enriched in specific transporters, is involved in the transport of molecules between the cytosol and the matrix, whereas CM is involved in energy production since it hosts the ETC complexes.

The IMM encloses the mitochondrial matrix, which is enriched in proteins and metabolites that are essential for fatty acid oxidation and the tricarboxylic acid (TCA) cycle. Therefore, mitochondrial matrix harbours most of the metabolic processes. Besides, multiple copies of mtDNA are also located within the matrix.

A gap of 20 nm exists between the OMM and the IMM, known as the intermembrane space (IMS). The composition of IMS and cytosol is similar due to the presence of porins in the OMM (Prasai, 2017), but its enriched with specific proteins involved in mitochondrial functions and H^+ (Herrmann and Riemer, 2010; Porcelli et al., 2005). Besides, the low IMM permeability allows to the establishment and maintenance of a mitochondrial membrane potential ($\Delta\psi m$) across the IMM, due to the high matrix pH (~7.9) compared to IMS (~6.9), leading the IMS side positively

charged and the matrix side negatively charged. This pH gradient drives ATP synthesis via the ETC and oxidative phosphorylation (OXPHOS) (Porcelli et al., 2005).

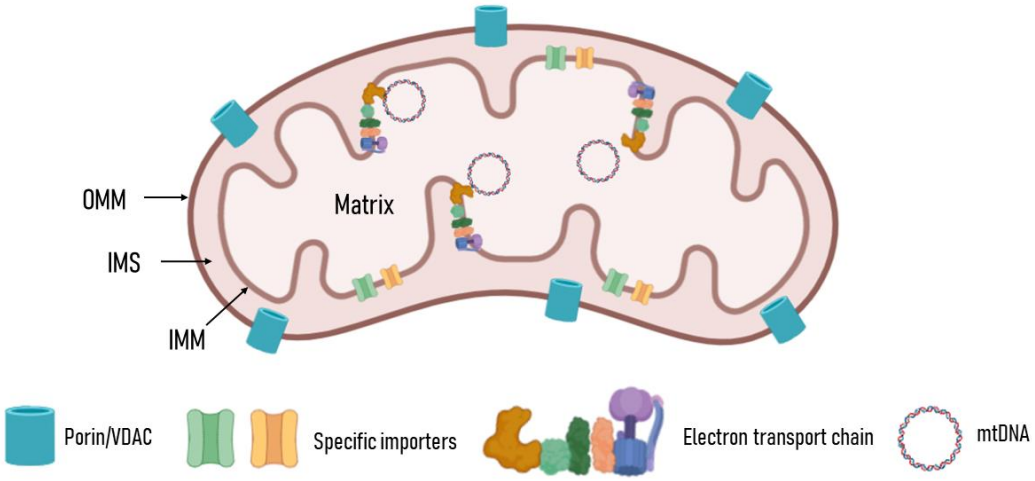

Figure 5. Mitochondrial architecture is complex and fragmented. A highly specialized double membrane encloses the mitochondrion. The OMM is enriched in porin/VDAC, allowing the exchange of nutrients and molecules between the IMS and the cytoplasm. Contrarily, the permeability of the IMM is limited and regulated by the presence of specific importers. Two different domains can be distinguished within the IMM with distinct functions. The IMB concentrates the transmembrane importers, and thus is involved in metabolite transport. CM, in turn, harbours the protein complexes of the ETC, hence it participates in the energetic metabolism. The IMM limits the mitochondrial matrix, where several molecules of mitochondrial DNA. OMM, outer mitochondrial matrix; IMS, inter membrane space; IMM, inner mitochondrial matrix; mtDNA, mitochondrial DNA. Adapted from Prasai, 2017 and Spinelli and Haigis, 2018. Created with BioRender.com.

1.4.2. MITOCHONDRIA FUNCTIONS AS THE CELL POWERHOUSES

Inarguably, the most important function of mitochondria is to provide cells with sufficient ATP in the OXPHOS. In aerobic organisms, 85-90% of cellular oxygen is consumed by mitochondria to produce energy. However, it is also a biosynthetic hub since it participates in the biosynthesis of metabolic precursors for macromolecules such as lipids, proteins, DNA and ribonucleic acid (RNA). Due to the relationship between OXPHOS derived ROS and longevity, we will focus our attention in on the energetic functions performed within the mitochondria.

1.4.2.1. Different substrates fuel mitochondrial metabolism

Cells consume glucose, fatty acids and amino acids to obtain energy (Walsh et al., 2018). These biomolecules, or its catalytic products (i.e., pyruvate derived from glucose), are translocated into the mitochondria through specific transporters located in the OMM and IMM (**Figure 6**). Once in the mitochondrial matrix, pyruvate, fatty acids and amino acids metabolised into acetyl-coenzyme A (CoA) (Pietrocola et al., 2015), a central metabolic intermediate that enters the TCA cycle to generate electron donors (NADH and $FADH_2$) that will finally feed the ETC to boost ATP production through the OXPHOS.

Glucose is the main energetic source in cells under normoxia conditions. Glycolysis culminates in the production of pyruvate, which is imported into mitochondria by the mitochondrial pyruvate carrier. Mitochondrial pyruvate is decarboxylated to form acetyl-CoA, CO_2 and NADH by the pyruvate dehydrogenase complex. However, under low-energy conditions, pyruvate can be used to synthetize the TCA cycle intermediate oxaloacetate via the enzyme pyruvate

carboxylase, which constitutes an anaplerotic reaction (a process to replenish TCA cycle intermediates under nutrient depleted circumstances).

Under conditions of nutrient stress, glycolysis is inhibited and fatty acid oxidation is favoured due to its energetic density (Randle, 1998). In fact, the palmitate (C16:0) fatty acid stores 39 KJ/g of energy compared to 16 KJ/g stored in glucose (Röhrig and Schulze, 2016). Cytosolic long-chain fatty acids (LC-FA) are sequentially oxidised and transformed into acyl-CoA in a reaction catalysed by the LC-FA acyl-CoA synthetase. Afterwards, acyl-CoA requires the carnitine shuttle system to be translocated into the mitochondria. The enzyme carnitine palmitoyl transferase 1 (CPT1) located in the OMM condenses acyl-CoA and carnitine, producing acylcarnitine and free CoA. Acylcarnitine is imported into the mitochondria and, once in the matrix, it is reconverted by CPT2 into carnitine and Acyl-Coa, which will be finally metabolised thought the fatty acid β-oxidation into acetyl-CoA.

No storage molecule is generated to control the concentration of excessive amino acids. In fact, excess of branched chain amino acids (BCAA) (leucine (Leu), isoleucine (Ile) and valine (Val)) are transaminated to branched-chain α-ketoacids (BCKA) in the cytosol by the enzyme BCAA transaminase 1. BCKA are imported into the mitochondria via the carnitine shuttle, and metabolised into acetyl-CoA by BCKA dehydrogenase in the mitochondrial matrix.

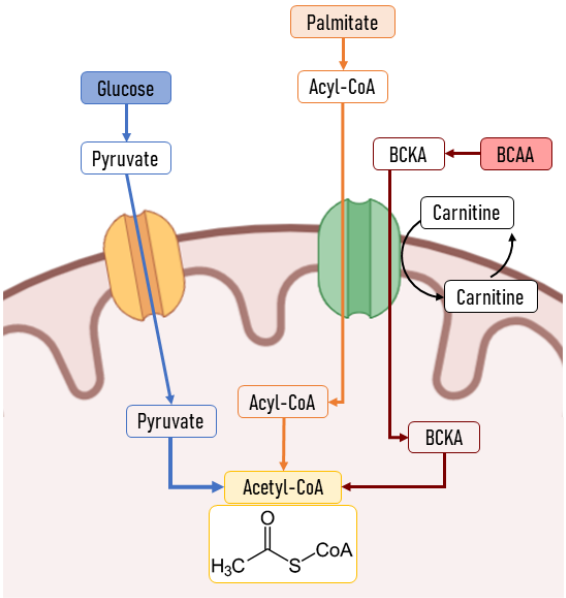

Figure 6. Glucose, palmitate and branched-chain amino acids are imported into the mitochondrial to fuel the TCA cycle. Pyruvate, which derives from glycolysis, is imported into the mitochondria through a specific carrier protein. Acyl-CoA and BCKA derived from palmitate and BCAA respectively, are imported through the carnitine shuttle. Once in the mitochondrial matrix, pyruvate, acyl-CoA and BCKA are metabolized into acetyl-CoA to fuel the TCA cycle. BCAA, branched-chain amino acids; BCKA, branched-chain α-ketoacids. Adapted from Pietrocola et al., 2015 and Spinelli & Haigis, 2018a. Created with BioRender.com.

1.4.2.2. The tricarboxylic acid cycle

The TCA cycle, also referred to as Krebs Cycle, occurs within the mitochondrial matrix, and constitutes a metabolic epicentre because multiple substrates can feed into it (Martínez-Reyes and Chandel, 2020). It includes a series of eight sequential metabolic reactions that lead to the production of metabolic intermediates, guanosine triphosphate (GTP) and electron donors (e.g. NADH and $FADH_2$) (**Figure 7**).

The first TCA cycle reaction is catalysed by citrate synthase (CS) that condensates acetyl-CoA (2C) and oxaloacetate (4C) to generate citrate (6C). In the second step, citrate undergoes a reversible isomerization catalysed by aconitase (ACO) to produce isocitrate. The oxidative decarboxylation of isocitrate leads to the generation of α-ketoglutarate (5C) and succinyl-CoA (4C) in a series of reactions catalysed by isocitrate dehydrogenase (IDH) and α-ketoglutarate dehydrogenase (KGDH) respectively, releasing CO_2 and generating two NADH molecules. Afterwards, succinyl-CoA is metabolised into succinate (4C) generating GTP by succinyl-CoA synthetase (SCS). Succinate is oxidized by succinate dehydrogenase (SDH), which is also part of the ETC, generating fumarate (4C). Hydrogen atoms are transferred to $FADH_2$. Next, fumarate hydratase or fumarase (FH) hydrates fumarate into malate (4C). Finally, malate dehydrogenase (MDH) reversibly oxidizes malate into OAA, which combines with another acetyl-CoA molecules to continue the TCA cycle. The global energetic balance for each acetyl-CoA that enters the cycle is the production of 1 GTP, molecule, and 2 NADH and 1 $FADH_2$ that will feed the ETC.

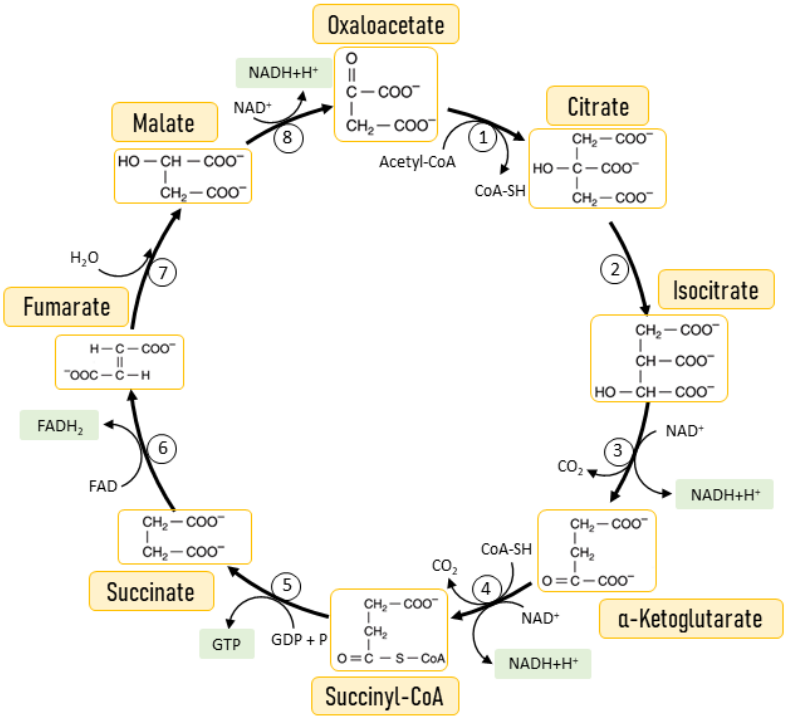

Figure 7. The TCA cycle is formed by a series of eight reactions that constitute a central hub of energetic metabolism as it is fuelled by multiple nutrients. The TCA cycle occurs within the mitochondrial matrix, and involve the participation of multiple enzymes: **1**, citrate synthase (CS); **2**, aconitase (ACO); **3**, isocitrate dehydrogenase (IDH); **4**, α-ketoglutarate dehydrogenase (KGDH); **5**, succinyl-CoA synthetase (SCS); **6**, succinate dehydrogenase (SDH); **7**, fumarase or fumarate hydratase (FH); and **8**, malate dehydrogenase (MDH). The final energetic balance per each acetyl-CoA that feeds the cycle is that of 1 GTP, 3 NADH and 1 $FADH_2$.

1.4.3. THE ELECTRON TRANSPORT CHAIN

The electron donors generated during the TCA cycle feed the ETC. Their containing electrons are sequentially transferred across ETC complexes and oxygen, the final acceptor. This electron transfer is coupled to ATP generation via ATP synthase, and inevitability linked to ROS production (**Figure 8**).

The enzymes of the ETC are huge multi-subunit protein assemblies embedded into the IMM that include NADH:ubiquinone oxidoreductase (complex I, Cx I), succinate dehydrogenase (Cx II),

succinate:ubiquinone oxidoreductase or succinate dehydrogenase (Cx II), ubiquinone:cytochrome *c* oxidoreductase or cytochrome *c* reductase (Cx III), cytochrome *c* oxidase (Cx IV) and ATP synthase (Cx V). Within Cx I-IV, redox cofactors facilitate electron transport. However, transport between complexes occurs through mobile carriers such as membrane-integrated ubiquinone (Q) and the soluble protein cytochrome *c*.

The electrons can enter the ETC at different sites (Scialò et al., 2017). In fact, NADH produced during glycolysis, β-oxidation and TCA cycle, gives two electrons to ubiquinone (Q), which is reduced to ubiquinol (QH_2) in a reaction catalysed by Cx I. Two electrons from $FADH_2$, which is produced during β-oxidation of fatty acids and as a consequence of Cx II-catalysed oxidation of succinate into fumarate, are transferred to Q to reduce it (QH_2). Ubiquinol (QH_2), derived from either Cx I or II activity, diffuse along and across the IMM to Cx III, where it releases two electrons to cytochrome *c* (Rich and Maréchal, 2010), and is oxidized back to ubiquinone (Q). Finally, Cx IV transfers electrons from cytochrome *c* (CytC) to reduce oxygen, which is combined with protons withdrawn from the matrix (Rich and Maréchal, 2010), generating water (Schultz and Chan, 2001).

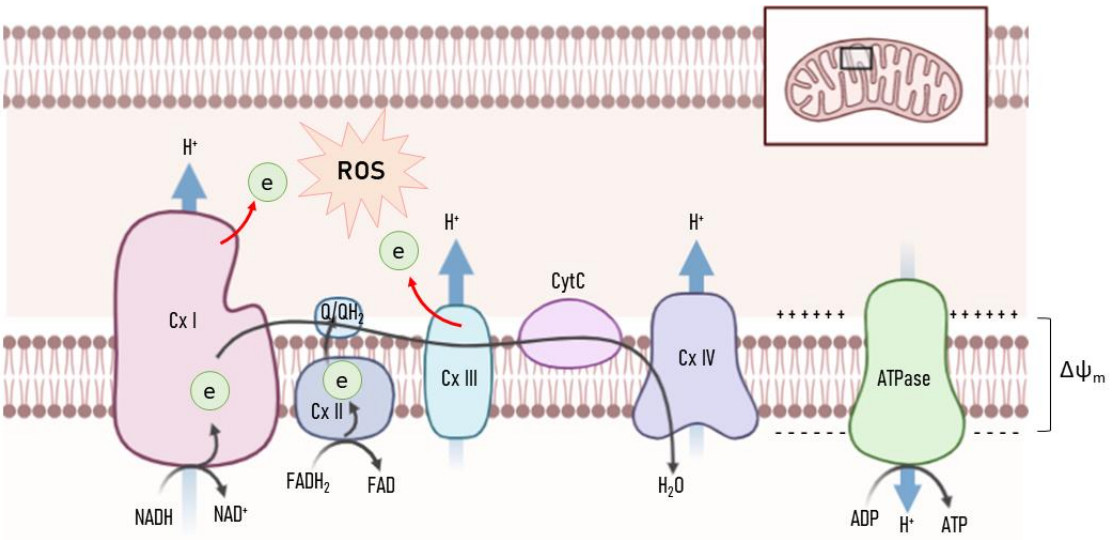

Figure 8. The physiological leak of electrons during the ETC is the main source of intracellular ROS. The ETC Cx I-IV and the ATPase are embedded within the IMM. The electrons flow from Cx I/II to III and IV, where are transferred to oxygen to form water. Electron transfer relies on redox reactions. Within complexes, transport is facilitated by the presence of electron acceptors (mostly iron-sulfur (FeS) clusters and heme groups), whereas between complexes, electrons are transported through soluble mobile carriers such as ubiquinol (QH_2) and CytC. The electron transport is coupled to the pumping of H^+ from the matrix to the IMM, through a process that has not been well understood. Consequently, an electrochemical gradient (membrane potential, Δψm) is generated and used by the ATPase to drive the H^+ back to the matrix and synthetize ATP. However, this process is not perfect, and electrons can escape from the main path, mostly in Cx I and III, and react with oxygen to oxidatively damage surrounding membranes and mtDNA. Adapted from Prasai, 2017. Q: Ubiquinone; QH_2: Ubiquinol; CytC: Cytochrome *c*. Created with BioRender.com.

As electrons flow through the ETC, redox potentials of electron donors and acceptors gradually increase, releasing free energy that is used by the coupling sites of the respiratory chain (Cx I, II and IV) to pump positively charged protons from the mitochondrial matrix into the IMS (Ramsay, 2019). However, little is known about the mechanisms of proton pumping within the complexes. Cx II is the only ETC complex whose activity is not coupled to proton pumping (Rich and Maréchal, 2010). As a consequence of proton pumping, negative charges in the mitochondrial matrix are increased, as well as the positive charges in the IMS, thus creating a mitochondrial membrane potential across the IMM. The created electrochemical gradient is used by ATP

synthase to generate ATP from adenosine diphosphate (ADP) and inorganic phosphate as protons are driven back to the mitochondrial matrix.

1.4.4. THE EFFECTS OF OXIDATIVE PHOSPHORYLATION DERIVED ROS

Electron transfer across the complexes during OXPHOS is not a perfect process. Under physiological conditions, electrons escape from the main transfer path and react with the oxygen present in the IMM, leading to the generation of ROS. In fact, the product of a one-electron reduction of oxygen leads to the formation of the free radical superoxide ($O_2^{\cdot-}$), which is the precursor of most ROS (Pamplona and Barja, 2011) (**Figure 9**).

Leakage of electrons occurs in 11 different sites across the ETC, although Cx I and III are conventionally recognised as the major sites of mitochondrial production of $O_2^{\cdot-}$ (Wong et al., 2017), which is released either to the mitochondrial matrix (Cx I and III) and IMS (Cx III) (Li et al., 2013). Although only 0.2-2% of oxygen consumed by the mitochondria generates $O_2^{\cdot-}$ (Madamanchi and Runge, 2007), it can be spontaneously or enzymatically dismutated to hydrogen peroxide (H_2O_2). The dismutation of superoxide occurs quickly in the mitochondrial IMS and matrix by the enzymatic activities of superoxide dismutase (SOD) 1 and SOD2, respectively (Li et al., 2013).

The fate of $O_2^{\cdot-}$ and H_2O_2 differs due to its electrochemical properties. Due to its "electrophilicity" and short half-life, $O_2^{\cdot-}$ can't hardly cross the OMM. In fact, it reacts with nitric oxide (NO) to produce peroxynitrite ($ONOO^-$) within mitochondria, which is capable to non-enzymatically oxidatively alter DNA, proteins and mitochondrial integrity (Madamanchi and Runge, 2007). Although H_2O_2 is not considered a free radical, it can act as a Trojan horse. H_2O_2 electrophobicity and stability allows it to diffuse across biological membranes and extend initial damage, since it might be reduced to water or form the highly reactive hydroxyl radical ($HO^{\cdot}$) in the presence of ferrous or cuprous ions. Indeed, the concentration of H_2O_2 is 100 times greater than that of $O_2^{\cdot-}$ (Cadenas and Davies, 2000).

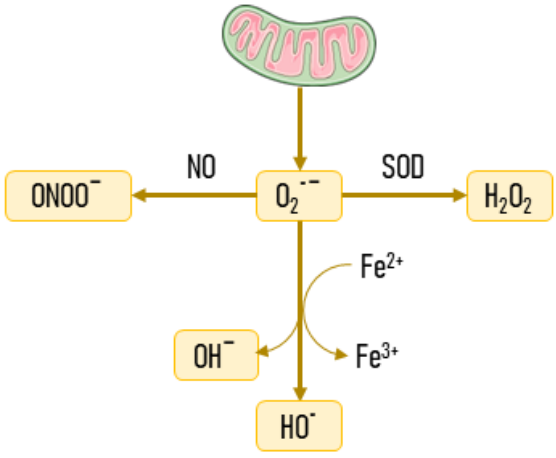

Figure 9. Intracellular mechanisms of ROS production. Electron that leak from the ETC react with oxygen producing the superoxide anion ($O_2^{\cdot-}$), the precursor of most ROS. In fact, it can follow different paths: i) be spontaneously or enzymatically dismutated into the non-radical hydrogen peroxide (H_2O_2); ii) in the presence of iron atoms, it can be transformed into the highly reactive hydroxyl radical ($HO^{\cdot}$), generating the hydroxyl ion (OH^-); iii) in the presence of nitric oxide (NO), generate peroxynitrite ($ONOO^-$).

Electron leakage and ROS production depends upon a number of factors, including mitochondrial membrane potential, metabolic state and dynamics, and oxygen concentration (Li et al., 2013). Nonetheless, electron leakage is unavoidable due to the structure of the ETC Cx I and III. The presence of electron carriers inside the ETC complexes (mostly FeS, clusters and heme groups) reduces the distance between redox cofactors minimizing electron leakage. However, most of these carriers span more than 14 Å, which is the maximum distance for physiological electron transfer between redox centres (Page et al., 1999; Ramsay, 2019). Besides, the rate of electron transfer also depends on the distance between electron carriers, with the rate decreasing roughly 10^6-fold per 10 Å. Hence, the rates of electron transfer are around 10^6 s^{-1} in Cx I and less than 1^{s-1} in Cx III (Ramsay, 2019).

The fact that, structurally, mitochondrial complexes are designed to allow electron leakage, supports the idea that ROS production might be necessary to regulate physiological processes, besides of its detrimental effects (Sena and Chandel, 2012a). In fact, it has been suggested that moderate ROS increases act as chemical messengers in cell signalling (Mailloux and Harper, 2012a) inducing the activation of transcription factors such as NF-kB or HIF-1α, which respond to cellular stresses (Prasai, 2017). The signalling ROS role has been mainly attributed to H_2O_2 (Mailloux and Harper, 2012b) that is generated as a consequence of a reverse electron transfer (RET). The previously described electron transfer, from Cx I and II to III, IV and V represents the canonical pathway, and is defined as a forward electron transfer (FET). However, it has been suggested that under specific circumstances, electrons entering through Cx II can flow back to Cx I via ubiquinol (QH_2) following a RET (Scialò et al., 2017). During both FET and RET, ROS are generated at Cx I, but it has been suggested that ROS-RET triggers physiological roles. Besides, it seems that ROS-RET is associated with lifespan extension (Scialò et al., 2016). Thus, when produced in controlled levels, ROS act as signalling molecules that facilitates communication between mitochondrial function and other cellular processes to maintain homeostasis and promote longevity (Sena and Chandel, 2012b); however, massive ROS production trigger structural alterations and cell death (Bolisetty and Jaimes, 2013).

1.4.5. THE ELECTRON TRANSPORT CHAIN COMPLEX I

Mitochondrial ROS production in long-lived species occurs at lower rates (Barja, 2013; Ku et al., 1993; Pamplona and Barja, 2007). Among the two main ROS generating ETC complexes, the low ROS production in long-lived species has been localized at Cx I (Barja and Herrero, 1998; Herrero and Barja, 1997, 1998).

1.4.5.1. Structure of complex I

The use of cryo-electron microscopy has solved the atomic structure of the mammalian Cx I (EC 1.6.5.3) (Fiedorczuk et al., 2016; Zhu et al., 2016), which is the largest component of the ETC weighting about 970 kDa (Carroll et al., 2003, 2006; Koopman et al., 2010). Within its L-shaped structure, a globular hydrophilic Y-shaped peripheral arm (130 Å long x 110 Å high x 100 Å large) protruding into the mitochondrial matrix can be distinguished from an hydrophobic elongated arm (210 Å long x 100 Å high x 75 Å large) embedded in the IMM (Guénebaut et al., 1998; Sazanov et al., 2003).

Cx I is a supercomplex built of 45 different subunits in mammals. From the inside, a conserved L-shaped core formed by 14 subunits is surrounded by 31 accessory subunits. These 14 core

subunits essential for its catalytic function include seven highly hydrophobic mtDNA encoded subunits (ND1, ND2, ND3, ND4, ND4L, ND5, and ND6), and seven hydrophilic nuclear DNA (nDNA)-encoded subunits (NDUFV1, NDUFV2, NDUFS1, NDUFS2, NDUFS3, NDUFS7, and NDUFS8) (Fiedorczuk and Sazanov, 2018). The accessory subunits form an interlinked, stabilizing shell around the conserved core with unclear function (Elurbe and Huynen, 2016; Sánchez-Caballero et al., 2016a), although they have been proposed to regulate Cx I stabilization, assembly, subunit interactions or limit of ROS production (Zhu et al., 2016).

From a functional point of view, Cx I is organized into three modules (Sánchez-Caballero et al., 2016b; Zickermann et al., 2015a): N (involved in NADH oxidation), Q (involved in CoQ reduction), and P (involved in proton pumping) (**Figure 10A**). Modules N and Q are located in the hydrophilic Cx I arm, which is involved in electron transfer and is the main site of ROS production (Barja, 2007; Brand, 2016; Sazanov, 2006; Wong et al., 2017). The NADH binding site, the primary electron acceptor FMN (Flavin mononucleotide), and the seven nDNA-subunits are located in the hydrophilic arm. The FeS clusters are located within each subunit, enabling single-electron transfer reactions over *wide* distances (Bridges et al., 2012; Mulder et al., 2011). Although the number of FeS clusters varies depending on animal species (up to ten), only eight of them are conserved during evolution (Gnandt et al., 2016). The P module located in the matrix arm, in turn, is constituted by the mtDNA-encoded subunits.

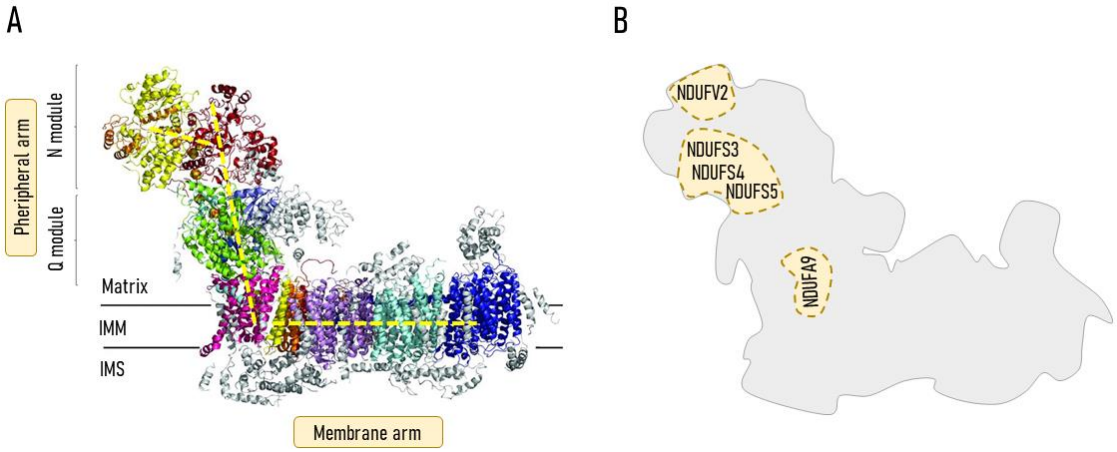

Figure 10. Structure of mammalian Cx I. A) Cryo-electron microscopy structure modified from Zickermann et al., 2015 with permission. Cx I have a characteristic L-shaped structure (see yellow line within Cx I), with a hydrophilic peripheral arm protruding into the mitochondrial matrix and a hydrophobic arm embedded in the inner mitochondrial lipid bilayer. The fourteen subunits of the core enzyme are shown in different colour. IMM, inner mitochondrial membrane; IMS, intermembrane space. Dimensions are in angstroms. **B)** Schematic representation of Cx I and expected location of the selected subunits that are mostly affected by longevity according to Miwa et al., 2014. NDUFA9 is stable across longevity, but it is identified as is used to normalize the results to the total amount of Cx I.

1.4.5.2. The transfer of electrons within complex I

Cx I catalyses NADH oxidation reducing ubiquinone (Q) to ubiquinol (QH_2) (Koopman et al., 2010). The FMN acceptor (NDUFV1 subunit) accepts electrons from NADH (Blinova et al., 2008; Grivennikova and Vinogradov, 2006). Then, these electrons are transported sequentially through the different subunits by seven FeS clusters: N3 (NDUFV1), N1b (NDUFS1), N4 (NDUFS1), N5 (NDUFS1), N6a (NDUFS8), N6b (NDUFS8), and ending with cluster N2 (NDUFS7) (**Figure 11**). Finally, electrons are transferred from FeS cluster N2 to ubiquinone (Q), which is reduced to ubiquinol (QH_2). Although it is still under study, it has been suggested that electron leakage could

be due to flavin semiquinone, to some of the eight different FeS of the hydrophilic domains or both to flavin and FeS centres (Genova et al., 2001; Herrero and Barja, 2000; Kushnareva et al., 2002).

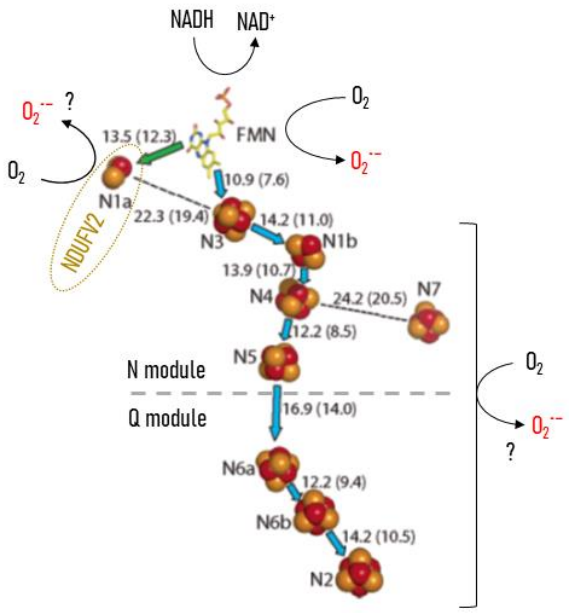

Figure 11. The electron transfer pathway inside Cx I relies on multiple FeS clusters. The sites of ROS generation within the hydrophilic Cx I domain have been pointed to FMN, ubisemiquinones and FeS clusters. Average distance within the Cx I redox centres is that of 14 Å. Distances are in angstroms. Adapted from Sazanov, 2006.

1.4.5.3. Complex I is involved in longevity determination

The underlying mechanisms leading to a lower mitochondrial ROS production at Cx I in long-lived species has been attributed to a smaller degree of electronic reduction of complex I under physiological conditions (Barja, 2013; Barja and Herrero, 1998). Cx I content seems to be also determinant for ROS production, since the reduced content of Cx I found in long-lived species occurs with a decreased rate of ROS production (Lambert et al., 2010; Pamplona et al., 2005). Thus, the lower Cx I content, the lower electron leakage and ROS production. In fact, pro-longevity interventions such as dietary (DR) and methionine restriction (MetR), as well as rapamycin, have also been associated with decreased mitochondrial ROS production at Cx I (Ayala et al., 2007; Gómez et al., 2007; Miwa et al., 2014; Pamplona and Barja, 2006, 2007; Sanchez-Roman et al., 2011; Sanz et al., 2006b).

In this line, a recent study comparing the mitochondrial proteome of long-lived mice (as a result of DR) with control should be highlighted (Miwa et al., 2014). The results demonstrated that longevity extension occurred along with a modulation of the content of specific Cx I subunits located in the hydrophilic arm. In fact, marked reduction of the conserved NDUFV2 subunit, along with NDUFS3, NDUFS4 and NDUFS5 is observed under DR (**Figure 10B**). Therefore, suggesting that these subunits might be involved in the electron leakage and subsequent ROS production, leading to a shortened longevity. Besides, they have suggested that the content of these subunits determines a proper Cx I assembly, which might also be essential to achieve a higher longevity. Therefore, long-lived species have decreased the Cx I content and modulate the content of specific subunits involved in ROS production, to maintain a correctly assembled and more efficient Cx I with a reduced electron leakage. Hence, specific genetic variations in

mtDNA (C150T transition in the T-loop) from Northern Italian centenarians (Salvioli et al., 2008) are associated with lower mitochondrial ROS production without affecting respiratory capacity (Chen et al., 2012), and specific Cx I genotype in Japanese centenarian confers resistance to degenerative diseases (Tanaka et al., 2000).

1.5. THE EVOLUTION OF THE AMINO ACID CODE

Life evolution requires a stable source of energy (Sousa et al., 2013). Geoscientists have proposed that the first living organisms depended on submarine hydrothermal vents that provided a stable concentration of ions including the transition metals iron and nickel ready for exploitation (Martin and Russell, 2003). Besides, its spherical captivities might have acted as mechanical scaffolds allowing the formation of lipid-covered cells. The mineral surfaces enriched in transition metals, might have become a blueprint for the construction of the most important group of ancient redox cofactors, the FeS clusters (Martin and Russell, 2003; Wächtershäuser, 2008).

The evolution of ancient cells implied their emancipation from amorphous FeS precipitates, which conferred them a stable source of nutrients. In order to maintain the catalytic properties of FeS clusters, cells gave rise to the first amino acids to anchor the FeS to the membranes. These early abiotic amino acids, which were hydrophobic and capable to insert into membranes (Bechinger, 2001), probably comprised the amino acid alanine (Ala), aspartate (Asp), glutamate (Glu), glycine (Gly), Ile, Leu, proline (Pro), serine (Ser), threonine (Thr) and Val (Granold et al., 2018; Longo and Blaber, 2012; Moosmann et al., 2020).

As oxygen concentration continued increasing, the emergence of new amino acids capable to flexibly react with ROS without compromising protein structure and function was forced (Granold et al., 2018; Moosmann et al., 2020). Thus, the fixation of amino acids with increased redox properties such as arginine (Arg), asparagine (Asn), cysteine (Cys), glutamine (Gln), histidine (His), lysine (Lys), Met, phenylalanine (Phe), tyrosine (Tyr) and tryptophan (Try), lead to the transition to the actual genetic code (Granold et al., 2018).

1.5.1. AMINO ACIDS STRUCTURE AND CLASSIFICATION

Amino acids are the basic units of proteins. Structurally, they contain an amino (-NH_2) and a carboxyl (-COOH) group, along with a varying side chain (R group), which is specific for each amino acid. To date, more than five hundred amino acids exist naturally, although only twenty-two are coded and used to synthetize proteins in all living organisms (Gordon et al., 1943). Aside from their structural role in composing proteins, amino acids have many biological functions. In fact, most of them are essential nutrients that can act as intermediate energetic metabolites and precursors of glucose biosynthesis, chemical messengers and methylating agents.

The structural diversity found within all amino acids, due to its side chain, leads to a complex classification of proteinogenic amino acids and according to different criteria, such as polarity of the R group, the presence of specific atoms (sulphur-containing amino acids) or structures (aromatic rings), the nutritional needs (essential amino acids) and metabolic roles (glycogenic or ketogenic) (**Figure 12**).

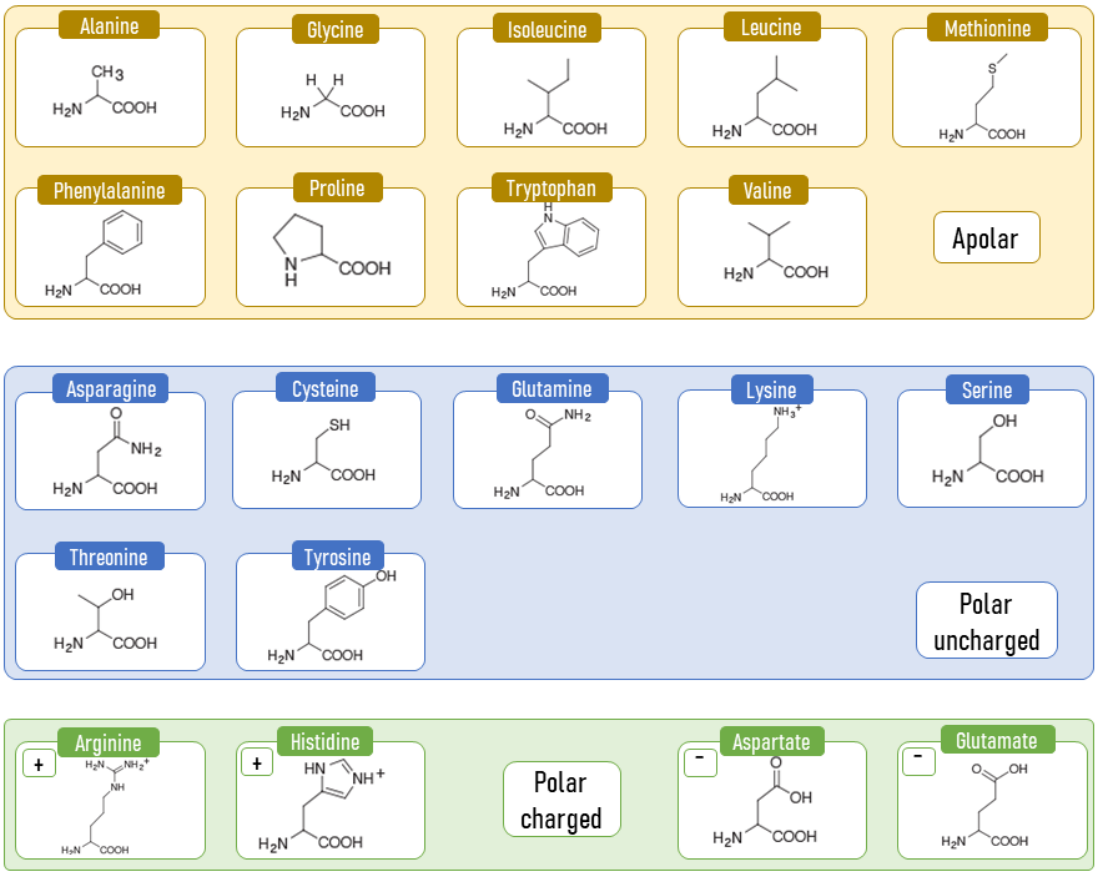

Figure 12. Structure of the twenty proteinogenic amino acids. Classification is performed on the basis of its side-chain polarity. Eleven of the proteinogenic amino acids are polar, although only four of them are charged (2 positively and 2 negatively). The nine amino acids left are non-polar.

1.5.2. THE SULPHUR-CONTAINING AMINO ACIDS IN LONGEVITY DETERMINATION

The emergence of sulphur atoms in the amino acids side chains can be considered a late event in the amino acids evolution. In fact, Cys and Met, the two proteinogenic sulphur-containing amino acids, are thought to be the 17 and 18 amino acids (Granold et al., 2018; Moosmann et al., 2020). Their redox properties might be attributed to the fact that, chemically, sulphur electronegativity is higher than that of oxygen (Brosnan and Brosnan, 2006). Therefore, it makes sulphur atoms to be attracted to undergo redox reactions, which were essential to adapt and survive to the new oxygenic atmosphere conditions.

Interestingly, the protein composition of Met and Cys is species-specific and is associated with animal longevity. In fact, long-lived animal species have lower Met (Aledo et al., 2011; Pamplona et al., 2005; Portero-Otín et al., 2004; Ruiz et al., 2005) and Cys (Moosmann, 2011) protein content. Free tissue Met content is also lower in long-lived animal species (Lewis et al., 2018; Mota-Martorell et al., 2020a). Besides, the reduced intake of Met is a widely described pro-longevity intervention (Pamplona and Barja, 2006), capable to increase longevity with a potency around half that of that of DR in rodents (Sanchez-Roman and Barja, 2013).

1.5.2.1. Cysteine is essential for evolution but detrimental for longevity

The first emergent sulphur-containing amino acids was Cys. Scientific evidence suggest that it may have been introduced into the genetic code to anchor FeS clusters to cellular membranes

and stabilize them (Moosmann et al., 2020). In fact, central Cys from the tripeptide glutathione (GSH) is sufficient to stabilize redox functional FeS clusters in aqueous solution (Qi et al., 2012).

Although essential for life evolution, incorporation of Cys residues in aerobic animals is limited. Within animals, nuclear-encoded Cys usage is stable and reduced to 2-2.5% of all encoded amino acids (Moosmann and Behl, 2008). However, mitochondrial-encoded Cys varies substantially. In fact, in aerobic taxa mitochondrial-encoded proteins are depleted of Cys in comparison with nuclear-encoded (Moosmann and Behl, 2008), and the content of Cys is negatively correlated with species lifespan (Kunath and Moosmann, 2020; Moosmann and Behl, 2008). Thus, the longer the longevity, the lower the mitochondrial-encoded Cys. Besides, Cys has been removed from protein surfaces (Marino and Gladyshev, 2010, 2012), although its frequently associated with protein function (Marino and Gladyshev, 2010).

Atmosphere oxygenation drove the limitation of Cys incorporation in protein surfaces from aerobic organisms, due to its structural and chemical properties. Sulphur atoms from Cys are contained in thiol groups (R-SH), and its free electrons allow for multiple oxidation states (**Figure 13**) (Chung et al., 2013; Netto et al., 2007). When located into protein surfaces, Cys residues are estimated to have, on average, the closest pK_a to the physiological pH (Marino and Gladyshev, 2010). Thus, exposed Cys residues easily experience electrostatic changes that might lead to its deprotonation even after small variations within the physiological range of pH values. Due to its chemical properties, Cys are capable to undergo reversible redox reactions, which are essential for aerobic life and protein function (Chung et al., 2013). For instance, thiol groups participate in the formation of covalent interaction with other thiols to create intra- and intermolecular disulphide bonds (R_1-SH + SH-R_2 → R_1-S-S-R_2) that are essential for protein function.

However, not all Cys residues have the same redox properties, which can vary according to protein environment. In fact, thiol groups from Cys residues that are surrounded by positively charged amino acids (Arg and His) in proteins, are deprotonated and converted into reactive thiolates (R-S^-) (Netto et al., 2007). These thiolates are better nucleophiles than their protonated counterparts, and react easily with oxidants (Winterbourn and Metodiewa, 1999) and other intracellular structures (Aledo et al., 2012). Accordingly, Cys has been often referred to as an oxidant amino acid (Aledo et al., 2011), and thus its incorporation in proteins from aerobic organisms is limited.

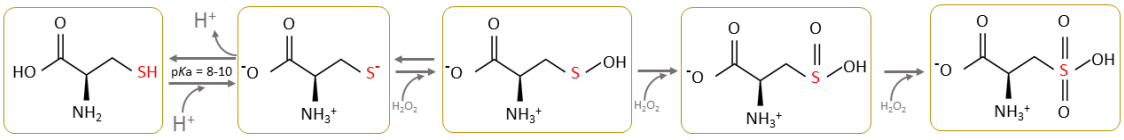

Figure 13. Chemistry of Cys redox states. Under physiological conditions, Cys thiol group (R-SH) is deprotonated into highly reactive thiolates (R-S^-). Thiolates can react within each other forming disulfide bounds (not shown). However, under oxidative stress conditions, it can be transformed into a sulfenic (R-SOH), sulfinic (R-SOOH) or sulfonic (R-SOOOH) group. Sulfenic formation can be reverted into thiolates through GSH dependent reactions. However, formation of sulfinic and sulfonic groups are irreversible. Adapted from Chung et al., 2013 and Marino and Gladyshev, 2010a.

1.5.2.2. Methionine accumulation is essential for the evolution of longevity

The introduction of the second sulphur-containing amino acid Met is closely associated with lipid evolution (Moosmann et al., 2020). Lipid membranes are present in all living organisms,

suggesting that they emerged early in history evolution (Lombard et al., 2012). In fact, these structures are essential to provide a stable barrier to separate cells from the environment, and allow the selective import of molecules. However, these two functions require the maintenance of proper membrane fluidity and viscosity.

Ancient cells emancipating from submarine hydrothermal vents to primordial ocean had to cope with a temperature drop of 40°C (from 70 to 30°C) (Martin and Russell, 2003; Moosmann et al., 2020). As little temperature changes of 5°C alter membrane function (Wunderlich et al., 2009), ancient cells had to develop mechanisms to maintain proper membrane physicochemical properties (homeoviscous adaptation). Probably, the most used strategy involves the introduction of PUFA in biological membranes (Pamplona et al., 2002). However, since PUFA are the most susceptible macromolecules to be oxidatively damaged, aerobic life occurs with the initiation of spontaneous membrane peroxidation reactions (Pamplona and Barja, 2007). In this oxidative context, the introduction of new hydrophobic amino acids, such as Met, capable to be embedded into biological membranes as transmembrane proteins to limit and prevent peroxidation reactions arguably became the most attractive option for ancient cells.

In animals, as Cys, Met usage is limited and accounts for 2.2-2.8% of encoded amino acids (Bender et al., 2008). Nonetheless, the content of mitochondrial-encoded Met is higher than that of nuclear encoded levels (Moosmann, 2011), accounting of a 4% of encoded amino acids or more, and is negatively correlated with species longevity (Aledo et al., 2011). Thus, the higher the longevity, the lower the mitochondrially-encoded Met. Mitochondrial DNA evolution occurred with the reassignment of the codon AUA from Ile to Met, leading to an increased accumulation of Met in the surface of respiratory chain complexes, physically interacting with the IMM (Bender et al., 2008; Schindeldecker and Moosmann, 2015). Notably, the accumulation of Met residues in animal proteins correlates with its aerobic metabolic rate (Schindeldecker and Moosmann, 2015).

Met is one of the late amino acids that were fixed in the genetic code. Although the introduction of amino acids in the genetic code is easy (Liu and Schultz, 2010), changing the composition of an already stable and operative genetic code is difficult. Therefore, the late introduction of Met into the genetic code must have been driven by selective pressures (Jones et al., 2013). Recapping the functions of Met in modern cells allows to discern what drove its fixation into the genetic code. Met is codified for the initiation codon AUG, and thus its necessary for protein synthesis initiation. However, its delayed introduction into the genetic code suggest that it was not essential for protein synthesis in ancient cells (Trifonov, 2000, 2009), suggesting that this was not the main force that drove its fixation. Besides, Met residues are not involved in catalysis reactions (Levine et al., 1996; Lim et al., 2019). Nonetheless, Met introduction temporally overlaps with the origin of oxygenic photosynthesis (Cardona, 2019), thus suggesting that its fixation is essential to allow cell survival under oxygenic conditions.

Although containing sulphur, Met structure is different than that of Cys. In fact, unlike Cys, sulphur atom is contained as a sulphide group (R_1-S-R_2) on its hydrophobic side chain (**Figure 14**). The four free sulphur electrons of Met sulphide can be attacked by oxygen (Schöneich, 2005), leading to the formation of Met sulfoxide (MetO), which converts its apolar side chain into a highly polar one (Aledo, 2019). Unexpectedly, the formation of MetO in some Met residues occurs with a minimal distortion of protein structure (Levine et al., 1996) and function

(Reddy et al., 1994). Besides, MetO can be solved by the enzymatic activity of Met sulfoxide reductases (Mrs) with the little metabolic cost of one NADPH molecule (Stadtman et al., 2005). Accordingly, specific methionine residues act as ROS scavengers, mainly those located in the inner mitochondrial membrane, where ROS is produced (Aledo et al., 2011). Therefore, one equivalent of ROS is destroyed for every equivalent of MetO that is reduced back to methionine (Levine et al., 1996). Therefore, Met has been defined as an anti-oxidant amino acids (Aledo et al., 2011; Schindeldecker and Moosmann, 2015).

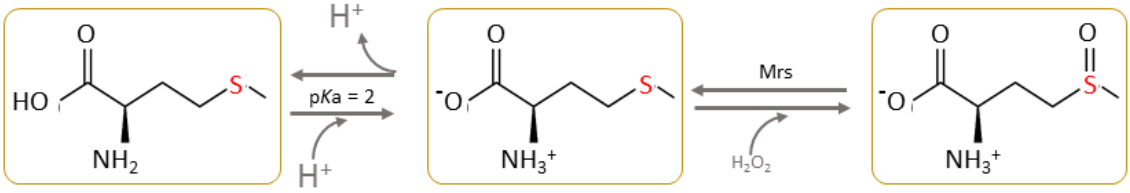

Figure 14. Chemistry of Met redox states. Under oxidative stress conditions, Met can be converted into MetO. However, the formation of MetO can be reverted by the enzymatic activity of Mrs. MetO, methionine sulfoxide; Mrs, methionine sulfoxide reductase. Adapted from Aledo, 2019.

Incorporation of Met residues in transmembrane proteins, such as the respiratory complexes, protects them from high radicals like hydroxyl radical (HO$^{\bullet}$) (Davies, 2016). Therefore, Met prevents protein oxidation ensuring its proper activity, but its reactivity towards peroxyl radicals derived from PUFA oxidation is limited. Therefore, evolution required the incorporation of the aromatic amino acids Tyr and Try, which were stable enough to resist to one-electron oxidation derived from lipid oxidation (Trifonov, 2000, 2009). In fact, these two amino acids can act as aqueous and lipophilic radical scavengers (Moosmann and Behl, 2008). Protein residues of Tyr and Try can interact with those of Met, forming the named S-aromatic motifs (Reid et al., 1985), which are involved in protein stabilization (Valley et al., 2012; Zauhar et al., 2000). Interestingly, these structures are found within non-oxidized Met residues, suggesting that Tyr and Try might also be involved in preventing Met oxidation (Aledo, 2019).

1.5.2.3. Establishing a relationship between methionine and cysteine

Beyond its redox functions as ROS scavenger, Met is central in a complex metabolic pathway that can be divided in three parts (**Figure 15**): Met cycle or the transmethylation pathway, the transsulfuration pathway, and Met salvage pathway (Parkhitko et al., 2019; Sanderson et al., 2019).

Free Met residues, obtained from either diet or intracellular catabolic processes such as autophagy, are metabolized through a series of four cyclic reaction referred to as the Met cycle or the transmethylation pathway. Briefly, the highly conserved methionine adenosyltransferase (MAT) converts Met into the universal methyl donor S-adenosylmethionine (SAM), which upon donation of one methyl group is enzymatically converted to S-adenosylhomocysteine (SAH) through one over the 200 known methyltransferases (MT) identified, at least in human genome (Parkhitko et al., 2019). The reversible hydrolysis of SAH into homocysteine and adenosine depends upon the enzymatic activity of S-adenosylhomocysteine hydrolase (SAHH/AHCY). Remethylation of homocysteine to form methionine completes the cycle. The final reaction involves either methionine synthase (MS), which participates in the folate cycle and uses 5-methyl tetrahydrofolate (5-MTHF) as methyl donor, or betaine-homocysteine 5-

methyltransferase (BHMT), which consumes betaine. Apart from these two enzymes, Met can be synthetized via the Met salvage pathway, which consumes SAM and is responsible for the production of polyamines, such as spermidine (Parkhitko et al., 2019).

Apart to serve as Met precursor, homocysteine can enter into the transsulfuration pathway. Sulphur atoms from homocysteine, are sequentially transferred to synthetize cystathionine and Cys. These reactions are catalysed by cystathionine-β-synthase (CBS) and cystathionine-γ-lyase (CTH), which require the vitamin B6 active form pyridoxal-5'-phosphate (PLP) as cofactor and produce hydrogen sulfide (H_2S) as by-product. Finally, Cys can be enzymatically combined with the amino acids Glu and Gly to synthetize the tripeptide GSH. In fact, it has been reported that approximately 50% of Cys derived from the transsulfuration pathway is utilized for GSH biosynthesis in liver (Mosharov et al., 2000). Besides GSH and H_2S, Cys can be oxidized and decarboxylated into taurine.

Scientific evidence reported that genetic alterations in the enzymes involved in the transmethylation and transsulfuration pathway modulate longevity (Parkhitko et al., 2019). However, it seems that these effects are mainly associated with the regulation of activity of the transsulfuration enzymes (Sbodio et al., 2019). Although constitutively expressed, CBS is allosterically activated by SAM (Majtan et al., 2014). On the contrary, CTH is expressed under nutritional, oxidative or endoplasmic stress conditions, triggering the biosynthesis of sulphur-containing antioxidants such as H_2S, GSH and taurine (Sbodio et al., 2019).

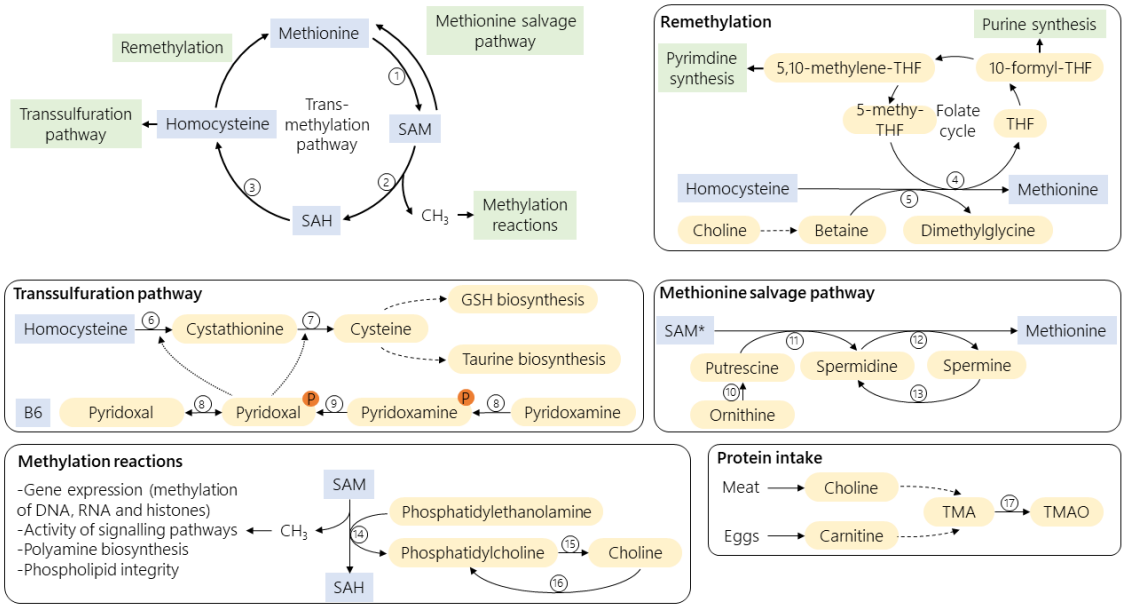

Figure 15. Methionine metabolism and related metabolic processes. Numbers refer to enzymes: 1, Methionine adenosyltransferase I/II (MAT1/MAT2); 2, Methyltransferases (MTs); 3, S-Adenosylhomocysteine hydrolase (SAHH/AHCY); 4, Methionine synthase (MS); 5, Betaine-Homocysteine S-methyltransferase (BHMT); 6, Cystathionine-β-synthase (CBS) ; 7, Cystathionine-γ-lyase (CTH); 8, Pyridoxal kinase (PDXK) or pyridoxal phosphatase (PDXP); 9, Pyridoxine 5'-phosphate oxidase (PNPO); 10, Ornithine decarboxylase (ODC1); 11, Spermidine synthase (SRM); 12, Spermine synthase (SMS); 13, Spermine oxidase (SMOX); 14, Phosphatidylethanolamine N-methyltransferase (PEMT); 15, Phospholipase C; 16; CPD-choline pathway; 17, Flavin mono-oxygenase 3 (FMO) in the liver. SAM* represents S-adenosyl-3-(methylsulfanyl)propylamine, synthesized from SAM via S-adenosylmethionine decarboxylase proenzyme (AMD1).

1.6. SIGNALLING PATHWAYS INVOLVED IN LONGEVITY DETERMINATION

Phenotype diversity, in terms of longevity achievement, is the consequence of a global intracellular modulation orchestrated by intracellular signalling systems that are finally modulated by external factors. Thereby, a recently published review (Barja, 2019) aimed to bring together the mechanisms leading to specific traits of longevity, which are not mutually excluding, present in all cells, and integrated into a cell aging regulating system (CARS). As the achievement of an extended longevity goes through a reduction of the aging rate, CARS is involved in longevity determination. In fact, Barja suggested that CARS system is composed of three main parts: i) cytoplasmic pre-nuclear signalling; ii) the nuclear genetic aging program; and iii) post-nuclear aging effectors.

The mechanism of CARS is straightforward. Nutrient availability in the external environment is sensed by cells using humoral factors like insulin, or blood amino acids like methionine. These extracellular factors, in turn, modify the activity of specific cytoplasmic signalling proteins like PI3K, AKT, AMPK, sirtuins, mTOR complex, ERK, among others (Dibble and Cantley, 2015; Johnson et al., 2013; Pan and Finkel, 2017). Many of these signals are sent to the nucleus, where specific transcription factors like FOXOs, PGC1α, SREBP and HIF-1α, among others (Fu et al., 2006), modify the expression of genes of the aging program involved in the control of longevity. The final effect of the aging program is to modulate the activity of post-nuclear ageing effectors, which include the rate of mitochondrial ROS production at Cx I, the composition of structural components such as the degree of unsaturation of biological membranes, and likely the autophagy system. Thus, those animal species that produce less ROS, are provided of oxidation-resistant structures, and are able to get rid of altered intracellular structures, diminish the rate of ageing and live longer.

1.6.1. THE MTOR SIGNALLING PATHWAY

The mechanistic target of rapamycin (mTOR) signalling pathway is one of the most studied intracellular pathways that regulates longevity, constituting a member of the CARS. Its description is closely related to the discovery of the antifungal rapamycin, which was isolated from *Sreptomyces hygroscopius* in the late 70s. Immunosuppressant and antitumor activities were attributed to rapamycin before its mechanism of action was understood. In the 90s, the genes codifying for the putative targets of rapamycin in yeast (*target of rapamycin (TOR) 1* and *TOR2*) were identified, but it wasn't until 1994 that the mammalian homologous was isolated from mammalian cells (Johnson et al., 2013).

mTOR is a member of an evolutionary conserved group of serine/threonine kinases from the PIKK (phosphatidylinositol-3 kinases (PI3K)-related kinase) family that is present as two distinct complexes: mTOR complex 1 (mTORC1) and mTOR complex 2 (mTORC2) (Valvezan and Manning 2019). It has been suggested that mTORC1 and 2 regulate different processes. In fact, mTORC1 is sensitive to rapamycin and its inhibition has been widely associated with an extended longevity, therefore most scientific efforts have been directed to study this complex. However, mTORC2 integrity has been recently suggested to regulated longevity in worms (Chellappa et al., 2019). As our work is focused in longevity, we will focus our attention into mTORC1.

mTORC1 plays a central role in the highly conserved mTOR signalling network (**Figure 16**), which integrates intracellular and extracellular signals to regulate cell physiology and metabolism

(Laplante and Sabatini, 2009). Thus, mTORC1 can regulate cell metabolism, growth, and proliferation, and can modulate complex physiological processes such as aging and longevity (Barja, 2019; Kapahi et al., 2010; Khayati et al., 2017; Papadopoli et al., 2019; Valvezan and Manning, 2019; Weichhart, 2018) through a wide range of downstream pathways such as mRNA translation, biosynthesis pathways, mitochondrial function, autophagy, endoplasmic reticulum stress, and stress responses, among others. Globally, under high nutrient availability, mTORC1 is activated and promotes the induction of anabolic processes, such as protein and lipid synthesis. Contrarily, when nutrient availability is scant mTORC1 is not activated, and catabolic processes, such as autophagy, are promoted to feed the cell and maintain proper energetic levels.

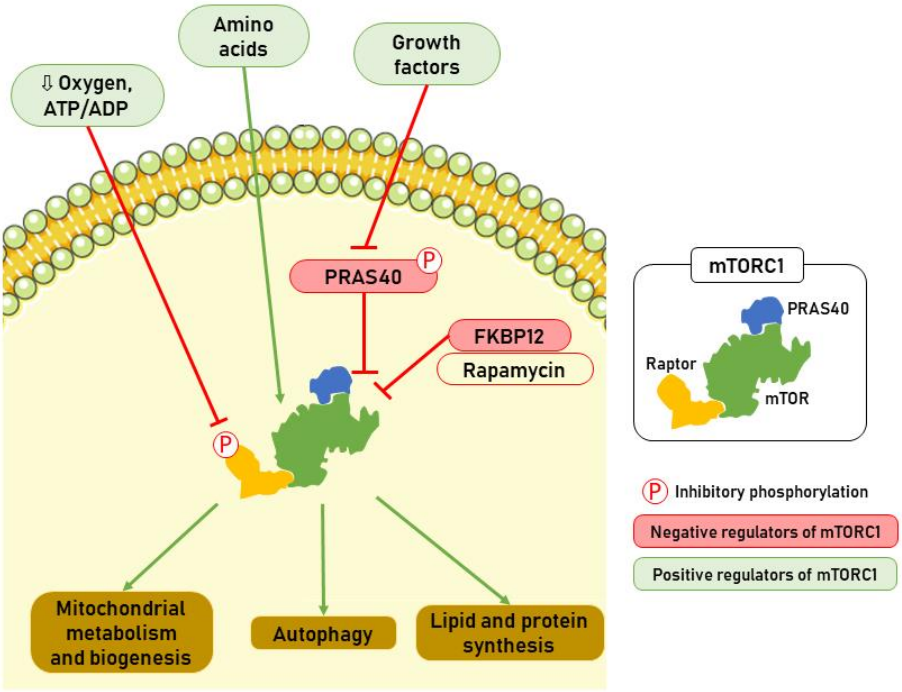

Figure 16. mTORC1 signaling at a glance. mTORC1 is activated under the presence of amino acids and growth factors, and in situations of low oxygen and energy (ATP/ADP ratio). Besides, its activity is also negatively regulated by PRAS40 and FKBP12. In response to these extracellular signals, mTORC1 regulates a diversity of intracellular processes such as mitochondrial metabolism and biogenesis, autophagy and lipid and protein synthesis.

1.6.1.1. The structure of the mTOR complex 1

In mammals, mTORC1 is composed by mTOR and its associated proteins Raptor (regulatory associated protein of TOR), mLST8 (mammalian lethal with SEC13 protein 8), and Deptor (DEP domain-containing mTOR-interacting protein) (Valvezan and Manning, 2019) (**Figure 17**). mTOR, Raptor, and mLST8 are core components, and Deptor is an inhibitory subunit. PRAS40 (Proline-rich AKT1 substrate of 40 kDa) is a polypeptide that is phosphorylated by mTORC1, but also negatively regulates mTORC1 activity. It binds to Raptor and thus it is commonly stably associated with mTORC1 (Chao and Avruch, 2019). FKBP12 (FK506 binding protein) is a regulatory subunit of the rapamycin sensitive mTORC1 activity. Importantly, Raptor and mTOR regulators PRAS40 and FKBP12 are exclusive of mTORC1.

Extra- and intracellular signals regulating mTORC1 include growth factors, hormones, glucose, ATP, oxygen, metabolic intermediates, and amino acids (Valvezan and Manning, 2019). Among

amino acids, arginine, leucine, and methionine cycle metabolites play a relevant role as activators of mTORC1 through their interaction with several intracellular mediators (Li and Yan, 2019; Valvezan and Manning, 2019).

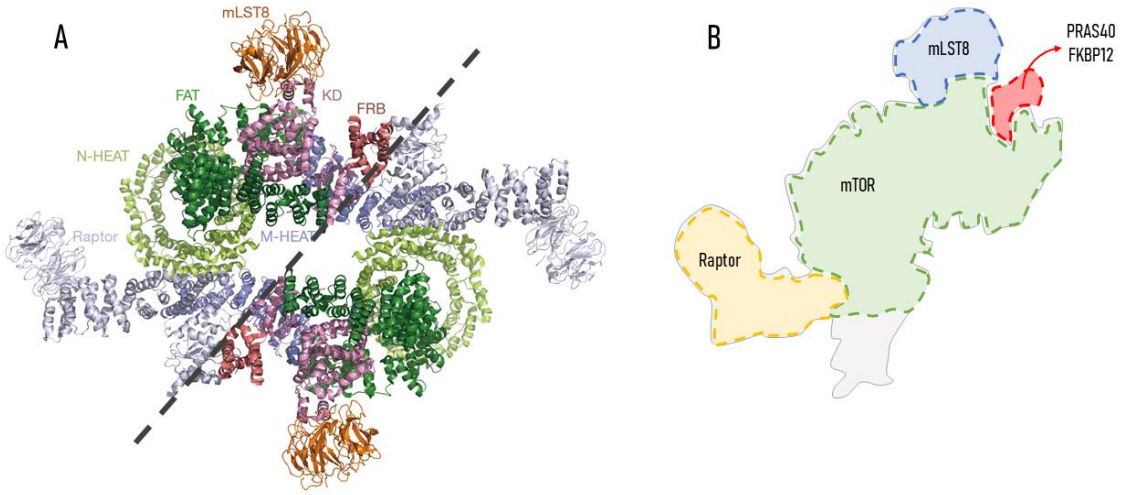

Figure 17. Structure of human mTORC1. A) Cryo-electron microscopy structure obtained from Yang et al., 2018. mTORC1 forms a symmetric dimmer of an heterotrimer constituted by mTOR itself, Raptor and mLST8. mTOR structure consists of an N-terminal HEAT repeats (N-HEAT), a FATD (Frap, ATM, TRRAP domain), an FRBD (FKBP12-Rapamycin binding domain) and a C-terminal kinase domain (KD). Each domain and subunits are indicated in different colours. **B)** Schematic representation of an mTORC1 heterotrimer and expected binding site of its regulators FKBP12 and PRAS40 adapted from Yang et al., 2018 and Aylett et al., 2016. FKBP12 binds to mTOR through its FRBD. PRAS40 binding domain is structurally very close to those of FKBP12, as it binds to an α-helix from the FBD and to mLST80.

1.6.2. mTOR SIGNALLING AND LONGEVITY

Inhibition of the mTOR pathway results in a longevity extension in several animal models (Kapahi et al., 2010; Lushchak et al., 2017; Papadopoli et al., 2019; Weichhart, 2018). These effects are independent on the site of inhibition. Hence, upstream mTOR inhibition with rapamycin increases mice lifespan (Martínez-Cisuelo et al., 2016; Singh et al., 2019), as the downstream inhibition of its effectors does (Selman et al., 2009; Wu et al., 2013b). Besides, mTOR activation shortens longevity (Johnson et al., 2013; Kapahi et al., 2010; Papadopoli et al., 2019) and its activity is decreased in long-lived whales (Ma and Gladyshev, 2017). Not only mTORC1 activity but its integrity has been recently to be essential for mTOR signalling (Hoeffer et al., 2008) and, thus, longevity.

mTOR is strongly regulated by specific proteins and nutrient availability, whose regulation is also associated with longevity. Accordingly, decreased content of amino acids are found in the exceptionally long-lived specimens (Lewis et al., 2018; Seim et al., 2016). In the same line, MetR extended longevity occurs along with an mTORC1 inhibition (Gomez et al., 2015). Thus, if the activity or the content of its activators is lowered, mTORC1 is not activated, and its activity is decreased.

The mechanisms by which mTORC1 inhibition leads to an extended longevity are diverse. In fact, mTORC1 targets mitochondria and regulates its metabolism (Saxton and Sabatini, 2017) and decreases ROS production at Cx I and oxidative stress (Gomez et al., 2015; Martínez-Cisuelo et al., 2016). Besides, lifespan extension under nutritional interventions leading to mTORC1 inhibition requires autophagy (Bárcena et al., 2019; Ruckenstuhl et al., 2014), thus pointing the

maintenance of proper protein turnover as an essential mechanism to achieve an extended longevity.

1.7. METABOLOMICS IN THE STUDY OF LONGEVITY

Longevity is a complex phenomenon that is mainly determined by two factors: endogenous damage production and the resistance to it. Hence, to achieve an extended longevity, evolution have induced a selective pressure to provide cells from stress-resistant structures and globally optimise its energetic metabolism. Notwithstanding scientific efforts, we are far from getting a global view of the longevity process.

Many studies performed in animal models aimed to determine specific genes affecting longevity. Although most of them are highly conserved across animal species, the determination of longevity in higher animals is more complex than that of animal models, and most of these individual gene alterations are not enough to enhance longevity. The emergence of omics technologies allowed to obtain a wider view of the genomic, transcriptomic and proteomic determinants of longevity. However, these approaches offer limited information due to the fact that: i) although species longevity is genetically determined, individual longevity is mostly affected by the environment; ii) mRNA levels doesn't necessarily correlate with protein content; and iii) proteomics lack of functional information. However, metabolomics seems to overcome these issues, as its object of study, metabolites, are the products of the enzymatic activities, and thus are closer to the longevity phenotype (**Figure 18**).

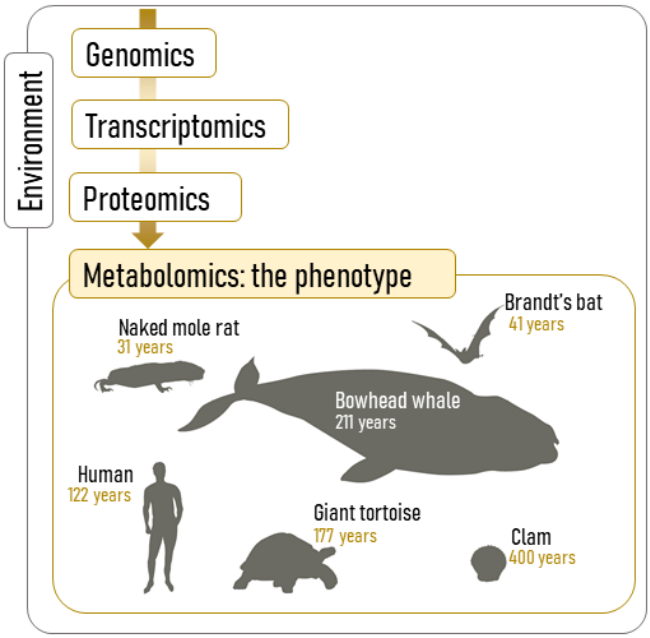

Figure 18. The omics workflow. Adapted from Hoffman et al., 2017.

The understanding of metabolomics requires the prior definition of related concepts such as metabolite, metabolome and metabolic profile. Metabolites are "small molecules that are chemically transformed during metabolism and, as such, provide a functional readout of cellular state" (Patti et al., 2012). Metabolome is the entirety of endogenous and exogenous metabolites of a cell, tissue or organisms, resulting from the enzymatic activity and exposition to environmental stimulus, that are essential for normal cell functionality. Hence, a metabolic

fingerprint is the set of metabolites that are associated to a specific condition, such as longevity, and thus can be a source of biomarkers.

The word "metabolomics" was firstly used in the early 20th century (van der Greef et al., 2013), and englobe the techniques that aim to measure the metabolites present within a cell, tissue or organism under a specific condition, either physiological or pathological (Nicholson et al., 1999). Metabolomics emergence is linked to the development of high sensitivity and accurate mass spectrometry and chromatographic systems and its continuous improvements.

1.7.1. THE CHALLENGES OF METABOLOMICS ANALYSES

The performance of metabolomics studies is complex and involves multiple steps that are summarised in **Figure 19**.

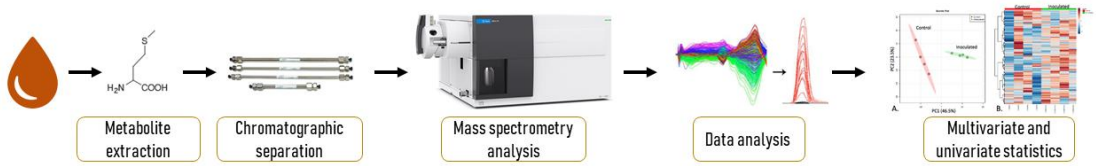

Figure 19. General workflow for metabolomics analyses. Briefly, metabolites are extracted from the sample and undergo a chromatographic separation (according to its retention time). Afterwards, metabolites are ionized and fragmented in a mass spectrometer, to obtain its specific mass to ratio abundances. Finally, data is analysed and multivariate and univariate statistics are applied to give a biological sense to the data.

1.7.1.1. Experimental design

First, the design of a proper experimental design is essential. Two main approaches can be followed according to the objective and the number of metabolites that we are interested into. The performance of an untargeted approach allows for the identification of an unbiased metabolic fingerprint associated to a specific condition, such as longevity. This is useful to identify novel pathways associated with specific processes. However, when we have a hypothesis and want to specifically determine a small set of metabolites, a targeted approach is the best option. This step is crucial, as the number of metabolites will determine the equipment suitability. For instance, triple quadrupole (QqQ) mass spectrometer is mostly used to perform targeted metabolomics and absolute metabolite quantification (Patti et al., 2012).

1.7.1.2. Analytical procedures

Once the experiment is correctly designed, the metabolomic analysis begins. As it is a complex process, it can be split in multiple steps. First, metabolites need to be extracted from the sample. Multiple extraction methods have been developed based on different solvents and chemical properties of the desired metabolites (Cabré et al., 2016; Liu et al., 2017). Thus, polar metabolites will require more hydrophilic solvents, whereas more apolar metabolites rely on hydrophobic ones. Afterwards, extracted metabolites undergo a chromatographic separation and a mass spectrometry analysis. As our work is developed in a liquid chromatography system coupled to a hybrid mass spectrometer with electrospray ionization and a QqQ mass spectrometer (LC-ESI-QqQ-MS) platform, we will detail the performance of this system.

Individual metabolites are separated according to its affinity to a stationary phase (a column) at specific time points, named retention time. Thus, those metabolites showing a higher affinity

for the column, will be retained on it longer than those having a lower affinity. Finally, these metabolites are eluted after being flushed with solvents (either polar, non-polar or combination of both through specific gradients) showing a higher affinity for metabolites than that of metabolites with the column. Afterwards, individual metabolites enter sequentially into the mass spectrometer system.

The functionality of a mass spectrometer is based on the specific fragmentation patterns of each metabolite. Under specific voltage, metabolites are ionized and fragmented into unique fragmentation patterns (metabolite fragmentation spectra). Thus, we distinguish the exact mass (m) of a non-ionized metabolite and the mass-to-charge ratio (m/z) of an ionised metabolite. This ionisation can either be in positive (adding an electron to the metabolite, represent the wining of a unitary mass, M+H) or in negative (removing an electron from the metabolite, representing the loss of a unitary mass, M-H). Thus, after being ionised, a metabolite is defined by a m/z. The precursor metabolite is the ionised metabolite after being fragmented, and the product ions are the individual generated fragments. The m/z conversion of a parent into a specific product ion (parent m/z → product m/z) is a transition. The prior selection of appropriate and unique transitions for each metabolite will allow a proper identification of selected metabolites.

Unique fragmentation patterns and transitions are essential to unambiguously detect and quantify metabolites in a QqQ mass spectrometer. Simplifying its complex structure, a QqQ consists on an ionization source coupled to three chambers. Metabolites enter into the QqQ through the ionization source. After being ionised, specific requirements need to be accomplished to allow the passing of metabolites from one to another chamber. Thus, only those metabolites that are correctly ionised (parents) will enter the first chamber. Afterwards, in the second chamber, also referred to as the collision chamber, a voltage is applied to fragment the parents into their multiple product ions. Finally, only selected product ions (according to the desired transitions) will enter the third chamber, where the abundance of these is determined. As the abundance of product ions is equivalent to parent and metabolite abundance, quantification is performed.

1.7.1.3. Statistical analyses

Finally, if we have managed to pass all the analytical procedures, the odyssey of data analysis begins, which is one of the critical steps to perform a successful metabolomics analysis. Therefore, the use of bioinformatics is essential to properly analyse such amount of obtained data (Jarvis and Goodacre, 2005). First of all, as the aim is to quantify the detected metabolites, normalization, by means of internal standards, external standards and total signal is required (Roberts et al., 2012). Afterwards, multivariate statistics allows to analyse the data as a whole, and to identify metabolomics patterns associated to specific conditions, such as longevity. Finally, univariate statistics allow to identify little changes.

1.7.2. METABOLOMICS IN THE STUDY OF LONGEVITY

As we have stated before, longevity is a complex phenomenon that occurs through the global modulation of intracellular metabolism. Therefore, as metabolomics allows to analyse a wide range of variables (here metabolites), and due to the fact that metabolomics profile is closely

associated to longevity, it has become a widely used technique to unravel the longevity phenotype and its underlying mechanisms.

The first study that aimed to elucidate the metabolomics profile of longevity was performed in long-lived worm models (Fuchs et al., 2010). For the first time, a longevity-associated metabolomics profile, characterised by modulations in amino acids and carbohydrate metabolism, was described. Thus, single-gene mutations and nutritional interventions in worms leading to an extended longevity, occur along with a global metabolic modulation (Butler et al., 2010; Evans et al., 2010; Martin et al., 2011; Mouchiroud et al., 2011; Patti et al., 2014). The existence of a longevity-associated metabolomics profile is not only restricted to worms, as it also observed in rodents under MetR (Pradas et al., 2019a) and long-lived NMR and centenarians (Cheng et al., 2015; Collino et al., 2013).

Most studies have been focused in studying the metabolomics fingerprints of exceptionally-long lived species. However, until recently the basal metabolomics profile associated to species longevity hasn't been analysed. In fact, the first inter species study analysing the tissue metabolomics profile of a series of 25 mammals was recently published (Ma et al., 2015). They have identified metabolites associated with animal longevity, but the most intriguing result was the existence of a highly stable tissue metabolome in mammals. Although most of the efforts have been directed to determine the lipid determinants of longevity (Jové et al., 2013; Pradas et al., 2019a), metabolomics determinants of mammalian longevity are yet to be explored.

HYPOTHESIS AND OBJECTIVES

2.1. HYPOTHESIS

Longevity is a species-specific trait being about 115-120 years in humans. Centenarians are considered an exceptional human model of healthy aging and extreme longevity. Available evidence discloses the existence of a link between longevity and oxidative stress. Thus, the longer the longevity, the higher the resistance to stress. This resistance is considered to be an evolutionary adaptation, and is expressed in terms of lowered ROS production and stress resistant intracellular structures.

The intracellular ROS production is a consequence of, but not limited to, electron leakage from mitochondrial Cx I. Although the underlying mechanisms remain to be elucidated, it has been suggested that the reduced content of selected hydrophilic Cx I subunits might be responsible for a reduced ROS production in long-lived species. In a longevity context, whether mitochondrial structure is regulated to limit ROS generation, it is feasible to postulate that energetic metabolism occurring within mitochondrial matrix might also undergo specific modulations.

Sulphur amino acids (Met and Cys) regulate mitochondrial function. Accordingly, reduced intake of Met extends longevity by decreasing the content of mitochondrial Cx I and limiting the rate of ROS production. Furthermore, the achievement of a higher longevity is associated with the limited intracellular accumulation of Met and Cys. Hence, a regulation of sulphur-containing amino acid metabolism would be expected in a longevity context.

The longevity phenotype is controlled by specific intracellular pathways such as mTOR. In fact, nutritional interventions leading to an enhanced lifespan are associated with lower mTOR signalling activity and, more specifically, mTORC1. Hence, reduced activity of mTORC1 might be associated with the reduced ROS production and structural adaptations. However, whether basal mTORC1 constituents are modulated to achieve an enhanced longevity hasn't been described yet.

The use of metabolomics to elucidate the mechanisms underlying longevity is increasing. In fact, the achievement of an increased longevity occurs through a global reorganization of intracellular metabolism orchestrated by selected intracellular pathways. Hence, we propose that the combined application of a targeted metabolomics approach and molecular biology methodologies will allow to unravel structural and metabolic modulations associated with inter-species and inter-individual longevity.

Therefore, we hypothesise that long-lived species and exceptionally long-lived humans undergo specific metabolic and structural modulations involving methionine and energetic metabolism, amino acid composition, and structural Cx I and mTORC1 adaptations to achieve such an increased longevity.

2.2. OBJECTIVES

In order to elucidate the hypothesis, our work will be divided into two main objectives:

MAIN OBJECTIVE 1. TO DESCRIBE A METABOLIC PROFILE AND ITS MODULATION ASSOCIATED WITH SPECIES LONGEVITY

Objective 1.1. To analyse the role of gene and protein steady state levels of Cx I hydrophilic subunits in determining species longevity

The aim of this study is to determine the steady state levels of selected Cx I subunits that might be involved in the leak of electrons and subsequent ROS production. A comparative approach will be performed in heart tissue from eight mammals with different longevities ranging from 3.5 to 46 years. Gene expression and protein content of selected Cx I subunits (NDUFV2, NDUFS3, NDUFS4, NDUFS5 and NDUFA9) will be analysed using droplet digital PCR and western blot, respectively.

Objective 1.2. To define a metabolic profile associated with species longevity in a post-mitotic tissue

The aim of this study is to determine the existence of a heart species-specific metabolic profile associated with longevity in terms of Met and its related metabolites, amino acids and TCA cycle intermediates. A comparative approach will be performed in heart tissue from seven mammals with different longevities ranging from 3.5 to 46 years. Metabolite content will be measured using a LC-ESI-QqQ-MS platform following a targeted approach.

Objective 1.3. To define a metabolic profile associated with species longevity in plasma

The aim of this study is to determine the existence of a plasma species-specific metabolic profile associated with longevity in terms of Met and its related metabolites, amino acids and TCA cycle intermediates. A comparative approach will be performed in plasma tissue from eleven mammals with different longevities ranging from 3.5 to 120 years. Metabolite content will be measured using a LC-ESI-QqQ-MS platform following a targeted approach.

Objective 1.4. To analyse the role of gene and protein steady state levels of mTORC1 subunits and its regulators in determining species longevity

The aim of this study is to determine the steady state levels of specific mTORC1 subunits and its regulators in long-lived species. A comparative approach will be performed in heart tissue from eight mammals with different longevities ranging from 3.5 to 46 years. Gene expression and protein content of unique mTORC1 forming subunits (mTOR, Raptor, PRAS40) and its regulators (FKBP12) will be measured using droplet digital PCR and western blot, respectively.

MAIN OBJECTIVE 2. TO DESCRIBE A METABOLIC PROFILE AND ITS MODULATION ASSOCIATED WITH HUMAN EXTREME LONGEVITY

The aim of this study is to determine the existence of a plasma metabolic profile associated to human extreme longevity, in terms of Met and its related metabolites, amino acids and TCA cycle intermediates. Three different aged-groups will be compared: adults, aged and centenarian individuals. Metabolite content will be measured using a LC-ESI-QqQ-MS platform following a targeted approach.

MATERIALS AND METHODS

3.1. ANIMALS AND POPULATION

3.1.1. HEART CHANGES ACROSS SPECIES LONGEVITY

Mammalian species included in the study were male adult specimens with an age representing a 15-30% of their longevity. The recorded values for longevity (in years) were: mouse (*Mus musculus*, n=4), 3.5; rat (*Rattus norvegicus*, n=5), 4.5; gerbil (*Meriones unguiculatus*, n=6), 6.3, guinea pig (*Cavia porcellus*, n=5), 8; rabbit (*Oryctolagus cuniculus*, n=5), 24; pig (*Sus scrofa*, n=5), 27; cow (*Bos taurus*, n=4), 30; and horse (*Equus caballus*, n=5), 46. Rodents and rabbits were obtained from rodent husbandries and sacrificed by decapitation, whereas pigs, cows, and horses were obtained from farms. The animal care protocols were approved by the Animal Experimentation Ethics Committee of the University of Lleida, and all relevant ethical regulations were complied. Heart samples were taken from ventricles of 5-10 animals at the same time after death (5 minutes) and immediately frozen in liquid nitrogen and stored at -80°C before 2 h until gene expression, protein content and targeted metabolomics analyses.

3.1.2. PLASMA CHANGES ACROSS SPECIES LONGEVITY

Mammalian species included in the study were male adult specimens with an age representing a 15-30% of their longevity. The recorded values for longevity (in years) were: mouse (*Mus musculus*, n=4), 3.5; rat (*Rattus norvegicus*, n=5), 4.5; guinea pig (*Cavia porcellus*, n=5), 8; rabbit (*Oryctolagus cuniculus*, n=5), 13; sheep (*Ovis aries*, n=5), 20; dog (*Canis lupus*, n=5), 24; pig (*Sus scrofa*, n=5), 27; cow (*Bos taurus*, n=4), 30; cat (*Felis catus*, n=5), 30; horse (*Equus caballus*, n=5), 46; and human (*Homo sapiens*, n=6), 120. Rodents and rabbits were obtained from rodent husbandries and sacrificed by decapitation, whereas plasma from dogs, cats, sheeps, pigs, cows, and horses were obtained from farms. For humans, plasma samples were obtained from healthy adult individuals. The animal care protocols were approved by the Animal Experimentation Ethics Committee of the University of Lleida, and all relevant ethical regulations were complied. Human protocols were approved by the Committee for Ethics in Clinical Research of the Hospital Universitari Arnau de Vilanova, in accordance with the Declaration of Helsinki. All subjects were fully informed of the aims and scope of the research and signed an informed consent. Blood samples from 4-6 animals and subjects were obtained after fasting (8–12 h) by venipunction, centrifuged to separate plasma fraction, which was immediately frozen in liquid nitrogen and stored at -80°C before 4 h until targeted metabolomics analyses.

3.1.3. PLASMATIC TRAITS OF HUMAN EXTREME LONGEVITY

Potential healthy subjects were selected from the population data system of the 11th Health Department of the Valencian Community (Valencia, Spain), which is composed of 29 towns (240.000 inhabitants). The inclusion criteria were to live in the 11th Health Department for at least the last 6 years and to sign the informed consent. The exclusion criterion was to be under statin-therapy or any pharmacological treatment affecting lipid metabolism or to be terminally ill for any reason. We included 18 centenarians (100.8 ± 1.1 years), 21 randomly recruited aged subjects (76.4 ± 0.5 years), and 21 adult individuals (27.9 ± 1.4 years). All experimental procedures were approved by the Committee for Ethics in Clinical Research of the Hospital de la Ribera (Alzira, Valencia, Spain). All subjects or their relatives were fully informed of the aims

and scope of the research and signed an informed consent. Blood samples were obtained after fasting (8–12 h) by venipunction, centrifuged to separate plasma fraction, which was immediately frozen in liquid nitrogen and stored at -80°C before 4 h until targeted metabolomics analyses.

3.2. GENE EXPRESSION ANALYSES BY DIGITAL PCR

The polymerase chain reaction (PCR) enables the amplification of a specific DNA fragment. It is based on the use of a DNA polymerase enzyme, primers and nucleotides (**Figure 20**). Briefly, two primers bind specifically to the flanking regions of the target one-stranded DNA (by sequence complementarity), generating a double-stranded DNA structure that is recognized by the enzyme. After being attached to it, the enzyme starts adding complementary nucleotides to the single-stranded DNA sequence to generate the resultant PCR product.

The PCR reaction is regulated by temperature changes and can be split into three basic steps (**Figure 20A**). First, the temperature is increased above the melting point of the two-stranded DNA of the target DNA, allowing strands to separate (denaturation). Then, the temperature is decreased to allow the specific primers to bind the DNA segments (annealing). Finally, the temperature is raised to be optimal for enzymatic activity, to allow the DNA polymerase to extend the primers by adding nucleotides to the developing DNA strands (extension). Theoretically, after each reaction or cycle, the number of DNA segments is doubled, therefore 2^n copies can be produced after *n* cycles (exponential phase) (**Figure 20B**). However, in practice, the amplification process reaches a *plateau* phase as PCR reagents are depleted and PCR products self-anneal, preventing further amplification (**Figure 20C**).

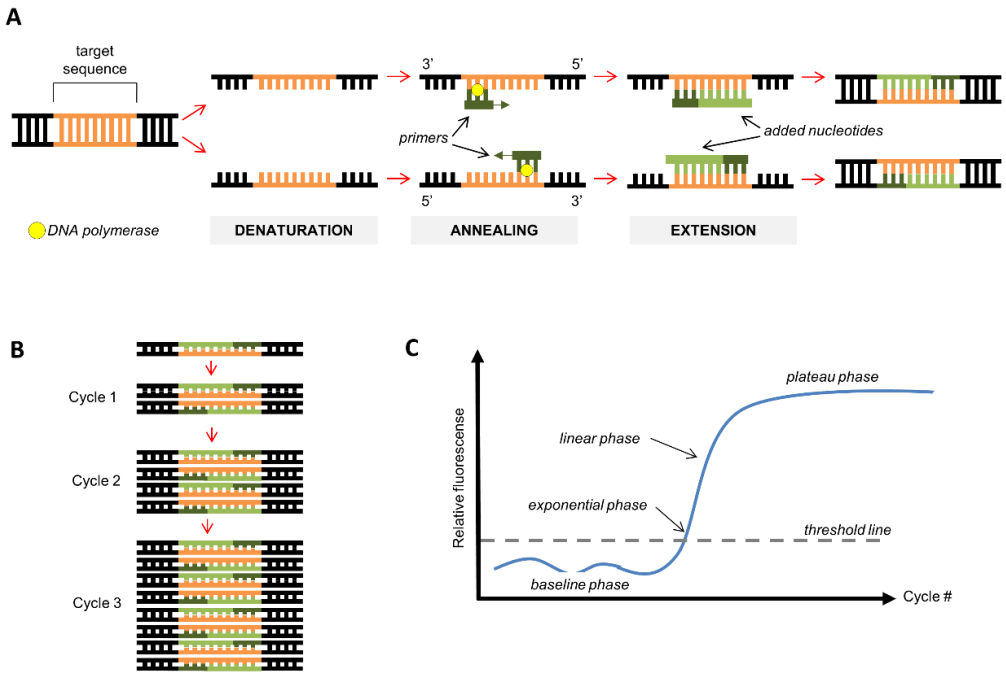

Figure 20. General workflow of a PCR. A) Steps of a single PCR cycle. **B)** Target sequence doubling during PCR cycles. **C)** Different phases of a real-time PCR amplification plot on a linear scale.

Amplified PCR products can be visualized after being stained. According to dye and the staining point it can be distinguished between qualitative and quantitative PCR. Staining of the amplified

DNA product with a chemical dye (ethidium bromide, SYBR safe) is used to qualitatively detect the presence of absence of a specific DNA. However, labelling the PCR primers or nucleotides with fluorescent dyes (SYBR green, EvaGreen) prior to PCR amplification is used to quantitatively measure the amount of PCR products.

The real-time PCR (qPCR) is widely used to perform a semi-quantification of the starting DNA. It relies on the construction of a standard curve of a known DNA concentration. A fluorescent readout is performed to measure the amount of PCR product after each amplification cycle during the exponential phase (**Figure 20C**), when the amplification efficiency is 100%. Therefore, this method implies equivalent amplification efficiencies of the sample and the standards, in order to maximize the quantification accuracy.

The performance of inter-species gene expression assays allows for the identification of shared and conserved mechanisms determining species longevity. However, even when gene sequences are conserved, small differences in DNA sequences can highly affect the capacity of primer binding and the amplification efficiency, thus limiting the use of qPCR on comparative assays. However, these difficulties can be overcome by the use of droplet digital PCR (ddPCR), which allows for an absolute quantification without the construction of standard curves and regardless of assay amplification efficiency.

The ddPCR technology is based in sample partitioning which, in combination with the use of fluorescent dyes, allows for a highly precise and sensitive absolute quantification (**Figure 21**). Prior amplification reaction, target background DNA is randomly distributed within 20.000 water-in-oil droplet partitions. Therefore, empty droplets or containing one or more copies of the target DNA will be generated. The amplification reaction occurs within each droplet, which is classified in a binary scale according to its fluorescence: fluorescent droplets (containing one or more copies of target DNA) are counted as positive whereas non-fluorescent droplets (empty droplets or non-containing target DNA) are counted as negative. Poisson's statistics is applied to statistically correct for the amount of target DNA and accurately obtain an absolute quantification of target sequence.

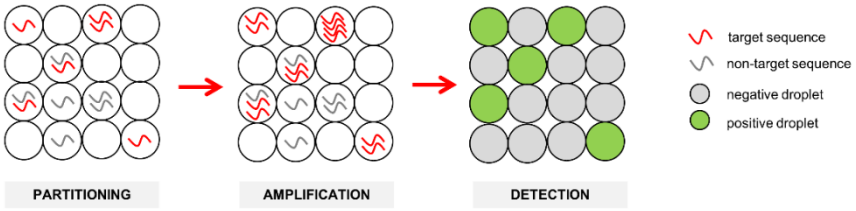

Figure 21. Principles of dddPCR amplification. Sample is partitioned into droplets prior amplification. The fluorescence of positive droplets will be counted and referred to the total number of droplets to accurately obtain the number of DNA units within a sample.

The general workflow for setting up a ddPCR assay includes the RNA extraction and its retrotranscription to a complementary DNA (cDNA), the primer design and the optimization of the parameters through qualitative and qPCR (**Figure 22**). The ddPCR assays allowed to obtain an absolute quantification of cDNA units coding for hydrophilic Cx I subunits (*ndufv2, ndufs3, ndufs4, ndufs5 and ndufa9*) and mTORC1-specific core elements (*mtor, rptor*) and its negative regulators (*fkbp1a* and *akt1s1*) in heart from animal species with different longevities.

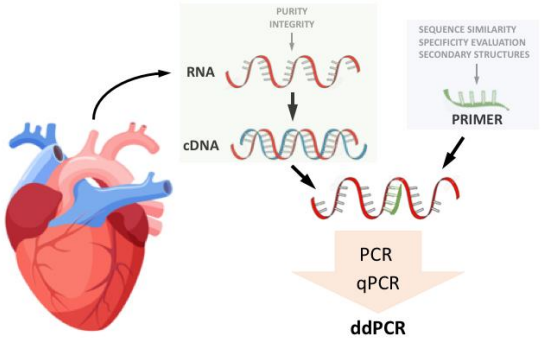

Figure 22. General workflow to set up a ddPCR assay. RNA is extracted from heart and retrotranscribed to cDNA. Afterwards, primer reactivity and specificity are checked by performing conventional PCR assays. Finally, qPCR assay allows for a proper determination of the starting cDNA concentration to perform the ddPCR assay.

3.2.1. Extraction of total RNA

Obtaining pure and high-quality RNA is the first and most critical step when performing many molecular techniques, including PCR. In order to prevent RNA degradation, several handling precautions had been taken, including the cleaning of the workspace and the material with 70% ethanol (v/v) and ribonuclease (RNAse) inhibitor RNAse Zap (Sigma-Aldrich, MO, USA), and the use of RNAse free 1.5-mL tubes, filtered pipette tips and nuclease-free water. After its purification, RNA purity, integrity and concentration were measured.

3.2.1.1. Purification of RNA

RNA purification from heart samples was carried out using RNeasy Fibrous Tissue Mini Kit (Qiagen, Germany) following the protocol provided by the supplier. Basically, RNA purification is based on its affinity to silica membranes.

Briefly, whole tissue (15 mg approximately) was lysed with 300 µL Buffer RLT* and homogenized using an Ultra-Turrax (IKA, Germany). Buffer RLT contains chaotropic agents (guanidine isothiocycanate) to support binding of RNA to the silica membrane, and β-mercaptoethanol to inactivate RNases in the lysate. After homogenization, 590 µL of RNase-free water and 10 µL proteinase K were added to the homogenate, mixed and let incubate at 55°C for 10 minutes. Proteinase allows to remove contractile proteins, connective tissue and collagen. Samples were centrifuged at 10.000 x *g* for 3 minutes and the supernatant, which contains the cellular debris, was transferred to a new 1.5 mL tube where 0.5 volumes of 96% ethanol (v/v) were added. Ethanol is used to enhance the binding of RNA to the silica membrane. Samples were transferred to an RNeasy Mini Column and centrifuged for 15 seconds at ≥ 8000 x *g*. Centrifugation forces RNA to bind to the silica gel membrane that is inside the spin column. Flow-through was discarded and 350 µL of Buffer RW1* was added to the column and centrifuged 15 seconds at ≥ 8000 x *g*. Buffer RW1, which contains guanidine salt and ethanol, is used to remove biomolecules that are non-specifically bound to the silica membrane. Flow-through was discarded and 10 µL DNAse and 70 µL Buffer RDD* were added to the RNeasy membrane and centrifuged 15 seconds at ≥ 8000 x *g*. Buffer RDD provides efficient medium to digest DNA that may co-purify with the RNA. Flow-though was discarded and 350 µL Buffer RW1 were added to the column and centrifuged 15 seconds at ≥ 8000 x *g*. Flow-through was discarded and 500 µL Buffer RPE* were added to the column and centrifuged 15 seconds at ≥ 8000 x *g*. Buffer RPE is used to remove traces of salts. Flow-through was discarded and the column was washed with buffer RPE twice.

After discarding the flow-through, RNeasy column was placed in a new 1.5 mL tube and 50 µL RNase-free water was added and centrifuged 1 minute at ≥ 8000 x *g* to elute RNA. *The exact composition of Buffer RLT, RW1, RDD and RPE is confidential and proprietary of Qiagen.

3.2.1.2. Concentration, purity and integrity of RNA

Sample concentration (ng/µl) and RNA purity were measured at NanoDrop 2000 spectrophotometer (Thermo Scientific, MA, USA).

RNA integrity was assessed by running an aliquot of RNA on a denaturing agarose gel. Briefly, RNA was mixed with loading buffer 6x containing 6 mM of ethylenediaminetetraacetic acid (EDTA), 30% of glycerol (v/v) and 0.25% bromophenol blue (m/v) and loaded into a 1 % agarose gel (m/v) (Condalab, Spain) stained for 10 minutes in fresh prepared 1:10000 SYBR-safe (Invitrogen, CA, USA). After electrophoresis at 100 V for 1 hour, bands were visualized under UV light and images were captured using a Multi-Image Light Cabinet (Alpha Innotech, CA, USA). Intact total eukaryotic RNA was defined by sharp and clear 28S and 18S ribosomal RNA (rRNA) bands. Moreover, the 28S rRNA band should be approximately twice as intense as the 18S rRNA band.

3.2.2. RETROTRANSCRIPTION OF RNA TO CDNA

RNA has to be retrotranscribed into cDNA (synthesised from a single stranded RNA template) to perform PCR analyses. Retrotranscription of RNA to cDNA was carried out with the High-Capacity cDNA Reverse Transcription kit (Applied Biosystems, CA, USA), which is based on the use of random primers that ensured an efficient synthesis of the first strand of each RNA molecule within the sample, including mRNA and RNA. Briefly, reverse transcription mixture contained 1x of MultiScribe™ reverse transcriptase, 2x of reverse transcription buffer, 2x of random primers, 8 nM of dNTP mix and nuclease-free water up to 10 µL for each reaction. Amplification was performed on a Gene Amp PCR system 2700 (Applied Biosystems, CA, USA) starting with a primer annealing step (25°C, 10 minutes), followed by a DNA polymerization step (37°C, 2 h) and a final enzyme deactivation step (85°C, 5 minutes).

3.2.3. PRIMER DESIGN

Gene expression was assessed using primers capable to recognise a specific and conserved gene region shared among the different mammals included in the analyses. Given the complexity of the analyses (10 genes from 8 mammalian species), the use of degenerated primers (mixture of primers with different bases in a specific position) decreased time and cost of the analyses.

3.2.3.1. Gene sequence similarity

The identification of conserved regions in our genes was performed through the performance of multiple sequence alignment (Chowdhury and Garai, 2017). Sequence alignment refers to arranging two or more sequences in such a way that maximum number of identical or similar residues are matched. As the level of similarity is reported as the percentage of the same residues at the same position, it is a measure of conserved sequences and evolutionary distance. Mammalian sequence similarity against mouse or pig was measured using the National Center for Biotechnology Information's (NCBI) Basic Local Alignment Search Tool (BLAST®, https://blast.ncbi.nlm.nih.gov) and is summarized in **Table 1**. cDNA sequences were obtained

from Ensembl database (https://www.ensembl.org). Globally, gene sequences appeared to be highly conserved across animals. However, we've found two clades in *ndufs5*, *ndufa9, rptor* and *akt1s1*, representing rodents and non-rodents, which were taken into account for further primer design.

Table 1. Nucleotide sequence similarity across different species. Values are expressed as percentage of similarity against mouse ([a]) or pig ([b]) gene sequences. Minimum level of signification was set at E-value < 0.05. N.S. = not significant similarity found against mouse or pig. N.D. = Not described gene. E-value = Expected value, represents the number of different alignments with scores equivalents to the obtained that is expected to occur in a database search by chance.

	Mouse	Rat	Guinea pig	Rabbit	Pig	Cow	Horse
Cx I subunits							
ndufv2	100[a]	94[a]	90[a]	91[a]	92[a]	90[a]	92[a]
ndufs3	100[a]	94[a]	83[a]	85[a]	87[a]	87[a]	88[a]
ndufs4	100[a]	94[a]	88[a]	87[a]	91[a]	88[a]	89[a]
ndufs5	100[a]	N.S.	N.S.	85[b]	100[b]	88[b]	93[b]
ndufa9	100[a]	94[a]	80[a]	85[b]	100[b]	87[b]	88[b]
mTORC1							
mtor	100[a]	95[a]	90[a]	90[a]	89[a]	89[a]	90[a]
rptor	100[a]	96[a]	89[a]	87[a]	100[b]	92[b]	91[b]
fkbp1a	100[a]	97[a]	92[a]	92[a]	93[a]	92[a]	91[a]
akt1s1	100[a]	95[a]	85[a]	N.D.	100[b]	93[b]	92[b]

3.2.3.2.Degenerate primers sequence

Initially, cDNA sequences were masked to identify interspersed repeats and low complexity DNA sequences that could interfere on the following PCR analysis. Masking was performed using RepatMasker (www.repeatmasker.org). After that, sequences were aligned using Clustal Omega (https://www.ebi.ac.uk/Tools/msa/clustalo) in order to identify conserved regions among the different animals. Multiple sequence alignment was performed on the bases of sequence clusterization.

After alignment, as several insert-deletion mutations and SNP's across different sequences were identified, we have designed degenerated primer pairs against genes sharing conserved regions across animals using PriFi (Fredslund et al., 2005). For those genes with unique sequences across animals, we have designed non-degenerated primer pairs using Primer3Plus (Untergasser et al., 2012). Parameter settings for primer sequence design were: Primer length, 17-25 nucleotides; primer melting temperature, 50-65°C; primer content, 300 nM; primer GC content, 50-60%, amplicon length, 60-200 nucleotides; MgCl buffer content, 3.8 mM; and dNTPs buffer content, 0.8 mM. Primer sequences are listed in **Table 2**, and melting temperatures were calculated following nearest-neighbour method (Untergasser et al., 2012). Oligonucleotides were purchased from Isogen (Netherlands).

Table 2. Primer sequences. Bold letters represent degenerated nucleotides: R(A/G), Y(C/T), W(A/T), K(G/T), M(A/C), D(A/G/T), H(A/C/T). Length and Product size, measured as base pairs. T_a, annealing temperature, measured following the formula ($[T_{m1} + T_{m2}]$)/2)-5. T_m, melting temperature.

				Forward			Reverse		
Gene	**Reactivity**	**Product**	**T_a**	**Primer sequence (3'-5')**	**Length**	**T_m**	**Primer sequence (3'-5')**	**Length**	**T_m**
ndufv2	All	116	57.8	CCTGACAA**R**CTTTTCACTCTTATAGA**R**GT**D**GAATG	35	62.9	TCTTCAATATC**Y**TT**R**GGTGTCAGATCCTC	29	62.7
ndufs3	All	137	57.8	CC**Y**AAGTATGTCCA**R**CA**M**GTTCAGGTG	27	62.2	GTCA**R**GTCAGCCA**R**GGATTTGAA**Y**TG	26	63.4
ndufs4	All	102	58.3	GTTCCTGCTCG**M**AATAACATGCAG	24	64.6	CCA**R**CCCATCA**R**AGGATTTTCCCATC	26	62
	Mouse	193	57.9	CGGTGCCACGCATTTGAAAA	20	62.8	GTGGAGGGGTGTATTTGCCC	20	63
	Rat	175	57.7	CACATGGGATCGGTGCTACC	20	62.8	TCCTTGCCCAAATGGTGAGG	20	62.6
	Guinea pig	106	58.0	TACCCGGGCACAGAAAGAGT	20	63.2	ATCCCGCTGCTTCTTGATGG	20	62.8
	Rabbit	168	58.0	TCCCTACTCGATGCCATGCT	20	63.1	TGTCCCGCTGCTTCTTGATG	20	62.9
ndufs5	Non-rodents	152	58.9	GGATAGA**R**TGTGCACATGGAATCGG	25	63.4	CCCTTCCTT**K**ATTAGCTT**W**TCCCGC	25	64.3
	Rodents, Rabbit	127	59.1	ACAGG**M**TTCCTGGG**H**CGATA**Y**GTTGT	26	63.6	TAA**K**CTGGCC**Y**AGGTCACCCAT	22	64.6
ndufa9	Non-rodents	104	59.4	CCAGCGCCAGCTTCATC	17	63.9	GGCCCAGGAATCC**Y**GTTGCTC	21	64.9
mtor	All	116	59.8	CTTCATCTTCAAGTCCCTGGGGCTC	25	64.6	GCTGGAACAGAAATTCCCGGATGGC	25	64.9
	Rabbit	191	58.0	CAGCTGCCGACCATCATTGA	20	63	CTTCCCAGCAGATCCAAGGC	20	63
	Rodents	110	59.9	GACCTGTTCACATCCTG**Y**CTCACCACTCC	29	64.8	TTTTCTATCAAATCCAGTGTGACTCCAGGCACC	33	65
rptor	Non-rodents	101	59.5	GGCGTCCCCTCCGTGGTC	18	64.1	AGCTTCTCCCCTTTCTCCCAGTCC	24	64.9
fkbp1a	All	145	59.7	GAGACGGGCGCACCTTCC	18	64.6	CCTC**K**GATCACCTCCTGCTTG	21	64.7
	Mouse	148	57.5	CTGCTCCTAGTCCACCACCT	20	62.9	AGGGTGGCATCCTCATCCAT	20	62.1
	Rat	179	58.6	CAGGACCT**R**CCCCCCTTCTG	20	64.8	CTCTT**Y**TCCTTGAAGGCCCASAC	23	62.3
	Guinea pig	191	58.0	ACCCCGAGAGCACAGATGAT	20	63	AGGCTGTCCGTTCTCCTCAT	20	62.9
	Pig	158	58.0	GAGAGCACAGACGATGGCAG	20	63	CGCGCTTCTGTCCTCTTCTC	20	63
	Cow	118	58.0	TGTGAGTCAGACCCCGAGAG	20	62.9	ACTTGGCGTACTGCTGTGTG	20	63.1
akt1s1	Horse	138	58.9	CAGGACCT**R**CCCCCCTTCTG	20	64.8	GGACTTGGCATACTGCTGGG	20	63

3.2.3.3.Primer specificity and efficiency

Proper primer design is essential to improve primer specificity and efficiency (Dieffenbach et al., 1993). Specificity is defined as the frequency with which a mispriming event occurs, and relies on primer sequence and annealing temperature. Efficiency is defined as how close a primer pair is able to double the number of molecules of the target during each replication cycle.

In silico sequence specificity was checked by running a BLAST® analysis against the animal's whole genome, in order to ensure that each primer pair recognised a unique genome sequence. As efficiency could be decreased by the formation of primer dimer or secondary structures, its formation at the annealing temperature was evaluated *in silico* using OligoEvaluator (http://www.oligoevaluator.com/).

3.2.4. CONVENTIONAL PCR

In silico primer validation allows for a global overview of primer specificity and theoretical annealing temperature, although those features need to be tested *in vivo* by running a conventional PCR.

Briefly, PCR amplification mixture contained 1.25 U of DreamTaq green DNA polymerase, 1x DreamTaq green buffer, 200 nM dNTP mix, 200 nM forward and reverse primer mix, 20 ng of DNA template and nuclease-free water up to 20 µL for each reaction. All reagents were purchased from ThermoFisher (MA, USA). Amplification was performed in a Gene Amp PCR system 2700 (Applied Biosystems, CA, USA) following an initial DNA denaturation (98°C, 5 minutes), and 34 cycles of a DNA denaturation (94°C, 1 minute), annealing (57.5 or 58.8°C, 1 minute), and extension (72°C, 30 seconds). A final DNA extension step was included (72°C, 30 seconds). Annealing temperature was set at 58.5°C for all the assays, but 57.5°C for *rptor* (rabbit) and *akt1s1* (non-rodents). All reactions were prepared in a 96-well plate, including the appropriate negative controls.

Running an aliquot of the PCR products in a no-denaturing gel, as described previously (see 3.2.2. Concentration, purity and integrity of RNA) allowed the visualization of amplified non-specific cDNA product.

3.2.5. REAL-TIME PCR

The adequate concentration of starting cDNA to perform the ddPCR was set by performing a qPCR standard curve assay, as it allows for semi-quantification by obtaining threshold cycle (C_t) values. The C_t is defined as the number of cycles required for the fluorescent signal to be detected above a threshold and is inversely correlated to the initial amount of DNA sample. Adequate cDNA concentration for ddPCR assay corresponds to a $C_t < 25$.

Standard curve from different cDNA concentrations per each assay was constructed, ranging from 70 to 1.4 ng/µL. Amplification of cDNA was carried out with the SYBR Select Master Mix (Applied Biosystems, CA, USA). PCR amplification mixture contained 1x SYBR Select Master Mix, 200 nM of forward and revers primer mix, 70 ng of DNA template and nuclease-free water up to 10 µl for each reaction. All reactions were prepared in a 96-well plate, including the appropriate negative controls. Amplification was performed in in a Gene Amp PCR system 2700 (Applied Biosystems, CA, USA) following an initial UDG (50°C, 2 minutes) and DNA polymerase

activation (95º°, 2 minutes), and 40 cycles of a DNA denaturation (95°C, 15 seconds), annealing (57.5 or 58.8°C, 1 minute) and extension (72°C, 30 seconds). A final DNA extension step was included (72°C, 30 seconds). Results were analysed using Bio-Rad CFX Manager (BioRad, CA, USA).

3.2.6. DROPLET DIGITAL PCR

The amount of absolute cDNA copy numbers for each gene was obtained by performing a ddPCR after following the workflow described in **Figure 23**.

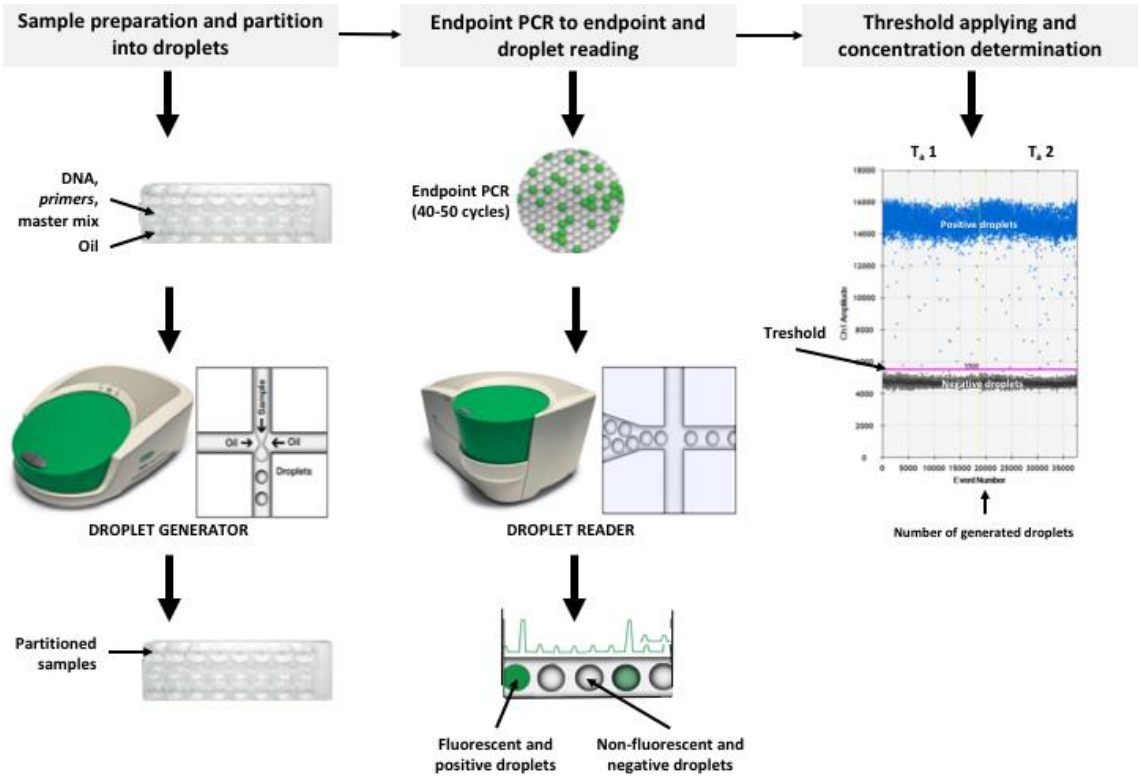

Figure 23. General workflow for ddPCR assays. Adapted from Pinheiro et al., 2012.

For DNA amplification, reaction mixture contained 1x of EvaGreen ddPCR Supermix, 200 nM of primers and 0.01 to 16 ng of template DNA, corresponding to a C_t<25. All materials and reagents were purchased from BioRad (CA, USA). Due to common alterations during droplet generation, duplicates for each assay were prepared.

For droplet generation, 20 µL reaction mixture was loaded into the sample wells of an eight-channel disposable Droplet generation cartridge (DG8 Cartridge), along with 70 µL of Droplet Generation Oil for EvaGreen in the oil wells, containing stabilizing surfactant. Afterwards, the cartridge was placed into the Droplet generation, where vacuum is applied to the outlet wells to simultaneously partition each sample into nanolitre-sized droplets at a rate of 1000 droplets/channel/second (Pinheiro et al., 2012). Consequently, surfactants-stabilized droplets quickly concentrate on the outlet well due to density differences between the oil and aqueous phases (Hindson et al., 2011). After 1.5 min, the cartridge was removed from the generator, and the droplets were transferred to a 96-well plate.

Amplification of cDNA was performed after heat-sealing the plate with foil using a PC1 PCR Plate sealer in a C1000 Touch Thermal Cycler (BioRad, CA, USA). Assay optimization was performed by running across a thermal gradient (55.4, 57.4, 58.8 and 60°C) to determine the annealing

temperature that increases separation between positive and negative droplets while minimizing rain (droplets that fall between the major positive and negative populations). Appropriate annealing temperature was set at 58°C.

After amplification, the 96-well plate was loaded into the QX200 Droplet Reader (BioRad, CA, USA), and appropriate assay information was entered into the analysis software QuantaSoft (BioRad, CA, USA). Droplets were automatically aspirated from each well and aligned to pass a fluorescence detector and cDNA concentrations were calculated on the bases of Poisson statistics (Hindson et al., 2013). Positive and negative droplet populations were defined manually by setting a threshold. Values are reported as absolute cDNA units per µL.

3.3. IMMUNODETECTION BY WESTERN BLOT

The immunodetection by western blot technique was used to compare the protein content of hydrophilic Cx I subunits (NDUFV2, NDUFS3, NDUFS4, NDUFS5, NDUFA9) and the mitochondrial protein VDAC, and the mTORC1-specific core elements (mTOR and RPTOR) and its negative regulators (FKBP12 and PRAS40) in heart from animal species with different longevities.

3.3.1. PROTEIN SEQUENCE SIMILARITY

The main struggle when measuring protein content across different animals is that not all the antibodies are known to react against all the species. Structural biology is strongly connected with protein sequence similarity (Morgenstern et al., 2006), therefore for highly similar sequences we can infer similar function, and hence similar protein structure.

Multiple protein sequence alignment was performed as described previously and summarized in **Table 3**. In contrast to genes, protein similarity score accounted for amino acids having similar physicochemical properties (Chowdhury and Garai, 2017). Amino acid sequences were obtained from NCBI protein database.

Globally, the protein sequences appeared to be highly conserved across mammalian. However, we've found the lower conservation for NDUFS5 (except for mouse and rat) and NDUFA9 (non-rodents), which should be taken into account when performing the western blot analyses.

Table 3. Amino acid sequence similarity across different mammals. Values are expressed as % similarity against mouse (a) amino acid sequences. Minimum level of signification was set at E-value < 0.05. ns = not significant similarity found against mouse or pig. n.d = Not described gene. E-value = Expected value, represents the number of different alignments with scores equivalents to the obtained that is expected to occur in a database search by chance.

	Mouse	Rat	Guinea pig	Rabbit	Pig	Cow	Horse
Cx I subunits							
NDUFV2	100[a]	97[a]	94[a]	94[a]	94[a]	94[a]	93[a]
NDUFS3	100[a]	95[a]	85[a]	88[a]	88[a]	88[a]	89[a]
NDUFS4	100[a]	93[a]	90[a]	90[a]	88[a]	88[a]	91[a]
NDUFS5	100[a]	89[a]	74[a]	72[a]	74[a]	74[a]	72[a]
NDUFA9	100[a]	96[a]	79[a]	80[a]	76[a]	76[a]	76[a]
mTORC1							
mTOR	100[a]	99[a]	99[a]	98[a]	99[a]	99[a]	99[a]
RPTOR	100[a]	98[a]	97[a]	95[a]	94[a]	96[a]	96[a]
FKBP12	100[a]	98[a]	96[a]	97[a]	96[a]	95[a]	81[a]
PRAS40	100[a]	95[a]	89[a]	n.d	92[a]	90[a]	89[a]
VDAC	100[a]	100[a]	100[a]	99a	100[a]	100[a]	100[a]

3.3.2. SAMPLE HOMOGENIZATION

The homogenization solution used contained 180 mM of potassium chloride (KCl), 5 mM of 3-(*N*-morpholino)propaensulfonic acid (MOPS), 2 mM of ethylendiamine-tetraacetic acid (EDTA), 1 mM diethylenetriamine-penta acetic acid (DTPAC), 1 µM of butylhydroxytoluene (BHT) adjusted to pH 7.4. This solution prevented the effect of metal chelators and lipid oxidation due to sample processing. A commercial mix of proteases inhibitors (Amersham Bioscience, Spain) and phosphatase inhibitors (1 mM of sodium orthovanodate (Na_3VO_4) and 1 M of sodium fluoride (NaF)) were added. For homogenization, 50 mg of whole heart were weighted and homogenized with an Ultra-Turrax (IKA, Germany), followed by a brief centrifugation (120 x *g* for 3 minutes at 4°C) to pellet and remove cellular debris. The supernatants obtained were quantified.

3.3.3. PROTEIN QUANTIFICATION

In order to determine the protein amount of the supernatant, the Bradford's method was used (Bradford, 1976). Protein concentration of each sample has been analysed by the interpolation of the data obtained from the corresponding concentrations in the standard curve performed with known concentrations (rang 0-250 µg/µL) of bovine serum albumin (BSA). The Bradford reagent (Bio-Rad, CA, USA) was added to every sample and BSA standards and then mixed. After 10 minutes of incubation at room temperature, the absorbance was determined by spectrophotometry with a microplate reader (Thermo Labsystem, CA, USA) at a wavelength of 595 nm in a 96 well plate.

3.3.4. SAMPLE PROCESSING

Protein concentrations of each sample have been equalized and normalized with the solution containing 62.5 mM of tris(hydroxymehtyl) aminomethane hydrochloridre (Tris-HCl) at pH=6.8, 2 % of sodium dodecyl sulfate (SDS) (m/v), 10 % of glycerol (v/v), 20% of β-mercaptoethanol (v/v) and 0.02% of bromophenol blue (m/v). For the protein denaturalization samples were heated at 95°C for 3 minutes in a dry bath (Termobloc Selecta, Spain).

3.3.5. ELECTROPHORESIS

Protein separation of the samples according to their molecular weight was performed using acrylamide gels with SDS detergent. The anionic detergent SDS solubilizes and denaturalizes the proteins in the sample. Over and above, SDS allows the proteins to separate according to their molecular weight once the gel with the samples are subjected to an electric field. Proteins will migrate from the anode to the cathode more or less fast depending on their size.

The acrylamide gels used for the separation were of different percentage of acrylamide/bisacrylamide depending on the molecular weight of the proteins to be separated, this percentage varied from 7.5% (only for the high molecular weight proteins mTOR and Raptor) to 10% (v/v) with a thickness of 1.5 mm. Stacking gels to deposit the samples were 5% of acrylamide/bisacrylamide (v/v). Both, separating and stacking gels, polymerize after the addition of the catalysers ammonium persulfate at 10% (v/v) and N,N,N',N'-tetramethylethylenediamine (TEMED) at 0.03% (v/v). As a control and identification measure, 2.5 µL of a molecular weight marker was used (Precision Plus Protein™ Dual Color Standards, BioRad, CA, USA). The

electrophoretic separation was performed in electrophoresis Mini-PROTEAN II cells (BioRad, CA, USA) filled with a buffer solution made of 25 mM of Tris, 192 mM of glycerol and of 0.1% of SDS (m/v) and applying a constant amperage of 15 mA/gel.

3.3.6. ELECTROBLOTTING

After electrophoretic protein separation, proteins are transferred to a polyvinylidene difluoride (PVDF) membrane (Millipore, MA, USA) previously activated by incubation with 99.9% methanol (v/v) for 5 minutes and equilibrated with transfer buffer made of 25 mM of Tris, 192 of mM glycerol and methanol. The percentage of methanol varied between 10% (only for the high molecular weight proteins mTOR and Raptor) to 20% (v/v). The separating gel is in touch with the PVDF membrane inside a sandwich system (from the anode to the cathode) for a wet transfer in a Mini Trans-Blot Transfer Cell (BioRad, CA, USA). The voltage applied was constant at 100 V for 90 minutes.

3.3.7. MEMBRANE BLOCKING

Once the proteins have been transferred to the PVDF membrane, next step is blocking the membrane. This step serves to avoid false positives in those places of the membrane where there is not protein coupled. The blocking solution contained 5% of BSA (m/v) in TBS-T 0.1% buffer, containing 2 M of Tris, 2.5 M of sodium chloride (NaCl) 0.01% of Tween (v/v). After the blocking step, membranes were washed for 5 minutes with TBS-T 0.05% solution, containing 2M of Tris, 2.5 M of NaCl and 0.05 of Tween (v/v) in order to remove the excess of blocking solution.

3.3.8. IMMUNODETECTION

For the immunodetection the PVDF membranes were incubated with the primary antibody at a final concentration of 1:1000 in a BSA 5% (m/v) in TBS-T 0.01% solution overnight at 4^{o}C and with mild shaking. All the primary antibodies used in this work are summarized in **Table 4.** After the incubation with the primary antibody, three washes of 5 minutes were performed with TBS-T 0.05% solution. Then, the PVDF membranes were incubated with the appropriate secondary antibody linked to peroxidase. In this work two different types of secondary antibodies were used, anti-mouse and anti-rabbit (**Table 5**). In every immunodetection the secondary antibody is been dissolved in the same solution of incubation which lasts one hour and it was performed in mild shaking. After this incubation, the membranes were washed three times for 5 minutes each wash with TBS-T 0.05% solution and two more washes with TBS and strong shaking for 5 minutes each wash.

3.3.9. CHEMILUMINESCENT DETECTION AND DATA ANALYSIS

For the exposure, PVDF membranes were incubated at room temperature for 5 minutes with the chemiluminescent (Luminol™ Western Chemiluminiscent HRP substrate (Millipore, MA, USA). The luminescence emission was detected with a ChemiDoc™ MP imaging System (BioRad, CA, USA) and analysed with the software Image Lab v4.0 (BioRad, CA, USA). The amount of luminescence is directly proportional to the amount of protein in the membrane. In every immunodetection by western blot the signal obtained was relativized with a loading control applied to the same membrane after washing. Those loading controls were VDAC and actin,

depending on the molecular weight of the detected protein. Finally, the PVDF was stained with Coomassie Blue in order to obtain a more accurate loading control.

Table 4. Experimental conditions of the primary antibodies used for the immunodetection. Reactivity is not ensured when *(animal)*.

Antibodies	Reactivity	MW	µg
NDUFV2 (SAB2107279, Sigma)	Mouse, guinea pig, rabbit, horse	27	17
NDUFS3 (459130, Invitrogen)	Mouse, rat	29	17
NDUFS4 (ab96549, Abcam)	(Mouse), (rat), (cow)	20	17
NDUFS5 (ab188510, Abcam)	Mouse, rat	13	17
NDUFA9 (459100, Life technologies)	Mouse, rat	39	17
mTOR (2972, Cell signalling)	Mouse, rat, (pig), (horse)	289	80
$mTOR^{Ser2448}$ (2917, Cell signalling)	Mouse, rat, (horse)	289	80
Raptor (ab189158, Abcam)	Mouse, rat	149	80
FKBP12 (ab2981, Abcam)	Mouse, rat, pig	12	80
PRAS40 (ab134087, Abcam)	Mouse	40	80
$PRAS40^{Thr246}$ (ab151719, Abcam)	Mouse	40	80
VDAC (ab15898, Abcam)	Mouse, rat, (rabbit), (pig), (cow)	31	17

Table 5. Experimental conditions of the secondary antibodies used for the immunodetection.

Antibodies	Description
Anti-mouse (NA934, GE healthcare)	ECL Anti Mouse IgG, Horseradish Peroxidase-linked Species-Specific Whole Antibody (from sheep), 1:30.000
Anti-rabbit (31460, Pierce)	Anti-rabbit IgG, H&L, Horseradish Peroxidase-linked species (from goat), 1:50.000

3.4. TARGETED METABOLOMIC ANALYSIS

A targeted metabolomic approach using a LC -MS platform was used to unambiguously detect and quantify the content of: a) Met and its related metabolites, including the intermediates of the transmethylation pathway (SAM, SAH and homocysteine); betaine and spermidine as metabolites involved in the regeneration of methionine; the intermediates of the transsulfuration pathway Cys and cystathionine; taurine and GSH as downstream metabolites of the transsulfuration pathway; and vitamin B6 metabolites pyridoxal, pyridoxamine and PLP, as cofactors of the transsulfuration enzymes; b) additional amino acids including 8 non-polar amino acids (Ala, Gly, Leu, Ile, Phe, Pro, Try and Val), 4 polar uncharged amino acids (Asn, Ser, Thr and Tyr), 2 polar negatively charged amino acids (Asp and Glu), and 2 polar positively charged amino acids (Arg and His); c) TCA cycle metabolites, including pyruvate, citrate, isocitrate, α-ketoglutarate, succinate, fumarate and malate; and d) methionine-derived lipid intermediates such as choline and carnitine. The targeted analysis was performed in heart and plasma from mammals with different longevities, and plasma from humans with extreme longevities.

3.4.1. SETTING UP A NEW METABOLOMICS METHOD

Standard solutions of all metabolites were prepared by weighing and dissolving the compounds in the proper solvent. All reagents were purchased from Sigma Aldrich (MI, USA).

To detect the individual metabolites, multiple reaction monitoring (MRM) in negative and in positive ion mode was performed with individually optimize fragmentation voltage and collision energies. Most of the MRM parameters were achieved by flow injection of pure standards and the MassHunter Optimizer software (Agilent Technologies, CA, USA). However, some of metabolites required manual optimization using MassHunter Qualitative Analyses (Agilent Technologies, CA, USA). All the MRM parameters obtained from optimization were compared to the literature when available for certain compounds. Finally, a chromatographic system was applied to determine retention time of each standard. Peak determination and peak area integration were carried out with MassHunter Quantitative Analyses (Agilent Technologies, CA, USA).

3.4.2. SAMPLE PROCESSING

Samples were randomized and decoded prior extraction. Plasma metabolites extraction was performed based on the methodology previously described (Cabré et al., 2016). Briefly, 10 µL of plasma or tissue homogenate were added to 30 µL of cold methanol containing 1 µg/mL of Phe-^{13}C as internal standard and 1 µM BHT as antioxidant. Then, samples were incubated at -20°C for 1 hour and centrifuged at 12000 *g* for 3 minutes at 4°C. Finally, the supernatant was filtrated through a 0.22-µm organic diameter filter (Agilent Technologies, CA, USA) and transferred to Agilent vials with glass inserts for further analysis.

Sulphur-containing metabolites were extracted on the bases of the methodology previously described (Liu et al., 2017). Briefly, 2 µL of 5% DTT diluted in methanol (m/v) were added to 10 µL of plasma or tissue homogenates. The resulting solution was vortexed for 1 minute and allowed to stand at room temperature for 10 minutes. For protein precipitation, 40 µL of 0.1% formic acid (v/v) plus 0.05% trifluoroacetic acid (v/v) in acetonitrile containing 1 µg/mL of Phe-^{13}C as internal standard was added to the sample, and the solution was vortexed for 2 min. Then, samples were incubated at room temperature for 15 minutes and centrifuged at 12000 *g* for 3 min. Finally, the supernatant was filtrated through a 0.22-µm organic diameter filter (Agilent Technologies, CA, USA) and transferred to vials with glass inserts for further analysis.

3.4.3. EQUIPMENT

The analysis was performed through a liquid chromatography coupled to a hybrid mass spectrometer with electrospray ionization and a triple quadrupole mass spectrometer (LC-ESI-QqQ-MS). The liquid chromatography system was an ultra-performance LS model 1290 coupled to an ESI-QqQ-MS model 6420 both from Agilent Technologies (Spain).

3.4.4. ANALYSIS CONDITIONS

The detection and quantification of a metabolomic panel including 39 metabolites (**Table 6**) was developed on the bases of previous described targeted approaches (Cabré et al., 2016; Liu et al., 2017). Samples were decoded and randomized before injection. Every 5 samples, internal and external standards were injected as a quality control.

For sulphur-containing metabolites, 10 µL of extracted sample was injected based on the method described (Liu et al., 2017). Chromatographic separation was achieved on a reversed-phase Supelcosil LC-CN column (Supelco of 4.6 x 250 mm and 5 µL particle size, Sigma, MI, USA) with a column temperature of 30°C. The flow rate was 0.5mL/min during a 10 minutes at 10 %

B (v/v). Solvent A was composed of water containing 0.1% formic acid (v/v) and solvent B was composed of acetonitrile containing 0.1% formic acid (v/v). Electrospray ionization was performed in both positive and negative ion mode (depending on the target metabolite) using N_2 at a pressure of 50 psi for the nebulizer with a flow of 12 L/min and a temperature of 325°C, respectively.

For non-sulphur-containing metabolites, 2 µL of extracted sample was injected based on the method described (Cabré et al., 2016). Chromatographic separation was achieved on a reversed-phase column (Zorbax SB-Aq 1.8 µm 2.1×50mm, Agilent Technologies, CA, USA) equipped with a precolumn (Zorba-SB-C8 Rapid Resolution Cartridge 2.1×30mm 3.5 µm; Agilent Technologies, CA, USA) with a column temperature of 60°C. The flow rate was 0.6mL/min during 19 minutes. Solvent A was composed of water containing 0.2% acetic acid (v/v) and solvent B was composed of methanol containing 0.2% acetic acid (v/v). The gradient started at 2 % B (v/v) and increased to 98 % B (v/v) in 13 minutes and held at 98 % B (v/v) for 6 minutes. Post-time was established in 5 minutes. Electrospray ionization was performed in both positive and negative ion mode (depending on the target metabolite) using N_2 at a pressure of 50 psi for the nebulizer with a flow of 12 L/min and a temperature of 325°C, respectively.

Data was collected using the MassHunter Data Analysis Software (Agilent Technologies, CA, USA). Peak determination and peak area integration were carried out with MassHunter Quantitative Analyses (Agilent Technologies, CA, USA).

3.4.5. METABOLITE QUANTIFICATION

Metabolite quantification was performed by constructing standard curves for each metabolite. Expected plasma concentration for each metabolite was based on the Human Metabolome Database (HMDB, http://www.hmdb.ca). Solutions were produced by spiking 10 µL of 10x standard solutions of each metabolite into 9 µL of water. Metabolites were extracted and subjected to mass spectrometry analyses as described before. Standard curves were constructed by plotting the peak area ratio against the final metabolite concentration.

Table 6. Analytical traits of the metabolites measured following a targeted metabolomics approach. Precursor (Prec ion) and product (Prod ion) are given as m/z**.** Fragmentor, collision energy (CE) and cell acceleration voltage (CAV) are given as voltage; retention time (RT) in minutes. Method 1 (see material and methods, Cabré et al. 2016); Method 2 (see material and methods, Liu et al. 2017). ND=Not detected metabolite.

Compound	Prec Ion	Prod Ion	Frag (V)	CE (V)	Cell Acc (V)	RT (min)	RT Window	Polarity	Extraction	Method
Methionine metabolism										
Betaine	118.09	59.2	136	16	7	0.425	2	Positive	Methanol	1
Betaine	118.09	58.2	136	32	7	0.425	2	Positive	Methanol	1
Cysteine	122.02	76	64	12	7	6.312	4	Positive	ACN-DTT	2
Cysteine	122.02	59	64	24	7	6.312	4	Positive	ACN-DTT	2
Cystathionine	223.07	134	88	8	7	6.818	4	Positive	ACN-DTT	2
Cystathionine	223.07	88	88	28	7	6.818	4	Positive	ACN-DTT	2
Glutathione	308.09	179	88	8	7	0.5	2	Positive	ACN-DTT	1
Glutathione	308.09	76	88	24	7	0.5	2	Positive	ACN-DTT	1
Homocysteine	136.18	90.1	135	15	7	7.225	4	Positive	ACN-DTT	2
Homocysteine	136.18	56.2	135	15	7	7.225	4	Positive	ACN-DTT	2
Methionine	150.05	104	64	4	7	0.48	2	Positive	ACN-DTT	1
Pyridoxal	168.05	150	64	8	7	0.522	2	Positive	Methanol	1
Pyridoxal	168.05	94	64	24	7	0.522	2	Positive	Methanol	1
PLP	248.03	150	112	12	7	0.7	2	Positive	Methanol	1
PLP	248.03	67	112	32	7	0.7	2	Positive	Methanol	1
Pyridoxamine	169.09	152	64	8	7	0.366	2	Positive	Methanol	1
Pyridoxamine	169.09	134	64	20	7	0.366	2	Positive	Methanol	1
SAH	385.1	136	112	20	7	1.13	2	Positive	Methanol	1
SAH	385.1	88	112	48	7	1.13	2	Positive	Methanol	1
SAM	399.1	250	112	12	7	0.396	2	Positive	ACN-DTT	1
SAM	399.1	136	112	28	7	0.396	2	Positive	ACN-DTT	1
Spermidine	146.1	84	88	24	7	0.3	2	Positive	Methanol	1
Spermidine	146.1	72	88	12	7	0.3	2	Positive	Methanol	1
Taurine	126.02	108	88	8	7	0.38	2	Positive	ACN-DTT	1
Taurine	124	80	112	20	7	0.38	2	Negative	ACN-DTT	1
Amino acids										
Alanine	90.06	44.2	40	8	7	0.376	2	Positive	Methanol	1
Arginine	175.1	70.2	60	20	7	0.32	2	Positive	Methanol	1
Arginine	175.1	60.2	60	15	7	0.32	2	Positive	Methanol	1

Asparagine	133	74.1	60	15	7	0.376	2	Positive	Methanol	1
Aspartate	134	43.2	60	15	7	0.362	2	Positive	Methanol	1
Aspartate	132	88.1	60	15	7	0.362	2	Negative	Methanol	1
Glutamate	146	102.1	60	15	7	0.363	2	Negative	Methanol	1
Glutamate	146	41	60	15	7	0.363	2	Negative	Methanol	1
Glycine	76.04	48	40	0	7	0.34	2	Positive	Methanol	1
Glycine	76.04	30	40	4	7	0.34	2	Positive	Methanol	1
Histidine	156	110.1	60	15	7	0.32	2	Positive	Methanol	1
Histidine	156	56.2	60	25	7	0.32	2	Positive	Methanol	1
Isoleucine	132.1	86	64	8	7	0.591	2	Positive	Methanol	1
Isoleucine	132.1	69	64	16	7	0.591	2	Positive	Methanol	1
Leucine	132.1	86	64	8	7	0.591	2	Positive	Methanol	1
Leucine	132.1	69	64	16	7	0.591	2	Positive	Methanol	1
Phenylalanine	164	147	100	15	7	0.841	2	Negative	Methanol	1
Phenylalanine	164	103.1	100	15	7	0.841	2	Negative	Methanol	1
Proline	116	70.2	60	15	7	0.392	2	Positive	Methanol	1
Serine	106.05	60	64	8	7	0.35	2	Positive	Methanol	1
Serine	106.05	42	64	24	7	0.35	2	Positive	Methanol	1
Serine	104.03	74	64	8	7	0.35	2	Negative	Methanol	1
Threonine	120	74.2	60	15	7	0.358	2	Positive	Methanol	1
Threonine	120	56.2	60	15	7	0.358	2	Positive	Methanol	1
Tryptophan	205	188.1	60	15	7	1.23	2	Positive	Methanol	1
Tryptophan	205	146.1	60	15	7	1.23	2	Positive	Methanol	1
Tyrosine	180.1	163.1	100	15	7	0.548	2	Negative	Methanol	1
Tyrosine	180.1	119.1	100	15	7	0.548	2	Negative	Methanol	1
Valine	118.08	72	64	8	7	0.43	2	Positive	Methanol	1
Valine	118.08	55	64	20	7	0.43	2	Positive	Methanol	1
TCA cycle intermediates										
α-Ketoglutarate	145.01	101	64	4	7	0.435	2	Negative	Methanol	1
α-Ketoglutarate	145.01	57	64	20	7	0.435	2	Negative	Methanol	1
(Iso)Citrate	191.01	111	88	8	7	0.637	2	Negative	Methanol	1
(Iso)Citrate	191.01	87	88	16	7	0.637	2	Negative	Methanol	1
Fumarate	115.01	71	64	4	7	0.55	2	Negative	Methanol	1
Fumarate	115.01	27	64	4	7	0.55	2	Negative	Methanol	1

Malate	133.02	115	64	8	7	0.4	2	Negative	Methanol	1
Malate	133.02	71	64	12	7	0.4	2	Negative	Methanol	1
Pyruvate	87.01	43	64	4	7	0.413	2	Negative	Methanol	1
Succinate	117.02	73	64	8	7	0.57	2	Negative	Methanol	1
Succinate	117.02	55	64	20	7	0.57	2	Negative	Methanol	1
Lipid and protein intermediates										
Carnitine	162.12	103.1	88	16	7	0.393	2	Positive	Methanol	1
Choline	104.11	60.2	112	16	7	0.39	2	Positive	Methanol	1
TMAO	76.08	59.2	64	8	7	0.4	2	Positive	Methanol	1
TMAO	76.08	58.2	64	20	7	0.4	2	Positive	Methanol	1
ISTD										
PheC13	167.09	120.1	70	8	7	0.87	2	Positive	Methanol/ACN-DTT	1/2
PheC13	167.09	77	70	44	7	0.87	2	Positive	Methanol/ACN-DTT	1/2
PheC13	167.09	103	70	28	7	0.87	2	Positive	Methanol/ACN-DTT	1/2
PheC13	167.09	51.1	70	60	7	0.87	2	Positive	Methanol/ACN-DTT	1/2

3.5. STATISTICAL ANALYSIS

Prior to statistical analyses, data was pre-treated (auto-scaled and log-transformed). Multivariate statistics was performed using Metaboanalyst software (Chong et al., 2019). Principal component analysis (PCA), partial least squares-discriminant analyses (PLS-DA), hierarchical clustering analysis represented by a heat map, and Random Forest used as a classification algorithm were performed using Metaboanalyst. Inter-group differences were tested using ANOVA followed by a post-hoc Tukey multiple test in GraphPad prism (v8.0.1). Correlation analyses and linear models such as Pearson correlation, Pearson correlation matrix, linear models and phylogenetic generalised least squares (PGLS) regression) were performed using RStudio (v1.1.453). Correlation functions were included in the packages *Hmisc* (Harrel Jr and Dupont, 2020) and *corrplot* (Wei and Simko, 2017), and plotted with *ggplot2* (Wickham, 2016). Network plot were constructed and plotted using the functions included in the package *igraph* (Csardi and Nepusz, 2006). Linear regression was plotted using GrapPhad Prism (v8.0.1). PGLS regression functions were included in the package *caper* (Orme et al., 2018), and used to analyse the correlation of individual metabolites with animal longevity after controlling for phylogenetic relationships, defined by a phylogeny. The phylogenetic tree was constructed using taxa names as described previously (Kumar et al., 2017).

RESULTS

The results obtained in this thesis will be presented as published or pre-printed articles, each of one aiming to respond the previously described individual objectives. References section from manuscripts are removed and included in the reference section of this thesis.

MAIN OBJECTIVE 1. TO DESCRIBE A METABOLIC PROFILE AND ITS MODULATION ASSOCIATED WITH SPECIES LONGEVITY

Objective 1.1. To analyse the role of gene and protein steady state levels of Cx I hydrophilic subunits in determining species longevity

Results have been already published in the following manuscript:

Mota-Martorell N, Jove M, Pradas I, Sanchez I, Gómez J, Naudi A, Barja G, Pamplona R. **Low abundance of NDUFV2 and NDUFS4 subunits of the hydrophilic complex I domain and VDAC1 predicts mammalian longevity**. Redox Biol. 2020; 34:101539. doi: 10.1016/j.redox.2020.101539.

Objective 1.2. To define a metabolic profile associated with species longevity in a post-mitotic tissue

Results are under editorial review in the following manuscript:

Mota-Martorell N, Jove M, Berdún R, Pamplona R. **Heart methionine metabolic profile is associated with longevity in mammals**. FASEB Journal.

Objective 1.3. To define a metabolic profile associated with species longevity in plasma

Results are under editorial review in the following manuscript:

Mota-Martorell N, Jove M, Berdún R, Pamplona R. **Reduced content of sulphur-containing metabolites and increased succinate is associated with species longevity**. Communications Biology.

Objective 1.4. To analyse the role of gene and protein steady state levels of mTORC1 subunits and its regulators in determining species longevity

Results have been already published in the following manuscript:

Mota-Martorell N, Jove M, Pradas I, et al. **Gene expression and regulatory factors of the mechanistic target of rapamycin (mTOR) complex 1 predict mammalian longevity.** Geroscience. 2020;42(4):1157-1173. doi: 10.1007/s11357-020-00210-3.

MAIN OBJECTIVE 2. TO DESCRIBE A METABOLIC PROFILE AND ITS MODULATION ASSOCIATED WITH HUMAN EXTREME LONGEVITY

Results have been already published in the following manuscript:

Mota-Martorell N, Jove M, Borrás C, Berdún R, Sol J, Cabré R, Pradas I, Galo-Licona JD, Puig J, Viña J, Pamplona R. **Methionine transsulfuration pathway is upregulated in long-lived humans**. Free Radical Biology and Medicine. 2020; 162:38-52. doi: 10.1016/j.freeradbiomed.2020.11.026.

Low abundance of NDUFV2 and NDUFS4 subunits of the hydrophilic complex I domain and VDAC1 predicts mammalian longevity

Natalia Mota-Martorell[1], Mariona Jove[1], Irene Pradas[1], Isabel Sanchez[2], José Gómez[4], Alba Naudi[1], Gustavo Barja[3], Reinald Pamplona[1,*]

[1] Department of Experimental Medicine, University of Lleida-Lleida Biomedical Research Institute (UdL-IRBLleida), Lleida, Catalonia, Spain

[2] Proteomics and Genomics Unit, University of Lleida, Lleida, Catalonia, Spain

[3] Department of Genetics, Physiology and Microbiology, Complutense University of Madrid, Madrid, Spain

[4] Department of Biology and Geology, Physics and Inorganic Chemistry, University Rey Juan Carlos I, ESCET-Campus de Móstoles, Móstoles (Madrid), Spain

*** Corresponding author:**

Prof. Dr. Reinald Pamplona. Department of Experimental Medicine, University of Lleida-Lleida Biomedical Research Institute (UdL-IRBLleida), Biomedicine 1 building, Av. Rovira Roure 80, Lleida 25198, Spain. E-mail: reinald.pamplona@mex.udl.cat

E-mail addresses of the rest of the authors:

NMM: Natalia.mota@mex.udl.cat

MJ: mariona.jove@udl.cat

IP: ipradas@mex.udl.cat

IS: Isabel.sanchez@udl.cat

JG: jose.gomezs@urjc.es

AN: alba.naudi@mex.udl.cat

GB: gbarja@bio.ucm.es

Abstract

Mitochondrial reactive oxygen species (ROS) production, specifically at complex I (Cx I), has been widely suggested to be one of the determinants of species longevity. The present study follows a comparative approach to analyse complex I in heart tissue from 8 mammalian species with a longevity ranging from 3.5 to 46 years. Gene expression and protein content of selected Cx I subunits were analysed using droplet digital PCR (ddPCR) and western blot, respectively. Our results demonstrate: 1) the existence of species-specific differences in gene expression and protein content of Cx I in relation to longevity; 2) the achievement of a longevity phenotype is associated with low protein abundance of subunits NDUFV2 and NDUFS4 from the matrix hydrophilic domain of Cx I; and 3) long-lived mammals show also lower levels of VDAC (voltage-dependent anion channel) amount. These differences could be associated with the lower mitochondrial ROS production and slower aging rate of long-lived animals and, unexpectedly, with a low content of the mitochondrial permeability transition pore in these species.

Keywords: Complex I, droplet digital PCR, longevity, mammals, mitochondria, NDUFV2 subunit, NDUFS4 subunit, VDAC, western blot

Introduction

Complex I (Cx I) (NADH-ubiquinone oxidoreductase; EC 1.6.5.3) is an electron entry point in the mitochondrial respiratory electron transport chain (ETC). Cx I catalyzes NADH oxidation reducing ubiquinone to ubiquinol, importantly contributing to the proton motive force used to synthesize ATP by the oxidative phosphorylation (Koopman et al., 2010). Cx I also produce reactive oxygen species (ROS), initially superoxide radicals, which can damage all cellular components. Although at least 11 sites producing ROS have been identified, Cx I and complex III (Cx III) are conventionally recognized as the major sources of ROS at the ETC (Wong et al., 2017). Mitochondrial ROS production (mitROSp) has been considered one of the main effectors responsible for aging and longevity (Barja, 2013; Pamplona and Barja, 2007).

Low rates of mitROSp have been described in many long-lived mammalian and bird species (Barja, 2013; Ku et al., 1993; Pamplona and Barja, 2007). These studies generally demonstrated the existence of a negative correlation between mitROSp and longevity. Among the two main ROS generating ETC complexes, the low ROS production of various long-lived species has been localized at Cx I (Barja and Herrero, 1998; Herrero and Barja, 1997, 1998). Interestingly, different pro-longevity nutritional and pharmacological interventions like dietary (DR) and methionine restriction, and rapamycin treatment have been also associated with decreased mitROSp at Cx I (Pamplona and Barja, 2006, 2007). Although is a matter of controversy, within complex I longevity-related ROS production has been observed in the hydrophilic domain (Miwa et al., 2014), which could be due either to the flavin semiquinone, to some of the eight different FeS clusters of this domain (Genova et al., 2001; Herrero and Barja, 2000; Kushnareva et al., 2002) or both to flavin and FeS centers.

The underlying mechanism responsible, at least in part, for the low mitROSp of some long-lived species has been attributed to a smaller degree of electronic reduction of Cx I under basal conditions (Barja, 2013; Barja and Herrero, 1998). Additional studies demonstrated that a lower Cx I content could also explain the low ROS production of those long-lived species (Lambert et al., 2010; Pamplona et al., 2005). Pro-longevity nutritional interventions also induced decreased Cx I content concomitantly with a lower mitROSp (Ayala et al., 2007; Gómez et al., 2007; Miwa et al., 2014; Sanchez-Roman et al., 2011; Sanz et al., 2006b).

Mammalian Cx I is the largest component of the ETC built of 45 different subunits in mammals (Koopman et al., 2010). The conserved L-shaped core, formed by 14 subunits sufficient for catalysis, is surrounded by 31 accessory subunits forming an interlinked shell with unclear function (Fiedorczuk et al., 2016; Zhu et al., 2016). Among the 14 core subunits, the 7 mitochondrial-encoded ND subunits are present in the hydrophobic membrane domain, and the other 7 nuclear-encoded (NDUF) subunits are present in the hydrophilic matrix domain (Fiedorczuk and Sazanov, 2018). The 31 supernumerary NDUF accessory subunits are also nuclear coded (Fiedorczuk et al., 2016). However, it is totally unknown if some particular Cx I subunits, especially some NDUF subunits of the Cx I hydrophilic domain, could be involved in the determination of the longevity-related low complex I ROS production of long-lived animal species.

On the other hand, the mitochondrial permeability transition pore (mPTP) is a protein complex that permits diffusion of molecules of molecular mass up to 1500 Da across the mitochondrial

inner membrane (Hunter and Haworth, 1979; Panel et al., 2018). Many substrates can pass from mitochondrial matrix to cytosol through this pore. The mPTP opening is promoted through oxidation of lipids and proteins of mitochondrial membrane by ROS (Panel et al., 2018) and is related to pathological stages. However, some studies suggest that mPTP opening by mitROS can also drive the progression of aging (Panel et al., 2018; Rottenberg and Hoek, 2017). It has been hypothesized that mPTP comprises inner and outer mitochondrial membrane proteins such as the ATP synthase, key in the channel formation, and a diversity of regulatory components including the voltage-dependent anion channel (VDAC), the pro-death Bcl-2 family member proteins Bax and Bak, the translocator protein (TSPO), the hexokinase (HK), the adenine nucleotide translocase (ANT), the phosphate carrier (PiC), and the cyclophilin-D (Halestrap, 2009; Mnatsakanyan et al., 2017, 2019), all of which have been studied as candidates for exact molecular mPTP identity which remains uncertain. Recent studies have shown that decreased VDAC promotes longevity by decreasing mitochondrial permeability in *C. elegans* (Zhou et al., 2019).

The purpose of this study was to investigate the abundance of Cx I hydrophilic domain selected subunits and VDAC as possibly related to the low mitROSp of long-lived mammalian species. We used droplet digital PCR (ddPCR) and western blot methods to define the steady-state levels of gene expression and protein content of mitochondrial electron transport chain Cx I subunits and VDAC in heart tissue of eight mammalian species showing more than one order of magnitude of difference in longevity, from 3.5 years in mice to 46 years in horses. Cx I hydrophilic subunits were selected based on: i) previous partial proteomic studies of the ETC revealing the subunits more acutely decreasing in dietary restriction or varying in aged or longevity mutant mice (Miwa et al., 2014); ii) their core (NDUFV2 and NDUFS3) or supernumerary (NDUFS4 and NDUFS5) character; iii) their especial situation in the electron path of the hydrophilic domain (NDUFV2); or iv) their lack of variation in those longevity models to be potentially used as a reference (NDUFA9) . Abundance of the VDAC component of the mPTP was also measured due to its possible relationship with mitROSp and aging.

Results

Multivariate statistics reveals a species-specific Cx I profile

Multivariate statistics was applied to determine whether specific Cx I subunits gene expression (*ndufv2*, *ndufs3*, *ndufs4* and *ndufs5*) and protein content (NDUFV2, NDUFS3, NDUFS4 and NDUFA9) differ among mammals. Non-supervised principal component analysis (PCA) revealed the existence of a species-specific gene and protein profile of the Cx I, capable to explain up to 65.4% samples variability (**Figure 1A**). A hierarchical clustering of the samples represented by a heat map revealed specific Cx I patterns for rodents (mouse, rat and guinea pig) and non-rodents (rabbit, pig, cow and horse) (**Figure 1B and C**). These results were confirmed by performing a supervised analysis, such as partial least squares discriminant analysis (PLS-DA) (**Figure 1D**). Cross-validation values of PLS-DA model scored a maximum Q^2 of 0.3 and R^2 of 0.4 when using only one component (**Figure 1E**). Permutation tests (1000 repeats) yielded a low p=0.02, indicating that none of the distributions formed by the permuted data was better than the observed statistic based on the original data (**Figure 1F**). The inter-group discriminating power of the different measured features is evaluated by a variable importance projection (VIP) score > 1.5, which was obtained only for NDUFV2 (**Figure 1G**). These results were supported by applying a Random Forest (RF) classification algorithm which revealed a species overall classification error of 0.26, being *ndufv2* the variable with the highest contribution to classification accuracy (**Figures 1H and 1I**).

The species-specific Cx I profile is associated with animal longevity

Gene expression and protein content of Cx I were also correlated with mammalian longevity. Specifically, long-lived animals showed decreased gene expression of *ndufv2* and *ndufs3* (**Figure 2A**). Moreover, protein content of NDUFV2 and NDUFS4 were also decreased in long-lived mammals (**Figure 2B**). Yet no correlation between protein content and gene expression was found (**Supplementary Figure 1**).

The VDAC content is associated with animal longevity

VDAC is a component of the mitochondrial permeability transition pore (mPTP) and is commonly used as a loading control for mitochondrial proteins. In order to check its suitability when comparing different animals, we've compared total VDAC content by performing an ANOVA analysis. Unexpectedly, we've found that total VDAC content changes across the different animal species and is negatively correlated with animal longevity (**Figure 3A**). Furthermore, VDAC total content was positively correlated with NDUFV2 and NDUFS4 protein content (**Figure 3B and C, Supplementary Figure 1**).

ndufv2 and VDAC correlate with longevity after controlling for phylogenetic relationships

Animal species are evolutionarily related, and closely related species often have similar traits due to inheritance from a common ancestor. Most of statistical analysis, such as linear regression, assume the independence of the data, which might not be accomplished from data obtained from these close-related species. In order to find associations between longevity and gene expression and protein content of selected Cx I subunits and VDAC protein content, we have applied a phylogenetic comparative method, such as phylogenetically generalised least

squares (PGLS) regression. A phylogenetic tree allowing to evolutionary relate the species in our study was inferred and is constructed in **Supplementary Figure 2A**.

First of all, under the assumption of a Brownian motion model of evolution (a branching, random walk of trait values from an ancestral value at the root to the tips of the tree (Washburne et al., 2018)), we have estimated the Pagels λ. It allows to measure phylogenetic signal and indicates the relative extent to which a traits' correlation among close relatives match a Brownian motion model of trait evolution. Pagels λ range from 0 to 1, where λ=1 indicate that trait similarities between species are influenced by phylogenetic relationships; λ=0 indicate that trait similarities between species are independent of phylogenetic relationships; and 0<λ<1 indicate different levels of phylogenetic signal. According to the estimated λ value, we have classified the measured traits according to its association degree with phylogenetic relationships: i) independent (λ=0): *ndufs5* and NDUFS3; ii) low dependence: *ndufs3* and NDUFA9; iii) mild dependence: *ndufv2* (λ=0.65), NDUFV2 (λ=0.81) and VDAC (λ=0.53); and strong dependence (λ=1): *ndufs4* and NDUFS4. Finally, we have applied a PGLS regression, which revealed that only gene expression of *ndufv2* (p=0.041, r=-0.80) (**Supplementary Figure 2B**) and protein content of VDAC (p=0.015, r=-0.79) (**Supplementary Figure 2C**) were positively correlated with animal longevity after controlling for phylogenetic relationships.

Discussion

Longevity-associated Cx I profile

In this investigation we have found that the mitochondrial Cx I profile is associated with mammalian longevity. Our model revealed that Cx I accounts for 40% of inter-species variation, being *ndufv2* gene expression and protein content, followed by NDUFS4 protein, the highest longevity predictor. To the best of our knowledge, ours is the first study elucidating the genetic changes in particular Cx I subunits across mammals of different orders revealing new insights on animal longevity.

Low Cx I content in long-lived mammalian species

Mitochondrial-related genes have been positively selected in long-living invertebrates (Roux et al., 2014) and mammals, including rodents (Sahm et al., 2018a), bats (Shen et al., 2010) and primates (Muntané et al., 2018). Our results showed a decreased matrix Cx I subunits gene expression in the same direction that protein content. These findings agree with previous studies that show a positive selection during evolution of gene expression of Cx I subunits, as well as genes that regulate its assembly (Sahm et al., 2017). Our study design revealed decreased gene expression and/or amount of particular Cx I subunits, suggesting that longevity is associated with a genetic modulation targeted to maintain a lower content of those hydrophilic Cx I matrix domain subunits.

The core Cx I structure is highly conserved across animal species (Vinothkumar et al., 2014) and maintains a fixed stoichiometric relationship of 1:1 in their forming subunits (Wirth et al., 2016). Since we have found different protein content of the core subunits NDUFV2 and NDUFS4 in different animal species, we suggest that the lowest amount of core subunits determines the total amount of fully assembled Cx I. Accordingly, several studies extrapolated changes in specific Cx I subunits to total Cx I content variations (Ayala et al., 2007; Gomez et al., 2015; Martínez-Cisuelo et al., 2016; Pamplona et al., 2005). Furthermore, we are measuring the total content of these proteins, but not its intracellular location. Therefore, we cannot discard that these stoichiometric differences are due to the presence of free subunits at the mitochondrial matrix. Supporting the latter, it has been described different protein turnover rates for each Cx I subunit (up to 4.6-fold difference), which is higher in matrix subunits compared to those located in the membrane (Karunadharma et al., 2015).

Although ROS can be produced at many different mitochondrial sites, studies including those with endogenous reporters in the absence of inhibitors have localized the main ROS generator sites at the hydrophilic Cx I domain and at Cx III (Quinlan et al., 2012; Wong et al., 2017). Among these two, the low ROS production of long-lived species and dietary restricted animals has been localized at Cx I (Barja and Herrero, 1998; Herrero and Barja, 1997, 1998; Pamplona and Barja, 2006, 2007), particularly to its matrix hydrophilic domain (Miwa et al., 2014) which catalyses oxidation-reduction reactions, while the hydrophobic membrane domain catalyses proton pumping (**Figure 4**). ROS production at the hydrophilic Cx I domain can occur either at the flavin (I_F site) or at some of its FeS clusters (Genova et al., 2001; Herrero and Barja, 2000; Kushnareva et al., 2002), which can also further contribute to secondary ROS formation due to Fe liberation under oxidative stress (Koopman et al., 2010). Adscription of ROS production to the I_F site has been based on experiments increasing or decreasing flavin reduction concomitant with

increases and decreases in ROS production respectively. However, these experiments can't rule out Cx I FeS clusters as potential ROS generators because they are located downstream of the flavin, and then increases and decreases in FeS reduction will also occur in those experiments. Studying the amounts of particular Cx I subunits of the hydrophilic Cx I domain can further localize the sites, subunits and genes responsible for the longevity related decrease in mitROSp.

Low abundance of NDUFV2 and NDUFS4 subunits is associated with mammalian longevity

The functional role of the Cx I accessory subunits is fragmentary and not clear (Fiedorczuk and Sazanov, 2018; Zhu et al., 2016) although it has been proposed that they have regulatory roles participating in Cx I stabilization, assembly, subunit interactions or limitation of ROS production (Zhu et al., 2016).

Among the CxI subunits selected, NDUFVS3 and NDUFS5 did not show correlation with species longevity in spite of their decrease in DR and in the long-lived ICRFa mouse strain (moderate decreases), and the increase in NDUFS3 with age in C57Bl/6 mice (Miwa et al., 2014). The lack of correlation with longevity observed for NDUFS5 is not strange however, since recent description of the near atomic structure of bovine and ovine Cx I at around 4 Å resolution by cryoEM localized NDUFS5 at the bottom of the hydrophobic domain near the intermembrane space (Fiedorczuk et al., 2016; Zhu et al., 2016), far away from the Cx I hydrophilic domain sites of ROS production. Concerning NDUFS3, it is an accessory subunit without cofactor that does not take part directly on the main electron transfer but rather provides the platform required for complex assembly (Fiedorczuk and Sazanov, 2018). The lack of correlation of the NDUFA9 subunit with species longevity was expected since it did not show correlation in other longevity models (Miwa et al., 2014), it is a subunit essential for activity that binds NADPH to indirectly regulate the terminal N2 cluster (Fiedorczuk and Sazanov, 2018), and is present at the bottom of the hydrophilic domain near the hinge connecting the two Cx I domains. This protein also has a structural function because it stabilizes the junction between the membrane and matrix domains of Cx I (Stroud et al., 2013).

The remaining two subunits studied, the NDUFV2 and NDUFS4 proteins, showed negative correlation with species longevity. In principle, regulation of ROS production should be left for accessory subunits because the central core is needed for the most fundamental function, electron transfer coupled to H^+ pumping and ATP production. However, NDUFV2, which was lower in long-lived species both at mRNA and protein levels, is a special case because it does not take part in the main electron path of the hydrophilic domain of Cx I. Instead, the highly conserved off-pathway N1a FeS cofactor of NDUFV2 can take one electron from FMN but cannot give it to N3 because the distance from N1a (in subunit NDUFV2) to N3 (19.4 to 22.3 Å, **Figure 4**) is too long compared to the maximum distance for physiological electron transfer between redox centers, 14 Å (Page et al., 1999). It has been proposed that N1a can function to prevent excessive ROS production (Sazanov, 2006, 2015). The very low one electron potential of N1a (around -370mV) compared to all the other isopotential FeS clusters (N3 to N6b at around -250 mV) makes it highly susceptible to one electron reduction of oxygen to superoxide radical (**Figure 4**). The low NUDFV2 (and N1a) amount present in long-lived species agrees with the hypothesis that it can serve to limit ROS production, since the smaller the NDUFV2 amount, the less the number of electrons transferred from FMN to N1a, and thus less would reduce O_2 to $O_2^{\cdot}$, while more electrons would follow the central path from the flavin to N3 and then the rest

of the FeS until N2 (**Figure 4**). This could help to explain the smaller amount of ROS produced per unit electron flow in long-lived species. This mechanism is simple and avoids the need for electrons to travel bidirectionally between the flavin and N1a (Sazanov, 2006). Therefore, we postulate that the amount of NDUFV2 subunit could serve to modulate ROS production in each species in accordance with its longevity and would help to explain the functional significance of the off-path situation of cluster N1a. Interestingly, it has been found that phosphorylation of NDUFV2 tyrosine 118 decreases ROS production leading to cardioprotection after ischemia-reperfusion (Xu et al., 2017).

The supernumerary non cofactor containing NDUFS4 was the other subunit showing less protein level amount in long-lived species, although its mRNA levels did not show significant differences. Such low level agrees with its strongly decreased levels in long-lived DR mice (Miwa et al., 2014). The accessory NDUFS4 subunit is located where the NADH dehydrogenase domain meets the rest of the hydrophilic arm (Zhu et al., 2016) and is not likely to play a catalytic role but it is important for assembly of the complex (Stroud et al., 2016). Various NDUFS4 mutations lead to total loss of Cx I activity (Budde et al., 2000).

It is known that mammalian NDUFSV1, V3, S1, S4 and S6 interact with NDUFV2 (Fiedorczuk et al., 2016; Zhu et al., 2016). Among all those, only NDUFS4 shows a strong decrease in DR (Miwa et al., 2014) the rest being invariant or showing only modest decreases. Therefore, although NDUFS4 does not have an electron transport cofactor, it could modulate ROS production through its interaction with NDUFV2, which would be affected by the lower NDUFS4 levels of long-lived species. In agreement with this possibility, it is known that cAMP associated serine phosphorylation of NDUFS4 by PKA lowers ROS production and increases Cx I activity (Papa et al., 2008), and heart-specific NDUFS4 knockout mice have normal heart energetics and function together with less ROS generation and better functional recovery after ischemia-reperfusion while reintroduction of NDUFS4 abolishes this protection (Zhang et al., 2018).

Although our finding of smaller amounts of NDUFV2 and NDUFS4 can contribute to decrease Cx I ROS production in long-lived species, association of complex I within supercomplexes could perhaps also contribute to ROS regulation. Possible functional roles of respiratory supercomplexes remain controversial, proposals including roles in stability of individual complexes, CoQ substrate channeling between Cx I and Cx III_2, prevention of protein aggregation, and reduction in ROS production. Various authors have suggested that assembly of Cx I into supercomplexes prevents excessive ROS production during oxidation of NADH-linked substrates because more efficient CoQ channeling helps in maintaining the chain in a more oxidized state (Lopez-Fabuel et al., 2016; Maranzana et al., 2013). However, despite progress in the determination of the structures of respiratory supercomplexes their physiological role is not yet understood (Fiedorczuk and Sazanov, 2018) and more research is needed to clarify if they could also contribute to modulate mitROSp in relation to animal longevity.

There is an association between mitROSp and VDAC content in animal longevity

ROS production promotes the opening of the mitochondrial permeability transition pore mPTP (Rottenberg and Hoek, 2017) which is related to mitochondrial swelling and fragmentation, ischemia-reperfusion injury, and cell death (Koopman et al., 2010; Murphy and Steenbergen, 2008; Zhang et al., 2018). Specifically, ROS generation and reverse electron transport through

Cx I increase the sensitivity of mPTP opening (Briston et al., 2017). Previous studies have shown that dietary restriction decreases both mPTP (Amigo et al., 2017; Petrosillo et al., 2010) and mitROSp at Cx I (Pamplona and Barja, 2006, 2007). Since mPTP opening is promoted through oxidation of mitochondrial membrane lipids and proteins by ROS (Panel et al., 2018), the decrease in mitochondrial permeability in DR could be due to the decrease in mitROSp that occurs in this dietary manipulation.

VDAC is a component of mPTP (Halestrap, 2009; Leanza et al., 2019; Mnatsakanyan et al., 2017, 2019). Some studies indicate that VDAC content regulates the opening of mPTP in response to modifications in mitROSp (Panel et al., 2018; Rottenberg and Hoek, 2017). Since decreases in Cx I content correlate with reduction in mitROSp (Ayala et al., 2007; Gómez et al., 2007; Miwa et al., 2014; Sanchez-Roman et al., 2011; Sanz et al., 2006b), Cx I content could regulate the mPTP opening mediated by mitROSp modifications.

On the other hand, our results show that a lower VDAC content is associated with mammalian longevity. Furthermore, VDAC is positively correlated with NDUFV2 and NDUFS4 Cx I subunits which are present at higher levels in short-lived animals. Thus, we hypothesize that a lower level of NDUFV2 and NDUFS4 would lead to lower complex I ROSp, lower ROS-mediated VDAC modification and lower mPTP in long-lived animal species (**Figure 3**). This agrees with the recent description that high VDAC levels lead to mPTP and to a shortened lifespan (Zhou et al., 2019), as well as with the decrease in mPTP observed in dietary restriction studies (Amigo et al., 2017; Petrosillo et al., 2010).

Dealing with Cx I and VDAC variations in evolutionary-related species

Comparative studies across species with different lifespan are a powerful source of information to identify mechanisms linked to extended longevity (Bozek et al., 2017; Ma et al., 2015). However, those studies come up with several technical limitations. Specifically, in terms of protein recognition, the presence of SNPs inducing little sequence or amino acid changes might alter protein structure, even in highly conserved structure, possibly affecting antibody recognition. Since we lack of methods to improve inter-species antibody reactivity, we have increased the number of repeated measurements up to 7, in order to capture higher inter-individual variability in each specie, and measured gene expression using a very sensible technique in order to confirm those results. However, we didn't find significative correlations between gene expression and protein content. Although we cannot omit technical issues, the lack of correlation doesn't necessarily invalidate the presented results. Accordingly, it had been reported that mRNA and protein content doesn't need to be necessarily correlated (Maier et al., 2009), even in mammals (Tian et al., 2004). Furthermore, a comparative study has demonstrated an increasing protein divergence with higher evolutionary distance, since expression divergence seems to be more stable (Warnefors and Kaessmann, 2013), which agrees with the obtained data.

Even after dealing with technical issues, inter-species studies have to face that evolutionary relationships don't allow for independence of the data (Cooper et al., 2016). Therefore, it's important to elucidate whether a specific trait correlates with longevity differences, or alternatively, these differences arise because of the data similarity. To overcome this limitation, several longevity cross-species studies in birds (Minias and Podlaszczuk, 2017), bats (Wilkinson

and Adams, 2019), primates (Muntané et al., 2018), mammals (Jové et al., 2013; Lindborg et al., 2015) and vertebrates (Mayne et al., 2019) have applied phylogenetic comparative methods, such as PGLS. In our data, PGLS revealed that *ndufv2* gene expression and VDAC protein content changes associated with longevity weren't due interspecies relationships. Although robust, the main limitation of the methods for phylogenetic analysis is that they rely on the construction of a phylogenetic tree, which is unknown. Phylogenies are estimated, mainly by aligning homologue gene sequences and using models of mutation to infer most-likely evolutionary histories. However, depending on the genes chosen, how the sequences are aligned and which method is used to infer evolutionary histories we get different phylogenies. And errors in phylogenetic inferences propagate to errors in phylogenetic analyses (Washburne et al., 2018). These limitations arise the need of the development of more robust bioinformatic methodologies for phylogenetic tree inferences.

Conclusions

Our study indicates that long-lived mammalian species have low levels of NDUFV2 and NDUFS4 subunits of the hydrophilic domain of complex I which could be responsible in part for their lower mitROSp and superior longevity. The lower VDAC content of these animals could also contribute to their high longevity due to lower ROS-mediated opening of the mitochondrial permeability transition pore.

Methods

Animals

Mammalian species included in the study were male adult specimens with an age representing their 15-30% of their longevity. The recorded values for longevity (in years) were: mouse (*Mus musculus*), 3.5; rat (*Rattus norvegicus*), 4.5; gerbil (*Meriones unguiculatus*), 6.3 guinea pig (*Cavia porcellus*), 8; rabbit (*Oryctolagus cuniculus*), 13; pig (*Sus scrofa*), 27; cow (*Bos taurus*), 30; and horse (*Equus caballus*), 46. Rodents and rabbits were obtained from rodent husbandries and sacrificed by decapitation, whereas sheep, pigs, cow, and horses were obtained from abattoirs. The animal care protocols were approved by the Animal Experimentation Ethics committee of the University of Lleida. Heart ventricles from 5-7 animals were removed and immediately frozen in liquid nitrogen and transferred to -80°C until analyses.

Sample homogenization and quantification

Heart tissue (≈50 mg of whole tissue) was homogenized in a buffer containing 180 mM KCl, 5 mM MOPS, 2 mM EDTA, 1 mM DTPAC adjusted to pH=7.4. Prior homogenization, 1 µM BHT and a mix of proteases inhibitors (GE80-6501-23, Sigma, Madrid, Spain) and phosphatase inhibitors (1 mM Na_3VO_4, 1 M NaF) were added. After a brief centrifugation (1000 rpm for 3 min at 4°C), supernatants protein concentration was measured using the Bradford method (500-0006, Bio-Rad Laboratories, Barcelona, Spain).

Protein content determination

The amount of the specific Cx I subunits NDUFV2, NDUFS3, NDUFS4, NDUFS5 and NDUFA9, as well as VDAC-1/Porin, were estimated using western blot analyses as previously described (Gomez et al., 2015). Anticipating potential technical limitations mainly due to antibody reactivity, and before performing the comparative approach, we have evaluated the similarity of the protein sequences using a BLAST algorithm (**Supplementary Table 1; for details, see Table 3 of this Thesis**). Although the exact target sequence of the commercial antibodies is unknown, we have found a high similarity between sequences, and have chosen the most appropriate antibodies available according to their proved or predicted reactivity against the species of our study.

Briefly, heart homogenates were mixed with a buffer containing 62.5 mM Tris-HCl pH 6.8, 2% SDS, 10% glycerol, 20% β-mercaptoethanol and 0.02% bromophenol blue, and heated for 3 min at 95°C. Then, proteins were subjected to one-dimensional electrophoresis on SDS and transferred to PVDF membranes. Membranes were maintained in blocking solution containing Tris 2M, NaCl 2.5 M, 5% BSA and 0.01% Tween for 1h at room temperature. Immunodetection was performed using antibodies against NDUFV2 (SAB2107279, Sigma, Madrid, Spain), NDUFS3 (459130, ThermoFisher, Barcelona, Spain), NDUFS4 (ab96549, Abcam, Cambridge, UK), NDUFS5 (ab188510, Abcam, Cambridge, UK), NDUFA9 (459100, ThermoFisher, Barcelona, Spain), and VDAC-1/Porin (ab15898, Abcam, Cambridge, UK).

Secondary antibodies were anti-mouse (GENA931, Sigma, Madrid, Spain) and anti-rabbit (31460, ThermoFisher, Barcelona, Spain). Bands were visualized using an enhanced chemiluminescence HRP substrate (Millipore, MA, USA). Signal quantification and recording was performed with

ChemiDoc equipment (Bio-Rad Laboratories, Barcelona, Spain). The protein amount was calculated from the ratio of their densitometry values referred to its respective Coomassie staining (1610436, Bio-Rad Laboratories, Barcelona, Spain) (**Supplementary Figure 3**). Due to technical issues (antibody recognition), NDUFA5 amount is not reported. Lack of protein recognition might be due to technical issues, not to missing proteins, such as for NDUFS3 in guinea pig.

Primers design

Gene cDNA sequences coding for the Cx I subunits NDUFV2 (*ndufv2*), NDUFS3 (*ndufs3*), NDUFS4 (*ndufs4*), NDUFS5 (*ndufs5*) and NDUFA9 (*ndufa9*) were obtained from Ensmbl (http://www.ensmbl.org). Due to gene cDNA sequences limitations for gerbil, that specie wasn't included in the gene expression analyses. Degenerate primers were designed to amplify conserved regions among mammalian sequences using the software PriFi (Fredslund et al., 2005), and are listed in **Supplementary Table 2 (for details, see Table 2 of this Thesis)**. Primers were purchased from Isogen (LifeSciences, Utretch, Netherlands).

Gene expression: Droplet digital PCR

Prior DNA amplification, RNA from 15 mg whole heart tissue was extracted using RNeasy Fibrous Tissue Mini Kit (Qiagen, Hilden, Germany), and retro-transcribed to cDNA using the High-Capacity cDNA Reverse Transcription kit (Applied Biosystems, CA, USA).

For DNA absolute quantification (copies/µl), reaction mixture contained 1x of EvaGreen ddPCR Supermix, 200 nM primers and 0.01-16 ng of template cDNA. For droplet generation, 20 µL of reaction mixture and 70 µL of Droplet Generation Oil for EvaGreen were loaded in the Droplet Generation Cartridge, which was placed into the Droplet generator. From each PCR reaction mixture, 20 µL were transferred to a 96-well PCR plate, which was sealed with a foil heat using PX1 PCR plate sealer. Amplification was performed in a C1000 Touch Thermal Cycler following an initial DNA Polymerase activation (95°C, 5 min), and 40 cycles consisting of a DNA denaturation (95°C, 30 sec), primer annealing (58°C, 1 min) and extension (60°C, 1 min). A final dye-stabilization step was included (4°C 5 min, and 90°C 5 min). Droplets were read with a QX200 Droplet Reader and analysed using QuantaSoft software (Bio-Rad). The results from more than 12,000 droplets were accepted and normalised to an appropriate housekeeping gene (*ndufa9*) as suggested by previous work (Miwa et al., 2014). Values are reported as cDNA gene units per cDNA housekeeping units. All equipment and reagents were purchased from Bio-Rad (Bio-Rad Laboratories, Barcelona, Spain).

Statistics

Multivariate statistics was performed using Metaboanalyst software (Chong et al., 2019). Pearson correlation and Pearson partial correlation were performed using RStudio (v1.1.453). Linear models and phylogenetic generalised least squares regression (PGLS) were constructed using RStudio (v1.1.453). The phylogenetic tree was constructed using taxa names as described previously (Kumar et al., 2017). Functions used were included in the package *caper*. Data was log-transformed and mean-centred prior statistical analyses in order to accomplish the assumptions of linearity.

Conflict of interest

The authors declare no conflict of interest

Funding

This work was supported by the Spanish Ministry of Economy and Competitiveness, Institute of Health Carlos III (grant number PI14/00328), the Spanish Ministry of Science, Innovation and Universities (RTI2018-099200-B-I00), and the Generalitat of Catalonia, Agency for Management of University and Research Grants (2017SGR696) and Department of Health (SLT002/16/00250) to R.P, and PR[19] BIO MET 0155 to GB.This study has been co-financed by FEDER funds from the European Union ("A way to build Europe"). IRBLleida is a CERCA Programme/Generalitat of Catalonia.

Acknowledgements

M.J. is a 'Serra Hunter' Fellow. N.M-M received a predoctoral fellowship from the Generalitat of Catalonia (AGAUR, ref 2018FI_B2_00104). We thank Dr. Eloi Gari, from the Basic Medical Sciences Department (UdL-IRBLleida) for technical support in gene expression analysis. We thank Salvador Batolome, from the Laboratory of Luminescense and Biomolecular Spectroscopy (Autonomous University of Barcelona, Barcelona, Catalonia, Spain), for ddPCR technical support.

Author Contributions

G.B and R.P designed the study. N.M.M., M.J., I.P., I.S., J.G., and A.N. performed experimental work. N.M.M and R.P. analysed the data. R.P. supervised the design and data interpretation. The manuscript was written by N.M.M, J.G, G.B. and R.P. and edited by R.P. All authors discussed the results and commented on the manuscript.

Figures

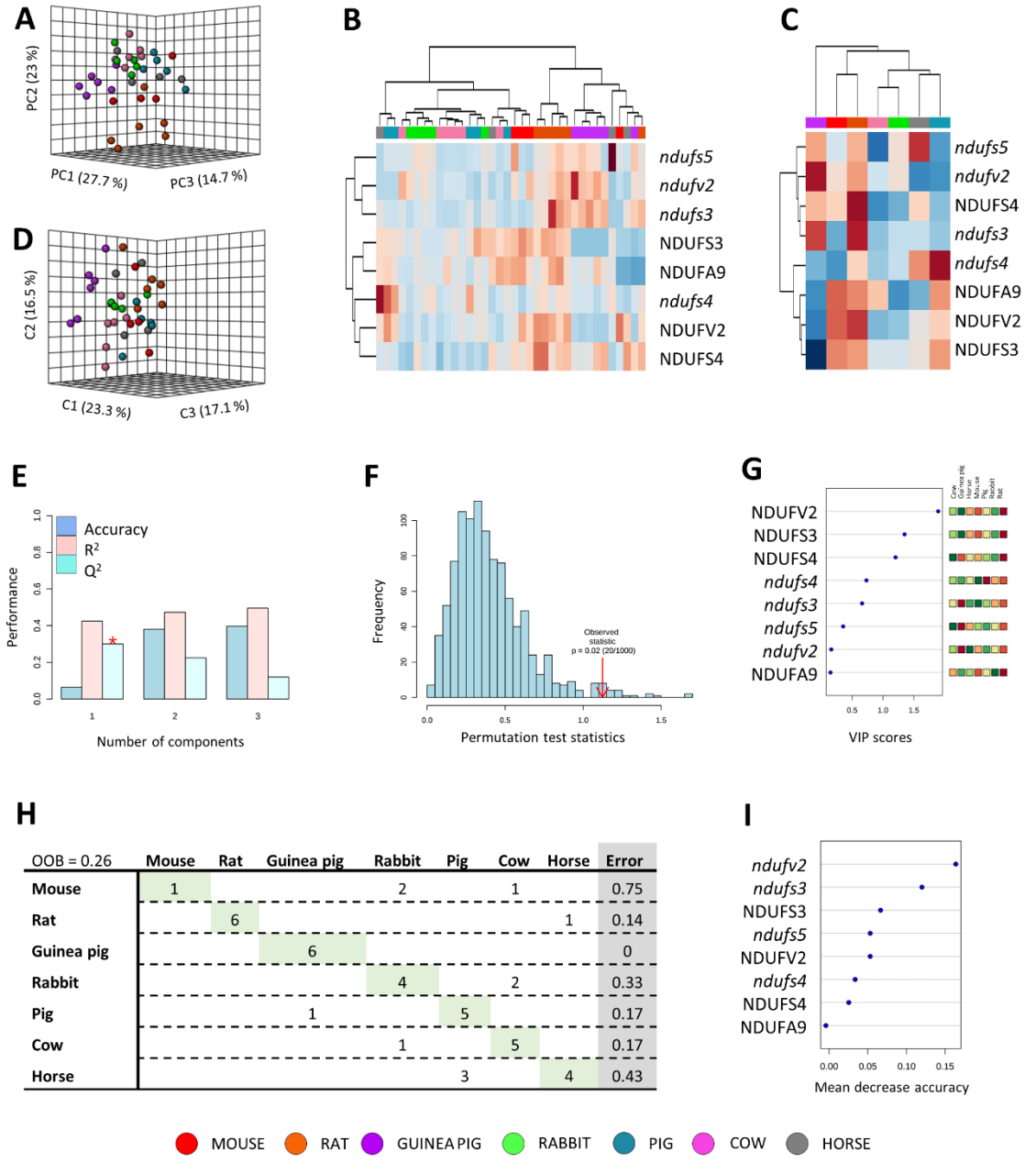

OOB = 0.26	Mouse	Rat	Guinea pig	Rabbit	Pig	Cow	Horse	Error
Mouse	1			2		1		0.75
Rat		6					1	0.14
Guinea pig			6					0
Rabbit				4		2		0.33
Pig			1		5			0.17
Cow				1		5		0.17
Horse					3		4	0.43

Figure 1. Multivariate statistics reveals a species-specific gene expression and protein content of Cx I. A) Principal component analyses (PCA) representation of gene expression and protein content of CI subunits. X: Principal component 1 (PC1); Y: Principal component 2 (PC2); Z: Principal component 3 (PC3). **B)** Hierarchical clustering of individual animal samples according to gene expression and protein content of CI. **C)** Hierarchical clustering of animal species according to average sample values of gene expression and protein content of CI. **D)** Partial least squares discriminant analysis (PLS-DA) representation of gene expression and protein content of CI. X: Component 1 (C1); Y: Component 2 (C2); Z: Component 3 (C3). **E)** Cross validation (CV) analyses (10-fold CV method) of the PLS-DA model. **F)** Permutation test (1000 repeats) using separation distance. **G)** Variable importance projection (VIP) scores indicating the elements which contribute the most to define the first component of a PLS-DA. **H)** Random Forest (RF) classification algorithm. **I)** VIP scores for RF

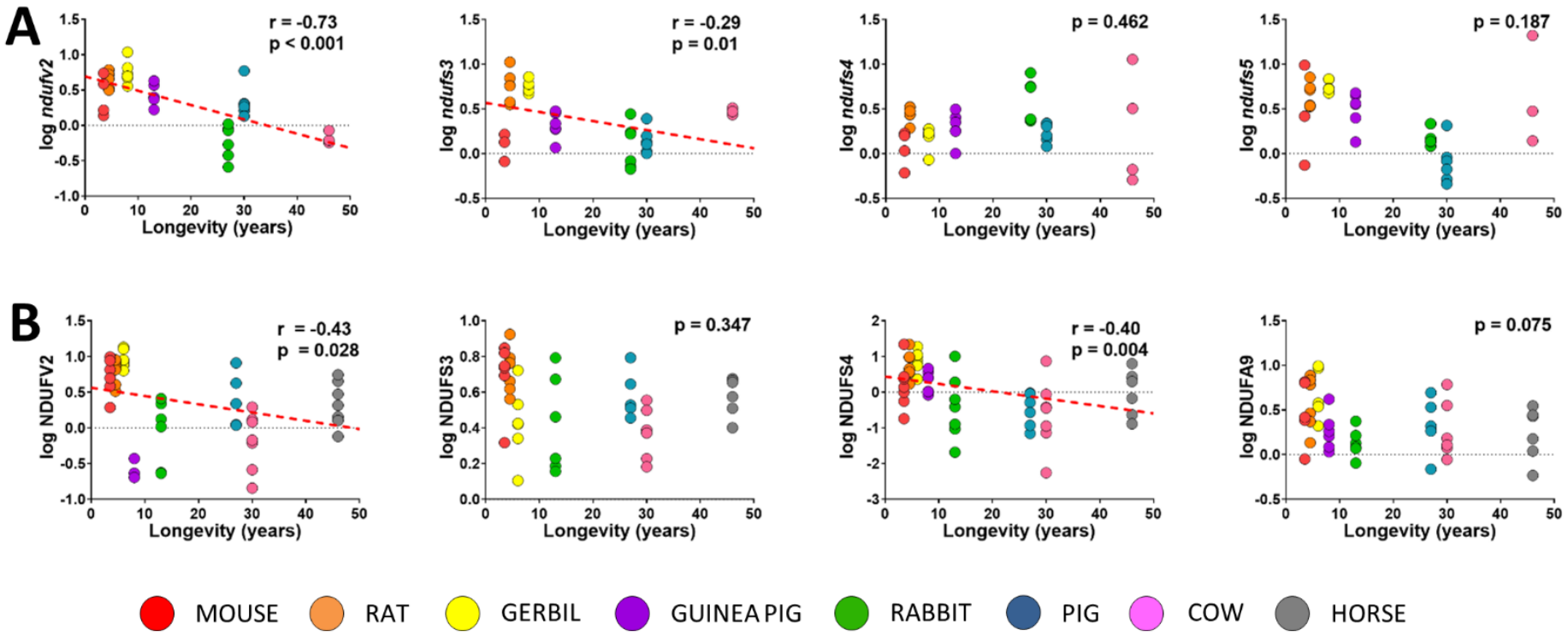

Figure 2. Cx I gene expression (A) and protein content (B) are linearly correlated with mammalian longevity. Pearson correlation was performed between maximum longevity (ML) and gene expression or protein content. Linear regression was applied when significant relationships were found. R^2(*ndufv2*) = 0.48; R^2(*ndufs3*) = 0.20; R^2(NDUFV2) = 0.10; R^2(NDUFS4) = 0.15. NDUFA5 protein results aren't reported due to technical issues. Expression of *ndufs9* is not reported since is used as a housekeeping to normalize the data. Minimum signification level was set at $p<0.05$. Gene expression and protein content were log-transformed to accomplish the assumptions of normality.

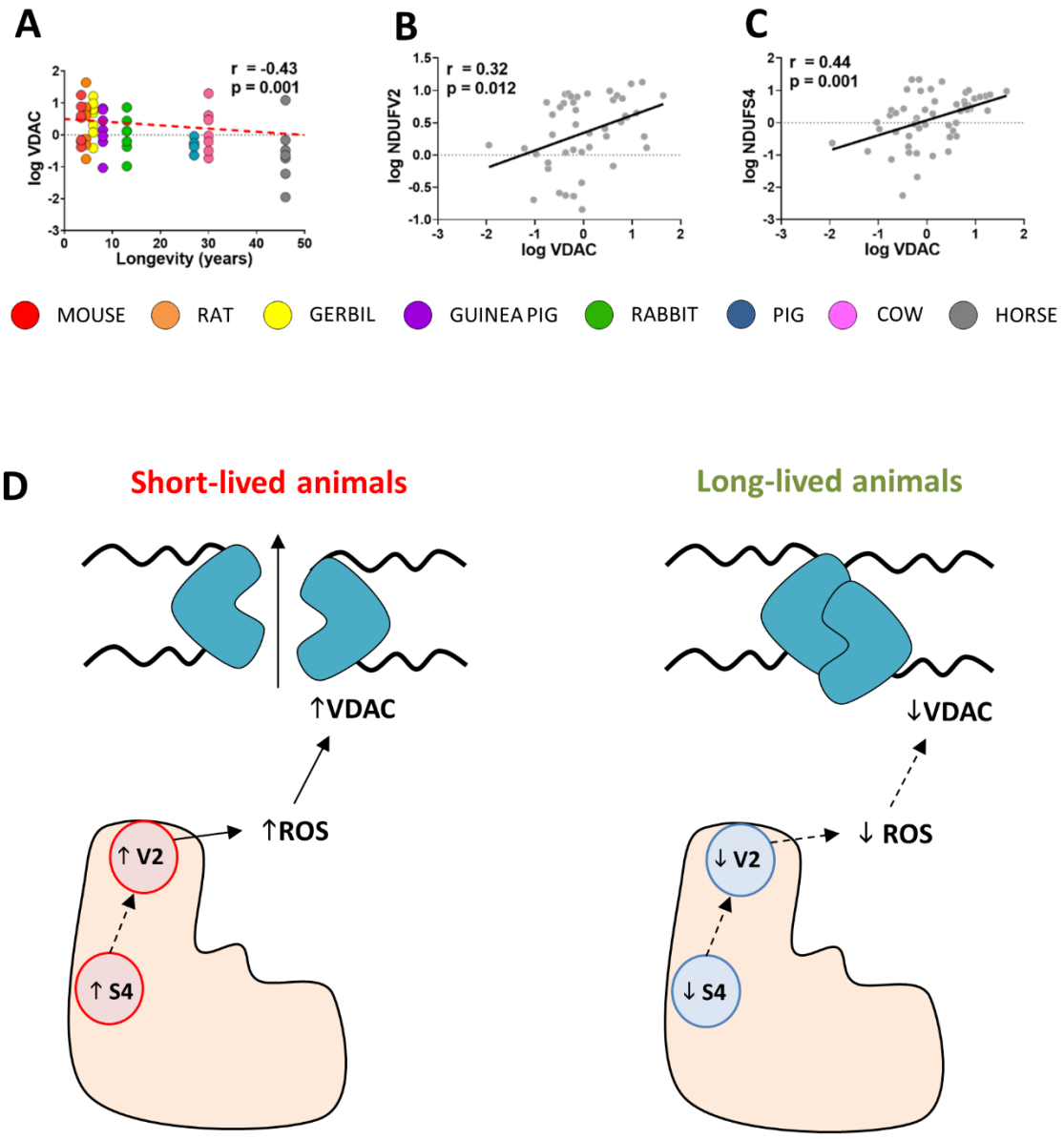

Figure 3. VDAC-1 changes across animal longevity and its association with Cx I subunits and animal longevity. A) Pearson correlation between VDAC-1 protein content and animal longevity. R^2(VDAC) = 0.18. **B)** PGLS regression between VDAC-1 protein content and animal longevity according to phylogenetic tree reported in Figure 3A. **C)** Pearson correlation between VDAC-1 and complex 1 subunit. Linear regression (LR) model was performed when significant relationships were found. R^2(VDAC vs. NDUFV2) = 0.13; R^2(VDAC vs. NDUFS4) = 0.19. Minimum signification level was set at $p<0.05$. Protein content was log-transformed to accomplish the assumptions of normality. **D)** Longevity model of longevity modulation via Cx I, ROS and VDAC.

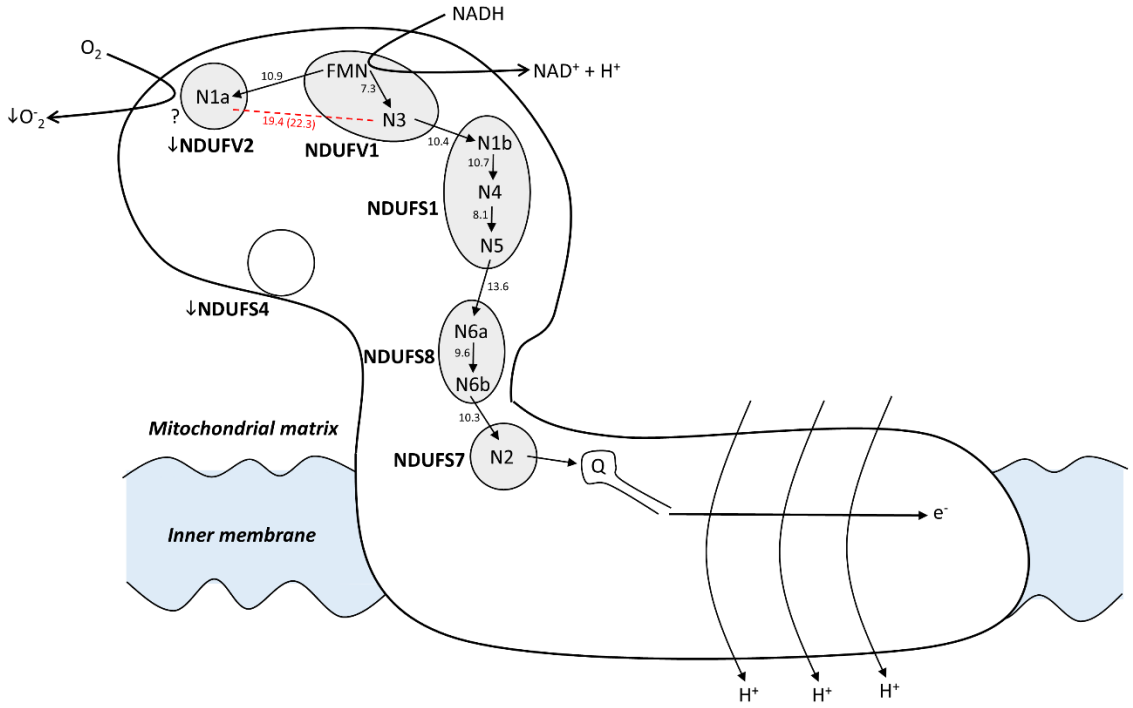

Figure 4. Low NDUFV2 and NDUFS4 in long-lived species can decrease mitROSp from the hydrophilic domain of Cx I. The figure shows the pathway of electron transfer. The human nomenclature for Cx I subunits (NDUF) is used. Electron transfer is indicated by solid arrows from FMN to Fe S clusters N1a, N3, N1b, N4, N5, N6a, N6b and N2 which reduces the quinone. The conserved off-pathway bifurcation from the flavin to FeS cluster N1a (in NDUFV2) is shown as alternative to main electron transfer to N3. Edge-to-edge distances between cofactors indicated in Å correspond to those described for the mammalian ovine enzyme studied by cryo-Electron Microscopy (Fiedorczuk et al., 2016). The distance between iron-sulphur clusters N1a and N3 (*T. thermophilus,* Sazanov 2015) is too long for physiological electron transfer to occur either edge-to-edge (19,4 Å) or centre-to-centre (22.3 Å, shown inside brackets). Therefore, the electron transferred from FMN to 2Fe2s cluster N1a could then reduce oxygen to superoxide radical at NDUFV2. A low amount of NDUFV2 in long-lived species would divert less electrons from the main pathway and would thus lead to a lower rate of complex I ROS production. A lower amount of the accessory subunit NDUFS4 in long-lived species can also downregulate ROS generation at N1a through its known interaction with NDUFV2.

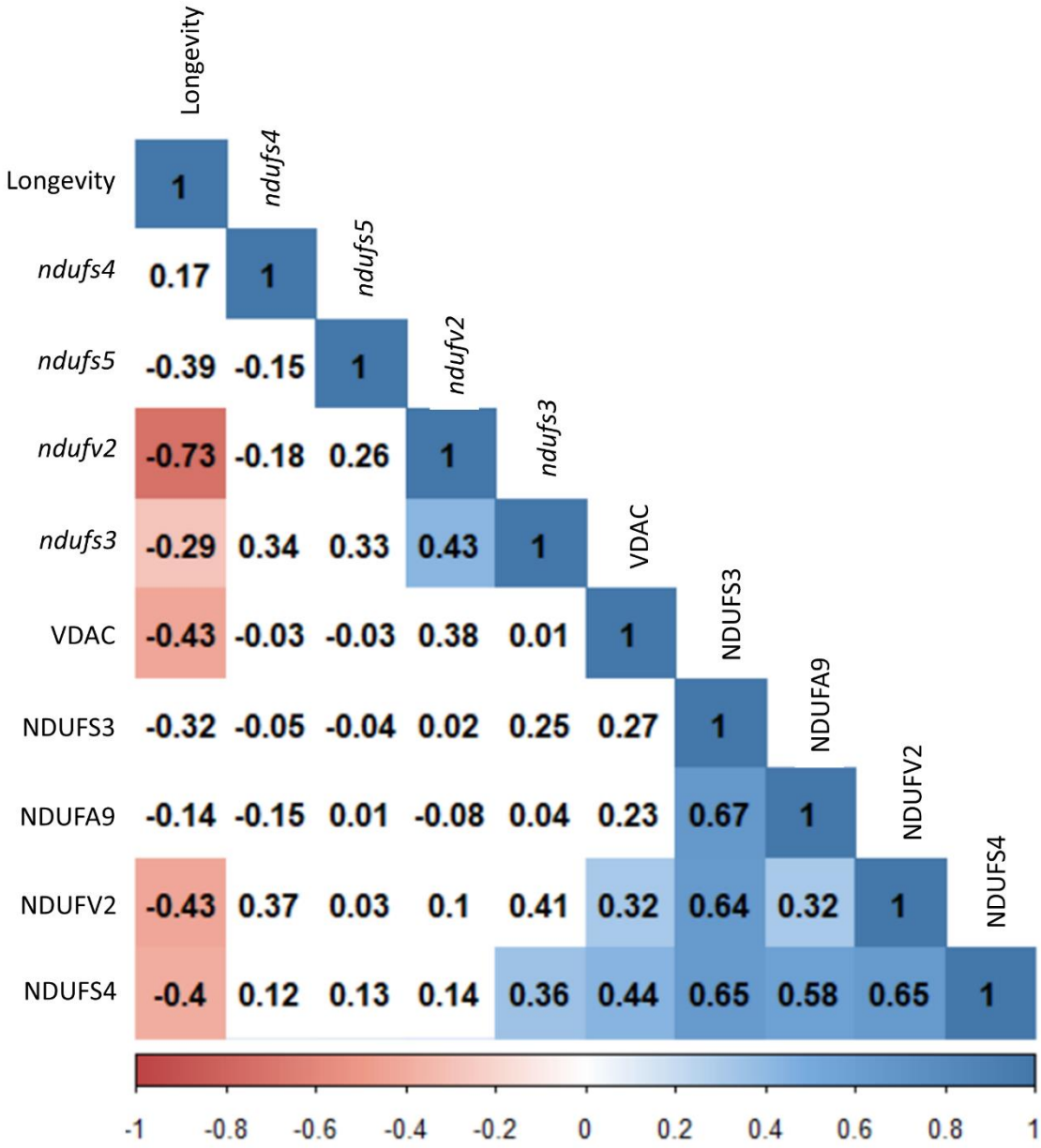

Supplementary figure 1. Pearson correlation matrix of gene expression and protein content of Cx I. Pearson r-value for pairwise comparisons is reported. Non-significant correlations are left in blank. Minimum signification level was set at $p<0.05$. Gene expression and protein content were log-transformed to accomplish the assumptions of normality.

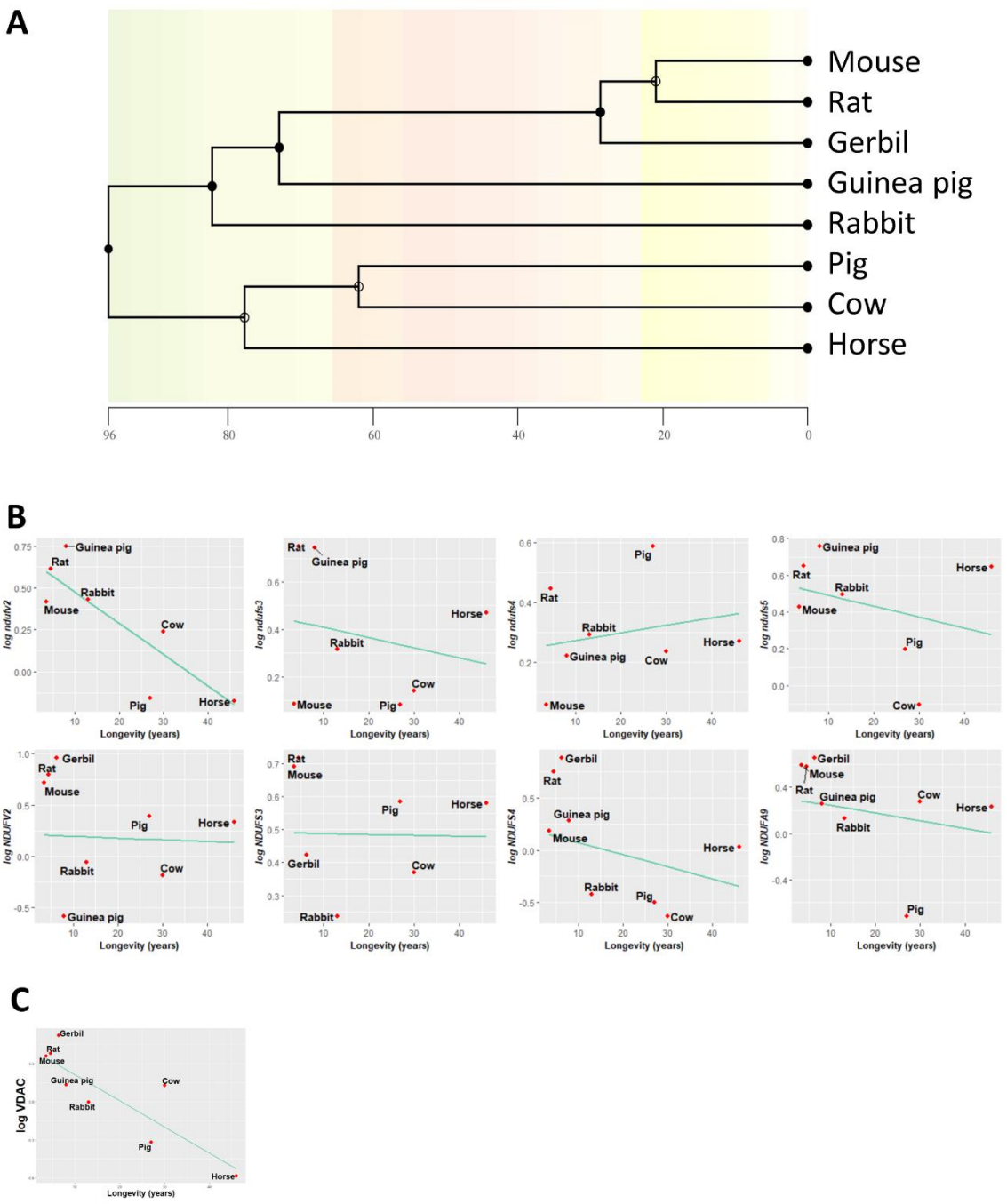

Supplementary figure 2. Cx I subunits and VDAC-1 gene expression and protein content changes across mammalian longevity after correcting for phylogenetic relationships. **A)** Phylogenetic tree with a timescale of million years ago. **B)** Phylogenetic generalised least squares regression (PGLS) between longevity and gene expression and protein content of Cx I subunits. **C)** PGLS between longevity and protein content of VDAC-1. Gene expression and protein content were log-transformed to accomplish the assumptions of normality.

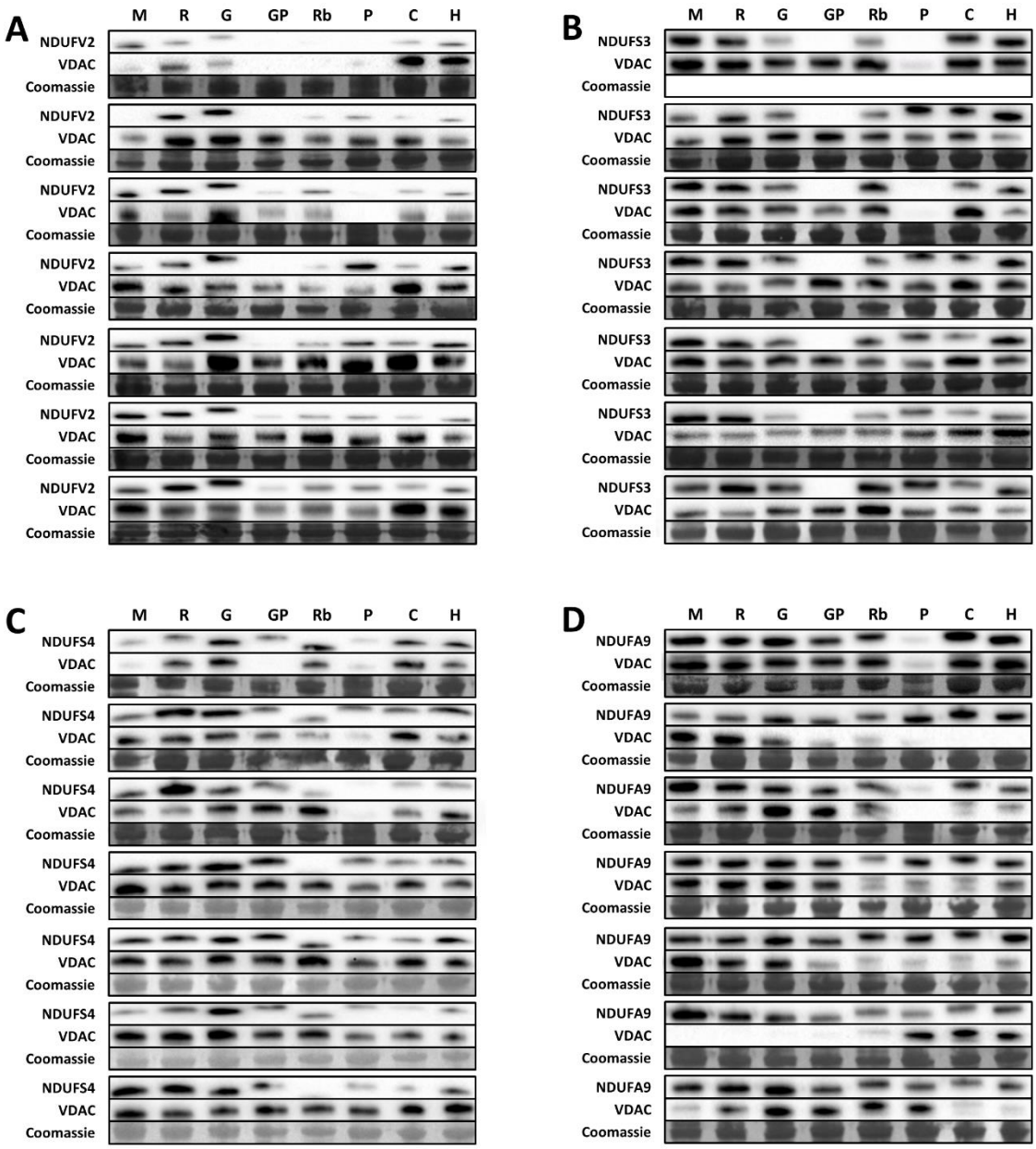

Supplementary figure 3. Individual Cx I protein content from animal's heart. A) NDUFV2 protein content and its respective VDAC and Coomassie. **B)** NDUFS3 and its respective VDAC and Coomassie. **C)** NDUFS4 protein content and its respective VDAC and Coomassie. **D)** NDUFA9 protein content and its respective VDAC and Coomassie. NDUFA5 results aren't reported due to technical issues. M = Mouse; R = Rat; G = Gerbil; GP = Guinea pig; Rb = Rabbit; P = Pig; C = Cow; H = Horse.

Heart methionine metabolic profile is associated with longevity in mammals

Mota-Martorell N[1], Jové M[1], Berdún R[1], Pamplona R[1,*]

[1] Department of Experimental Medicine, Lleida University-Lleida Biomedical Research Institute (UdL-IRBLleida), Lleida, Catalonia, Spain.

[*] **Corresponding author**:

Prof. Reinald Pamplona. Department of Experimental Medicine, University of Lleida-Lleida Biomedical Research Institute (UdL-IRBLleida), Biomedicine 1 building, Av. Rovira Roure 80, Lleida 25198, Spain. E-mail: reinald.pamplona@mex.udl.cat

E-mail addresses of the rest of the authors:

NMM: nataliamotamartorell@gmail.com

MJ: mariona.jove@udl.cat

RB: rebecaberdun@gmail.com

Abstract

Methionine constitutes a central metabolic hub of intracellular adaptations leading to an extended longevity. The present study follows a comparative approach to analyse heart methionine metabolic profile using a LC-MS/MS platform from 7 mammalian species with a longevity ranging from 3.5 to 46 years. Our findings demonstrate the existence of a species-specific heart profile for methionine metabolism associated with longevity characterised by: i) reduced methionine and its related sulphur-containing metabolites; ii) reduced content of metabolites with anti-oxidant properties; iii) reduced amino acid pool; iv) reduced TCA metabolites but increased succinate; v) reduced choline. Our results support the existence of heart longevity features that might respond to an optimised methionine and mitochondrial metabolism, as well as protein turnover mechanisms, in long-lived species.

Keywords: Amino acids; mass spectrometry; metabolites TCA cycle; transmethylation pathway; transsulfuration pathway.

Introduction

Longevity achievement is the consequence of an optimised intracellular metabolism. Globally, the modulations leading to this phenotype include a low generation rate of reactive oxygen species (ROS) and subsequent endogenous damage (Barja, 2013; Ku et al., 1993; Pamplona and Barja, 2007), and the incorporation of biomolecules highly resistant to oxidation on cellular structures (Pamplona and Barja, 2007). The main source of intracellular ROS is the mitochondrial complex I (Cx I) (Barja and Herrero, 1998; Herrero and Barja, 1997, 1998), which has undergone metabolic adaptations leading to quantitative (Lambert et al., 2010; Mota-Martorell et al., 2020b; Pamplona et al., 2005) and qualitative (Barja, 2013; Barja and Herrero, 1998; Miwa et al., 2014) changes to decrease the rate of ROS production in longevous specimens. The macromolecular adaptation concerning nucleotides in DNA, proteins and lipids (Ma and Gladyshev, 2017; Pamplona and Barja, 2007, 2011), respond to controlled gene expression patterns (Tyshkovskiy et al., 2019) that are exhibited as specific proteomic, metabolomic and lipidomic profiles (Faulkes et al., 2019; Jové et al., 2013; Lewis et al., 2018; Mota-Martorell et al., 2019; Naudí et al., 2013; Pradas et al., 2019b; Swovick et al., 2018). Globally, these features seem to be regulated by specific signalling pathways (Barja, 2019), including the mechanistic target of rapamycin (mTOR) pathway.

Proteins evolved to become more resistant by tightly regulating the content of sulphur-containing residues, such as methionine and cysteine. Their sulphur atoms are susceptible to react with oxygen, leading to the formation of different structures according to the location of sulphur atoms on their side chains. Methionine sulphide (R_1-S-R_2) reacts with oxygen leading to the formation of methionine sulfoxide (MetO), which converts an apolar side chain into a highly polar one (Aledo, 2019), whereas cysteine sulfhydryl groups (R-SH) from cysteines are oxidized forming a disulphide linkage (Kim et al., 2014), leading to protein structural modifications (Patil et al., 2015). Longevous phenotype occurs through the adaptative (Moosmann et al., 2020; Pamplona and Barja, 2011) reduction of methionine (Aledo et al., 2011; Pamplona et al., 2005; Portero-Otín et al., 2004; Ruiz et al., 2005) and cysteine (Moosmann, 2011) protein content, as well as its free tissue content (Lewis et al., 2018; Mota-Martorell et al., 2020a). In addition to their structural roles, methionine and cysteine are involved in a complex metabolic network (globally referred to as methionine metabolism) that can divided into: methionine cycle o transmethylation pathway, the transsulfuration pathway and polyamine biosynthesis (Parkhitko et al., 2019; Sanderson et al., 2019). Significantly, modulation of these branches occurs in long-lived models (McIsaac et al., 2016). Available evidence points to methionine metabolism and its specific modulations as feasible determinants of animal longevity.

The aim of this study was to investigate the methionine metabolic phenotype of long-lived mammalian species. Specifically, we had been able to unambiguously detect and quantify 36 different molecular species in heart of 7 mammalian species with different longevities, from 3.5 years in mice to 46 years in horse. The metabolites detected and quantified were: a) methionine and its related metabolites, including the intermediates of the transmethylation pathway S-adenosylmethionine (SAM), S-adenosylhomocysteine (SAH) and homocysteine; betaine and spermidine as metabolites involved in the regeneration of methionine levels; the intermediates of the transsulfuration pathway cystathionine and cysteine; taurine and glutathione as downstream metabolites of the transsulfuration pathway; and vitamin B6 metabolites pyridoxal,

pyridoxal 5’ phosphate (PLP) and pyridoxamine, as cofactors of the transsulfuration enzymes; b) additional amino acids including 8 non-polar amino acids (alanine, glycine, isoleucine, leucine, phenylalanine, proline, tryptophan and valine), 4 polar uncharged amino acids (asparagine, serine, threonine and tyrosine), 2 polar negatively charged amino acid (aspartate and glutamate) and 2 polar positively charged amino acids (arginine and histidine); c) TCA cycle metabolites, including pyruvate, citrate/isocitrate, succinate, fumarate and malate; and d) methionine-derived lipid intermediates such as choline and carnitine. The heart metabolites profile was determined using a LC-MS/MS platform to define specific phenotypic profiles associated with animal longevity.

Results

Multivariate statistics reveals a species-specific methionine-related metabolites heart profile

In order to determine whether heart methionine and its related metabolites concentration differed among mammals, multivariate statistics were applied. Non-supervised principal component analysis (PCA) suggested the existence of a species-specific methionine-related metabolites heart profile (**Figure 1A**), capable to explain 70.9% of sample variability. These results were confirmed after performing a hierarchical clustering of the samples represented by a heat map, which revealed a good sample clusterization of individual specimens according to its specie (**Figure 1B**). Furthermore, average specimen values suggested the existence of different methionine heart profile for short-living species, such as rodents (mouse, rat and guinea pig), and long-living species (**Figure 1C**). A supervised analysis, such as partial least squares discriminant analysis (PLS-DA) allowed to determine the ability to predict the mammalian specie of a specific specimen according to its methionine metabolomic profile (**Figure 1D**). Cross-validation values of PLS-DA model showed that methionine heart metabolome content is a good model to define the animal species scoring a R^2=0.6 and Q^2=0.5, obtaining a maximum accuracy of 0.6 using 4 components (**Figure 1E**). Permutation tests (1000 repeats) yielded a low $p < 0.001$, indicating that none of the distributions formed by the permutated data was better than the observed statistics based on the original data. The discriminating power between groups of the different measured features was ranked by applying a variable importance projection (VIP) score. After selecting those features with VIP score>1.5 as significant, taurine heart content was found to be the top-ranked feature (**Figure 1F**).

Methionine related metabolites are decreased in heart from long-lived animals

The specific changes in heart methionine and its related metabolites content across animal longevity was evaluated. Globally, transmethylation and transsulfuration metabolites were negatively correlated with species longevity (**Figure 2A, Supplementary table 2-3**). Transmethylation intermediates, such as methionine, SAM and homocysteine, as well as spermidine, were decreased in long-lived species. No changes in betaine heart content were found across animal longevity. Transsulfuration intermediates, such as cystathionine and cysteine, as well as sulphur-containing metabolites synthetized from cysteine such as glutathione and taurine were also decreased in long-lived species. Accordingly, vitamin B6 intermediates, which are cofactors of transsulfuration enzymes, were also negatively correlated with species longevity (**Figure 2B**). Altogether, these results suggest a global reduction of methionine-metabolism and, consequently, sulphur-containing metabolites, in long-lived species.

Amino acid content is decreased in heart from long-lived animals

Since heart methionine metabolism is associated to animal longevity, we hypothesized the possibility that other amino acids could also be involved in the achievement of increased longevity. Specifically, we have been able to unambiguously detect 16 additional amino acids apart from cysteine and methionine. In order to determine whether heart amino acid content defines animal species, multivariate statistics were applied. Non-supervised PCA suggested the existence of a different heart amino acid profile within animal species (**Figure 3A**), capable to

explain 76.4% of sample variability. A hierarchical clustering of the samples represented by a heat map revealed a good sample clusterization for individual specimens according to its specie (**Figure 3B**). Again, average specimen values suggested the existence of different amino acids heart profile for short-living species, such as rodents (mouse, rat and guinea pig), and long-living species (**Figure 3C**). A supervised analysis, such as PLS-DA allowed to determine the ability to predict the mammalian specie of a specific specimen according to its methionine metabolomic profile (**Figure 3D**). Cross-validation values of PLS-DA model showed that amino acids heart metabolome content is a limited model to define the animal species scoring a R^2=0.5 and Q^2=0.3, obtaining a maximum accuracy of 0.5 using 5 components (**Figure 3E**). Permutation tests (1000 repeats) yielded a low $p < 0.001$, indicating that none of the distributions formed by the permutated data was better than the observed statistics based on the original data. The discriminating power between groups of the different measured features was ranked by applying a variable importance projection (VIP) score. After selecting those features with VIP score>1.3 as significant, threonine and aspartate heart content were found to be the top-ranked features (**Figure 3F**).

The specific changes in heart amino acid content across animal longevity were also evaluated. Among the 16 additionally detected amino acid (methionine and cysteine amino acids are not included), we have found a global decrease of heart amino acids in long-lived animals (**Figure 4, Supplementary table 2-3**). Specifically, we have decreased levels of non-polar amino acids such as glycine, isoleucine, leucine, phenylalanine, proline, tryptophan and valine; decreased levels of polar amino acids such as asparagine, threonine and tyrosine; and decreased levels of polar charged amino acids such as arginine, histidine, aspartate and glutamate. Alanine and serine heart content remained unchanged across animal longevity.

TCA cycle intermediates are globally decreased in heart from long-lived animals

Considering that amino acids can be metabolised into TCA cycle intermediates, we have analysed the heart changes for TCA cycle metabolites. Specifically, we had been able to unambiguously detect 5 intermediates, including pyruvate, (iso)citrate, succinate, fumarate and malate. In order to determine whether animal species have a specific heart profile for TCA cycle intermediates, multivariate statistics were applied using the heart concentration of the mentioned metabolites. A hierarchical clustering of the samples represented by a heat map revealed the existence of a shared TCA cycle intermediates heart profile within animal species (**Figure 5A**). Again, average specimen values suggested the existence of different amino acids heart profile for short-living species, such as rodents (mouse, rat and guinea pig), and long-living species (**Figure 5B**). However, PLS-DA model obtained was overfitted, probably due to the small number of variables (data not shown).

The specific changes in heart intermediates of TCA cycle across animal longevity were also evaluated (**Figure 5C, Supplementary table 2-3**). Except for pyruvate, heart content of the analysed metabolites correlated with species longevity. Specifically, (iso)citrate, fumarate and malate content were decreased in heart from long-lived animals, whereas succinate was increased.

Heart metabolome is also related with specific lipid intermediates in long-lived animals

Methionine metabolism participates in the biosynthesis of lipid intermediates such as choline and carnitine (**Supplementary table 2-3**). Although carnitine heart content remained unchanged across animal longevity, choline was found to be decreased in long-lived species (**Figure 6**).

Methionine related metabolites, amino acids and TCA cycle intermediates correlate with longevity after controlling for phylogenetic relationships

Animal species are evolutionarily related, and closely related species often have similar traits due to inheritance from a common ancestor. Most of statistical analysis, such as linear regression, assume the independence of the data, which might not be accomplished from data obtained from these close-related species. In order to find associations between longevity and heart methionine metabolites, amino acids and TCA cycle intermediates, we have applied a phylogenetic comparative method, such as phylogenetically generalised least squares (PGLS) regression. A phylogenetic tree allowing to evolutionary relate the species in our study was inferred and is constructed in **Figure 7A**.

First of all, under the assumption of a Brownian motion model of evolution (a branching, random walk of trait values from an ancestral value at the root to the tips of the tree (Washburne et al., 2018)), we have estimated the Pagels λ. It allows to measure phylogenetic signal and indicates the relative extent to which a traits' correlation among close relatives match a Brownian motion model of trait evolution. Pagels λ range from 0 to 1, where λ=1 indicate that trait similarities between species are influenced by phylogenetic relationships; λ=0 indicate that trait similarities between species are independent of phylogenetic relationships; and 0<λ<1 indicate different levels of phylogenetic signal. According to the estimated λ value, we have classified the measured traits according to its association degree with phylogenetic relationships (**Supplementary table 3**): i) independent (λ=0), ii) low dependence (λ<0.6); iii) mild dependence (λ>0.6); and strong dependence (λ=1), representing 63% of the analysed metabolites. Finally, we have applied a PGLS regression, which revealed that methionine-related metabolites, such as methionine (p=0.007, r=-0.74) and PLP (p=0.001, r=-0.67); amino acids, such as proline (p=0.019, r=-0.74) and tyrosine (p=0.04, r=-0.66); and TCA cycle intermediates, such as (iso)citrate (p=0.011, r=-0.76) and fumarate (p=0.035, r=-0.71) (**Figure 7B, Supplementary table 3**) heart content were negatively correlated with animal longevity after controlling for phylogenetic relationships.

Discussion

Cell, organ and tissue functions are determined by the expression of specific gene expression patterns (Sahm et al., 2018b; Seim et al., 2016; Zhang et al., 2020), which are tightly regulated. The transcription of specific proteins, lipids and metabolites respond to cellular functions, and undergoes a continuous remodulation providing a dynamic and integrated view of cell metabolism status (Hou et al., 2020). Multiple inter-species studies had already reported the existence of species-specific tissue and plasma transcriptomics (Fushan et al., 2015; Tyshkovskiy et al., 2019), proteomics (Heinze et al., 2018), lipidomics (Bozek et al., 2017; Gonzalez-Covarrubias et al., 2013) and metabolomics (Faulkes et al., 2019; Hoffman et al., 2020; Lewis et al., 2018; Ma et al., 2015; Viltard et al., 2019; Walters et al., 2018) profile which is often associated with animal longevity. In this line, our study reported the existence of a species-specific tissue profile restricted to a small set of metabolites related to methionine, being heart content of spermidine and taurine, metabolites related to methionine metabolism, the highest species-predictors. Therefore, as far as we are concerned, ours is the first study capable to define mammalian species with different longevities according to a single pathway intracellular status.

Methionine has been widely associated to longevity. Decreased encoded-methionine in mitochondrial DNA (Aledo et al., 2011), as well as decreased plasma (Lewis et al., 2018; Viltard et al., 2019) and tissue (Ruiz et al., 2005) methionine has been found in long-lived species. Reinforcing these data, methionine restriction (MR) has been described to extend species lifespan (McIsaac et al., 2016; Pamplona and Barja, 2006, 2011) and to modulate intracellular metabolism (Pradas et al., 2019a). Apart from being essential for translation initiation in eukaryotic cells, an antioxidant role has been attributed to methionine (Aledo et al., 2011; Bender et al., 2008; Levine et al., 1996; Luo and Levine, 2009). Specific methionine residues in proteins can be oxidized into methionine sulfoxide (MetO), without affecting protein function (Reddy et al., 1994). Oxidation of these methionine residues can be reverted via MrsA and MrsB enzymes at the low metabolic cost of one molecule of NADPH (Stadtman et al., 2005). In this way, one equivalent of ROS is destroyed for every equivalent of MetO that is reduced back to methionine (Levine et al., 1996). The fact that only specific methionine residues are oxidized, and that oxidable methionines doesn't alter protein function, reinforces the role of methionine as ROS scavenger (Aledo, 2019). In fact, the scavenger role seems to be restricted to a small subset of mitochondrial proteins located in the inner mitochondrial membrane, where ROS is produced (Aledo et al., 2011). Evolutionary studies analysing genetic sequence variations support the acquisition of methionine residues in tissue proteins from short-lived species, rather than the reduction of methionine content in long-lived species (Aledo et al., 2011). The evolution of mitochondrial genome in mammals occurred through the reassignment of the AUA codon from isoleucine to methionine, both of them provided by apolar side chains, which has been interpreted as an adaptative process leading to antioxidant methionine accumulation in respiratory chain complexes (Bender et al., 2008). A meta-analysis of mitochondrial genomes from mammalian species revealed that natural selection, not mutational bias or nucleotide bias, was the driving force in determining protein methionine content in short-lived species (Aledo et al., 2011, 2012). Given these bunch of evidence, Aledo and collaborators suggested that methionine might have been positively selected in short-living species to protect their tissues from ROS attack (Aledo, 2019; Aledo et al., 2015). Specific modulation of methionine

metabolism in a longevity context has already been described in animal models of extended longevity (Parkhitko et al., 2016; Uthus and Brown-Borg, 2006) or under nutritional interventions (Hine et al., 2015). Accordingly, our data supports the idea of a global metabolism remodulation targeted to enrich protein content of not only methionine, but also its related trans-sulphuration and trans-methylation metabolites, in short living species.

Cysteine is a sulphur-containing amino acid that is metabolized from methionine through the trans-sulphuration pathway. As cysteine content depends upon methionine catabolism, reduced content of mitochondrially-encoded cysteine (Moosmann and Behl, 2008), plasma (Lewis et al., 2018) and tissue cysteine is also found in long-lived species. Accordingly, our data revealed a decreased steady-state content of heart cysteine in long-lived species. The fact that mitochondrially-encoded electron transport chain complexes from long-lived species are depleted from cysteine (Moosmann and Behl, 2008), and that cysteine supplementation reverses the decreased ROS production at complex I induced by methionine restriction (Gomez et al., 2015), suggest that there may be adaptative pressures against mitochondrial residues that are easily oxidized. It might be the fact that cysteine thiyl radicals are capable to start irreversible and detrimental protein cross-linking reactions that had led to a negative selection of cysteine through mitochondrial DNA evolution (Aledo et al., 2012). Contrarily to methionine, which has been defined as an anti-oxidant amino acid, cysteine has been proposed to be pro-oxidant (Aledo et al., 2011).

Transsulfuration involves the sequential conversion of homocysteine into cystathionine and cysteine through the enzymes cystathionine-β-synthase and cystathionine-γ-lyase, respectively. A growing body of evidence reported that enhanced transsulfuration promotes longevity (Hine et al., 2015; Tyshkovskiy et al., 2019; Uthus and Brown-Borg, 2006; Wang et al., 2019). The injection of 3-H or 35-S labelled methionine in long-lived Ames dwarf mice revealed an enhanced transsulfuration activity in liver, brain and kidney, in comparison to their short-lived counterparts (Uthus and Brown-Borg, 2006). Cystathionine-γ-lyase was one of the most significant commonly upregulated genes among fifteen different lifespan-extending interventions in mice (Tyshkovskiy et al., 2019). Furthermore, methionine restriction has been found to promote lifespan extension via enhanced cystathionine-γ-lyase and hydrogen sulfide (H_2S) production (Hine et al., 2015; Wang et al., 2019), which upregulates AMPK and inhibits mTORC1, and its downstream effectors 4EBP1 and S6K (Wang et al., 2019). Our data revealed a global decrease of transsulfuration intermediates, as it had been found in long-lived fly strains (Parkhitko et al., 2016). Stress conditions seems to induce the translocation of cystathionine-γ-lyase from the cytoplasm to mitochondria, were it promotes cysteine metabolization along with the H_2S and ATP production (Fu et al., 2012). This mechanism seems to be attributed to the maintenance of sustained ATP mitochondrial production under stress condition.

Other sulphur-containing metabolites are derived from methionine metabolism. Spermidine is a polyamine that feeds trans-methylation metabolism and is associated with longevity. Increased plasma spermidine was found in long-lived Naked mole rat (NMR) (Viltard et al., 2019), and under MR (Bárcena et al., 2018). Neuroprotective and cardioprotective properties have been attributed to spermidine (Clarkson et al., 2004; Eisenberg et al., 2016), which has been described to be an autophagy inductor (Bárcena et al., 2018) and a metabolic mediator of the stress response (Rhee et al., 2007). Taurine and glutathione (GSH), in turn, are synthetised from

cysteine and can be defined as trans-sulphuration products. Antioxidant properties have been ascribed to both metabolites (Gould and Pazdro, 2019; Ito et al., 2014), being taurine an autophagy inductor (Kaneko et al., 2018). Beneficial effects have been reported after the intake of taurine (Yamori et al., 2009) and GSH precursors (Gould and Pazdro, 2019). Furthermore, increased taurine and GSH, along with decreased oxidized GSH (GSSG), was found in long-lived rodents (Lewis et al., 2018; Viltard et al., 2019; Vitvitsky et al., 2013). However, heart content of the three of them, taurine, glutathione and spermidine, were decreased in long-lived species.

Amino acids are the building blocks of proteins, which are the macromolecules responsible for protein function. Globally, amino acids were reduced in heart from long-lived species, which is in good agreement with previous studies in long-lived worms (Castro et al., 2013) and NMR plasma (Lewis et al., 2018; Viltard et al., 2019). The decreased pool of amino acids can be either due to an increased protein catabolism or decreased protein turnover. Few metabolomics studies performed in long-lived animal models suggest an increased protein catabolism, due to an increased levels of plasma degradation products (Lewis et al., 2018) and an up-regulation of amino acid catabolism genes (Hoffman et al., 2020). However, cross-species studies revealed a down-regulation of genes involved in amino acid catabolism (Fushan et al., 2015) and proteolysis (Ma et al., 2016). Furthermore, proteomics data revealed a negative correlation between longevity and global protein turnover rates in fibroblasts (Swovick et al., 2018).

Mitochondria has been pointed as the central organelle regulating longevity. A number of publications have described its structural and metabolic remodulations (mainly at Cx I) leading to an extended longevity (Ayala et al., 2007; Gómez et al., 2007; Lambert et al., 2010; Miwa et al., 2014; Pamplona et al., 2005; Sanchez-Roman et al., 2011; Sanz et al., 2006b) Accordingly, it is not surprising that major metabolic pathways occurring on mitochondrial are also undergoing specific modulations in a longevity context (Faulkes et al., 2019; Heinze et al., 2018; Viltard et al., 2019). In fact, manipulation of longevity-associated genes affect energy metabolism (Yanai et al., 2017). Globally, TCA cycle genes are up-regulated in long-lived mutants (Amador-Noguez et al., 2004; Perron et al., 2000; Wang et al., 2010) and mice subjected to pro-longevity interventions (Tyshkovskiy et al., 2019), suggesting an enhanced TCA activity. However, our metabolomics data suggest a decreased TCA activity, since decreased heart content of (iso)citrate, fumarate and malate was found in heart from long-lived species. Supporting this data, an inter-organ transcriptomic study including 33 species of mammals revealed that genes involved in TCA cycle are down-regulated in liver from long-lived species (Fushan et al., 2015).

Succinate is the only metabolic intermediate of the TCA cycle that increased in heart from long lived species, supporting previous data from long-lived models (Fuchs et al., 2010) and nutritional interventions (Plummer and Johnson, 2019; Weckmann et al., 2018). Metabolization of succinate occurs through $FADH_2$ oxidation, which derives from fatty acids β-oxidation, and relies on electron transport chain complex II (Cx II, also referred as succinate dehydrogenase) (Bezawork-Geleta et al., 2017). Therefore, complex II constitutes a link between lipid and glucose catabolism, which are mutually exclusive of each other (Randle, 1998). Mitochondrial metabolism modulations in NMR have been described (Faulkes et al., 2019; Heinze et al., 2018; Viltard et al., 2019) Specifically, liver proteomics analyses suggested a shift in mitochondrial metabolism from mitochondrial respiration to fatty acid metabolism for energy production (Heinze et al., 2018). Electrons that enter the electron transport chain through Cx II can flow in

a reverse direction (reverse electron transport, RET), and are transferred to Cx I via ubiquinol (Scialò et al., 2017). Although ROS is also produced (Schönfeld et al., 2010), these seems to have signalling roles since it has been reported that ROS derived from RET extends longevity in flies (Scialò et al., 2016). Mechanistic studies also revealed that succinate accumulation is responsible for RET induction (Chouchani et al., 2014). Altogether, these results suggest that long-lived species favour the β-oxidation and the entrance of electrons on the electron transport chain through Cx II by maintaining increased succinate heart content. Accordingly, it has been reported that glucose restriction results in a metabolic reprograming targeted to decrease glycolysis intermediates but increase succinate (Weckmann et al., 2018). Furthermore, β-oxidation influences ETC activity, and cooperate to modulate lipid metabolism and organism fitness (Ramachandran et al., 2019).

Choline is the precursor of phosphocholines (PC), which can be metabolised into lysoPC or phosphoserine by exchanging choline and serine groups (Li and Vance, 2008). Since choline is synthetised from betaine, it can be considered as a lipid intermediate that connects methionine and mitochondrial metabolism. Its association with longevity has already been reported (Pradas et al., 2019b), being plasma choline content decreased in long-lived specimens (Collino et al., 2013; Viltard et al., 2019). Our results reported a negative correlation between heart choline and animal longevity. Recent studies have suggested that choline promotes lipid oxidation (Shen et al., 2020), which might be through increasing succinate (Sivanesan et al., 2018). Since β-oxidation seems to be already boosted in long-lived species, as discussed previously, increasing heart choline might be a strategy developed by short-lived species to improve their metabolic status.

The obtained results suggest that long-lived species undergo a global metabolic modulation targeted to extend longevity. Two premises should be taken into account when discussing these data. Firstly, the difference between factors exerting a small and high longevity effect (Barja, 2019). Inter species studies, as the one that we had performed, are useful to determine high longevity determinators, since it allows to identify molecular traits shared between species that naturally live longer than others. Studies involving long-lived models or exceptionally long-lived species, such as NMR, allow to identify those features having a small longevity effect. These studies are useful to unravel the inter-specimen differences among a specific order o specie, allowing to determine the intracellular adaptations leading to a specimen from a specific specie to achieve a longer longevity, always within a longevity range. Secondly, long-lived species produce less ROS and are provided of intracellular structure stress-resistant (Pamplona and Barja, 2007). Therefore, they have an optimised metabolism targeted to maintain lower basal levels of oxidative damage, rather than invest energy to continuously maintain anti-oxidant mechanisms. Therefore, the induction of anti-oxidant mechanisms should be understood as a cellular mechanism that is acutely induced in response to the intracellular damage that is produced.

Considering those premises, we suggest that longevity is achieved through different intracellular mechanisms, including mitochondrial metabolic remodulation, transsulfuration induction in short-lived species and proper maintenance of proteostasis in long-lived species (**Figure 8**). Mitochondria from long-lived species are optimised through Cx I modulations. We had previously described that long-lived species maintain a lower steady-state content of Cx I, as

well as NDUFV2 subunit (Mota-Martorell et al., 2020b), which might be responsible for the higher electron leak and subsequent ROS production observed in Cx I from short-lived species (Barja, 2013; Ku et al., 1993; Pamplona and Barja, 2007). Glycolysis and β-oxidation occur within mitochondrial matrix. As we had discussed previously, it seems that fatty acid catabolism is the major energy supplier in long-lived species. We propose that by favouring β-oxidation and $FADH_2$ production, long-lived species feed the electron transport chain through Cx II, by-passing the major source of ROS production. Contrarily, short lived-species may promote glycolysis and the subsequent TCA cycle activity and $NADH_2$ production, feeding Cx I and promoting ROS production.

Less ROS is produced in long-lived species, which also protected their cells providing their cellular components with stress-resistant macromolecules. Accordingly, it has been reported that skin-derived protein fibroblasts from long-lived animals are more resistant to oxidative stress (Pickering et al., 2015a). Therefore, long-lived species doesn't need to continuously maintain the activity of antioxidant systems, although they maintain higher basal levels of heat shock proteins (Pride et al., 2015), which might allow them to temporarily induce a fast and efficient anti-oxidant response. Since damage is higher in tissues from short-lived species (Pamplona and Barja, 2007), they structurally protect their proteins by increasing the number of methionine residues, as we had previously discussed, we suggest that short-lived species also modulate intracellular pathways such as transmethylation and transsulfuration, to enhance the synthesis of antioxidant molecules, such as spermidine, taurine and GSH.

mTORC1 has been described to be a master regulator of intracellular metabolism (Kapahi et al. 2010; Antikainen et al. 2017; Weichhart 2018; Papadopoli et al. 2019; Barja 2019; Valvezan and Manning 2019). Furthermore, we had previously reported a basal decreased content and activity of mTORC1 in long-lived species (Mota-Martorell et al., 2020a). The activation of mTORC1 leading leads to the induction of anabolic processes, such as protein synthesis (Caron et al., 2015), and the inhibition catabolic pathways, such as autophagy (Simonsen et al., 2008). Therefore, mTORC1 might be responsible for the global increase of amino acid pool, which also induce mTORC1 activity. Accordingly, we propose that decreased mTORC1 content and activity might be involved in the maintenance of proper proteostasis in long-lived species.

The present work describes a heart species-specific longevity profile associated to a global reorganisation of methionine and energetic metabolism. Specifically, we suggest that enhanced TCA cycle in short-lived species promotes ROS production, whereas enhanced transsulfuration promotes antioxidant synthesis to prevent oxidative damage. Furthermore, our data supports an enhanced proteostasis in long-lived species. Although we had proposed mitochondria and mTORC1 as master regulators of these processes, more work is needed to unravel the specific intracellular modulations leading to these phenotypes and the specific interactions between methionine metabolism, mitochondria and protein turnover systems.

Methods

Chemicals

Unless otherwise specified, all reagents were from Sigma-Aldrich, and of the highest purity available.

Samples

Mammalian species included in the study were male adult specimens with an age representing their 15-30% of their longevity. The recorded values for longevity (in years) were: mouse (*Mus musculus*, n=4), 3.5; rat (*Rattus norvegicus*, n=5), 4.5; guinea pig (*Cavia porcellus*, n=5), 8; rabbit (*Oryctolagus cuniculus*, n=5), 24; pig (*Sus scrofa*, n=5), 27; cow (*Bos taurus*, n=4), 30; and horse (*Equus caballus*, n=5), 46. Rodents and rabbits were obtained from rodent husbandries and sacrificed by decapitation, whereas pigs, cows, and horses were obtained from farms. The animal care protocols were approved by the Animal Experimentation Ethics Committee of the University of Lleida, and all relevant ethical regulations were complied. Heart samples were taken from ventricles of 5-10 animals at the same time after death (5 minutes) and immediately frozen in liquid nitrogen and stored at -80ºC before 2h until analyses.

Sample homogenization and quantification

Heart tissue (≈50 mg of whole tissue) was homogenized in a buffer containing 180mM KCl, 5mM MOPS, 2mM EDTA, 1mM DTPAC adjusted to pH=7.4. Prior homogenization, 1 µM BHT and a mix of proteases inhibitors (GE80-6501-23, Sigma, Madrid, Spain) and phosphatase inhibitors (1mM Na_3VO_4, 1M NaF) was added. After a brief centrifugation (1000 rpm for 3 min at 4°C), supernatants protein concentration was measured using the Bradford method (500-0006, Bio-Rad Laboratories, Barcelona, Spain).

Sample processing

Plasma metabolites extraction was performed based on the methodology previously described (Method 1, Cabré et al., 2016). Briefly, 10 µL of sample homogenates were added to 30 µL of cold methanol containing 1 µg/mL of Phe-^{13}C as internal standard and 1 µM BHT as antioxidant. Then, samples were incubated at -20°C for 1 h and centrifuged at 12,000 *g* for 3 min at 4°C. Finally, the supernatant was filtrated through a 0.22-µm organic diameter filter (CLS8169, Sigma, Madrid, Spain) and transferred to vials with glass inserts for further analysis.

Sulphur-containing metabolites were extracted on the bases of the methodology previously described (Method 2, Liu et al., 2017). Briefly, 2 µL of 5 % DTT diluted in methanol (m/v) were added to 10 µL of sample homogenates. The resulting solution was vortexed for 1 min and allowed to stand at room temperature for 10 min. For protein precipitation, 40 µL of acetonitrile containing 0.1 % formic acid (v/v), 0.05 % trifluoroacetic acid (v/v) and 1 µg/mL of Phe-^{13}C as internal standard was added to the sample, and the solution was vortexed for 2 min. Then, samples were incubated at room temperature for 15 min and centrifuged at 12000 *g* for 3 min. Finally, the supernatant was filtrated through a 0.22-µm organic diameter filter (CLS8169, Sigma, Madrid, Spain) and transferred to vials with glass inserts for further analysis.

Analysis conditions

The individual conditions for the detection and quantification of plasma metabolites are listed in **Supplementary Table 1 (For details, see Table 6 of this Thesis)**. For non-sulphur-containing metabolites, 2 µL of extracted sample was injected based on the method described (Method 1, Cabré et al., 2016). Chromatographic separation was achieved on a reversed-phase column (Zorbax SB-Aq 2.1 × 50 mm, 1.8 µm particle size, Agilent Technologies, Barcelona, Spain) equipped with a pre-column (Zorba-SB-C8 Rapid Resolution Cartridge, 2.1 × 30 mm, 3.5 µm particle size, Agilent Technologies, Barcelona, Spain) with a column temperature of 60 °C. The flow rate was 0.6 mL/min during 19 min. Solvent A was composed of water containing 0.2 % acetic acid (v/v) and solvent B was composed of methanol containing 0.2 % acetic acid (v/v). The gradient started at 2 % of solvent B and increased to 98 % B in 13 min and held for 6 min. Post-time was established in 5 min. Electrospray ionization was performed in both positive and negative ion mode (depending on the target metabolite) using N_2 at a pressure of 50 psi for the nebulizer with a flow of 12 L/min and a temperature of 325 °C, respectively.

For sulphur-containing metabolites, 10 µL of extracted sample was injected based on the method described (Method 2, Liu et al., 2017). Chromatographic separation was achieved on a reversed-phase Supelcosil LC-CN column (Supelco of 4.6 x 250 mm, 5 µm particle size, Sigma, Madrid, Spain) with a column temperature of 30 °C. The flow rate was maintained at 0.5 mL/min during 10 min using a mobile phase of 10:90 acetonitrile/water with 0.1 % formic acid (v/v). Electrospray ionization was performed in both positive and negative ion mode (depending on the target metabolite) using N_2 at a pressure of 50 psi for the nebulizer with a flow of 12 L/min and a temperature of 325 °C, respectively.

Data was collected using the MassHunter Data Analysis Software (Agilent Technologies, CA, USA). Samples were decoded and randomized before injection. Metabolite extraction quality controls (plasma samples with internal Phe-^{13}C) were injected every 10 samples. Peak determination and peak area integration were carried out with MassHunter Quantitative Analyses (Agilent Technologies, CA, USA).

Equipment

The analysis was performed through liquid chromatography coupled to a hybrid mass spectrometer with electrospray ionization and a triple quadrupole mass analyser. The liquid chromatography system was an ultra-performance liquid chromatography model 1290 coupled to LC-ESI-QqQ-MS/MS model 6420 both from Agilent Technologies (Barcelona, Spain).

Statistics

Prior to statistical analyses, data was pre-treated (auto-scaled and log-transformed). Multivariate statistics was performed using Metaboanalyst software (Chong et al., 2019), and include principal component analysis (PCA), hierarchical clustering analysis represented by a heat map, and Random Forest used as a classification algorithm of animal species according to its heart metabolome. Univariate statistics (Pearson correlation, Pearson correlation matrix, linear models and phylogenetic generalised least squares (PGLS) regression) were performed using RStudio (v1.1.453). Correlation functions were included in the packages *Hmisc* (Harrel Jr

and Dupont, 2020) and *corrplot* (Wei and Simko, 2017), and plotted with *ggplot2* (Wickham, 2016). Linear regression was plotted using GrapPhad Prism (v8.0.1). PGLS regression functions were included in the package *caper* (Orme et al., 2018), and used to analyse the correlation of individual metabolites with animal longevity after controlling for phylogenetic relationships, defined by a phylogeny. The phylogenetic tree was constructed using taxa names as described previously (Kumar et al., 2017).

Conflict of interest

The authors declare no conflict of interest

Funding

This work was supported by the Spanish Ministry of Science, Innovation and Universities (RTI2018-099200-B-I00), and the Generalitat of Catalonia (Agency for Management of University and Research Grants (2017SGR696) and Department of Health (SLT002/16/00250)) to R.P. This study has been co-financed by FEDER funds from the European Union ("A way to build Europe"). IRBLleida is a CERCA Programme/Generalitat of Catalonia.

Acknowledgements

M.J. is a 'Serra Hunter' Fellow. N.M-M received a predoctoral fellowship from the Generalitat of Catalonia (AGAUR, ref 2018FI_B2_00104).

Author Contributions

R.P designed the study. N.M.M., M.J., and R.B. performed experimental work. N.M.M, M.J. and R.P. analysed the data. R.P. supervised the design and data interpretation. The manuscript was written by N.M.M, M.J. and R.P. and edited by R.P. All authors discussed the results and commented on the manuscript.

Figures

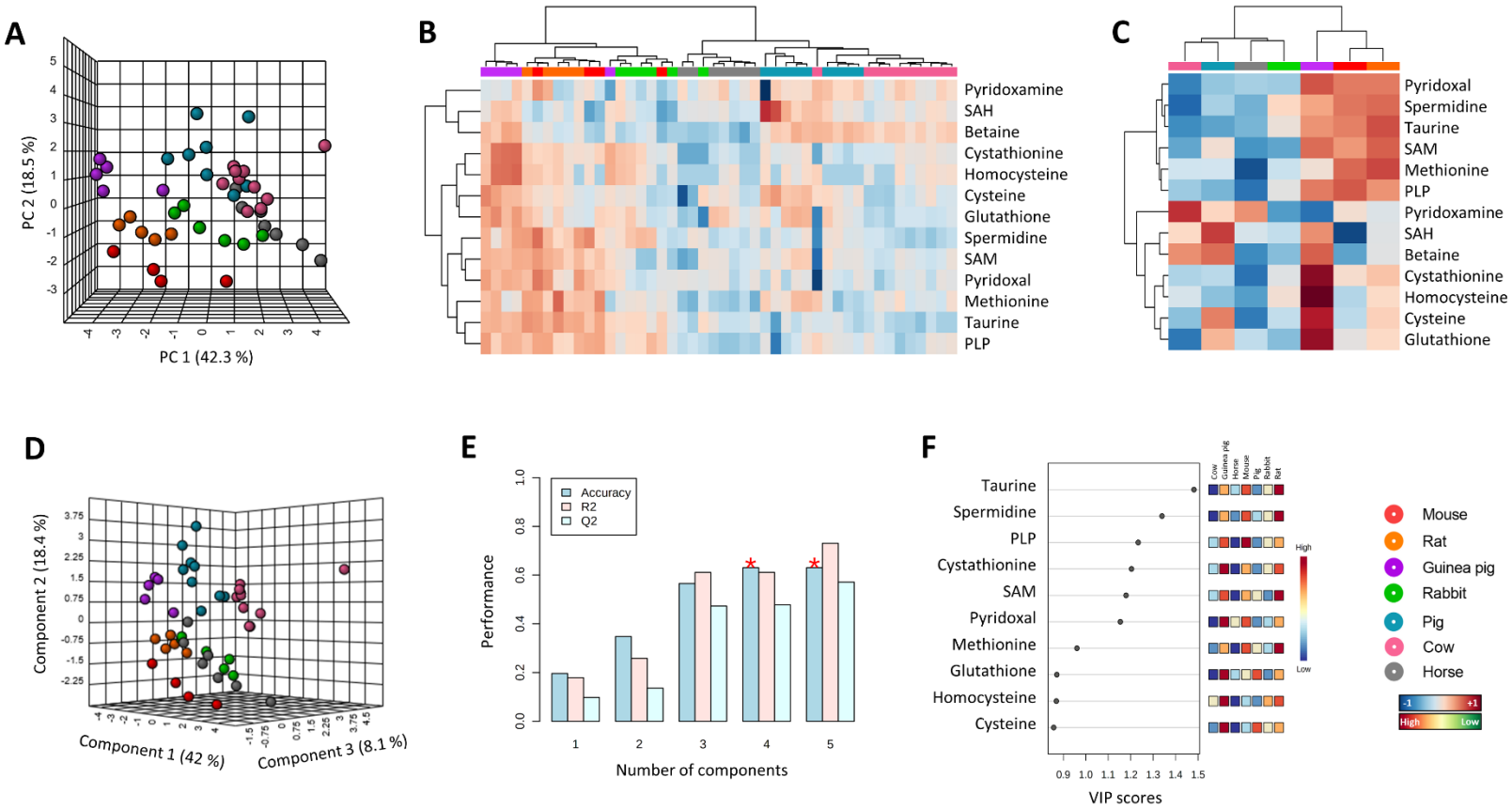

Figure 1. Multivariate statistics reveals a specific methionine heart profile for mammals. A) Principal component analyses (PCA) representation of methionine-related metabolites. X: Principal component 1 (PC1); Y: PC2; Z: PC3. **B)** Hierarchical clustering of individual animal samples according to metabolite abundance. **C)** Hierarchical clustering of animal species according to average metabolite abundance. **D)** Partial least squares discriminant analysis (PLS-DA) representation of metabolite abundance. X: Component 1 (C1); Y: C2; Z: C3. **E)** Cross validation (CV) analyses (10-fold CV method) of the PLS-DA model. **F)** Variable importance projection (VIP) scores indicating the elements which contribute most to define the first component of a PLS-DA.

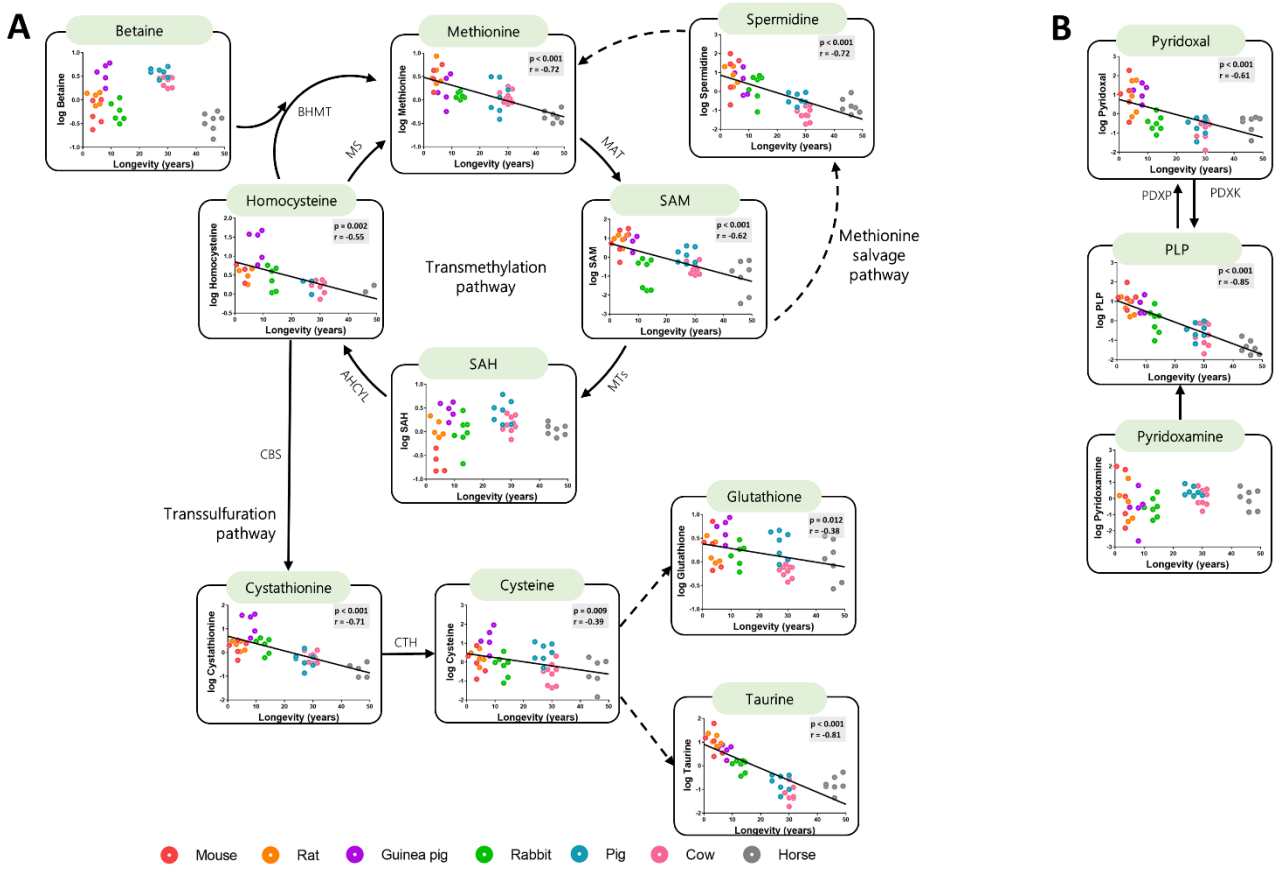

Figure 2. Heart methionine-related metabolites are negatively correlated with animal longevity. Individual heart concentration of the metabolites involved in the transmethylation and transsulfuration pathways (**A**) and vitamin B6 metabolites (**B**). Individual metabolite heart concentrations reported in log(mM /g tissue). Dashed lines refer to reactions in which more than one enzyme is involved. Gray-shaded boxes refer to non-detected metabolites. Pearson correlation was performed. Minimum signification level was set at $p<0.05$. All metabolites were log-transformed in order to accomplish the assumptions of normality. Enzyme codes refer to: Methionine synthase (MS); Betaine-Homocysteine S-methyltransferase (BHMT); Methionine adenosyltransferase (MAT); Methyltransferases (MTs); Adenosylhomocysteinase-like 1 (AHCYL); Cystathionine-β-synthase (CBS); Cystathionine-γ-lyase (CTH); Pyridoxal kinase (PDXK); Pyridoxal phosphatase (PDXP).

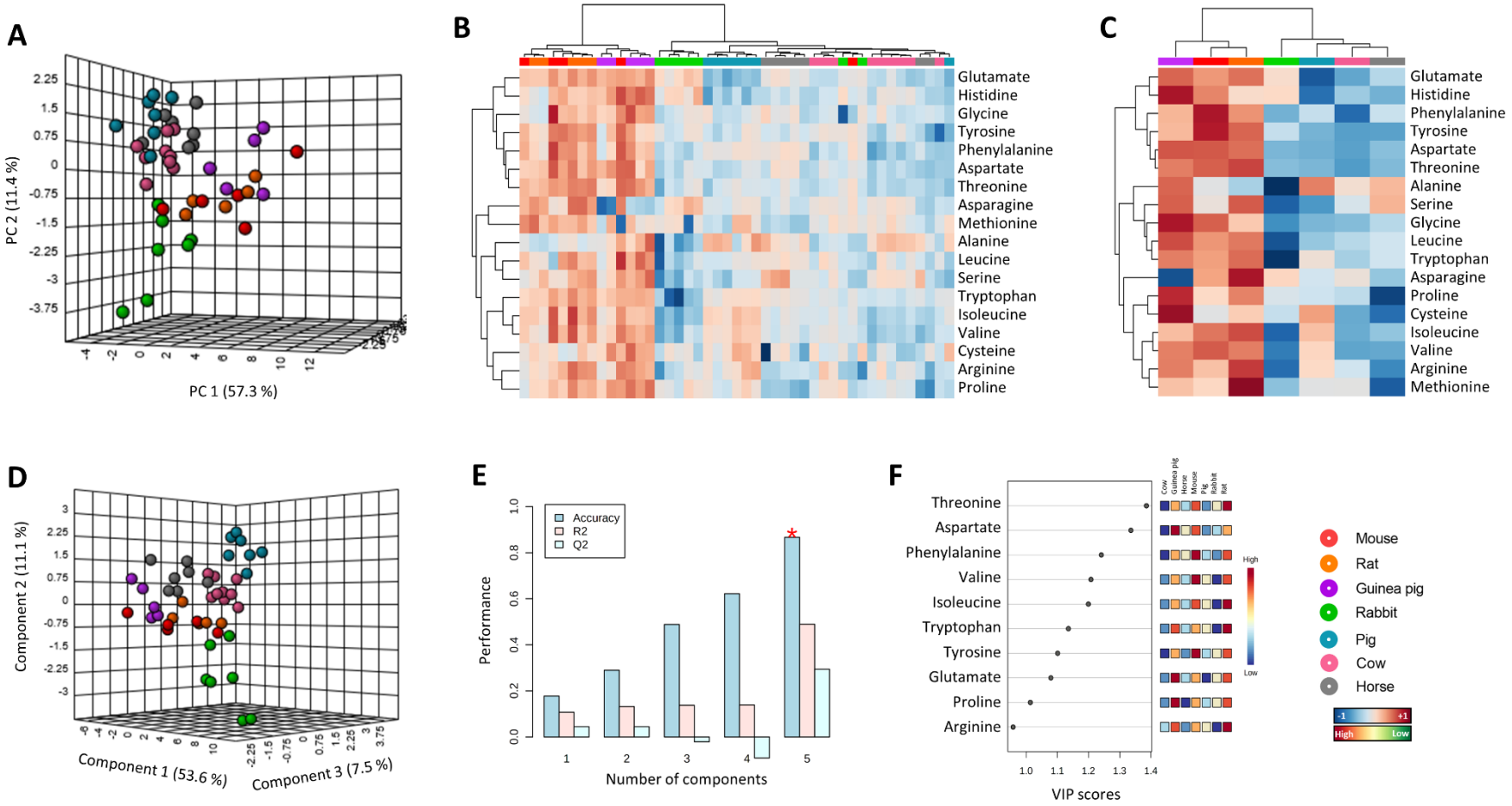

Figure 3. Multivariate statistics reveals a specific amino acids heart profile for mammals. A) PCA representation of methionine-related metabolites. X: PC1; Y: PC2; Z: PC3. **B)** Hierarchical clustering of individual animal samples according to metabolite abundance. **C)** Hierarchical clustering of animal species according to average metabolite abundance. **D)** PLS-DA analysis representation of metabolite abundance. X: C1; Y: C2; Z: C3. **E)** CV analyses (10-fold CV method) of the PLS-DA model. **F)** VIP scores indicating the elements which contribute most to define the first component of a PLS-DA.

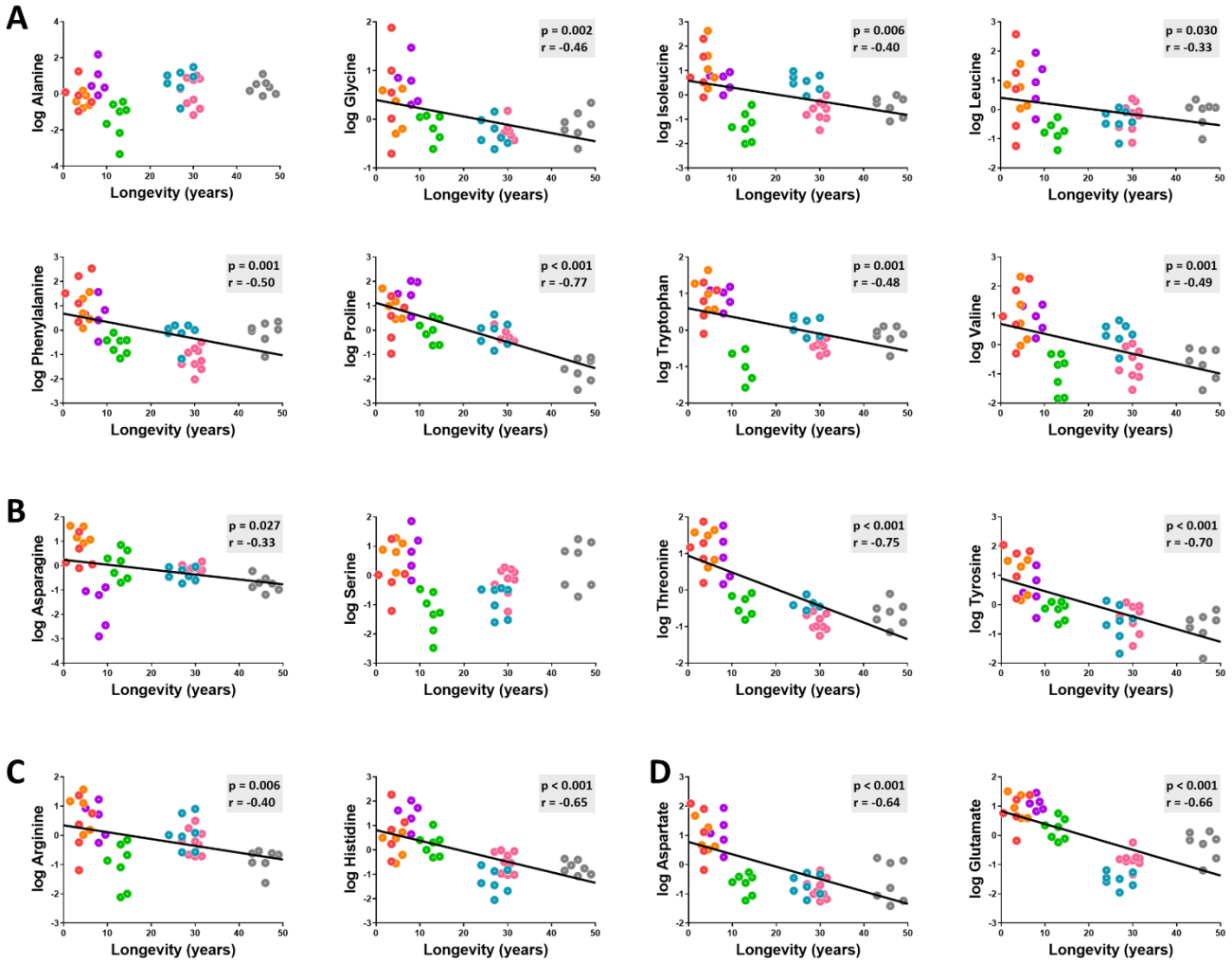

Figure 4. Individual heart concentration of non-polar (A), polar uncharged (B), positively charged (C) and negatively charged (D) amino acids. Individual metabolite heart concentrations reported in log(mM /g tissue). Pearson correlation between heart metabolites and animal longevity was performed (A-D). Minimum signification level was set at $p<0.05$. All metabolites were log-transformed in order to accomplish the assumptions of normality.

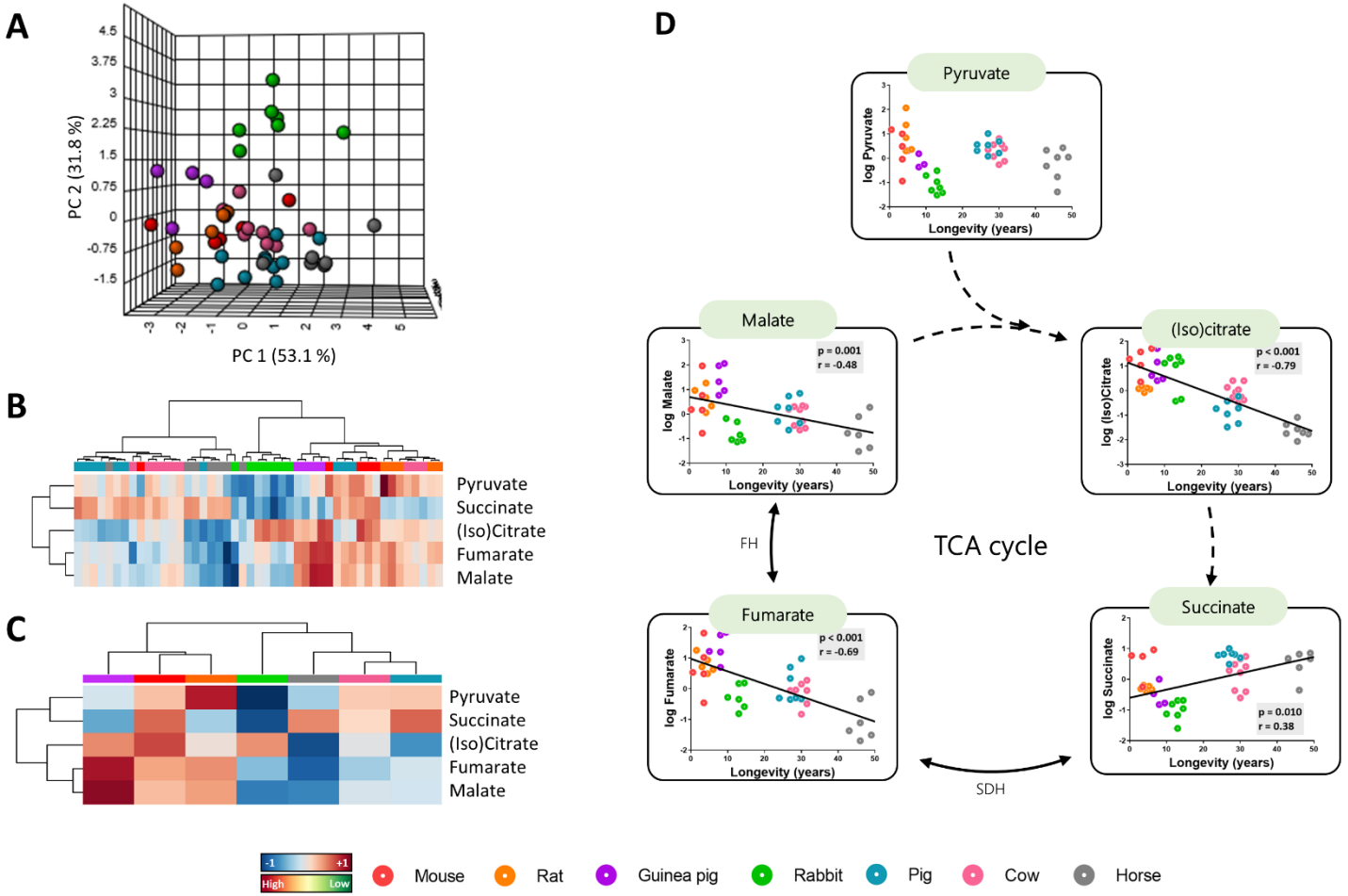

Figure 5. Multivariate statistics reveals a shared TCA cycle intermediates heart profile. A) PCA representation of methionine-related metabolites. X: PC1; Y: PC2); Z: PC3. **B)** Hierarchical clustering of individual animal samples according to metabolite abundance. **C)** Hierarchical clustering of animal species according to average metabolite abundance. **D)** Individual metabolite heart concentrations reported in log(MS Counts/g tissue). Dashed lines refer to reactions in which more than one enzyme is involved. Pearson correlation between heart metabolites and animal longevity was performed (D). Minimum signification level was set at $p<0.05$. All metabolites were log-transformed in order to accomplish the assumptions of normality. Enzyme codes refer to: Succinate dehydrogenase (SDH or Cx II); Fumarate hydratase (FH).

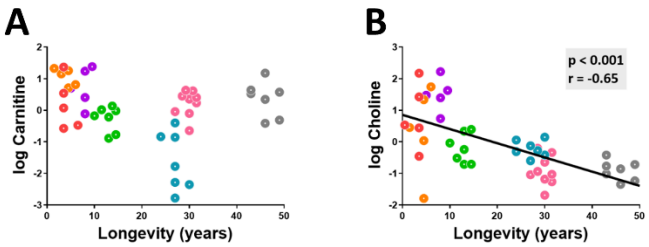

Figure 6. Heart choline is associated with animal longevity. Individual heart concentration of the lipid intermediates choline (**A**) and carnitine (**B**) reported in log(MS Counts/g tissue). Pearson correlation between heart metabolites and animal longevity was performed. Minimum signification level was set at p<0.05. All metabolites were log-transformed in order to accomplish the assumptions of normality.

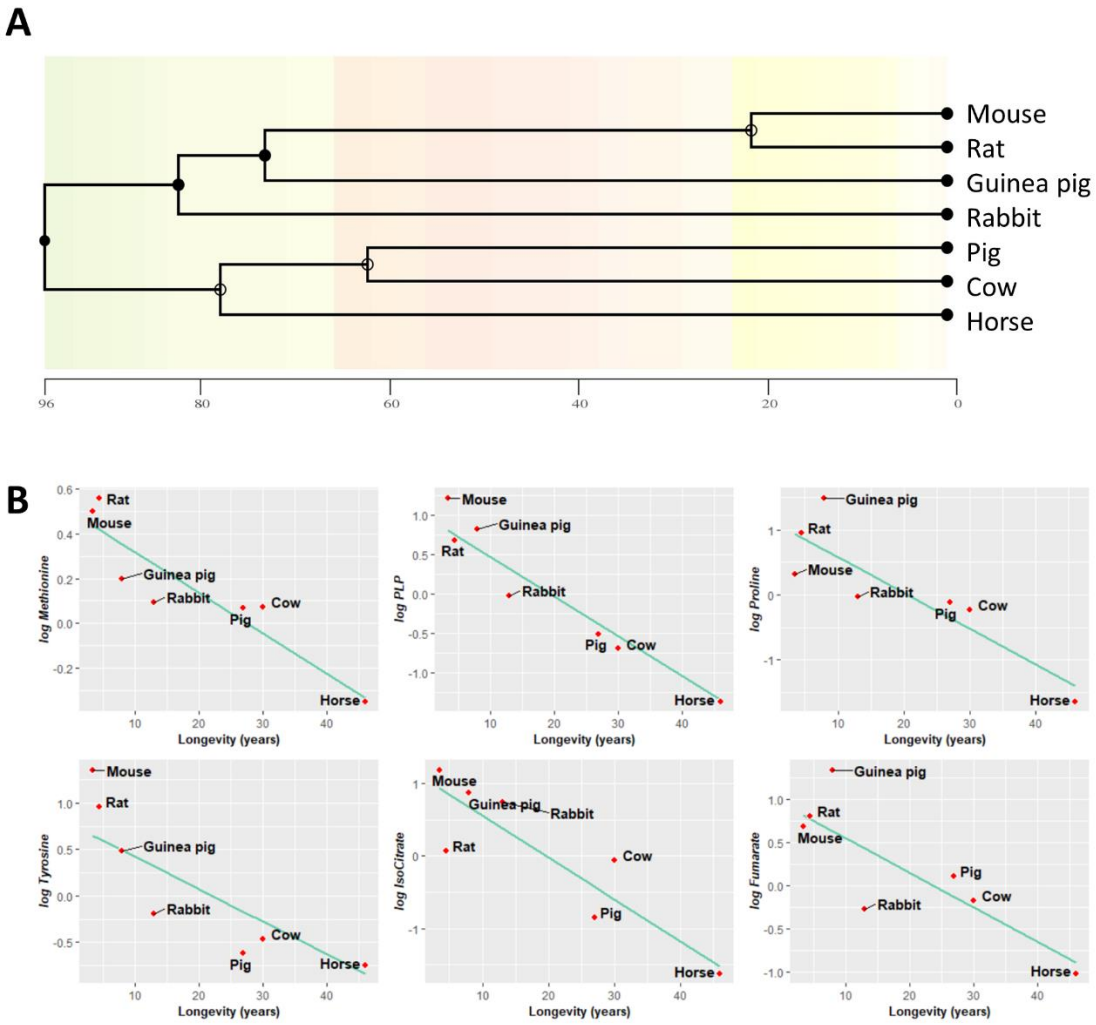

Figure 7. Heart metabolites changes across mammalian longevity after correcting for phylogenetic relationships. **A)** Phylogenetic tree with a timescale of million years ago. **B)** Phylogenetic generalized least squares regression (PGLS) between longevity and heart content of methionine-related metabolites, amino acids and TCA cycle intermediates. Minimum signification level was set at $p<0.05$. All metabolites were log-transformed in order to accomplish the assumptions of normality.

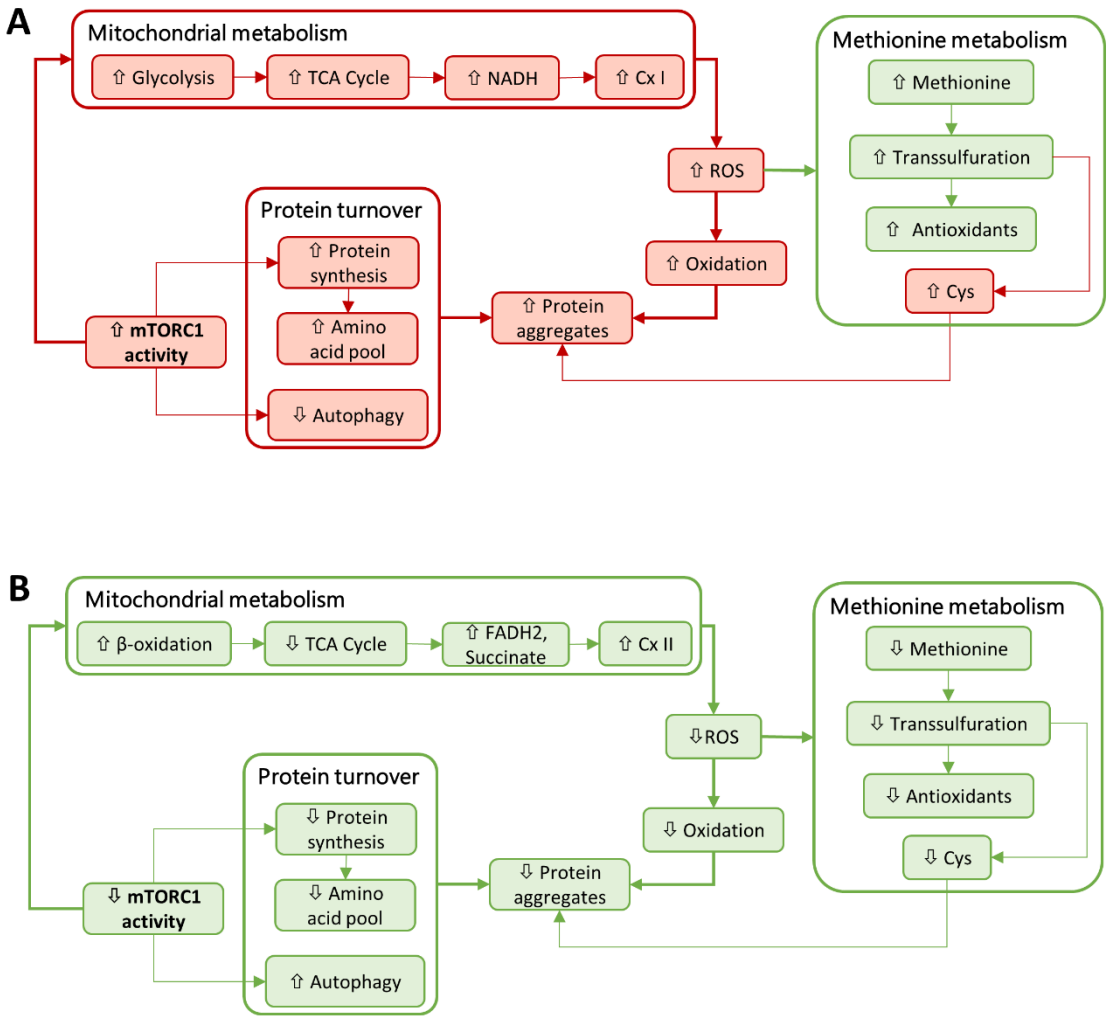

Figure 8. Longevity model for methionine and energetic metabolism modulation in short-lived (A) and long-lived (B) species. Colored boxes are used to indicate up-regulated pro-oxidative (red boxes) or anti-oxidative (green boxes) pathways.

Supplementary table 2. Heart metabolite concentration in mammals. Concentration values are reported in mM per g of heart tissue as mean ± SEM from 5-9 specimens. [a]Concentration values are reported in MS Counts per g of heart tissue.

	Mouse	Rat	Guinea pig	Rabbit	Pig	Cow	Horse
Methionine metabolism							
Betaine[a]	3292 ± 847	6016 ± 726	19814 ± 3683	3355 ± 650	16845 ± 1817	13995 ± 1173	2103 ± 301
Cystathionine	0.10 ± 0.03	0.12 ± 0.02	2.10 ± 0.72	0.13 ± 0.03	0.03 ± 0.01	0.04 ± 0.01	0.01 ± 0.00
Cysteine	0.14 ± 0.04	0.16 ± 0.03	0.49 ± 0.13	0.11 ± 0.02	0.30 ± 0.06	0.08 ± 0.02	0.07 ± 0.02
GSH	2.34 ± 1.16	1.45 ± 0.48	5.00 ± 1.19	1.23 ± 0.30	2.15 ± 0.43	0.41 ± 0.04	1.21 ± 0.43
Homocysteine[a]	1.84 ± 0.64	1.42 ± 0.33	22.5 ± 7.89	1.35 ± 0.41	0.67 ± 0.13	0.66 ± 0.13	0.45 ± 0.11
Methionine	0.91 ± 0.20	1.08 ± 0.24	0.65 ± 0.14	0.40 ± 0.02	0.47 ± 0.08	0.38 ± 0.03	0.22 ± 0.01
Pyridoxal[a]	66.0 ± 14.0	62.7 ± 11.6	67.0 ± 6.20	30.2 ± 2.40	29.1 ± 2.30	26.5 ± 2.00	30.1 ± 2.20
PLP[a]	44.9 ± 11.6	24.7 ± 5.10	28.3 ± 5.30	13.0 ± 3.10	9.90 ± 3.00	7.20 ± 1.40	2.80 ± 0.40
Pyridoxamine[a]	12.3 ± 4.60	7.50 ± 2.30	6.10 ± 1.70	5.7 ± 0.8	8.20 ± 1.30	8.70 ± 0.90	7.90 ± 1.00
SAH	0.02 ± 0.00	0.08 ± 0.01	0.15 ± 0.02	0.08 ± 0.02	0.16 ± 0.02	0.11 ± 0.01	0.08 ± 0.01
SAM	2.03 ± 0.65	1.98 ± 0.26	1.87 ± 0.30	0.32 ± 0.08	0.74 ± 0.10	0.33 ± 0.04	0.26 ± 0.07
Spermidine[a]	232 ± 93.0	134 ± 34.9	98.8 ± 33.8	67.2 ± 15.4	21.9 ± 2.90	8.40 ± 1.20	15.3 ± 3.60
Taurine	413 ± 132	362 ± 53.5	79.8 ± 23.2	28.0 ± 11.1	11.58 ± 2.42	8.32 ± 1.49	14.3 ± 2.54
Amino acids							
Alanine	2.16 ± 0.62	1.54 ± 0.12	2.95 ± 0.47	1.07 ± 0.23	5.17 ± 1.31	5.58 ± 1.42	5.05 ± 0.68
Arginine	1.21 ± 0.30	1.67 ± 0.29	1.38 ± 0.22	0.54 ± 0.09	1.01 ± 0.12	0.87 ± 0.08	0.57 ± 0.04
Asparagine	0.14 ± 0.06	0.33 ± 0.06	ND	0.09 ± 0.02	0.07 ± 0.01	0.06 ± 0.00	0.03 ± 0.00
Aspartate	14.3 ± 4.79	10.4 ± 2.38	12.4 ± 3.23	2.20 ± 0.25	2.69 ± 0.37	2.05 ± 0.25	2.71 ± 0.63
Glutamate	3.66 ± 0.71	4.29 ± 0.67	4.44 ± 0.42	2.24 ± 0.26	0.65 ± 0.10	0.92 ± 0.08	1.44 ± 0.19
Glycine	4.82 ± 2.32	2.33 ± 0.47	4.20 ± 1.14	1.26 ± 0.15	2.36 ± 0.72	1.12 ± 0.09	1.35 ± 0.17
Histidine	1.37 ± 0.50	0.70 ± 0.11	1.90 ± 0.30	0.76 ± 0.11	0.50 ± 0.17	0.47 ± 0.05	0.35 ± 0.03
Isoleucine	35.9 ± 9.77	44.5 ± 12.7	22.3 ± 2.06	7.81 ± 1.27	49.0 ± 10.8	13.7 ± 1.35	14.8 ± 1.33
Leucine	4.79 ± 1.42	4.40 ± 0.54	4.92 ± 0.82	2.12 ± 0.25	2.12 ± 0.35	2.98 ± 0.2	3.12 ± 0.21
Phenylalanine	1.18 ± 0.26	0.73 ± 0.12	0.65 ± 0.13	0.29 ± 0.02	0.67 ± 0.16	0.23 ± 0.02	0.40 ± 0.04
Proline	3.57 ± 1.06	5.77 ± 1.10	9.25 ± 1.64	2.81 ± 0.39	4.21 ± 1.22	2.28 ± 0.19	0.51 ± 0.10
Serine	0.61 ± 0.09	1.60 ± 0.20	1.72 ± 0.46	0.37 ± 0.07	0.62 ± 0.08	0.85 ± 0.09	1.39 ± 0.27

Threonine	3.50 ± 0.79	3.92 ± 0.63	3.07 ± 0.81	0.75 ± 0.12	1.11 ± 0.25	0.52 ± 0.03	0.69 ± 0.09
Tryptophan	0.31 ± 0.07	0.41 ± 0.09	0.36 ± 0.04	0.04 ± 0.01	0.22 ± 0.03	0.10 ± 0.01	0.13 ± 0.01
Tyrosine	1.83 ± 0.47	1.15 ± 0.29	0.67 ± 0.22	0.31 ± 0.03	0.44 ± 0.13	0.23 ± 0.04	0.17 ± 0.03
Valine	2.66 ± 0.60	2.42 ± 0.61	2.20 ± 0.25	0.82 ± 0.10	2.63 ± 0.59	1.04 ± 0.11	0.98 ± 0.10
TCA cycle intermediates							
(Iso)Citrate[a]	777 ± 208	127 ± 7.50	535 ± 218	492 ± 117	33.5 ± 7.60	125 ± 18.7	12.2 ± 2.30
Fumarate[a]	112 ± 27.0	110 ± 10.0	159 ± 20.6	50.2 ± 7.30	66.6 ± 8.50	60.9 ± 8.30	32.4 ± 6.60
Malate[a]	867 ± 245	871 ± 107.1	1365 ± 204	345 ± 49.4	583.5 ± 68.0	569 ± 43.0	370 ± 70.1
Pyruvate[a]	10.2 ± 3.90	26.8 ± 13.7	4.10 ± 0.90	0.90 ± 0.20	7.10 ± 1.40	7.30 ± 1.10	3.70 ± 0.90
Succinate[a]	1049 ± 264	109 ± 8.50	87.1 ± 38.9	28.2 ± 5.80	925 ± 138	500 ± 12+	763 ± 147
Lipid and protein intermediates							
Carnitine [a]	3402 ± 872	5418 ± 425	4589 ± 780	2298 ± 207	811 ± 211	3405 ± 327	3594 ± 482
Choline [a]	2585 ± 964	1981 ± 721	3707 ± 735	879.9 ± 130	2280 ± 848	528 ± 71.3	474 ± 47.9
TMAO [a]	35.5 ± 6.40	52.1 ± 7.30	83.6 ± 14.70	10.5 ± 2.80	21.1 ± 3.30	291 ± 42.4	34.1 ± 8.40

Supplementary table 3. Heart metabolite correlation with animal longevity. Pearson r values are reported. Pagels λ value measures phylogenetic signal for each individual metabolite. Phylogenetic generalized least squares (PGLS) regression between heart metabolites and longevity corrects for phylogenetic relationships. Minimum signification level was set at p<0.05. All metabolites were log-transformed to accomplish the assumptions of normality.

	Pearson		**PGLS**	
	***r* values**	**Sig.**	**λ**	**Sig.**
Methionine metabolism				
Betaine	-0.10	0.526	0	0.834
Cystathionine	-0.70	<0.001	0.7	0.070
Cysteine	-0.39	0.009	1	0.667
GSH	-0.38	0.012	0.7	0.590
Homocysteine	-0.55	0.002	1	0.391
Methionine	-0.72	<0.001	0.5	0.008
Pyridoxal	-0.61	<0.001	1	0.371
PLP	-0.85	<0.001	1	0.001
Pyridoxamine	0.17	0.265	1	0.724
SAH	0.20	0.190	1	0.754
SAM	-0.62	<0.001	1	0.089
Spermidine	-0.72	<0.001	1	0.287
Taurine	-0.81	<0.001	1	0.262
Amino acids				
Alanine	0.25	0.099	0.0	0.501
Arginine	-0.40	0.005	0.8	0.217
Asparagine	-0.33	0.027	0.0	0.434
Aspartate	-0.64	<0.001	1.2	0.336
Glutamate	-0.66	<0.001	1.1	0.492
Glycine	-0.46	0.001	1.2	0.556
Histidine	-0.65	<0.001	1.2	0.177
Isoleucine	-0.40	0.006	1.2	0.674
Leucine	-0.33	0.030	1.2	0.640
Phenylalanine	-0.50	<0.001	0.7	0.481
Proline	-0.77	<0.001	0.5	0.019
Serine	-0.05	0.741	1.0	0.639
Threonine	-0.75	<0.001	1.2	0.265
Tryptophan	-0.48	0.001	1.2	0.803
Tyrosine	-0.70	<0.001	1.2	0.041
Valine	-0.49	<0.001	1.3	0.401
TCA cycle intermediates				
(Iso)citrate	-0.79	<0.001	0.3	0.012
Fumarate	-0.69	<0.001	0.8	0.035
Malate	-0.48	0.001	0.8	0.209
Pyruvate	-0.02	0.893	0	0.686
Succinate	0.38	0.010	1	0.296
Lipid and protein intermediates				
Carnitine	-0.19	0.203	1	0.825
Choline	-0.65	<0.001	1	0.221
TMAO	0.14	0.363	0	0.857

Reduced content of sulphur-containing metabolites and increased succinate is associated with species longevity

Mota-Martorell N[1], Jové M[1], Berdún R[1], Pamplona R[1,*]

[1] Department of Experimental Medicine, Lleida University-Lleida Biomedical Research Institute (UdL-IRBLleida), Lleida, Catalonia, Spain.

[*] **Corresponding author**:

Prof. Reinald Pamplona. Department of Experimental Medicine, University of Lleida-Lleida Biomedical Research Institute (UdL-IRBLleida), Biomedicine 1 building, Av. Rovira Roure 80, Lleida 25198, Spain. E-mail: reinald.pamplona@mex.udl.cat

E-mail addresses of the rest of the authors:

NMM: nataliamotamartorell@gmail.com

MJ: mariona.jove@udl.cat

RB: rebecaberdun@gmail.com

Abstract

Methionine metabolism arises as a key target to elucidate the molecular adaptations underlying animal longevity due to the negative association between longevity and methionine content. The present study follows a comparative approach to analyse plasma methionine metabolic profile using a LC-MS/MS platform from 11 mammalian species with a longevity ranging from 3.5 to 120 years. Our findings demonstrate the existence of a species-specific plasma profile for methionine metabolism associated with longevity characterised by: i) reduced methionine, cystathionine and choline; ii) increased non-polar amino acids; iii) reduced succinate and malate; and iv) increased carnitine. Our results support the existence of plasma longevity features that might respond to an optimised energetic metabolism and intracellular structures found in long-lived species.

Keywords: Amino acids; mass spectrometry; metabolites TCA cycle; transmethylation pathway; transsulfuration pathway.

Introduction

All living organisms use the same twenty amino acids for protein synthesis. However, it seems that the minimum number to build functional proteins is around ten (Fan and Wang, 2003). Indeed, the first proteins were built with the available amino acids generated upon the early earth via abiotic processes (Longo and Blaber, 2012). This abiotic set probably comprised the amino acids alanine (A), aspartate (D), glutamate (E), glycine (G), isoleucine (I), leucine (L), proline (P), serine (S), threonine (T), and valine (V) (Longo and Blaber, 2012). These early amino acids were encoded adaptively by the early genetic code. The evolutionary transition from this initial genetic code to a genetic code where all 20 amino acids are fixated seems to be linked to the adaptations demanded by the appearance of oxygen in the biosphere during early evolution (Granold et al., 2018; Moosmann et al., 2020). Thus, amino acids with increased redox properties such as arginine (R), asparagine (N), cysteine (C), glutamine (Q), histidine (H), lysine (K), methionine (M), phenylalanine (F), tyrosine (Y), and tryptophan (W) were fixated into the new genetic code as adaption to preserve aerobic life (Granold et al., 2018).

Interestingly, the protein compositional content of the sulfur amino acids methionine and cysteine is species-specific and is associated with animal longevity. Thus, long-lived animal species show the lower methionine (Aledo et al., 2011; Pamplona et al., 2005; Portero-Otín et al., 2004; Ruiz et al., 2005) and cysteine (Moosmann, 2011) protein content, surely as adaptive response (Moosmann et al., 2020; Pamplona and Barja, 2011) to the low rate of endogenous damage and highly resistant macromolecular components also present in longevous species (Pamplona and Barja, 2006, 2007, 2011). Reinforcing these observations, the free tissue methionine content is also lower in diverse long-lived animal species (Lewis et al., 2018; Mota-Martorell et al., 2020a); and the pro-longevity effects of nutritional (methionine restriction, MetR) (McIsaac et al., 2016; Pamplona and Barja, 2006) and pharmacological (metformin) (Cabreiro et al., 2013) interventions are mediated by changes in methionine metabolism. In addition to its role in several intracellular processes, methionine is the core of a complex metabolic network which can be divided in three parts: methionine cycle, the transsulfuration pathway, and polyamine biosynthesis (Parkhitko et al., 2019; Sanderson et al., 2019) Significantly, manipulation of each of these branches affects longevity in diverse experimental animal models (McIsaac et al., 2016). Consequently, available findings point to the metabolism of methionine as a key target to study the molecular adaptive mechanisms underlying differences in animal longevity.

The purpose of this study was to investigate the methionine metabolic phenotype of long-lived mammalian species. Specifically, we have designed a study to detect and quantify a panel of metabolites including 35 different molecular species in plasma of eleven mammalian species showing more than one order of magnitude of difference in longevity, from 3.5 years in mice to 120 years in humans. The metabolites detected and quantified were: a) methionine and its related metabolites, including the intermediates of the transmethylation pathway S-adenosylmethionine (SAM), S-adenosylhomocysteine (SAH) and homocysteine; betaine as metabolites involved in the regeneration of methionine plasma levels; the intermediates of the transsulfuration pathway cysteine and cystathionine; taurine and glutathione as downstream metabolites of the transsulfuration pathway; and vitamin B6 metabolites pyridoxal and pyridoxamine, as cofactors of the transsulfuration enzymes; b) additional amino acids including

8 non-polar amino acids (alanine, glycine, leucine, isoleucine, phenylalanine, proline, tryptophan and valine), 4 polar uncharged amino acids (asparagine, serine, threonine and tyrosine), 2 polar negatively charged amino acid (aspartate and glutamate) and 2 polar positively charged amino acids (arginine and histidine); c) TCA cycle metabolites, including pyruvate, citrate, α-ketoglutarate, succinate, fumarate and malate; and d) methionine-derived lipid intermediates such as choline and carnitine. The plasma metabolites profile was determined using a LC-MS/MS platform to define specific phenotypic profiles associated with animal longevity.

Results

Multivariate statistics reveals a species-specific methionine-related metabolites plasma profile

In order to determine whether plasma methionine and its related metabolites concentration differed among mammals, multivariate statistics were applied. Non-supervised principal component analysis (PCA) suggested the existence of a species-specific methionine-related metabolites plasma profile (**Figure 1A**), capable to explain 63.2% of sample variability. A hierarchical clustering of the samples represented by a heat map revealed a good sample clusterization according to animal species (**Figure 1B**). Accordingly, the performance of a Random forest (RF) classification algorithm revealed a species overall classification error < 0.1 (**Figure 1C**), being cystathionine and pyridoxamine the variables with the highest contribution to classification accuracy (**Figure 1D**). These data suggest that RF is a good model to identify specimens of specific mammalian species according to its plasma methionine metabolism profile.

Methionine and cystathionine plasma content are decreased in long-lived animals

The specific changes in plasma methionine and its related metabolites content across animal longevity was evaluated (**Figure 2A, Supplementary Table 2- 3**). Specifically, methionine plasma content was decreased in long-lived animals, as well as the sulphur-containing metabolites cystathionine, taurine and glutathione. However, transmethylation metabolites such as SAM, SAH and betaine, as well as the sulphur-containing metabolites homocysteine and cysteine, remained unchanged across animal longevity. Vitamin B6 intermediate metabolites pyridoxal and pyridoxamine, in turn, were increased in long-lived animals (**Figure 2B**).

Plasma amino acid profile predicts animal species

Since plasma methionine is associated to animal longevity, we hypothesized the possibility that other amino acids could also be involved in the achievement of increased longevity. Specifically, we have been able to unambiguously detect 16 additional amino acids apart from cysteine and methionine. In order to determine whether plasma amino acid content defines animal species, multivariate statistics were applied. Non-supervised PCA suggested the existence of a different plasma amino acid profile within animal species (**Figure 3A**), capable to explain 71.6% of sample variability. A hierarchical clustering of the samples represented by a heat map confirmed the existence of a species-specific plasma amino acid profile (**Figure 3B**). Accordingly, RF classification algorithm revealed a species overall classification error of 0.11, being cow the specimens with the highest classification error (50% of cow specimens weren't properly classified according to its amino acids plasma profile) (**Figure 3C**), being serine the metabolite with the highest contribution to classification accuracy (**Figure 3D**). These data suggest that RF is a good model to identify specimens of specific mammalian species according to its methionine metabolism plasma profile.

The specific changes in plasma amino acid content across animal longevity were also evaluated (**Figure 4, Supplementary Table 2 and 3**). Among the 16 additionally detected amino acid (methionine and cysteine amino acids are not included), we have found a global increase of non-polar amino acids plasma levels in long-lived animals, such as isoleucine, leucine, phenylalanine,

proline, tryptophan and valine (**Figure 4A**). Plasma content of specific polar amino acids such as asparagine, tyrosine and histidine, was also increased in long-lived animals, unlike serine and glutamate, which were decreased (**Figure 4B-D**).

Succinate and malate plasma content are decreased in long-lived animals

Considering that amino acids can be metabolised into TCA cycle intermediates, we have analysed the plasma changes for TCA cycle metabolites. Specifically, we had been able to unambiguously detect 6 intermediates, including pyruvate, citrate, α-ketoglutarate, succinate, fumarate and malate. In order to determine whether animal species have a specific plasma profile for TCA cycle intermediates, multivariate statistics were applied using the plasma concentration of the mentioned metabolites. A hierarchical clustering of the samples represented by a heat map revealed the existence of a shared TCA cycle intermediates plasma profile within animal species (**Figure 5A-B**).

The specific changes in plasma intermediates of TCA cycle across animal longevity were also evaluated (**Figure 5C, Supplementary Table 2 and 3**). Among the 6 detected metabolites, only succinate and malate were associated with animal longevity, being decreased in long-lived animals.

Amino acids and TCA cycle intermediates are bidirectionally related: the amino acids carbon skeleton can be used to synthetize TCA cycle intermediates and vice versa. Therefore, we have estimated the conversion of specific amino acids into the measured TCA intermediates across animal longevity (**Supplementary Figure 1D**). In fact, long-lived animals were found to have increased ratio of pyruvate/glycine and fumarate/aspartate. Positive correlation between fumarate and aspartate was also found (**Supplementary Figure 1E**).

Methionine-derived lipid intermediates in long-lived animals

Methionine metabolism participates in the biosynthesis of lipid intermediates such as choline and carnitine (**Supplementary Table 2 and 3**). In long-lived animals, plasma carnitine was increased (**Figure 6A-B)**, whereas choline decreased (**Figure 6C**).

Pyridoxamine and succinate correlate with longevity after controlling for phylogenetic relationships

Animal species are evolutionarily related, and closely related species often have similar traits due to inheritance from a common ancestor. Most of statistical analysis, such as linear regression, assume the independence of the data, which might not be accomplished from data obtained from these close-related species. In order to find associations between longevity and plasma methionine metabolites, amino acids and TCA cycle intermediates, we have applied a phylogenetic comparative method, such as phylogenetically generalised least squares (PGLS) regression. A phylogenetic tree allowing to evolutionary relate the species in our study was inferred and is constructed in **Figure 7A**.

First of all, under the assumption of a Brownian motion model of evolution (a branching, random walk of trait values from an ancestral value at the root to the tips of the tree (Washburne et al., 2018)), we have estimated the Pagels λ. It allows to measure phylogenetic signal and indicates the relative extent to which a traits' correlation among close relatives match a Brownian motion

model of trait evolution. Pagels λ range from 0 to 1, where λ=1 indicate that trait similarities between species are influenced by phylogenetic relationships; λ=0 indicate that trait similarities between species are independent of phylogenetic relationships; and 0<λ<1 indicate different levels of phylogenetic signal. According to the estimated λ value, we have classified the measured traits according to its association degree with phylogenetic relationships (**Supplementary Table 3**): i) independent (λ=0), representing 60% of the analysed metabolites, including all the TCA cycle intermediates; ii) low dependence (λ<0.6): methionine, taurine , pyridoxamine, glutamate and phenylalanine; iii) mild dependence (λ>0.6): histidine, proline and tryptophan; and strong dependence (λ=1): cystathionine, homocysteine, aspartate, tyrosine, choline. Finally, we have applied a PGLS regression, which revealed that only pyridoxamine (p=0.045, r=-0.66) and succinate (p=0.044, r=-0.69) (**Figure 7B, Supplementary Table 3)** plasma content were positively correlated with animal longevity after controlling for phylogenetic relationships.

Discussion

Blood bathes cells and tissues, and serves as body's major metabolite carrier (Suarez-Diez et al., 2017). Cells release molecules to blood stream as a consequence of their active metabolism, which will be either excreted or transported, and up taken by cells located in different tissues and organs, according to their specific metabolic needs (Psychogios et al., 2011). Therefore, plasma (blood's liquid fraction) metabolome is modulated by cells and tissues, and its composition represents a global metabolic state from a living organism.

The achievement of a long-living phenotype requires the modulation of intracellular pathways which, in turn, regulate intracellular processes (Barja, 2019; Mota-Martorell et al., 2020a, 2020b) that converge in synthetizing resistant intracellular structures, and limiting endogenous damage production (Pamplona and Barja, 2007). Consequently, a globally optimized metabolic state is achieved and expressed as specific transcriptomic (Borrás et al., 2017; Fushan et al., 2015; Gambini et al., 2016; Inglés et al., 2019; Ma et al., 2016; Muntané et al., 2018; Passtoors et al., 2012), proteomic (Heinze et al., 2018; Lehallier et al., 2019), lipidomic (Jové et al., 2013, 2017; Mota-Martorell et al., 2019; Pradas et al., 2019b) and metabolomic (Cheng et al., 2015; Houtkooper et al., 2010; Lewis et al., 2018; Ma et al., 2015) profile for each tissue (Bozek et al., 2017; Ma et al., 2015; Sahm et al., 2018b). In the present study we have identified the methionine-related metabolites as clue molecules defining a species-specific plasma metabolic profile. Furthermore, our model suggests that using these metabolites it is possible to identify the species of a mammalian specimen, being plasma cystathionine and pyridoxamine, along with the amino acid serine, the highest predictors.

Reduced methionine content had been widely associated with extended longevity. Accordingly, previous studies had reported reduced DNA methionine-encoded (Aledo et al., 2011), as well as decreased tissue (Pamplona et al., 2005; Portero-Otín et al., 2004; Ruiz et al., 2005) and plasma (Lewis et al., 2018) content in long-lived species. Furthermore, MetR leads to an extended longevity in different experimental models (McIsaac et al., 2016; Pamplona and Barja, 2006, 2011). Few studies have unfocused from methionine and evaluated global changes in plasma (Lewis et al., 2018; Viltard et al., 2019) and tissue (Mota-Martorell et al., 2020a) methionine metabolism intermediates associated to animal longevity. Globally, these studies suggested that species longevity is associated with reduced sulphur-containing metabolites, and accompanied by decreased methionine plasma content (Lewis et al., 2018; Viltard et al., 2019). Accordingly, our study revealed reduced steady-state plasma levels of methionine and cystathionine in long-lived mammals.

Transsulfuration, which starts with the metabolization of homocysteine into cystathionine via cystathionine-β-synthase (CBS), has been widely associated with animal longevity. Specifically, transsulfuration is enhanced in long-lived flies (Parkhitko et al., 2019) and mice (Vitvitsky et al., 2013), in comparison to their non-longevous counterparts. The longevity effects of transsulfuration have been attributed to the generation of molecules with antioxidant properties such as hydrogen sulfide (H_2S) (Hine et al., 2015; Miller and Roth, 2007; Ng et al., 2020; Wei and Kenyon, 2016), glutathione and taurine (Ito et al., 2014; Yamori et al., 2009). However, our study reveals that plasma transsulfuration intermediates or products remain unchanged (homocysteine and cysteine) across species, and even decreased (cystathionine, glutathione and taurine) in long-lived mammalian species. Under the presumption that "less is

more" in long-lived species, we suggest that the steady state levels of these intermediates aren't increased since long-lived species produce less intracellular damage and are structurally built upon more resistant molecules. Therefore, these long-lived species don't need to synthetize a vast amount of antioxidant and can re-direct the energy saved to maintain other vital cellular functions. Altogether, these data support the existence of basal metabolic differences that are associated with inter-species longevity, such as decreased methionine and cystathionine plasma levels.

Proteins are essential structural components, but also the effectors of intracellular functions. Long-lived species have evolved by optimising protein composition to ensure proper protein structure, function and turnover. Synthesising more resistant proteins (Pickering et al., 2015a) and enhancing autophagy (Pickering et al., 2015b; Pride et al., 2015; Rodriguez et al., 2016) to efficiently clear altered and non-functional proteins results in a negative correlation between global protein turnover and species longevity (Swovick et al., 2018). Accordingly, our data reveals a globally increased plasma free amino acid pool in long-lived species. Furthermore, the decreased serine plasma content, which can provide one-carbon units to regenerate methionine from homocysteine under methionine depleted conditions (Maddocks et al., 2016), as we reported in the present study, supports the role of methionine metabolism as determinants of animal species and longevity.

Mitochondrion structural and functional adaptations associated with longevity had been widely described, and include decreased membrane unsaturation (Pamplona and Barja, 2007), lower permeability (Mota-Martorell et al., 2020b; Zhou et al., 2019) and modulation of mitochondrial dynamics (Sharma et al., 2019). Nonetheless, quantitative and qualitative complex I (Cx I) adaptations, such as reduced total content (Pamplona and Barja, 2007), and Cx I specific subunits (Mota-Martorell et al., 2020b) that support its assembly (Miwa et al., 2014), resulting in reduced reactive oxygen species (Barja and Herrero, 1998; Herrero and Barja, 1997, 1998; Miwa et al., 2014; Pamplona and Barja, 2006, 2007), constitutes a hallmark of longevity.

Electron transport chain is feed from electron donors derived from the tricarboxylic acid (TCA) cycle, such as NADH and $FADH_2$, which transfer electrons to Cx I and Cx II, respectively. As expected, TCA cycle modulations have also been associated with animal longevity, and include upregulation of TCA cycle genes (Amador-Noguez et al., 2004; Kamei et al., 2011; Ma et al., 2016; Wang et al., 2010; Yanai et al., 2017), which might result in an optimised energetic metabolism. In contrast with these data, our results revealed reduced basal content of succinate and malate in plasma from long-lived species, supporting the existence of metabolic adaptations associated to species longevity, different from those specific individual adaptations associated to specimen longevity. Succinate is the substrate of Cx II, and the only TCA cycle intermediate known to trigger organismal functions regulating the immune system (Martínez-Reyes and Chandel, 2020). We suggest that since long-lived species have an optimised metabolism with more efficient Cx I, they rely less in succinate and Cx II activity to enter electrons and generate ATP, therefore, they have reduced steady levels of succinate compared to short-lived ones. Accordingly, increased plasma levels of malate in aged individuals are associated with higher cardiovascular risk (Cheng et al., 2015).

Methionine metabolism and TCA cycle are connected with lipid metabolism through choline and carnitine, respectively. Choline is synthetized from betaine, and is the biosynthetic precursor of

phosphocholines (PC), which can be metabolised into lysoPC or catabolised into phosphoserine by exchanging choline by serine groups (Li and Vance, 2008). Previous studies in long-lived species had already reported the existence of a specific plasma PC profile in centenarians (Collino et al., 2013; Pradas et al., 2019b), as well as a reduction of PC content in centenarians (Collino et al., 2013) and the exceptionally long-living naked-mole rat (NMR) (Viltard et al., 2019). Our results revealed reduced plasma choline in long-lived species, which might result in a reduced PC biosynthesis, although its reduced plasma content as a consequence of increased PC biosynthesis cannot be discarded.

Carnitine acts as a shuttle essential to transport fatty acids from the cytosol to the mitochondrial matrix, where β-oxidation occurs (Calabrese et al., 2012). When combined with fatty acids, acyl-carnitines are formed. Previous studies revealed that carnitine plasma content is reduced in NMR compared to mice (Viltard et al., 2019). Our data revealed higher plasma carnitine content in long-lived species, which might suggest an improved β-oxidation. Accordingly, previous proteomic results revealed a shift in mitochondrial metabolism from mitochondrial respiration to fatty acid metabolism for energy production in NMR in comparison to short-lived guinea pig (Heinze et al., 2018). Supporting our results, recent studies found an association between reduced serum carnitine and human frailty (Rattray et al., 2019). Furthermore, carnitine intake has been demonstrated to have neuroprotective effects (Burks et al., 2019; Calabrese et al., 2012).

Comparative studies across species with different lifespan are a powerful source of information to identify mechanisms linked to extended longevity (Bozek et al., 2017; Ma et al., 2015; Mota-Martorell et al., 2020a, 2020b). However, due to species evolution, inter-species studies have to deal with the problem of non-independence of the data due to evolutionary relationships (Cooper et al., 2016). Therefore, it's important to elucidate whether a specific trait correlates with longevity differences, or alternatively, these differences arise because of the data similarity, by applying statistical phylogenetic comparative methods, such as PGLS (Jové et al., 2013; Lindborg et al., 2015; Mayne et al., 2019; Minias and Podlaszczuk, 2017; Mota-Martorell et al., 2020a, 2020b; Muntané et al., 2018; Wilkinson and Adams, 2019). In the present study, PGLS revealed that pyridoxamine and succinate plasma content changes associated with longevity weren't due inter-species relationships. Therefore, these results support the involvement of sulphur-containing metabolites biosynthesis and energetic metabolism in determining species longevity.

Globally, the obtained results reveal the existence of a species-specific plasma methionine metabolic profile. Furthermore, this metabolic profile is an optimised feature of species longevity, characterised by i) reduced plasma levels of sulphur-containing metabolites methionine and cystathionine and TCA cycle intermediates succinate and malate; ii) increased amino acids; iii) reduced choline; and iv) increased carnitine in long-lived species.

It is important to remark that although plasma composition reflects organismal metabolic status, we cannot disregard the possibility of the existence of controlled mechanisms regulating plasma composition, such as metabolite transports, which might differ across tissue and organs. Furthermore, intracellular function of the described metabolites has already been described, but a lack of knowledge is found regarding plasmatic function of plasma metabolites. Therefore,

more studies focused on elucidating the function of the plasmatic profiles associated to longevity is needed.

The present work describes a species-specific longevity profile, which is the result of a whole organismal metabolic reorganisation that exert a “big effect” on longevity, but needs to be differentiated from other metabolic adaptations exerting a “small effect” on longevity, as suggested previously (Barja, 2019). The later, represent the individual metabolic adaptations resulting from genetic modulations or nutritional interventions that determine whether a specimen from a specific specie becomes long-lived on not. Most of the efforts have been directed to study the longevity metabolomic determinants of long-lived specimens (García-Cañaveras et al., 2012; Lewis et al., 2018; Viltard et al., 2019), vertebrates (Hoffman et al., 2017; Vitvitsky et al., 2013) and invertebrate long-lived mutants (Gubina et al., 2019; Parkhitko et al., 2019), or its modulation by nutritional interventions increasing longevity (Jové et al., 2014; Pradas et al., 2019a; Walters et al., 2018). The results obtained from these studies are of big value since allow to describe strategies that would be feasible to apply to humans in order to improve our health span. However, these results only represent the “small effect” determinants of longevity, and might resemble, such as decreased Cx I (Miwa et al., 2014; Mota-Martorell et al., 2020b; Pamplona et al., 2005) and/or reduced intracellular damage (Gomez et al., 2015; Pamplona et al., 2005; Ruiz et al., 2005), or differ, such as plasma metabolic profile (García-Cañaveras et al., 2012; Hoffman et al., 2017; Lewis et al., 2018; Rattray et al., 2019; Viltard et al., 2019; Walters et al., 2018), from those obtained when comparing species of different longevities, as described previously. In the recent years, the number of inter-species studies have increased, since they provide the basal metabolic status of each species and to compare it with other species, which is essential to unravel the mechanisms underlying an improved longevity and to properly design strategies to improve human health span.

Methods

Chemicals

Unless otherwise specified, all reagents were from Sigma-Aldrich, and of the highest purity available.

Samples

Mammalian species included in the study were male adult specimens with an age representing their 15-30% of their longevity. The recorded values for longevity (in years) were: mouse (*Mus musculus*, n=4), 3.5; rat (*Rattus norvegicus*, n=5), 4.5; guinea pig (*Cavia porcellus*, n=5), 8; rabbit (*Oryctolagus cuniculus*, n=5), 13; sheep (*Ovis aries*, n=5), 20; dog (*Canis lupus*, n=5), 24; pig (*Sus scrofa*, n=5), 27; cow (*Bos taurus*, n=4), 30; cat (*Felis catus*, n=5), 30; horse (*Equus caballus*, n=5), 46; and human (*Homo sapiens*, n=6), 120. Rodents and rabbits were obtained from rodent husbandries and sacrificed by decapitation, whereas plasma from dogs, cats, sheeps, pigs, cows, and horses were obtained from farms. For humans, plasma samples were obtained from healthy adult individuals. The animal care protocols were approved by the Animal Experimentation Ethics Committee of the University of Lleida, and all relevant ethical regulations were complied. Human protocols were approved by the Committee for Ethics in Clinical Research of the Hospital Universitari Arnau de Vilanova, in accordance with the Declaration of Helsinki. All subjects were fully informed of the aims and scope of the research and signed an informed consent. Blood samples from 4-6 animals and subjects were obtained after fasting (8–12 h) by venipunction, centrifuged to separate plasma fraction, which was immediately frozen in liquid nitrogen and stored at -80ºC before 4h until analyses.

Sample processing

Plasma metabolites extraction was performed based on the methodology previously described (Method 1, Cabré et al., 2016). Briefly, 10 µL of plasma were added to 30 µL of cold methanol containing 1 µg/mL of Phe-^{13}C as internal standard and 1µM BHT as antioxidant. Then, samples were incubated at -20°C for 1 hour and centrifuged at 12.000 *g* for 3 min at 4°C. Finally, the supernatant was filtrated through a 0.22-µm organic diameter filter (CLS8169, Sigma, Madrid, Spain) and transferred to vials with glass inserts for further analysis.

Sulphur-containing metabolites were extracted on the bases of the methodology previously described (Method 2, Liu et al., 2017). Briefly, 2 µL of 5 % DTT diluted in methanol (m/v) were added to 10 µL of plasma. The resulting solution was vortexed for 1 min and allowed to stand at room temperature for 10 min. For protein precipitation, 40 µL of acetonitrile containing 0.1 % formic acid (v/v), 0.05 % trifluoroacetic acid (v/v) and 1 µg/mL of Phe-^{13}C as internal standard was added to the sample, and the solution was vortexed for 2 min. Then, samples were incubated at room temperature for 15 min and centrifuged at 12000 *g* for 3 min. Finally, the supernatant was filtrated through a 0.22-µm organic diameter filter (CLS8169, Sigma, Madrid, Spain) and transferred to vials with glass inserts for further analysis.

Analysis conditions

The individual conditions for the detection and quantification of plasma metabolites are listed in **Supplementary Table 1 (For details, see Table 6 of this Thesis)**. For non-sulphur-containing metabolites, 2 µL of extracted sample was injected based on the method described (Method 1, Cabré et al., 2016). Chromatographic separation was achieved on a reversed-phase column (Zorbax SB-Aq 2.1 × 50 mm, 1.8 µm particle size, Agilent Technologies, Barcelona, Spain) equipped with a pre-column (Zorba-SB-C8 Rapid Resolution Cartridge, 2.1 × 30 mm, 3.5 µm particle size, Agilent Technologies, Barcelona, Spain) with a column temperature of 60 °C. The flow rate was 0.6 mL/min during 19 min. Solvent A was composed of water containing 0.2 % acetic acid (v/v) and solvent B was composed of methanol containing 0.2 % acetic acid (v/v). The gradient started at 2 % of solvent B and increased to 98 % B in 13 min and held for 6 min. Post-time was established in 5 min. Electrospray ionization was performed in both positive and negative ion mode (depending on the target metabolite) using N_2 at a pressure of 50 psi for the nebulizer with a flow of 12 L/min and a temperature of 325 °C, respectively.

For sulphur-containing metabolites, 10 µL of extracted sample was injected based on the method described (Method 2, Liu et al., 2017). Chromatographic separation was achieved on a reversed-phase Supelcosil LC-CN column (Supelco of 4.6 x 250 mm, 5 µm particle size, Sigma, Madrid, Spain) with a column temperature of 30 °C. The flow rate was maintained at 0.5 mL/min during 10 min using a mobile phase of 10:90 acetonitrile/water with 0.1 % formic acid (v/v). Electrospray ionization was performed in both positive and negative ion mode (depending on the target metabolite) using N_2 at a pressure of 50 psi for the nebulizer with a flow of 12 L/min and a temperature of 325 °C, respectively.

Data was collected using the MassHunter Data Analysis Software (Agilent Technologies, CA, USA). Samples were decoded and randomized before injection. Metabolite extraction quality controls (plasma samples with internal Phe-^{13}C) were injected every 10 samples. Peak determination and peak area integration were carried out with MassHunter Quantitative Analyses (Agilent Technologies, CA, USA).

Equipment

The analysis was performed through liquid chromatography coupled to a hybrid mass spectrometer with electrospray ionization and a triple quadrupole mass analyser. The liquid chromatography system was an ultra-performance liquid chromatography model 1290 coupled to LC-ESI-QqQ-MS/MS model 6420 both from Agilent Technologies (Barcelona, Spain).

Statistics

Prior to statistical analyses, data was pre-treated (auto-scaled and log-transformed). Multivariate statistics was performed using Metaboanalyst software (Chong et al., 2019), and include principal component analysis (PCA), hierarchical clustering analysis represented by a heat map, and Random Forest used as a classification algorithm of animal species according to its plasma metabolome. Univariate statistics (Pearson correlation, Pearson correlation matrix, linear models and phylogenetic generalised least squares (PGLS) regression) were performed using RStudio (v1.1.453). Correlation functions were included in the packages *Hmisc* (Harrel Jr

and Dupont, 2020) and *corrplot* (Wei and Simko, 2017), and plotted with *ggplot2* (Wickham, 2016). Linear regression was plotted using GrapPhad Prism (v8.0.1). PGLS regression functions were included in the package *caper* (Orme et al., 2018), and used to analyse the correlation of individual metabolites with animal longevity after controlling for phylogenetic relationships, defined by a phylogeny. The phylogenetic tree was constructed using taxa names as described previously (Kumar et al., 2017).

Data availability

All data generated or analysed during this study are included in this published article (and its supplementary information files)

Conflict of interest

The authors declare no conflict of interest

Funding

This work was supported by the Spanish Ministry of Science, Innovation and Universities (RTI2018-099200-B-I00), and the Generalitat of Catalonia (Agency for Management of University and Research Grants (2017SGR696) and Department of Health (SLT002/16/00250)) to R.P. This study has been co-financed by FEDER funds from the European Union ("A way to build Europe"). IRBLleida is a CERCA Programme/Generalitat of Catalonia.

Acknowledgements

M.J. is a 'Serra Hunter' Fellow. N.M-M received a predoctoral fellowship from the Generalitat of Catalonia (AGAUR, ref 2018FI_B2_00104).

Author Contributions

R.P designed the study. N.M.M., M.J., and R.B. performed experimental work. N.M.M, M.J. and R.P. analysed the data. R.P. supervised the design and data interpretation. The manuscript was written by N.M.M, M.J. and R.P. and edited by R.P. All authors discussed the results and commented on the manuscript.

Figures

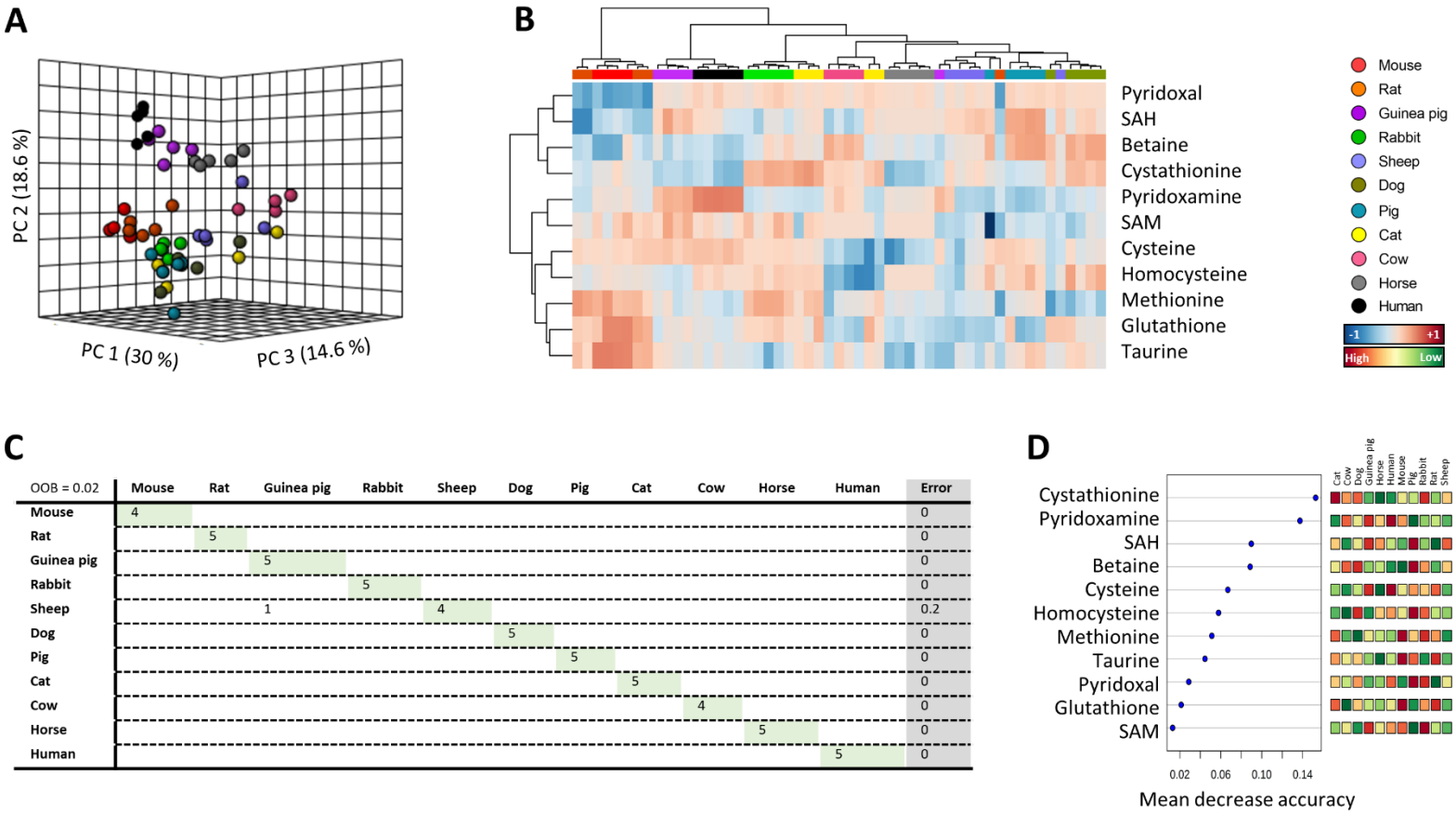

Figure 1. Multivariate statistics reveals a species-specific methionine plasma profile. A) Principal component analyses (PCA) representation of methionine-related metabolites. X: Principal component 1 (PC1); Y: PC2; Z: PC3. **B)** Hierarchical clustering of individual animal samples according to metabolite abundance. **C)** Random forest (RF) classification algorithm. **D)** VIP scores for RF.

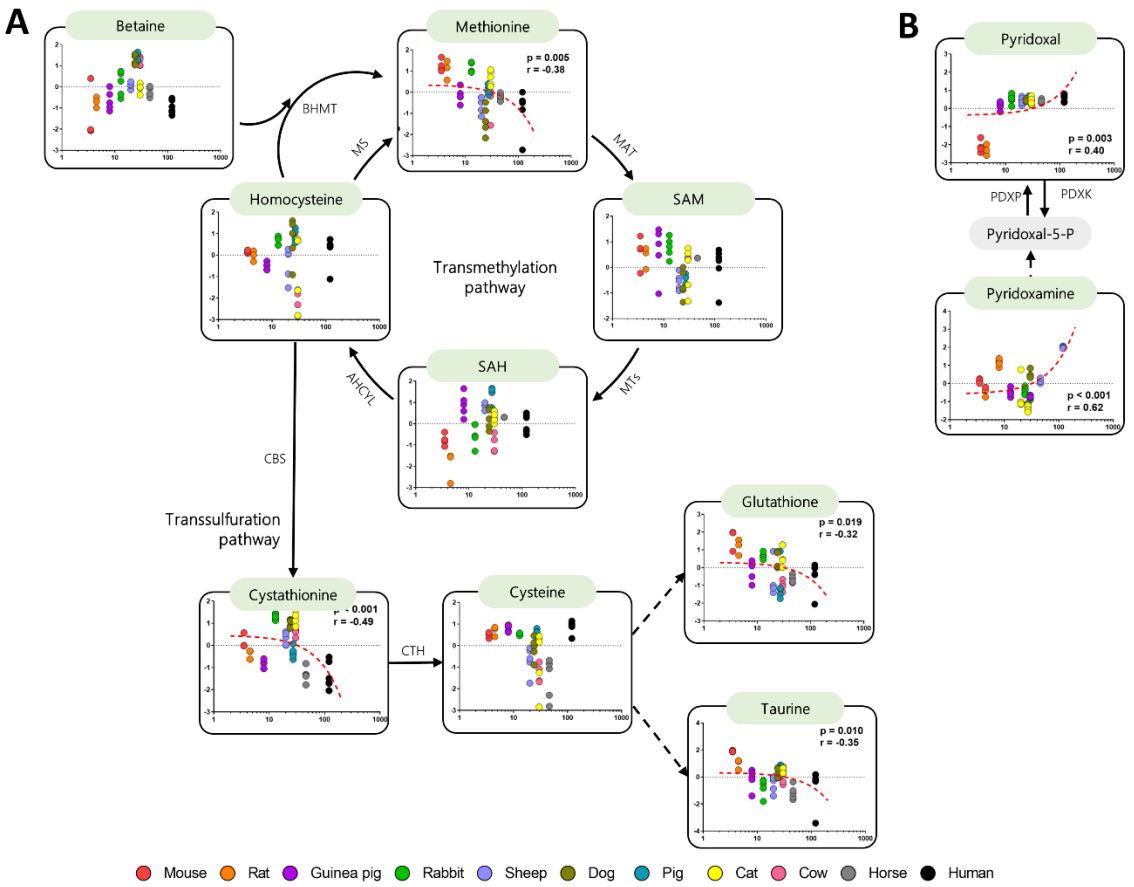

Figure 2. Plasma methionine-related metabolites and its correlation with animal longevity. Individual plasma correlation of the metabolites with animal longevity involved in the transmethylation and transsulfuration pathways (**A**) and vitamin B6 metabolites (**B**). Dashed lines refer to reactions in which more than one enzyme is involved. Gray-shaded boxes refer to non-detected metabolites. Pearson correlation was performed. Minimum signification level was set at $p<0.05$. All metabolites were log-transformed in order to accomplish the assumptions of normality. Enzyme codes refer to: Methionine synthase (MS); Betaine-Homocysteine S-methyltransferase (BHMT); Methionine adenosyltransferase (MAT); Methyltransferases (MTs); Adenosylhomocysteinase-like 1 (AHCYL); Cystathionine-β-synthase (CBS); Cystathionine-γ-lyase (CTH); Pyridoxal kinase (PDXK); Pyridoxal phosphatase (PDXP).

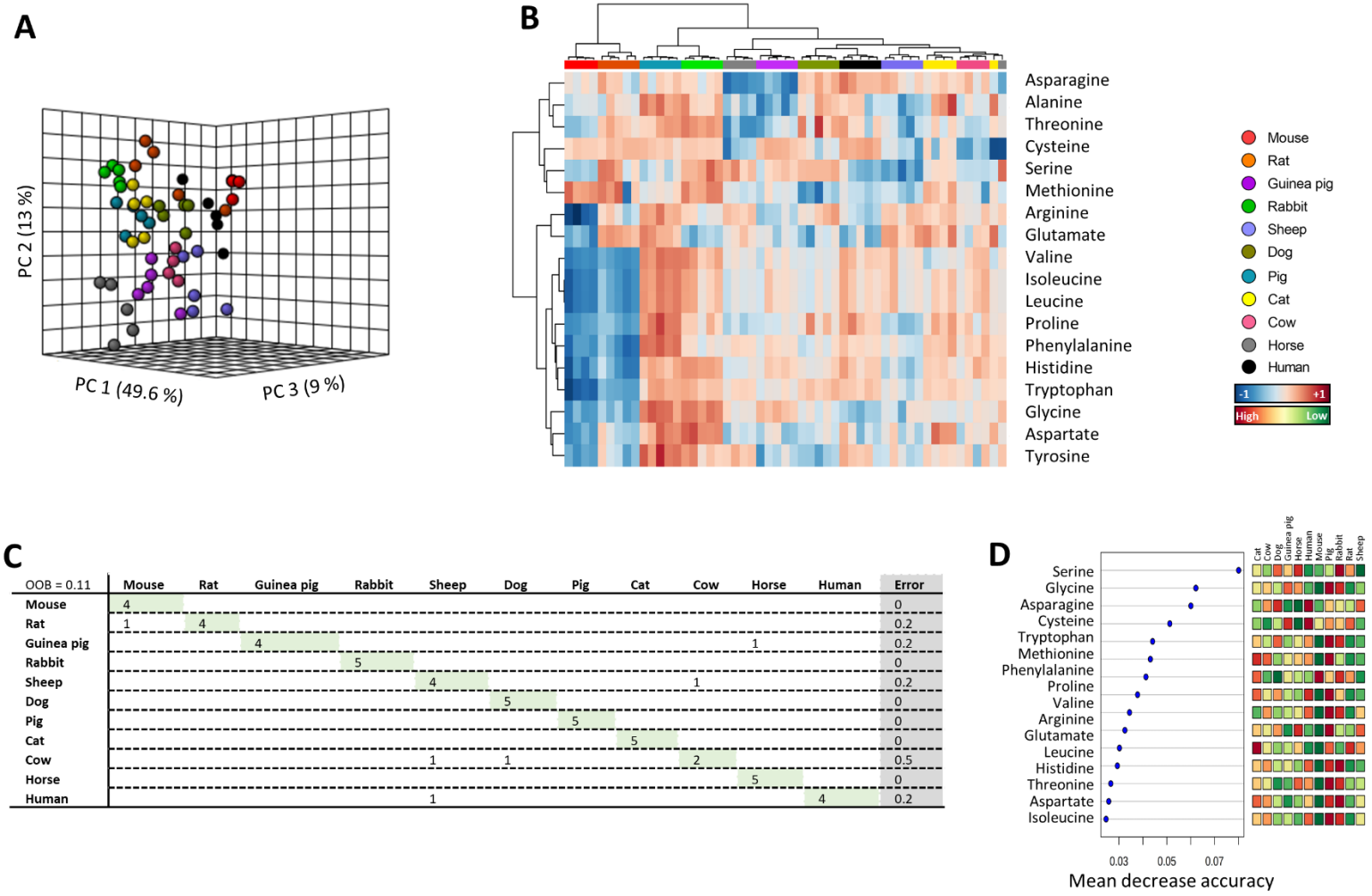

Figure 3. Multivariate statistics reveals a species-specific amino acids plasma profile. A) PCA representation of amino acids. X: PC1; Y: PC2; Z: PC3. **B)** Hierarchical clustering of individual animal samples according to metabolite abundance. **C)** RF classification algorithm. **D)** VIP scores for RF.

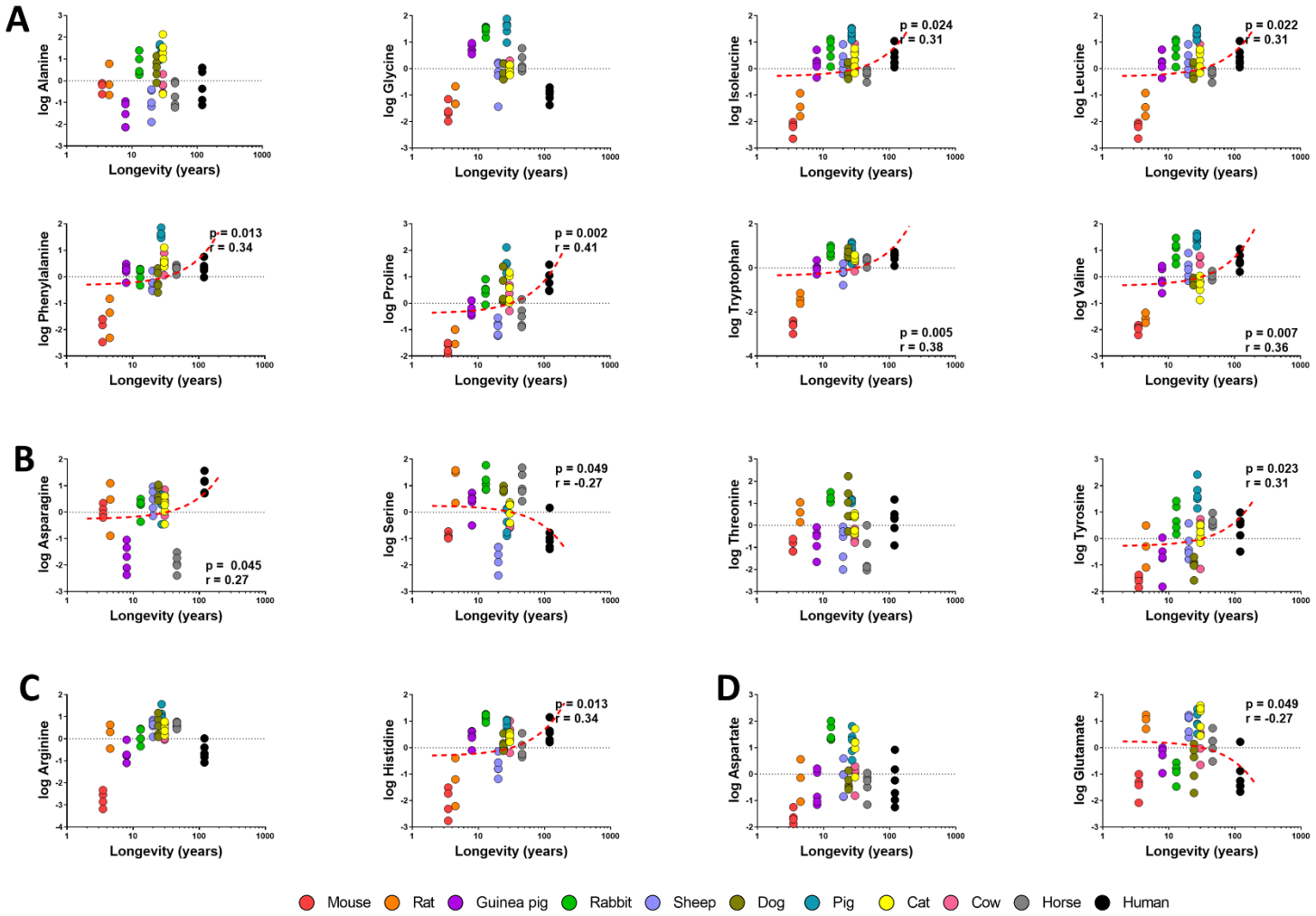

Figure 4. Individual plasma concentration of non-polar (A), polar uncharged (B), positively charged (C) and negatively charged (D) amino acids. Pearson correlation between plasma metabolites and animal longevity was performed (A-D). Minimum signification level was set at $p<0.05$. All metabolites were log-transformed in order to accomplish the assumptions of normality.

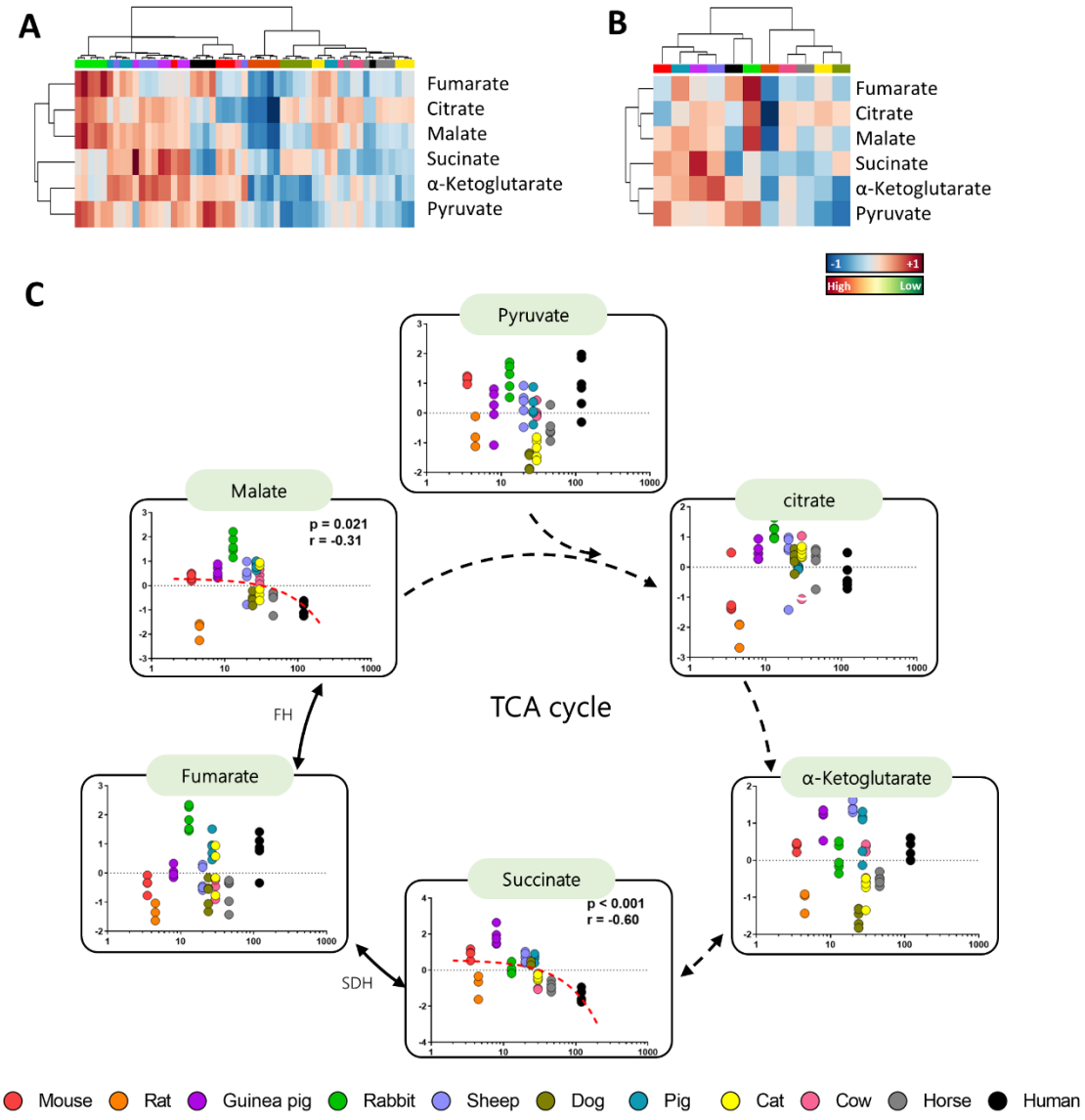

Figure 5. Multivariate statistics reveals a shared TCA cycle intermediates plasma profile. A) Hierarchical clustering of individual animal samples according to metabolite abundance. **B)** Hierarchical clustering animal species according to average metabolite abundance. **C)** Individual plasma correlation of the metabolites with animal longevity involved TCA cycle. Dashed lines refer to reactions in which more than one enzyme is involved. Pearson correlation between plasma metabolites and animal longevity was performed. Minimum signification level was set at $p<0.05$. All metabolites were log-transformed in order to accomplish the assumptions of normality. Enzyme codes refer to: Succinate dehydrogenase (SDH or Cx II); Fumarate hydratase (FH).

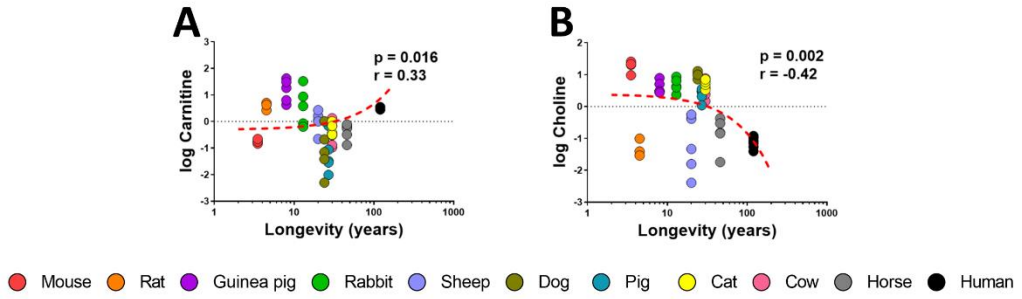

Figure 6. Individual plasma concentration of lipid intermediates carnitine (A) and choline (B). Pearson correlation between plasma metabolites and animal longevity was performed. Minimum signification level was set at $p<0.05$. All metabolites were log-transformed in order to accomplish the assumptions of normality.

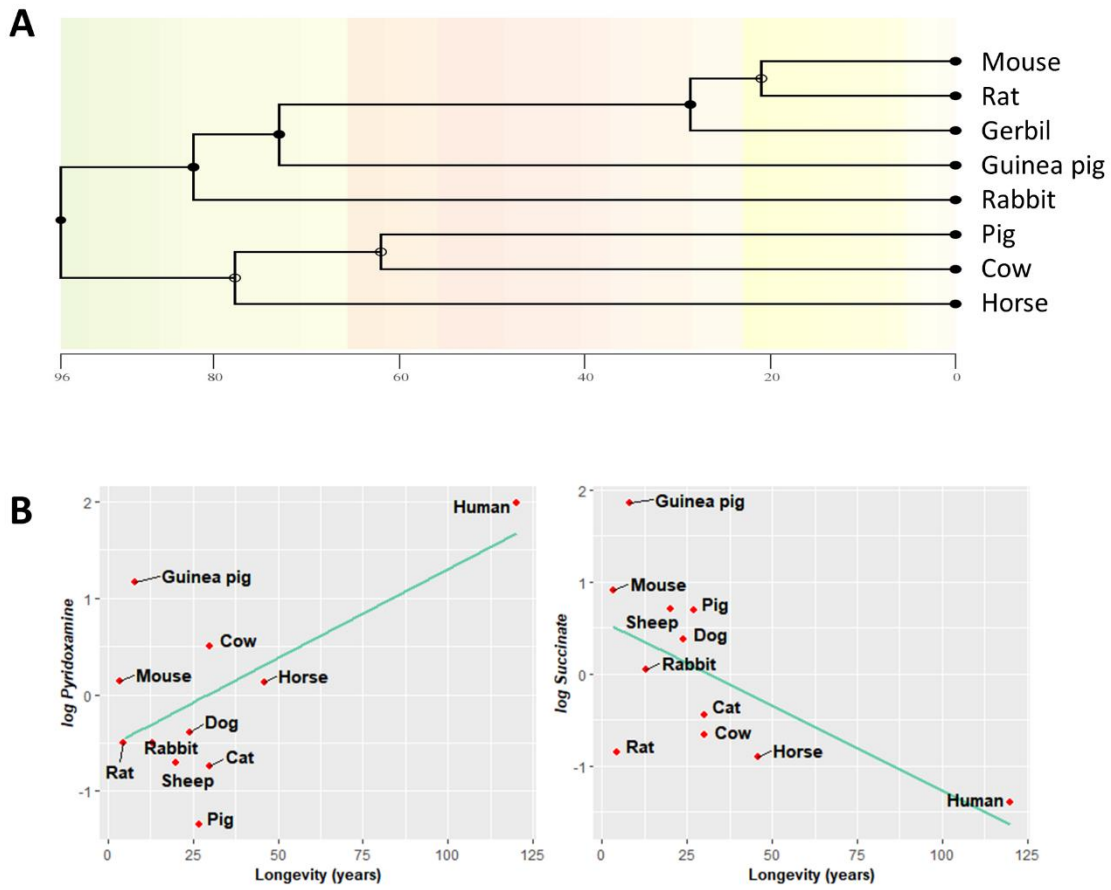

Figure 7. Plasma metabolites changes across mammalian longevity after correcting for phylogenetic relationships. **A)** Phylogenetic tree with a timescale of million years ago. **B)** Phylogenetic generalized least squares (PGLS) regression between longevity and plasma content of pyridoxamine and succinate. Minimum signification level was set at $p<0.05$. All metabolites were log-transformed in order to accomplish the assumptions of normality.

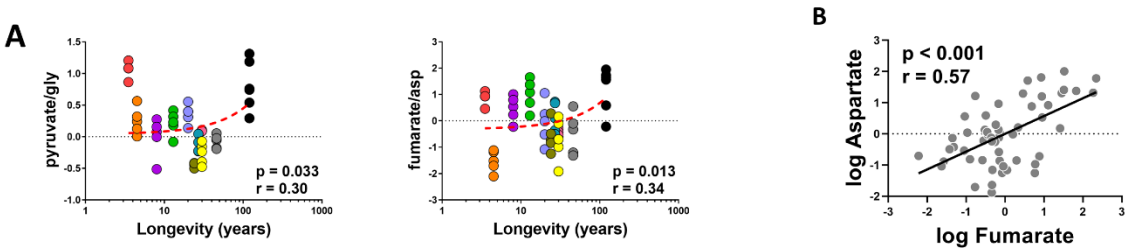

Supplementary figure 1. **Pearson correlation between longevity and TCA cycle intermediates/amino acids (A) and amino acids and TCA cycle intermediates (B)**. Minimum signification level was set at p<0.05. All metabolites were log-transformed in order to accomplish the assumptions of normality.

Supplementary table 2. **Plasma metabolite concentration in mammals**. Concentration values are reported in MS Counts as mean ± SEM from 4-6 individuals**.**

	Mouse	Rat	Guinea pig	Rabbit	Sheep	Dog	Pig	Cat	Cow	Horse	Human
Amino acids											
Alanine	9622 ± 389	10872 ± 920	6132 ± 548	13653 ± 1114	7559 ± 704	13055 ± 975	16949 ± 835	16248 ± 2307	10007 ± 647	8534 ± 755	10395 ± 1112
Arginine	1547 ± 214	12298 ± 2446	7486 ± 1089	13396 ± 1465	19279 ± 1776	19709 ± 3070	28465 ± 3000	17738 ± 1448	14505 ± 1995	19389 ± 902	7862 ± 993
Asparagine	400 ± 33	482 ± 109	123 ± 20	456 ± 41	546 ± 73	637 ± 52	496 ± 59	442 ± 51	542 ± 73	102 ± 10	800 ± 83
Aspartate	300 ± 15	464 ± 52	444 ± 46	927 ± 48	499 ± 49	475 ± 23	818 ± 63	772 ± 75	521 ± 42	465 ± 32	486 ± 60
Glutamate	135 ± 14	423 ± 18	233 ± 18	173 ± 12	405 ± 31	206 ± 30	425 ± 32	458 ± 45	279 ± 34	285 ± 27	140 ± 9
Glycine	658 ± 59	845 ± 80	2176 ± 83	3092 ± 113	1336 ± 171	1415 ± 92	3226 ± 236	1437 ± 49	1550 ± 81	1692 ± 142	906 ± 43
Histidine	991 ± 144	1363 ± 274	3613 ± 235	5325 ± 164	2042 ± 191	3134 ± 198	4558 ± 221	3767 ± 100	3808 ± 507	2891 ± 274	3991 ± 306
Isoleucine	785631 ± 57318	1158881 ± 138350	3177542 ± 305357	4243780 ± 435646	3356794 ± 393084	2701301 ± 185822	6018470 ± 282885	3390951 ± 315707	3718411 ± 442245	2527144 ± 120129	3647776 ± 325288
Leucine	777564 ± 55554	1146902 ± 137694	3145356 ± 308314	4180307 ± 427257	3341866 ± 393766	2664909 ± 185321	5937102 ± 279439	3343632 ± 298778	3688931 ± 448074	2501138 ± 121446	3629458 ± 318561
Phenylalanine	1051 ± 96	1135 ± 175	2868 ± 157	2692 ± 147	2311 ± 155	2426 ± 195	5672 ± 180	3567 ± 219	3261 ± 275	2985 ± 87	3067 ± 154
Proline	20118 ± 1349	26539 ± 2882	58724 ± 4389	99020 ± 11006	35894 ± 3372	109229 ± 22987	221255 ± 27458	112626 ± 18397	93396 ± 13687	50925 ± 7538	127761 ± 16943
Serine	3256 ± 66	6054 ± 719	5016 ± 338	6643 ± 411	2481 ± 164	5940 ± 78	3954 ± 287	4601 ± 222	3689 ± 33	6413 ± 507	3030 ± 117
Threonine	3375 ± 228	6993 ± 479	3866 ± 457	9387 ± 372	3694 ± 580	9018 ± 1811	7905 ± 618	5715 ± 492	4121 ± 280	3024 ± 626	6077 ± 779
Tryptophan	56098 ± 5119	138813 ± 9949	428879 ± 34935	758001 ± 54933	365132 ± 41243	698597 ± 43142	833938 ± 94473	605752 ± 22566	504841 ± 47232	545571 ± 32168	628770 ± 41400

Tyrosine	218 ± 9	344 ± 53	319 ± 38	602 ± 61	390 ± 42	275 ± 16	886 ± 83	469 ± 23	454 ± 71	561 ± 22	515 ± 43
Valine	72467 ± 3425	87998 ± 5309	245806 ± 27796	469870 ± 49934	307657 ± 36262	226402 ± 6738	606992 ± 30600	202688 ± 18589	337455 ± 42436	255574 ± 11038	367707 ± 27965
Methionine metabolism											
Betaine	29479 ± 415	87359 ± 6785	103778 ± 19168	207317 ± 41281	182902 ± 10513	531171 ± 45601	586314 ± 41654	165751 ± 13196	464612 ± 39664	137181 ± 11397	76199 ± 8708
Cystathionine	2555 ± 16	1662 ± 155	816 ± 96	15928 ± 1305	4301 ± 708	10849 ± 1086	1766 ± 305	18531 ± 3913	5841 ± 581	451 ± 102	528 ± 186
Cysteine	224861 ± 6950	266951 ± 20243	296224 ± 19633	220210 ± 5763	73664 ± 16370	125619 ± 25690	229049 ± 22829	116156 ± 39559	37615 ± 8549	36490 ± 11370	352668 ± 17110
GSH	13867 ± 203	2044 ± 976	186 ± 69	630 ± 71	13 ± 2	594 ± 249	8 ± 2	1398 ± 637	21 ± 6	44 ± 9	118 ± 34
Homocysteine	816 ± 41	706 ± 66	387 ± 34	1476 ± 139	551 ± 153	2187 ± 724	1950 ± 279	919 ± 349	70 ± 19	ND	1102 ± 203
Methionine	9956 ± 1581	8094 ± 2542	2398 ± 390	9631 ± 996	1551 ± 251	830 ± 240	3062 ± 294	5613 ± 853	2027 ± 509	2161 ± 152	1513 ± 338
Pyridoxal	219 ± 24	203 ± 15	819 ± 46	1016 ± 68	959 ± 50	970 ± 16	1024 ± 30	965 ± 46	946 ± 39	937 ± 24	1020 ± 50
Pyridoxamine	689 ± 52	289 ± 41	2923 ± 317	287 ± 41	124 ± 6	333 ± 40	88 ± 10	198 ± 12	1178 ± 220	678 ± 49	9150 ± 254
SAH	77 ± 8	35 ± 7	257 ± 45	95 ± 14	226 ± 11	159 ± 23	355 ± 35	161 ± 12	69 ± 11	ND	135 ± 17
SAM	100 ± 30	53 ± 16	129 ± 42	112 ± 23	21 ± 4	21 ± 6	19 ± 5	51 ± 17	ND	ND	55 ± 12
Taurine	1142 ± 23	475 ± 98	257 ± 50	157 ± 27	186 ± 33	331 ± 40	378 ± 47	361 ± 22	285 ± 69	113 ± 22	209 ± 41
TCA intermediates											
α-Ketoglutarate	444 ± 29	53 ± 13	1408 ± 56	325 ± 68	1827 ± 200	42 ± 5	866 ± 238	112 ± 17	358 ± 72	145 ± 12	424 ± 60
Citrate	351 ± 22	99 ± 24	7014 ± 1539	21748 ± 4594	8248 ± 2351	4669 ± 907	2741 ± 101	6259 ± 697	7790 ± 2932	4819 ± 1134	1467 ± 268

Fumarate	163 ± 12	89 ± 9	199 ± 10	540 ± 52	181 ± 18	138 ± 15	323 ± 31	217 ± 34	158 ± 13	143 ± 16	306 ± 34
Malate	1124 ± 69	161 ± 19	1373 ± 127	3686 ± 605	1217 ± 246	519 ± 45	1714 ± 97	1067 ± 294	1126 ± 134	526 ± 65	369 ± 35
Pyruvate	448 ± 18	141 ± 20	246 ± 45	488 ± 67	266 ± 39	72 ± 6	247 ± 37	95 ± 9	220 ± 20	157 ± 24	454 ± 103
Succinate	6625 ± 620	1934 ± 323	13900 ± 2490	3551 ± 331	5771 ± 525	4453 ± 153	5643 ± 326	2441 ± 101	2172 ± 350	1774 ± 144	1249 ± 122
Lipid intermediates											
Carnitine	3534 ± 112	12662 ± 495	19196 ± 2994	12592 ± 3491	7061 ± 963	3197 ± 1012	2683 ± 828	5194 ± 474	4847 ± 1107	4946 ± 532	25626 ± 5850
Choline	191008 ± 10036	42815 ± 2620	130092 ± 6916	135483 ± 7654	49365 ± 11165	163835 ± 3927	113692 ± 5753	139621 ± 4642	124035 ± 11272	56938 ± 6904	47049 ± 1985
TMAO	1905 ± 296	1528 ± 103	8210 ± 767	19964 ± 3149	87395 ± 8160	16161 ± 788	18773 ± 1066	21143 ± 4081	12363 ± 2902	66200 ± 11286	22424 ± 4914

Supplementary table 3. Plasma metabolite correlation with animal longevity. Pearson r values are reported. Pagel's λ value measures phylogenetic signal for each individual metabolite. Phylogenetic generalized least squares (PGLS) regression between plasma metabolites and longevity corrects for phylogenetic relationships. Minimum signification level was set at $p<0.05$. All metabolites were log-transformed to accomplish the assumptions of normality.

	Pearson		**PGLS**	
	***r* values**	**Sig.**	**λ**	**Sig.**
Amino acids				
Alanine	0.02	0.906	0	0.922
Arginine	0.01	0.924	0	0.796
Asparagine	0.27	0.045	0	0.440
Aspartate	-0.03	0.812	1	0.871
Glutamate	-0.27	0.049	0.40	0.500
Glycine	-0.22	0.102	0	0.623
Histidine	0.34	0.013	0.93	0.391
Isoleucine	0.31	0.024	0	0.305
Leucine	0.31	0.022	0	0.300
Phenylalanine	0.34	0.013	0.37	0.302
Proline	0.41	0.002	0.72	0.258
Serine	-0.27	0.049	0	0.468
Threonine	0.01	0.955	0	0.970
Tryptophan	0.38	0.005	0.79	0.334
Tyrosine	0.31	0.023	1	0.401
Valine	0.36	0.007	0	0.244
Methionine metabolism				
Betaine	-0.17	0.228	0	0.749
Cystathionine	-0.49	<0.001	1	0.140
Cysteine	0.06	0.675	0	0.981
GSH	-0.32	0.019	0	0.219
Homocysteine	0.07	0.643	1	0.902
Methionine	-0.38	0.005	0.19	0.155
Pyridoxal	0.40	0.003	0	0.195
Pyridoxamine	0.62	<0.001	0.42	0.045
SAH	0.14	0.330	0	0.625
SAM	-0.06	0.654	0	0.736
Taurine	-0.35	0.010	0.58	0.253
TCA cycle metabolites				
α-Ketoglutarate	0.05	0.706	0	0.917
Citrate	0.02	0.867	0	0.854
Fumarate	0.26	0.062	0	0.437
Malate	-0.31	0.021	0	0.350
Pyruvate	0.20	0.157	0	0.644
Succinate	-0.60	<0.001	0	0.045
Lipid and protein intermediates				
Carnitine	0.33	0.016	0	0.316
Choline	-0.42	0.002	1	0.481

Gene expression and regulatory factors of the mechanistic target of rapamycin (mTOR) complex 1 predict mammalian longevity

Natalia Mota-Martorell[1], Mariona Jove[1], Irene Pradas[1], Rebeca Berdún[1], Isabel Sanchez[2], Alba Naudi[1], Eloi Gari[3], Gustavo Barja[4,*], Reinald Pamplona[1,*]

[1]Department of Experimental Medicine, University of Lleida-Lleida Biomedical Research Institute (UdL-IRBLleida), Lleida, Catalonia, 25198, Spain

[2]Proteomics and Genomics Unit, University of Lleida, Lleida, Catalonia, 25198, Spain

[3]Department of Basic Medical Sciences, University of Lleida- Lleida Biomedical Research Institute (UdL-IRBLleida), Lleida, Catalonia, 25198, Spain

[4]Department of Genetics, Physiology and Microbiology, Complutense University of Madrid (UCM), Madrid, 28040, Spain

*** Corresponding authors:**

Dr. Gustavo Barja; e-mail: gbarja@bio.ucm.es;

Dr. Reinald Pamplona; e-mail: reinald.pamplona@mex.udl.cat

E-mail addresses of the rest of the authors:

NMM: nataliamotamartorell@gmail.com

MJ: mariona.jove@udl.cat

IP: irene.pradas@gmail.com

RB: rebecaberdun@gmail.com

IS: Isabel.sanchez@udl.cat

AN: alba.naudi@mex.udl.cat

EG: eloi.gari@udl.cat

Abstract

Species longevity varies significantly across animal species, but the underlying molecular mechanisms remain poorly understood. Recent studies and omics approaches suggest that phenotypic traits of longevity could converge in the mammalian target of rapamycin (mTOR) signalling pathway. The present study focuses on the comparative approach in heart tissue from 8 mammalian species with a ML ranging from 3.5 to 46 years. Gene expression, protein content, and concentration of regulatory metabolites of the mTOR complex 1 (mTORC1) were measured using droplet digital PCR, western blot, and mass spectrometry, respectively. Our results demonstrate 1) the existence of differences in species-specific gene expression and protein content of mTORC1; 2) that the achievement of a high longevity phenotype correlates with decreased and inhibited mTORC1; 3) a decreased content of mTORC1 activators in long-lived animals, and 4) that these differences are independent of phylogeny. Our findings, taken together, support an important role for mTORC1 down-regulation in the evolution of long-lived mammals.

Keywords: Arginine, FKBP12, methionine cycle metabolites, mTOR, PRAS40, raptor

Introduction

Maximum longevity ('longevity' from here on out) is a species-specific trait that differ more than 75,000-fold among animal species, and more than 200-fold among mammals (Ma and Gladyshev, 2017). The longevity of animal species is an endogenous genetically determined adaptation (Barja, 2010, 2019; Barja et al., 1994; Bowles, 1998; Jones et al., 2014; Libertini, 1988; Longo et al., 2005; Mitteldorf, 2016, 2018; Skulachev, 1997) expressed through regulation of highly conserved pathways (Fontana et al., 2010; Guarente and Kenyon, 2000) and modulation of gene expression (Fushan et al., 2015; Kim et al., 2011).

Long-lived animal models are frequently used when trying to discover the molecular bases of mammalian longevity (Selman et al. 2009; Wu et al. 2013; Fushan et al. 2015; Ma and Gladyshev 2017; Sahm et al. 2018), and the same is true of studies comparing animal species with different longevities (Barja 1998; Perez-Campo et al. 1998; Pamplona et al. 2002; Jové et al. 2013; Naudí et al. 2013; Ma et al. 2016; Bozek et al. 2017; Mota-Martorell et al. 2019), investigations inducing genetic manipulations, and pharmacological and nutritional interventions increasing longevity (Longo et al., 2015; Pamplona and Barja, 2006, 2011).

Phenotypic features associated with long-lived animal species include a lower generation of endogenous damage, highly resistant macromolecular components concerning nucleotides in DNA, proteins and lipids, and the specific transcriptomics and metabolomics profiles, among others (Lewis et al., 2018; Ma and Gladyshev, 2017; Naudí et al., 2013; Pamplona and Barja, 2007, 2011; Tyshkovskiy et al., 2019). Notably, several of these features seem to be supported by specific cell signalling pathways (Barja, 2019), including the mechanistic target of rapamycin (mTOR) pathway.

mTOR, a member of an evolutionary conserved group of serine/threonine kinases from the PIKK (phosphatidylinositol-3 kinases (PI3K)-related kinase) family, is present as two distinct complexes: mTOR complex 1 (mTORC1) and mTOR complex 2 (mTORC2) (Valvezan and Manning, 2019). mTORC1 is sensitive to rapamycin and plays a central role in the mTOR signalling network monitoring and integrating a broad diversity of extra- and intracellular signals controlling cell physiology. Thus, mTORC1 can regulate cell metabolism, growth, and proliferation, and can modulate complex physiological processes such as aging and longevity (Kapahi et al. 2010; Antikainen et al. 2017; Weichhart 2018; Papadopoli et al. 2019; Barja 2019; Valvezan and Manning 2019) through a wide range of downstream pathways such as mRNA translation, biosynthesis pathways, mitochondrial function, autophagy, endoplasmic reticulum stress, and stress responses, among others. Inhibition of the highly conserved mTOR pathway results in longevity extension in several animal models from yeast to mice (Kapahi et al., 2010; Lushchak et al., 2017; Papadopoli et al., 2019; Weichhart, 2018), and mTOR activation shortens longevity, likely through down regulation of aging and aging-associated degenerative diseases including cancer, diabetes, and neurodegeneration (Johnson et al., 2013; Kapahi et al., 2010; Papadopoli et al., 2019).

In mammals, mTORC1 is composed by mTOR and its associated proteins Raptor (regulatory associated protein of TOR), mLst8 (mammalian lethal with SEC13 protein 8), PRAS40 (Proline-rich AKT1 substrate of 40 kDa), and Deptor (DEP domain-containing mTOR-interacting protein) (Valvezan and Manning, 2019). Importantly, Raptor and PRAS40 are present exclusively in

mTORC1. mTOR, Raptor, and mLST8 are core components, and DEPTOR and PRAS40 are inhibitory subunits. FK506 binding protein (FKBP12) is a regulatory subunit of the rapamycin sensitive mTORC1 activity. Extra- and intracellular signals regulating mTORC1 include growth factors, hormones, glucose, ATP, oxygen, metabolic intermediates, and amino acids (Valvezan and Manning, 2019). Among amino acids, arginine, leucine, and methionine cycle metabolites play a relevant role as activators of mTORC1 through their interaction with several intracellular mediators (Valvezan and Manning, 2019).

Despite the high evolutionary conservation of the mTORC1, to our knowledge the possible existence of relevant differences in mTORC1 and its regulatory component levels across mammalian species with different longevities has never been investigated. In order to examine molecular traits associated with mammalian longevity we used droplet digital PCR (ddPCR) and western blot methods to define the steady-state levels of gene expression and protein content of the mTORC1, and targeted metabolomics to measure the concentration of its activators. Heart tissue of eight mammalian species showing more than one order of magnitude of difference in longevity —from 3.5 years in mice to 46 years in horses—, were analysed. The choice of selected subunits was: i) mTOR, Raptor, and PRAS40 as exclusive components of the mTORC1; ii) FKBP12 as regulatory subunit of the mTORC1 activity; and iii) arginine, leucine, methionine and its related metabolites as activators of the mTORC1 activity. Our results suggest that species-specific modulation on the mTORC1 might have contributed to extend longevity during evolution of long-lived animals.

Results

Multivariate statistics reveals a species-specific mTORC1 profile

In order to determine whether heart mTORC1 gene expression and protein content, and the concentration of its regulators differed among mammals, multivariate statistics were applied using the levels of gene expression of *mtor*, *rptor*, and *fkbp1a*, protein content of mTOR and its phosphorylation (measured as $mTOR^{Ser2448}$/mTOR ratio), PRAS40 and its phosphorylation (measured as $PRAS40^{Thr246}$/PRAS40) and FKBP12, and concentration of the amino acids leucine, arginine, methionine and the methionine cycle metabolites SAH, SAM and homocysteine. Non-supervised principal component analysis (PCA) revealed the existence of a species-specific protein and gene profile of the mTORC1 (**Figure 1A**), capable to explain up to 45.1% of sample variability. A hierarchical clustering of the samples represented by a heat map revealed specific mTORC1 patterns for rodents (mouse, rat, and guinea pig) (**Figure 1B**). Furthermore, this global pattern found in rodents was different from that found in non-rodents (rabbit, pig, cow and horse) (**Figure 1C**). These results were confirmed by performing a supervised analysis, such as partial least squares discriminant analysis (PLS-DA) (**Figure 1D**). However, cross-validation values of PLS-DA model showed that heart gene expression and protein amount of mTORC1, and the content of its regulators, is a limited model to define the animal species scoring a $R^2 = 0.6$ and $Q^2 = 0.4$, obtaining a maximum accuracy of 0.5 using 2 components (**Figure 1E**). Permutation tests (2000 repeats) yielded a low p=0.006, indicating that none of the distributions formed by the permuted data was better than the observed statistic based on the original data (**Figure 1F**). The discriminating power between groups of the different measured features was ranked by applying a variable importance projection (VIP) score (**Figure 1G**). After selecting those features with VIP score > 1.5 as significant, the *mtor* gene expression and FKBP12 protein content were found to be the top-ranked features.

The species-specific mTORC1 profile is associated with species longevity

The gene expression and protein content of mTORC1 were also correlated with species longevity (**Figure 2**). Specifically, long-lived animals have increased *mtor* expression, but decreased *raptor* (**Figure 2A**). Long-lived animals also had less protein content of mTOR and Raptor but higher PRAS40 (**Figure 2B**). Furthermore, gene expression and protein content of Raptor were positively correlated (**Supplementary figure 1**). Regarding protein phosphorylation, increased $mTOR^{Ser2448}$/mTOR and decreased $PRAS40^{Thr246}$/PRAS40 was found in long-lived animals (**Figure 2C**). Interestingly, the protein content of mTOR and PRAS40 is inversely correlated with their degree of phosphorylation (**Supplementary figure 1**).

The mTORC1 profile is associated with its regulators and methionine metabolites

Due to the relevance of regulatory factors such as FKBP12 and specific metabolites like arginine, leucine and methionine cycle components in determining mTORC1 activity, we have evaluated their relationship with species longevity and mTORC1 core components (**Figure 3**). Thus, two well-known positive activators of mTOR, arginine and methionine (**Figure 4A**), as well as two methionine-related metabolites, such as SAM and homocysteine (**Figure 4B**), were found to be negatively correlated with mammalian longevity. Gene expression of *fkbp1a* and protein content of FKBP12 were also negatively correlated with longevity (**Figure 4C**). Therefore, the greater the longevity of a mammalian species, the lower is the tissue concentration of the

mTORC1 regulatory metabolites. In addition, methionine metabolites were associated with mTOR, PRAS40 and Raptor (**Figure 3**). Accordingly, methionine and SAM were positively associated to Raptor and PRAS40^{Thr246}/PRAS40, but negatively related to PRAS40; SAM was also negatively correlated with mTOR^{Ser2448}/mTOR; whereas homocysteine was positively correlated with PRAS40^{Thr246}/PRAS40 (**Figure 5**). Arginine was positively correlated with PRAS40^{Thr246}/PRAS40 and FKBP12, but negatively with PRAS40 (**Figure 6**). Finally, the regulatory factor FKBP12 showed a positive correlation with *rptor* and RAPTOR, and a negative correlation with phosphorylated mTOR (**Figure 6**).

mTORC1 longevity changes are independent of phylogenetic relationships

Animal species are evolutionary related, raising the possibility that data from closely related species might not be statistically independent from one another. Therefore, to correct for phylogeny we performed a phylogenetically generalised least squares regression (PGLS) following the phylogenetic tree constructed in Figure 7A. First of all, we have measured the amount of phylogenetic signal of each trait (Pagel's λ). Basically, it indicates the degree up to which a specific trait is influenced by phylogeny, indicating whether the changes in those traits across different species might be due (λ=1) or not (λ=0) to phylogenetic relationships. After correcting for phylogeny, the expression of *mtor* (p=0.008, r=-0.20), *rptor* (p=0.008, r=0.05) and *fkbp1a* (p=0.019, r=-0.16), mTOR^{Ser2448}/mTOR (p=0.023, r=-0.94), PRAS40^{Thr246}/PRAS40 (p=0.023, r=-0.66), methionine (p=0.011, r=0.17) and SAM (p=0.049, r=0.11) continued to be correlated with mammalian longevity (**Figure 7B**, **Supplementary figure 2**, **Supplementary table 1**).

Discussion

Longevity-associated mTORC1 profile

We have found that animal species have a unique species-specific mTORC1 profile, which is associated with animal longevity. Furthermore, our results revealed that mTORC1 accounts for 60% of inter-species variation in longevity, mTORC1 gene expression and protein phosphorylation being the strongest longevity predictors. In agreement with this, previous studies have already described a unique gene expression profile (Caron et al., 2015; Fushan et al., 2015; Ma et al., 2016; Muntané et al., 2018), metabolome (Ma et al., 2015) and lipidome (Jové et al., 2013; Mota-Martorell et al., 2019) in long-lived species. Since mTORC1 is a master regulator of cellular metabolism including mRNA translation and lipid synthesis (Caron et al., 2015) those findings support the existence of important genetic adaptations in nutrient-sensing metabolic pathways, including those up- or downstream of mTOR, in the evolution of longevity (Singh et al., 2019).

Decreased mTORC1 content and activity to achieve a high longevity phenotype

Decreasing mTORC1 content and activity is associated with superior species longevity phenotypes. Long-lived animal species have decreased *rptor* but increased *mtor*. Accordingly, it has been reported that nonagenarians' blood has decreased mRNA content of *akt1s1* (PRAS40) and *rptor* (Raptor) when compared with middle-aged controls (Passtoors et al., 2013). Moreover, the offspring of those long-lived individuals also has decreased *rptor* gene expression, which emerges as a potential biomarker of familiar longevity (Passtoors et al., 2013). In the present investigation, protein content of mTOR and Raptor were also lower in long-lived animals, supporting a role for Raptor in longevity.

mTORC1 is regulated by opposite phosphorylation patterns in mTOR and PRAS40. Phosphorylation of mTOR at serine 2448 has inhibitory effects in skeletal muscle (Figueiredo et al., 2017). Nutrient availability promotes mTOR activation that, in turn, activates p70S6K which re-phosphorylates mTOR (at Ser^{2448}) inhibiting its activity. The existence of this negative feed-back loop could explain why some studies found that starvation increases Ser^{2448} (Chiang and Abraham, 2005). Proline-rich AKT substrate 40 kDa (PRAS40) is a component and negative regulator of the mTOR complex (Sancak et al., 2007). However, PRAS40 phosphorylation at Thr^{246} via Akt results on its dissociation from mTORC1 activating it (Nascimento et al., 2010). In agreement with this, we have found increased $mTOR^{Ser2448}$/mTOR and PRAS40, but decreased $PRAS40^{Thr246}$/PRAS40 in long-lived animals, all these three differences tending to inhibit mTORC1, suggesting that this inhibition is one among the various different signals to the nucleus that modulate gene expression of specific longevity-related genes. This, in turn, modulates protein synthesis of multiple aging effectors in the cytosolic or extracellular compartments, to finally cooperate together in the production of a high longevity phenotype (Barja, 2019). Previous studies had already reported inhibitory changes at mTORC1 activators in whales with an estimated longevity of 200 years (Ma and Gladyshev, 2017). Genetic mutations downregulating mTOR downstream signalling (Wu et al., 2013a) or its downstream effector S6K1 (Selman et al., 2009) increase lifespan in mice, similarly to its pharmacological inhibition by rapamycin (Singh et al., 2019). Furthermore, the lower phosphorylation of PRA40-Thr^{246} in long-lived animal species suggests a lower activation of AKT (the major kinase promoting PRAS40-

Thr^{246} phosphorylation is Akt (Nascimento et al., 2010)) probably associated with a down-regulation of the insulin signaling pathway which is a conserved regulatory system for aging and longevity (Kenyon, 2010). Further studies are, however, needed to develop a more detailed view.

Achievement of superior longevity is not exclusively due to changes on mTORC1 itself, but also on its activity regulators. Although it might sound controversial, decreased gene expression and protein content of the inhibitor FKBP12 was found in long-lived animals. However, since mTORC1 total content is decreased, less inhibitor is needed, allowing to save the energy that otherwise will be used to synthesize those proteins. Besides, recent studies have revealed that FKBP12 is associated with neurotoxicity (Caraveo et al., 2017), and its disruption enhances mTOR-Raptor interactions and memory (Hoeffer et al., 2008). Therefore, our results suggest that maintenance of proper mTORC1 stability by decreasing FKBP12 might be a molecular trait of mammalian longevity.

Decreased concentration of mTORC1 activators, such as arginine and methionine-related metabolites, might enhance its down-regulation. Accordingly, arginine content in primate fibroblasts is negatively correlated with longevity (Ma et al., 2016), and naked-mole rats have lower levels of plasma methionine than mice (Lewis et al., 2018), and increased methionine, SAM and homocysteine have been observed in ageing mice liver (Jeon et al., 2018).

mTORC1 and methionine-metabolism: the longevity connexion

mTORC1 is often described as a master regulator of cellular metabolism, due to its capacity to modulate anabolic and catabolic processes such as protein turnover. It has been proposed that mTORC1 inhibition during dietary restriction promotes autophagy, which clears old and dysfunctional organelles, promoting lifespan extension (Simonsen et al., 2008). Supporting this idea, it was found phenotypic expression of the methionine restriction life extension effect requires autophagy (Bárcena et al., 2019; Ruckenstuhl et al., 2014). Furthermore, a study in worms demonstrated that SAMTOR, a regulator of mTOR, detects methionine availability via SAM and is also involved in longevity extension during dietary restriction (Gu et al., 2017a). Overall, these results support that autophagy induction via mTORC1 down-regulation or inhibition might be among the various key mechanisms promoting a long lifespan.

In our model, we have been able to establish a correlation between the mTORC1-longevity associated changes and the methionine metabolism. Specifically, we have found that methionine, homocysteine and arginine might influence PRAS40 phosphorylation, whereas SAM could influence mTOR phosphorylation. Furthermore, methionine and SAM levels change Raptor, supporting the idea that it might be another key factor modulating animal longevity. However, more studies concerning mTORC1 modulation in animal longevity need to be done to confirm these new insights (**Figure 8**). mTORC1 activity has also been related to increased mitochondrial activity (Cunningham et al., 2007; Schieke et al., 2006), as well as increased *de novo* lipid biosynthesis and protein synthesis (Düvel et al., 2010), that might favour the long-lived phenotype.

Assessing inter-species issues

Comparative studies across species with different lifespan are a powerful source of information helping to identify mechanisms linked to extended longevity and to discard those not related to it (Bozek et al., 2017; Ma et al., 2015, 2016). However, those kinds of studies raise several problems that need to be addressed. First, evolutionary relationships do not allow to assume data independence (Cooper et al., 2016). Therefore, we cannot know, in principle, if a specific trait truly correlates with longevity differences, or alternatively, whether such correlation could be due to the existence of phylogenetic similarity among the species selected. To overcome this limitation, we have carried out statistical analyses accounting for theses phylogenetic relationships. In this way, we've found that phylogeny has greater influence on protein content and activity compared to gene expression, suggesting that gene expression is relevantly involved in endogenously generating the high longevity of long-lived animals. The second problem that needs to be assessed is technical, due to the presence of SNPs inducing amino acid variations. Although the mTOR pathway is highly conserved across living organisms (Fontana et al., 2010), small variations in protein amino acid sequence across species could decrease antibody recognition. To overcome these methodological issues, we used degenerated primers capable to recognise sequences with SNPs. Furthermore, sequencing of PCR products allowed us to confirm primer specificity and gene detection.

Conclusions

Our results, taken together, support a role for mTORC1 in the evolution of mammalian longevity. We provide new insights into the influence of gene expression, total protein content and modulation of basal levels of mTORC1 activation on species longevity. We suggest that maintaining mTORC1 on a lowered and inhibited state during adult life, after development, growing and maturation, is one among the main signals stimulating the cell nucleus to produce a long-lived phenotype. This is endogenously generated by varying the expression of hundreds of target genes, which changes the level of activity of the multiple aging effectors like mitochondrial ROS production, membrane fatty acid unsaturation, apoptosis, autophagy, telomere shortening, proteostasis or inflammaging (Barja, 2008, 2019). Thereby, the mechanisms or drugs that regulate mTOR activity might prompt new insights and potential applications to humans like rapamycin, aimed to slow down the rate of human aging.

Methods

Animals

Mammalian species included in this investigation study were male adult specimens with a chronological age equivalent to the first 15-30% of their (maximum) longevity. The longevity recorded values for each species (in years) were: mouse (*Mus musculus*), 3.5; rat (*Rattus norvegicus*), 4.5; gerbil (*Meriones unguiculatus*), 6.3; guinea pig (*Cavia porcellus*), 8; rabbit (*Oryctolagus cunniculus*), 13; pig (*Sus scrofa*), 27; cow (*Bos taurus*), 30; and horse (*Equus caballus*), 46. Rodents and rabbits were obtained from rodent husbandries and sacrificed by decapitation, whereas sheep, pigs, cow and horses were obtained from abattoirs. The animal care protocols were approved by the Animal Experimentation Ethics committee of the University of Lleida. Heart ventricles from 5-7 animals were removed and immediately frozen in liquid nitrogen and transferred to -80°C until analyses.

Sample homogenization and quantification

Heart tissue (≈50 mg of whole tissue) was homogenized in a buffer containing 180mM KCl, 5mM MOPS, 2mM EDTA, 1mM DTPAC adjusted to pH=7.4. Prior homogenization, 1µM BHT and a mix of proteases inhibitors (GE80-6501-23, Sigma, Madrid, Spain) and phosphatase inhibitors (1mM Na_3VO_4, 1M NaF) was added. After a brief centrifugation (1000 rpm for 3 min at 4°C), supernatants protein concentration was measured using the Bradford method (500-0006, Bio-Rad Laboratories, Barcelona, Spain).

Protein content determination

The amount of mTORC1 core elements mTOR and its phosphorylation $mTOR^{Ser2448}$, PRAS40 and its phosphorylation $PRAS40^{Thr246}$, and Raptor, as well as its negative regulator FKBP12, were estimated using western blot analyses as previously described by Gomez et al. 2015.

Briefly, heart homogenates were mixed with a buffer containing 62.5 mM Tris-HCl pH 6.8, 2% SDS, 10% glycerol, 20% β-mercaptoethanol and 0.02% bromophenol blue, and heated for 3 min at 95°C. Then, proteins were subjected to one-dimensional electrophoresis on SDS and transferred to PVDF membranes. Membranes were maintained in blocking solution containing Tris 2M, NaCl 2.5 M, 5% BSA and 0.01% Tween for 1h at room temperature. Immunodetection was performed using antibodies against mTOR (2972, Cell signalling, Barcelona, Spain), $mTOR^{Ser2448}$ (2971, Cell Signalling, Barcelona, Spain), PRAS40 (ab151718, Abcam, Cambridge, UK), $PRAS40^{Thr246}$ (ab134084, Abcam, Cambridge, UK), RAPTOR (ab189158, Abcam, Cambridge, UK) and FKBP12 (ab2981, Abcam, Cambridge, UK). Secondary antibodies were anti-mouse (GENA931, Sigma, Madrid, Spain) and anti-rabbit (31460, ThermoFisher, Barcelona, Spain). Bands were visualized using an enhanced chemiluminescence HRP substrate (Millipore, MA, USA). Signal quantification and recording was performed with ChemiDoc equipment (Bio-Rad Laboratories, Barcelona, Spain). Protein amount was calculated from the ratio of their densitometry values referred to the densitometry values of their own total protein content (for phosphorylated proteins, $mTOR^{Ser2448}$ and $PRAS40^{Thr246}$) and its respective Coomassie staining (1610436, Bio-Rad Laboratories, Barcelona, Spain) (**Supplementary figure 3**). Protein densitometry values are reported in the Dataset.

Primers design

Gene cDNA sequences coding for the mTORC1 elements mTOR (*mtor*), PRAS40 (*akt1s1*) and Raptor (*rptor*), as well as its negative regulator FKBP12 (*fkbp1a*), were obtained from Ensmbl (http://www.ensmbl.org). Due to gene cDNA sequences limitations for gerbil, that specie wasn't included in the gene expression analyses. Degenerate primers were designed to amplify conserved regions among mammalian sequences using the software PriFi (Fredslund et al., 2005), and are listed in **Supplementary table 2 (For details, see Table 2 of this Thesis)**. Primers were purchased from Isogen (LifeSciences, Utretch, Netherlands).

Gene expression: Droplet digital PCR

Prior to DNA amplification, RNA from 15 mg whole heart tissue was extracted using RNeasy Fibrous Tissue Mini Kit (Qiagen, Hilden, Germany), and reverse-transcribed to cDNA using the High-Capacity cDNA Reverse Transcription kit (Applied Biosystems, CA, USA).

For DNA amplification, reaction mixture contained 1x of EvaGreen ddPCR Supermix, 200 nM primers and 0.01-16 ng of template cDNA. For droplet generation, 20 µL of reaction mixture and 70 µL of Droplet Generation Oil for EvaGreen were loaded in the Droplet Generation Cartridge, which was placed into the Droplet generator. From each PCR reaction mixture, 20 µL were transferred to a 96-well PCR plate, which was sealed with a foil heat using PX1 PCR plate sealer. Amplification was performed in a C1000 Touch Thermal Cycler following an initial DNA Polymerase activation (95°C, 5 min), and 40 cycles consisting of a DNA denaturation (95°C, 30 sec), primer annealing (58°C, 1 min) and extension (60°C, 1 min). A final dye-stabilization step was included (4°C 5 min, and 90°C 5 min). Droplets were read with a QX200 Droplet Reader and analysed using QuantaSoft software (Bio-Rad). The results from more than 12.000 droplets were accepted and normalised to an appropriate housekeeping gene (*ndufa9*) as suggested by Miwa et al. 2014. Values are reported as cDNA gene units per cDNA housekeeping units. Since no amplification was obtained for PRAS40 (*akt1s1*), it was removed from the analyses. Gene cDNA units are reported in the Dataset. All equipment and reagents were purchased from Bio-Rad (Bio-Rad Laboratories, Barcelona, Spain).

Targeted metabolomics

Sample processing

Tissue metabolites extraction was performed based on the methodology previously described (Method 1, Cabré et al. 2016). Briefly, 10 µL of sample homogenates were added to 30 µL of cold methanol containing 1 µg/mL of Phe-^{13}C as internal standard and 1µM BHT as antioxidant. Then, samples were incubated at room temperature for 15 min and centrifuged at 12,000 *g* for 3 min. Finally, the supernatant was filtrated through a 0.22-µm organic diameter filter (CLS8169, Sigma, Madrid, Spain) and 200 µL were transferred to Agilent (Barcelona, Spain) vials with glass inserts for further analysis.

Sulphur-containing metabolites were extracted on the bases of the methodology previously described (Method 2, Liu et al. 2017). Briefly, 2 µL of 5% DTT were added to 10 µL of sample homogenates. The resulting solution was vortexed for 1 min and allowed to stand at room temperature for 10 min. For protein precipitation, 40 µL of 0.1% formic acid plus 0.05% trifluoroacetic acid in acetonitrile containing 1 µg/mL of Phe-^{13}C as internal standard was added

to the sample, and the solution was vortexed for 2 min. Then, samples were incubated at room temperature for 15 min and centrifuged at 12000 *g* for 3 min. Finally, the supernatant was filtrated through a 0.22-µm organic diameter filter (CLS8169, Sigma, Madrid, Spain) and 200 µL were transferred to Agilent (Barcelona, Spain) vials with glass inserts for further analysis.

Analysis conditions

The individual conditions for the detection and quantification of heart metabolites are listed in **Supplementary table 3 (For details, see Table 6 of this Thesis)**. For non-sulphur-containing metabolites, 2 µL of extracted sample was injected based on the method described (Method 1, Cabré et al. 2016). Chromatographic separation was achieved on a reversed-phase column (Zorbax SB-Aq 1.8 µm 2.1×50mm, Agilent Technologies, Barcelona, Spain) equipped with a pre-column (Zorba-SB-C8 Rapid Resolution Cartridge 2.1×30mm 3.5 µm, Agilent Technologies, Barcelona, Spain) with a column temperature of 60°C. The flow rate was 0.6mL/min during a 19 min. Solvent A was composed of water containing 0.2% acetic acid and solvent B was composed of methanol 0.2% acetic acid. The gradient started at 2% B and increased to 98% B in 13 minutes and held at 98% B for 6 minutes. Post-time was established in 5 minutes. Electrospray ionization was performed in both positive and negative ion mode (depending on the target metabolite) using N_2 at a pressure of 50 psi for the nebulizer with a flow of 12 L/min and a temperature of 325°C, respectively.

For sulphur-containing metabolites, 10 µL of extracted sample was injected based on the method described (Method 2, Liu et al. 2017). Chromatographic separation was achieved on a reversed-phase Supelcosil LC-CN column (Supelco of 4.6 x 250 mm and 5 µL particle size, Sigma, Madrid, Spain) with a column temperature of 30°C. The flow rate was 0.5mL/min during a 10 min at 10%B. Solvent A was composed of water containing 0.1% formic acid and solvent B was composed of acetonitrile 0.1% formic acid. Electrospray ionization was performed in both positive and negative ion mode (depending on the target metabolite) using N_2 at a pressure of 50 psi for the nebulizer with a flow of 12 L/min and a temperature of 325°C, respectively.

Data was collected using the MassHunter Data Analysis Software (Agilent Technologies, CA, USA). Peak determination and peak area integration were carried out with MassHunter Quantitative Analyses (Agilent Technologies, CA, USA).

Metabolite quantification

Metabolite quantification was performed by constructing standard curves for each metabolite. Expected tissue concentration for each metabolite was based on the Human Metabolome Database (HMDB, http://www.hmdb.ca). Standard curves were constructed by plotting the peak area ratio against the final metabolite concentration. Metabolites concentration per amount of tissue is reported in the Dataset.

Equipment

The analysis was performed through liquid chromatography coupled to a hybrid mass spectrometer with electrospray ionization and a triple quadrupole mass spectrometer. The liquid chromatography system was an ultra-performance liquid chromatography model 1290 coupled to ESI-TQ MQ/MS model 6420 both from Agilent Technologies (Barcelona, Spain).

Statistics

Multivariate statistics was performed using Metaboanalyst software (Chong et al., 2019). Pearson correlation and Pearson partial correlation were performed using RStudio (v1.1.453). Linear models and phylogenetic generalised least squares regression (PGLS) were constructed using RStudio (v1.1.453). The phylogenetic tree was constructed using taxa names according to Kumar et al. 2017. Functions used were included in the package *caper*. Data was log-transformed and mean-centred prior statistical analyses in order to accomplish the assumptions of linearity.

Acknowledgements

M.J. is a 'Serra Hunter' Fellow. N.M-M received a predoctoral fellowship from the Generalitat of Catalonia (AGAUR, ref 2018FI_B2_00104). R.B. received a predoctoral fellowship from the 'Impuls Program' funded by the University of Lleida and Banco Santander (UdL, ref 0864/2016). We thank Salvador Batolome, from the Laboratory of Luminescense and Biomolecular Spectroscopy (Autonomous University of Barcelona, Barcelona, Catalonia, Spain), for ddPCR technical support.

This work was supported by the Spanish Ministry of Economy and Competitiveness, Institute of Health Carlos III (grant number PI14/00328), the Spanish Ministry of Science, Innovation and Universities (RTI2018-099200-B-I00), and the Generalitat of Catalonia, Agency for Management of University and Research Grants (2017SGR696) and Department of Health (SLT002/16/00250) to R.P. This study has been co-financed by FEDER funds from the European Union ("A way to build Europe").

Author Contributions

G.B and R.P designed the study. N.M.M., M.J., I.P., R.B., I.S., A.N., and E.G. performed experimental work. N.M.M and R.P. analysed the data. R.P. supervised the design and data interpretation. The manuscript was written by N.M.M, G.B. and R.P. and edited by R.P. All authors discussed the results and commented on the manuscript.

Declaration of Interests

The authors declare no competing financial interest.

Figures

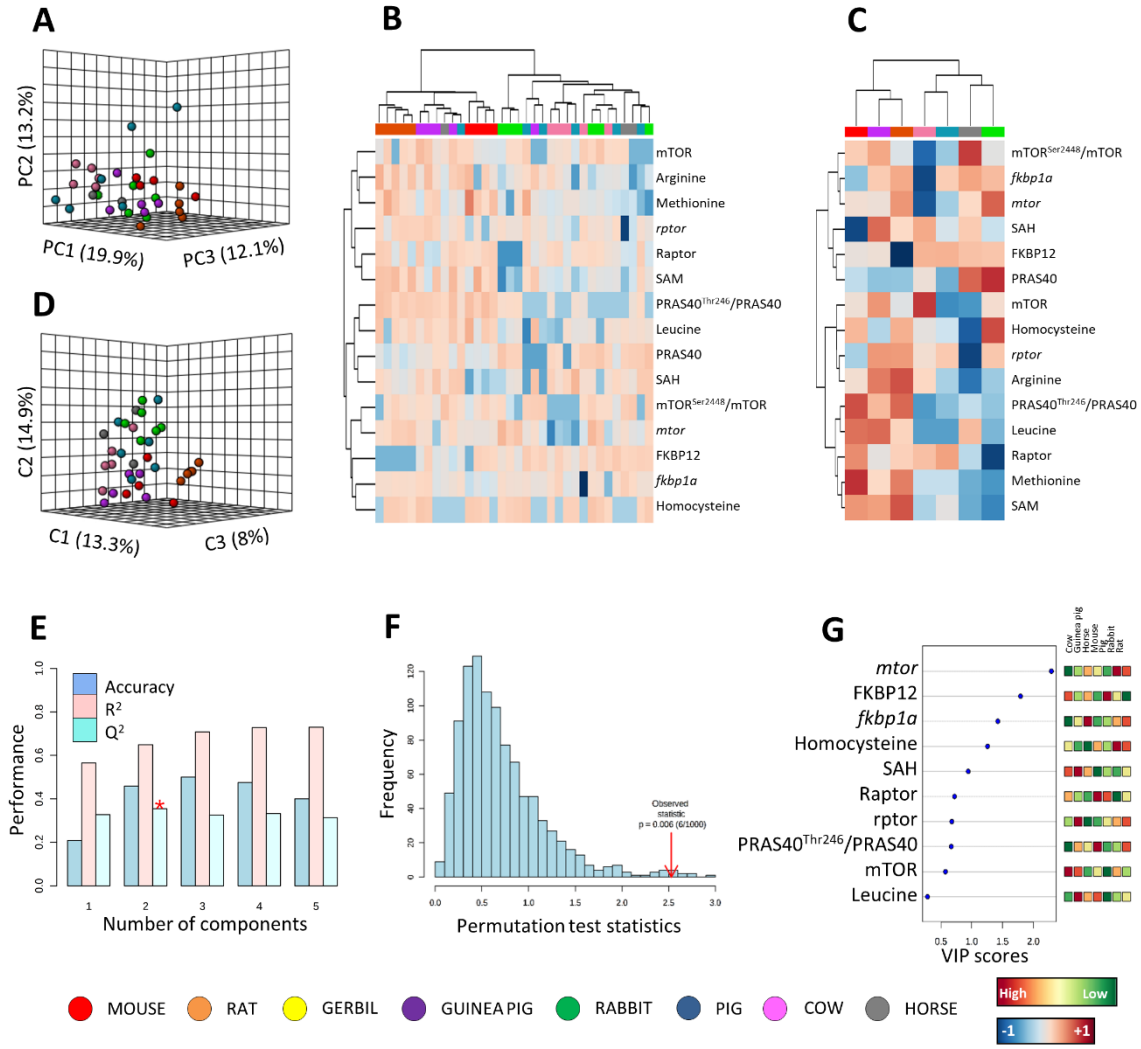

Figure 1. Multivariate statistics reveals a species-specific gene expression and protein content and phosphorylation of mTORC1 subunits, and metabolite concentration of its regulators. A) Principal component analyses (PCA) representation of gene expression and protein content and phosphorylation of mTORC1, and metabolite concentration (µM/mg of heart tissue) of its regulators. X: Principal component 1 (PC1); Y: Principal component 2 (PC2); Z: Principal component 3 (PC3). **B)** Hierarchical clustering of individual animal samples according to gene expression and protein content and phosphorylation of mTORC1, and metabolite concentration (µM/mg of heart tissue) of its regulators. **C)** Hierarchical clustering of animal species according to average sample values of gene expression and protein content and phosphorylation of mTORC1, and metabolite concentration (µM/mg of heart tissue) of its regulators. **D)** Partial least squares discriminant analysis (PLS-DA) representation of gene expression and protein content and phosphorylation of mTORC1, and metabolite concentration (µM/mg of heart tissue) of its regulators. X: Component 1 (C1); Y: Component 2 (C2); Z: Component 3 (C3). **E)** Cross validation (CV) analyses (10-fold CV method) of the PLS-DA model. **F)** Permutation test (1000 repeats) using separation distance. **G)** Variable importance projection (VIP) scores indicating the elements which contribute most to define the first component of a PLS-DA.

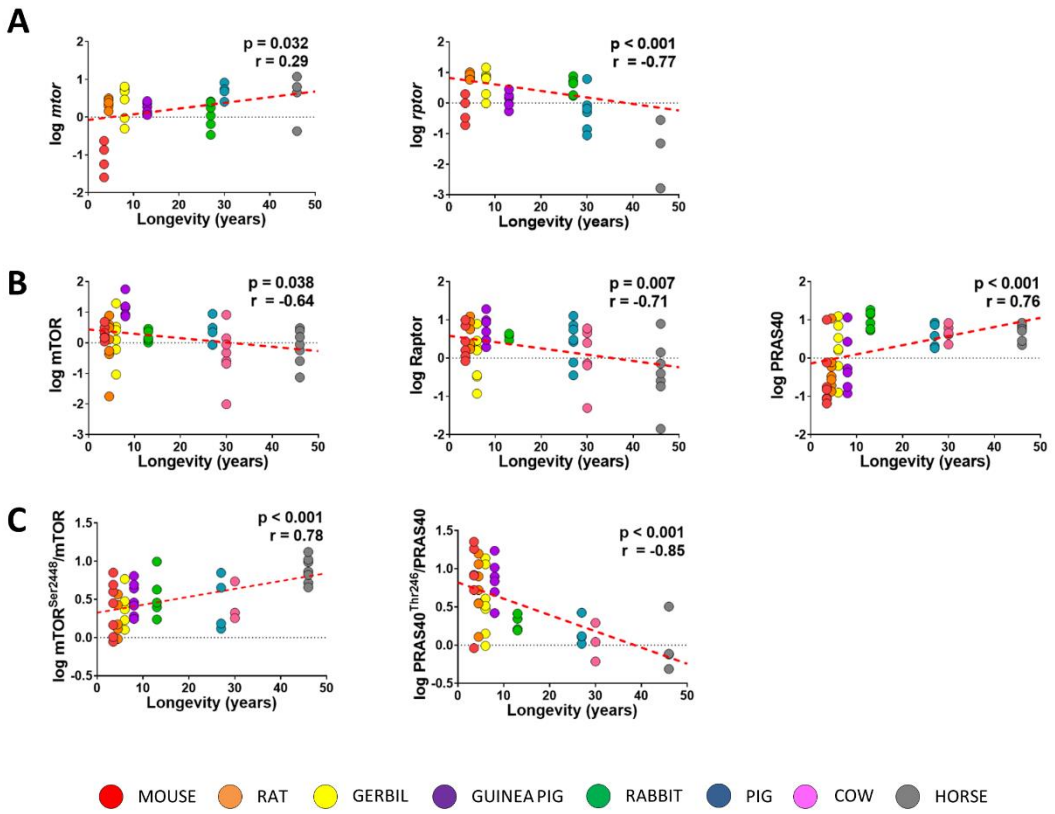

Figure 2. mTORC1 gene expression (A), protein content (B) and phosphorylation (C) are linearly correlated with mammalian longevity. Pearson correlations were performed between gene expression, protein content or phosphorylation, and longevity. Linear regression was applied when significant relationships were found. R^2(*mtor*) = 0.1; R^2(*rptor*) = 0.40; R^2(mTOR)<0.1; R^2(Raptor) = 0.14; R^2(PRAS40) = 0.22; R^2(mTOR^{Ser2448}/mTOR) = 0.27; R^2(PRAS40^{Thr246}/PRAS40) = 0.40. Minimum signification level was set at p<0.05. Gene expression, and protein content and phosphorylation were log-transformed to accomplish the assumptions of normality.

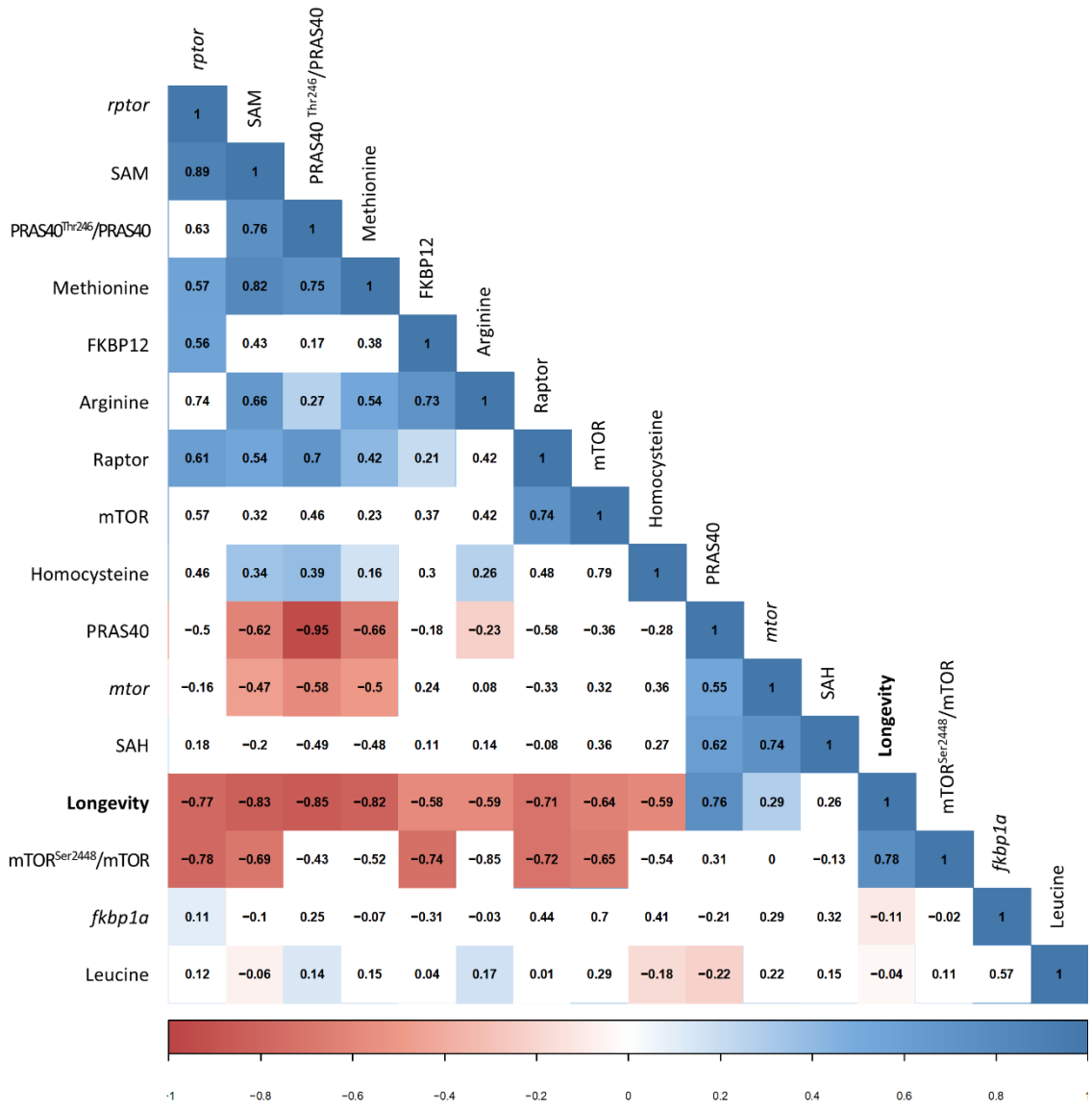

Figure 3. Gene expression, protein content and phosphorylation of mTORC1 subunits are correlated with metabolite concentration of its regulators. Pearson r-value for pairwise comparisons is reported. Non-significant correlations are left in blank. Minimum signification level was set at $p<0.05$. Gene expression, protein content and phosphorylation, and metabolite concentration (µM/mg of heart tissue) were log-transformed to accomplish the assumptions of normality.

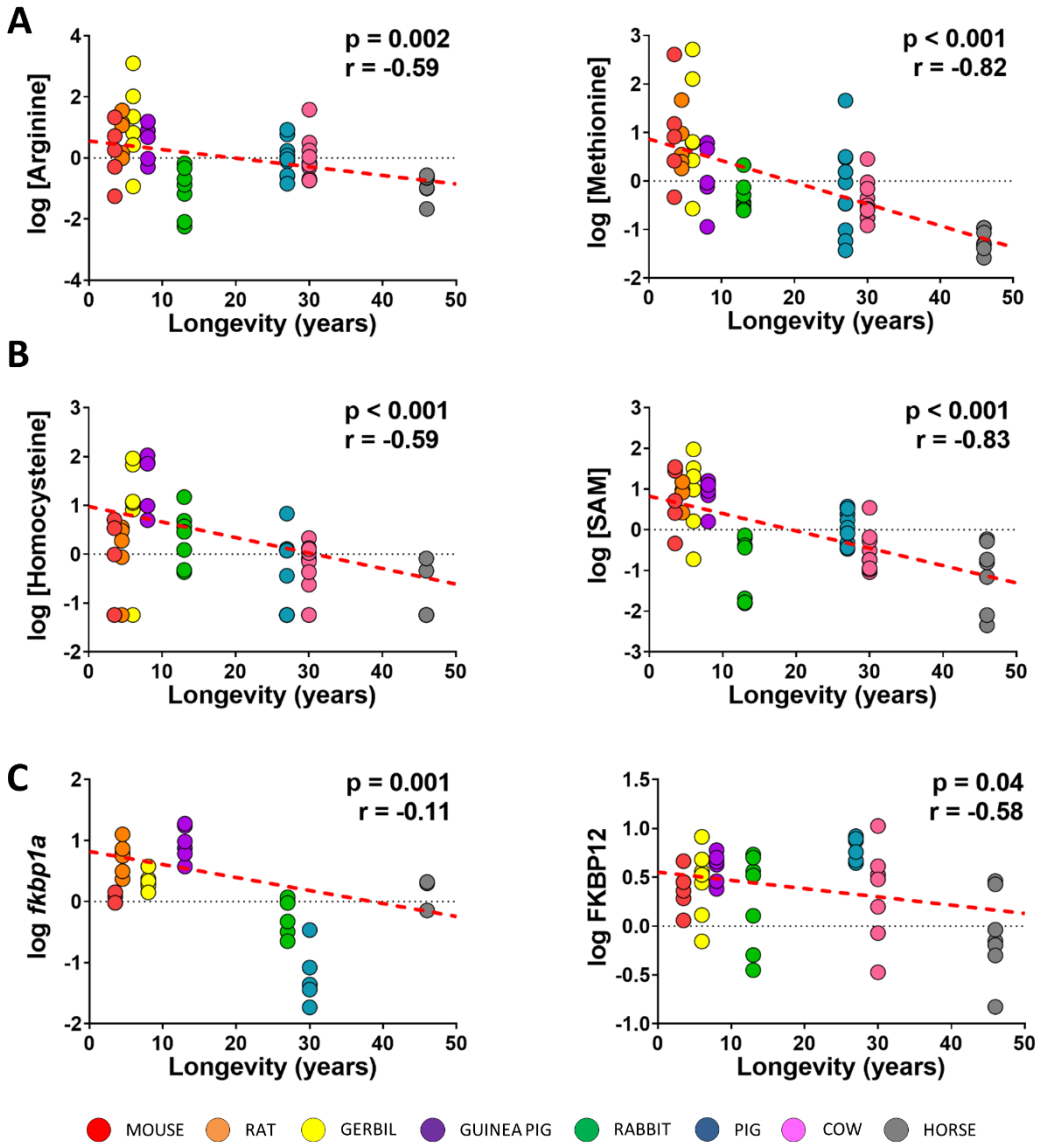

Figure 4. Regulatory factors of mTORC1 are correlated with mammalian longevity. A) Correlation between amino acids (arginine and methionine) and animal ML. **B)** Correlation between methionine cycle metabolites (SAM and homocysteine) and species longevity. **C)** Correlation between FKBP12 gene expression and protein content and longevity. Pearson correlation was performed between longevity and gene expression, protein content and phosphorylation, and metabolite concentration (µM/mg of heart tissue). Pearson r values are reported in **Figure 3**. Linear regression was applied when significant relationships were found. R^2(Methionine) = 0.42; R^2(Arginine) = 0.16; R^2(SAM) = 0.38; R^2(Homocysteine) = 0.24; R^2(*fkbp1a*) = 0.33; R^2(FKBP12) < 0.1; Minimum signification level was set at $p<0.05$. Gene expression, protein content and metabolite concentration were log-transformed to accomplish the assumptions of normality.

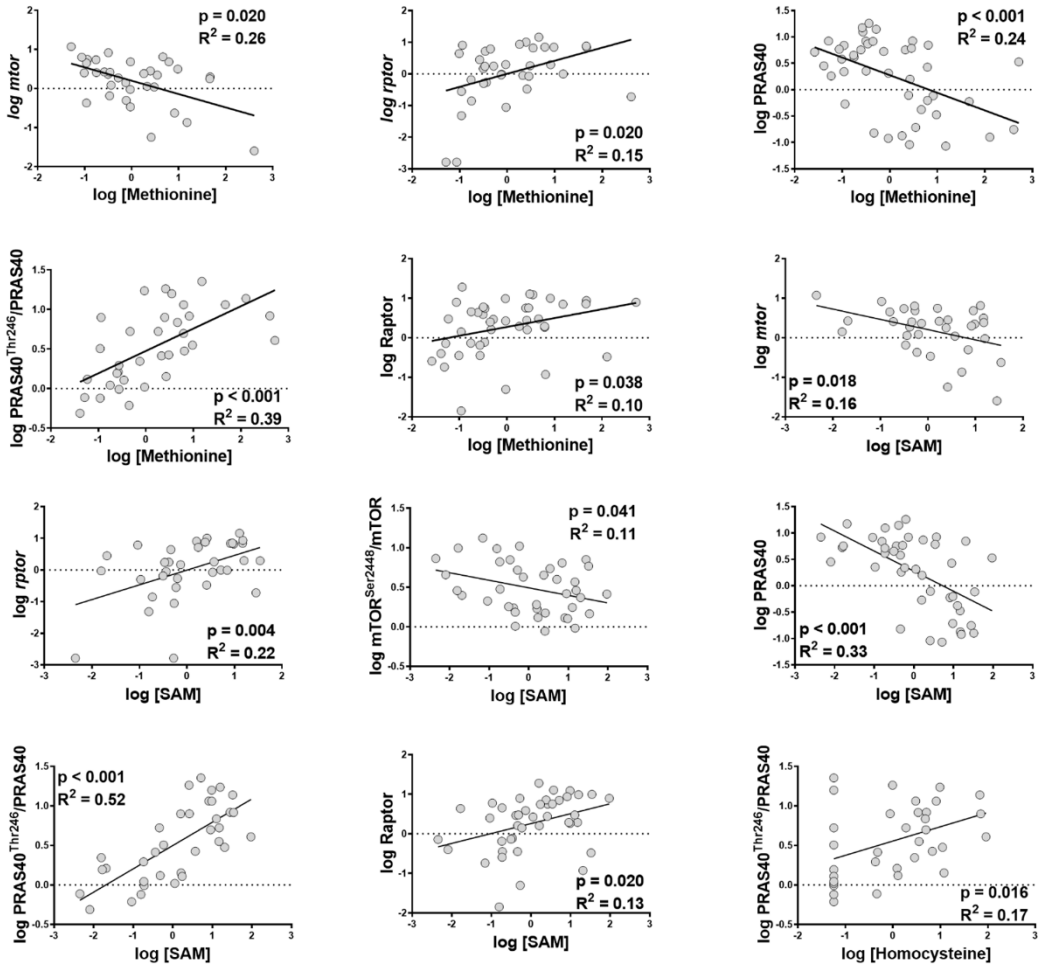

Figure 5. mTORC1 and methionine-related metabolites are correlated in heart tissue from mammalian species. Pearson correlation was performed among gene expression, protein content or phosphorylation and metabolite concentration (µM/mg of heart tissue). Pearson r values are reported in **Figure 3**. Linear regression (LR) model was performed when significant relationships were found. Minimum signification level was set at $p<0.05$. Gene expression, protein content and phosphorylation, and metabolite concentration were log-transformed to accomplish the assumptions of normality.

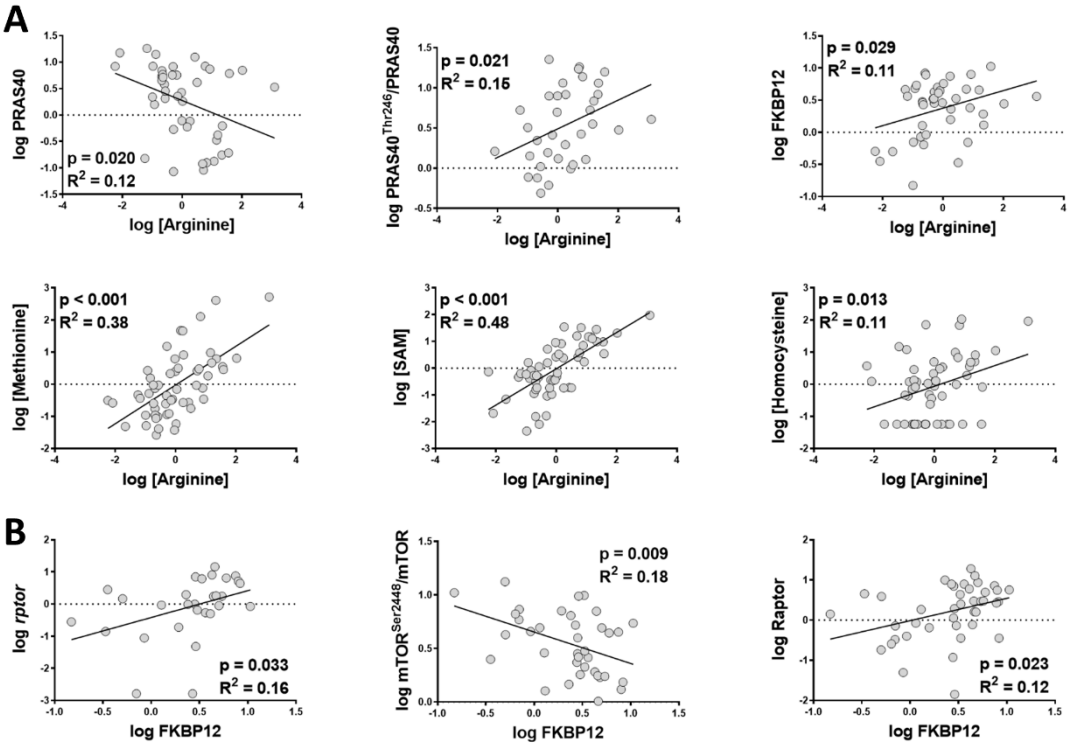

Figure 6. mTORC1 and its regulators arginine and FKBP12 are correlated in heart tissue of mammals. Pearson correlation was performed among gene expression, protein content and phosphorylation, and metabolite concentration. Pearson r values are reported in **Figure 3**. Linear regression (LR) model was performed when significant relationships were found. Minimum signification level was set at $p<0.05$. Gene expression, protein content and phosphorylation, and metabolite concentration were log-transformed to accomplish the assumptions of normality.

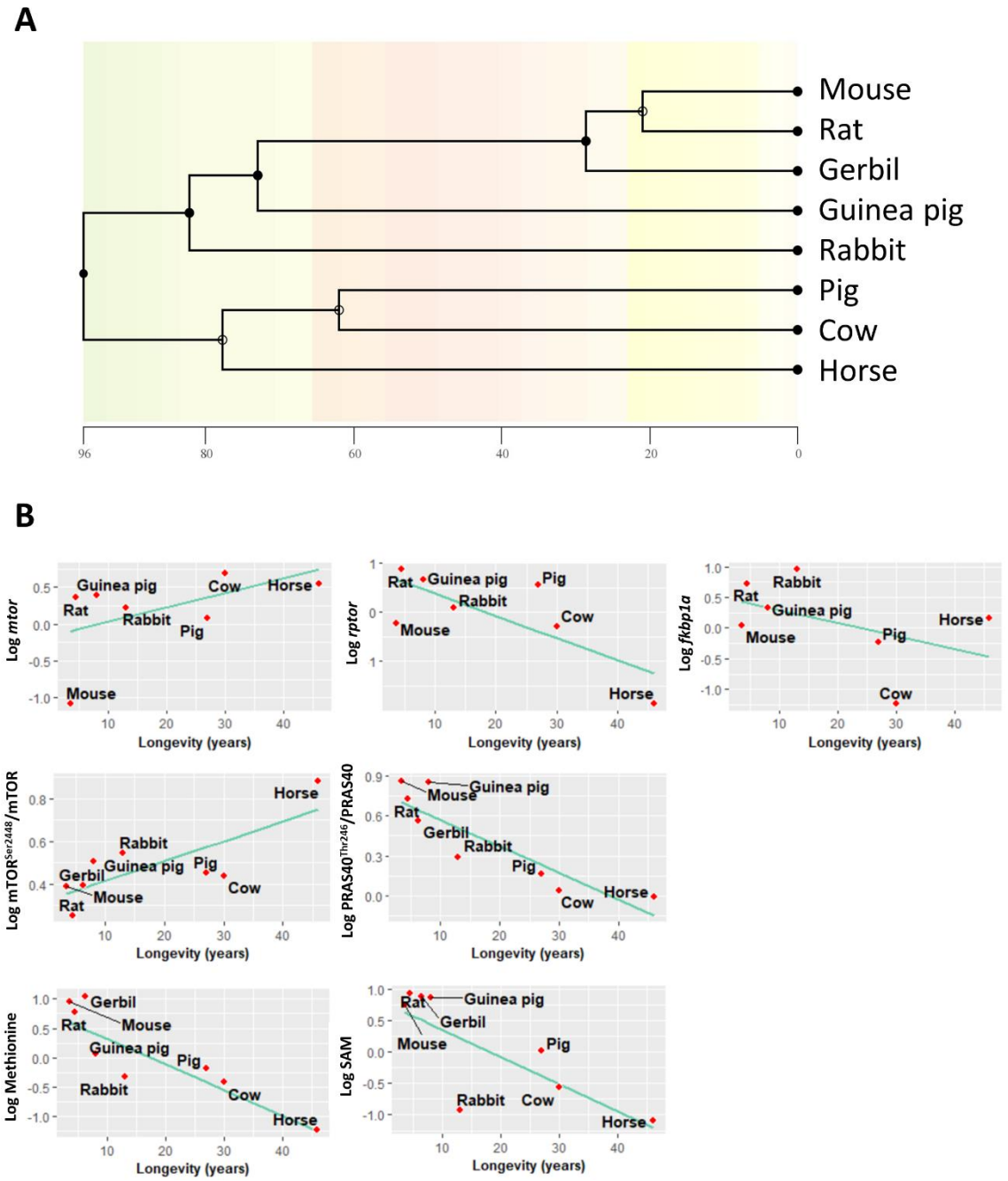

Figure 7. mTORC1 is correlated with animal longevity after correcting for phylogenetic relationships. A) Phylogenetic tree with a timescale of million years ago. **B)** mTORC1 subunits and regulators that are correlated with animal longevity after performing a phylogenetic generalised least squares regression. Metabolite concentration, gene expression and protein content were log-transformed to accomplish the assumptions of normality.

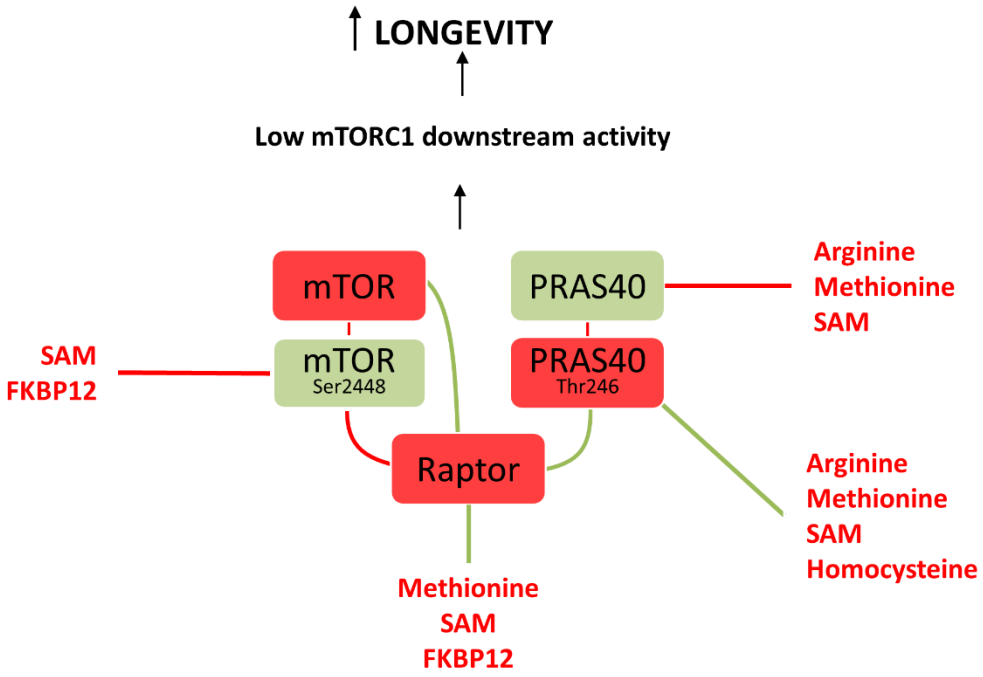

Figure 8. Longevity model of the mTORC1 modulation. Coloured boxes are used to indicate increased (green boxes) or decreased (red boxes) mTORC1 elements in long-lived animals. Coloured text is used to indicate increased (green text) or decreased (red text) mTORC1 regulatory factors in long-lived animals. Coloured lines are used to indicate positive (green lines) or negative (red lines) correlations between mTORC1 and its regulatory factors, as reported in **Figures 3, 5, 6**, or among mTORC1 elements, as reported in **Figure 3** and **Supplementary figure 1**.

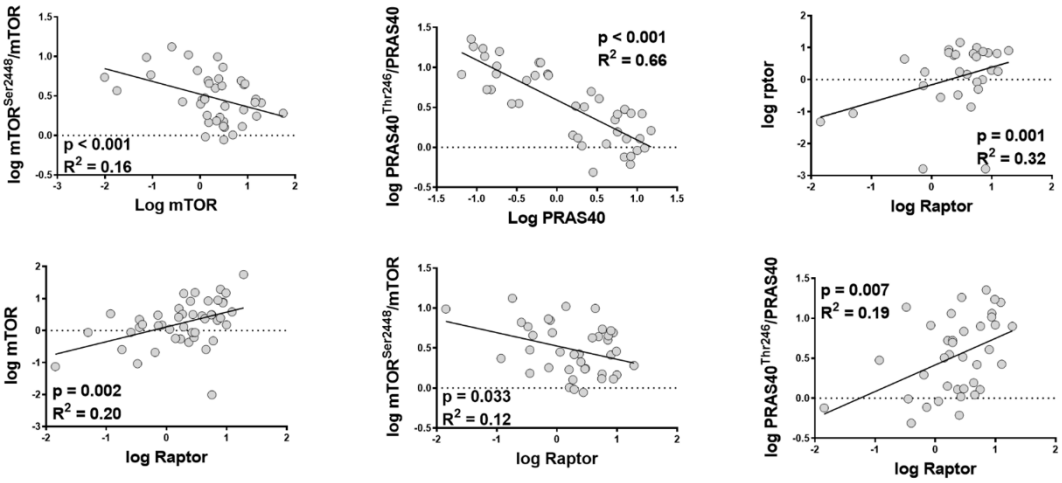

Supplementary figure 1. mTORC1 core components are correlated in heart tissue from mammalian species. Pearson correlation was performed. Pearson r values are reported in **Figure 3**. Linear regression (LR) model was performed when significant relationships were found. Minimum signification level was set at $p<0.05$. Gene expression, protein content and phosphorylation were log-transformed to accomplish the assumptions of normality.

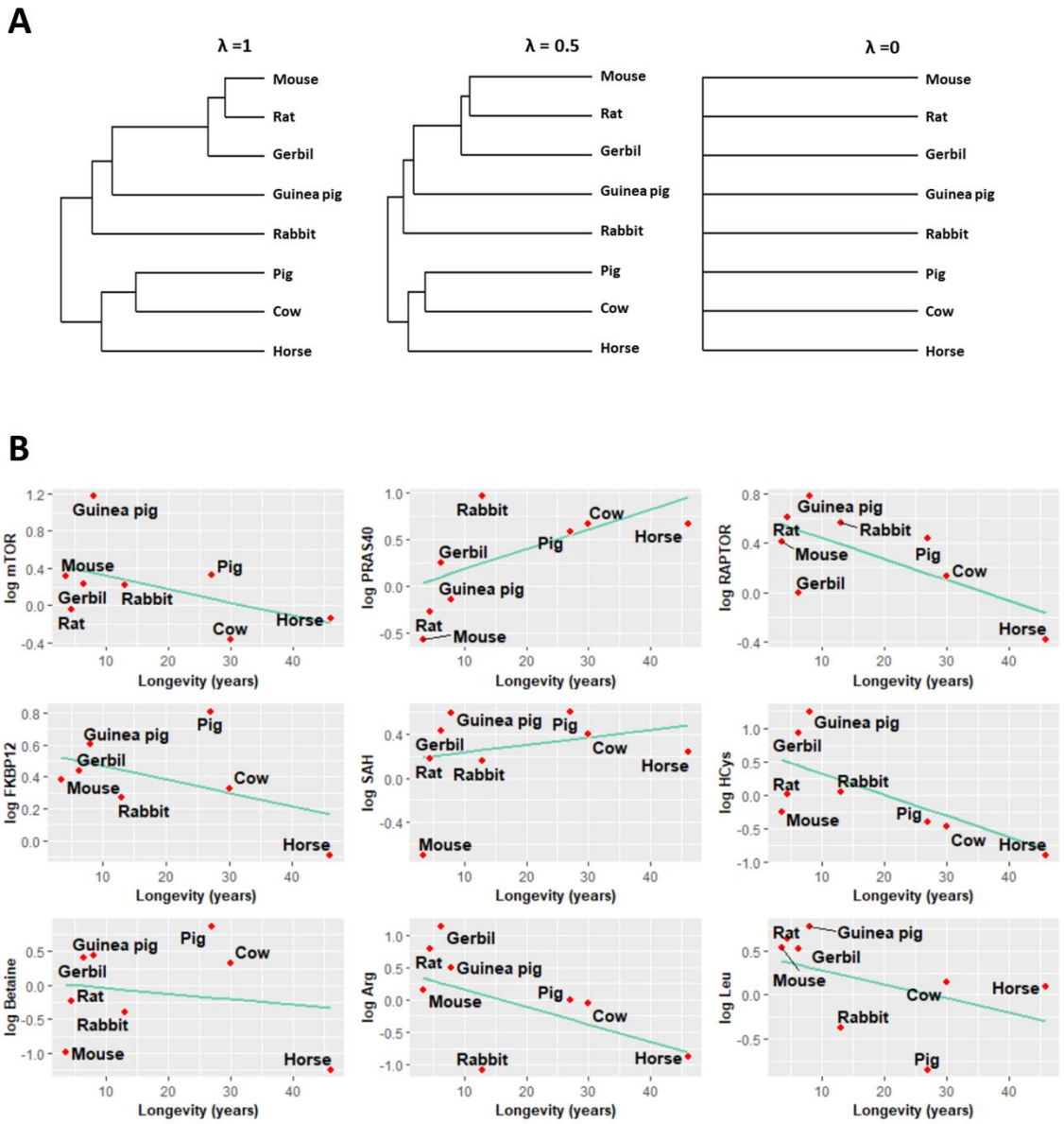

Supplementary figure 2. mTORC1 subunits and regulators that are not correlated with animal longevity after correcting for phylogenetic relationships. **A)** Effect of Pagel's λ value on phylogeny branch length, when assuming absent (λ=0) or strong (λ=1) phylogenetic signal in the data.

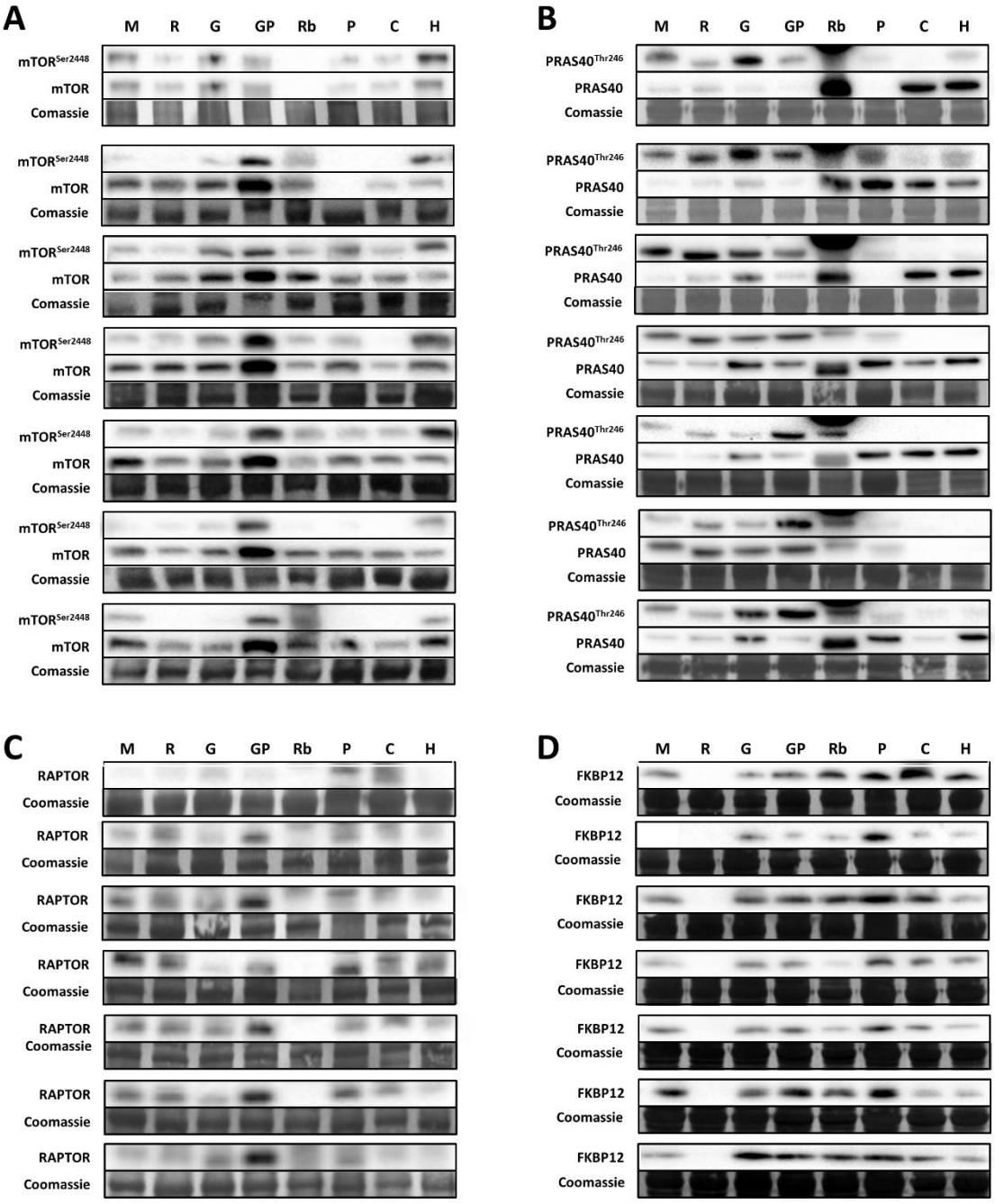

Supplementary figure 3. Individual mTORC1 protein content and phosphorylation from animal's heart. A) mTOR total protein content, mTOR^{Ser2448} and its respective Coomassie. **B)** PRAS40 total protein content, PRAS40^{Thr246} and its respective Coomassie. **C)** Raptor protein content and its respective Coomassie. **D)** FKBP12 protein content and its respective Coomassie. M = Mouse; R = Rat; G = Gerbil; GP = Guinea pig; Rb = Rabbit; P = Pig; C = Cow; H = Horse

Tables

Supplementary table 1. Phylogenetic generalized least squares (PGLS) regression between mTORC1 gene expression and protein content and phosphorylation of its subunits and its regulators content and animal longevity.

	λ	Pearson r	Sig.
Gene expression			
mtor	1	-0.21	0.009
rptor	0.17	0.05	0.009
fkbp1a	0	-0.16	0.020
Protein content			
mTOR	0	-0.44	0.233
PRAS40	1	-0.49	0.252
RAPTOR	0	-0.67	0.060
FKBP12	0	-0.83	0.291
Protein phosphorylation			
mTOR^{S2448}	0	-0.94	0.024
PRAS40^{T246}	1	-0.66	0.023
Metabolite concentration			
Methionine	0.90	0.17	0.011
SAH	1	-0.34	0.768
SAM	0.86	0.11	0.050
Homocysteine	1	0.02	0.250
Betaine	0	0.14	0.688
Arginine	1	0.12	0.336
Leucine	0.29	-0.24	0.309

Methionine transsulfuration pathway is upregulated in long-lived humans

Mota-Martorell N[1], Jové M[1], Borras C[2], Berdún R[1], Obis E[1], Joaquim Sol[1,3,4], Cabré R[1], Pradas I[1], Galo-Licona JD[1], Puig J[5], Viña J[2], Pamplona R[1,*]

[1] Department of Experimental Medicine, University of Lleida-Biomedical Research Institute of Lleida (UdL-IRBLleida), Lleida, Catalonia, Spain.

[2] Freshage Research Group, Department of Physiology, University of Valencia, CIBERFES, INCLIVA, Valencia, Spain.

[3] Institut Català de la Salut, Atenció Primària, Lleida, Spain.

[4] Research Support Unit Lleida, Fundació Institut Universitari per a la recerca a l'Atenció Primària de Salut Jordi Gol i Gurina (IDIAPJGol), Lleida, Spain

[5] Department of Radiology (Institut de Diagnòstic per la Imatge, IDI), University Hospital Dr Josep Trueta, Girona Biomedical Research Institute (IDIBGI), Girona, Catalonia, Spain.

[*] **Corresponding author**:

Prof. Reinald Pamplona. Department of Experimental Medicine, University of Lleida-Lleida Biomedical Research Institute (UdL-IRBLleida), Biomedicine 1 building, Av. Rovira Roure 80, Lleida 25198, Spain. E-mail: reinald.pamplona@mex.udl.cat

E-mail addresses of the rest of the authors:

NMM: nataliamotamartorell@gmail.com

MJ: mariona.jove@udl.cat

CB: consuelo.borras@uv.es

RB: rebecaberdun@gmail.com

EO: elia.obis@udl.cat

JS: solcullere@gmail.com

RC: rosannacabre@gmail.com

IP: irene.pradas@gmail.com

JDGL: jgalolic25@gmail.com

JP: jpuigmd@gmail.com

JV: jose.vina@uv.es

Abstract

Available evidences point to methionine metabolism as a key target to study the molecular adaptive mechanisms underlying differences in longevity. The plasma methionine metabolic profile was determined using a LC-MS/MS platform to systematically define specific phenotypic patterns associated with genotypes of human extreme longevity (centenarians). Our findings demonstrate the presence of a specific plasma profile associated with human longevity characterized by an enhanced transsulfuration pathway and tricarboxylic acid (TCA) cycle intermediates, as well as a reduced content of specific amino acids. Furthermore, our work reveals that centenarians maintain a strongly correlated methionine metabolism, suggesting an improved network integrity, homeostasis and more tightly regulated metabolism. We have discovered a particular methionine signature related to the condition of extreme longevity, allowing the identification of potential mechanisms and biomarkers of healthy aging.

Keywords

Amino Acids; Centenarians; TCA Cycle Metabolites; Longevity; Methionine Cycle; Plasma; Transsulfuration pathway

Introduction

Methionine is an essential proteinogenic amino acid selected and incorporated to the universal genetic code based on their functional properties and in response to the appearance of biospheric molecular oxygen during early evolution (Granold et al., 2018; Moosmann et al., 2020). In fact, molecular oxygen demanded early organisms to incorporate additional amino acids with increased redox properties into the genetic code like lysine, histidine, phenylalanine, cysteine, tyrosine, tryptophan, and selenocysteine as adaptation to preserve aerobic life (Granold et al., 2018). Interestingly, the protein content of the sulfur amino acids methionine and cysteine keeps a relationship with animal longevity. Thus, the longer the animal longevity, the lower the methionine (Aledo et al., 2011; Pamplona et al., 2005; Portero-Otín et al., 2004; Ruiz et al., 2005) and cysteine (Moosmann, 2011) protein content, probably as adaptive response (Pamplona and Barja, 2011) to the lower oxidative stress also present in long-lived animal species (Pamplona and Barja, 2006, 2007, 2011). Later, these observations were extended to the free tissue methionine content in diverse long-lived animal species (Lewis et al., 2018; Mota-Martorell et al., 2020b). Reinforcing these findings, methionine restriction is a nutritional intervention that extend animal longevity (McIsaac et al., 2016; Pamplona and Barja, 2006, 2011). Consequently, available evidences point to methionine metabolism as a key target to study the molecular adaptive mechanisms underlying differences in longevity.

Beyond its function in several intracellular processes, methionine is central in a complex metabolic pathway which can be divided in three parts: methionine cycle, the transsulfuration pathway, and polyamine biosynthesis (Parkhitko et al., 2019; Sanderson et al., 2019) (**Figure 1; for details see Figure 15 of this Thesis**). Methionine is an essential sulphur-containing metabolite that is mainly metabolized through the transmethylation pathway or the methionine cycle. Briefly, methionine is converted to the universal methyl donor S-adenosylmethionine (SAM), which upon donation of one methyl group is converted to S-adenosylhomocysteine (SAH). SAH is hydrolyzed into homocysteine, which can be used to regenerate methionine via betaine or folate cycle. However, homocysteine can enter into the transsulfuration pathway, and be sequentially converted into cystathionine and cysteine in a series of reactions catalyzed by enzymes that use vitamin B6 as cofactor. Finally, this cysteine can be directed to the glutathione synthesis or, via several metabolic reactions, to the synthesis of taurine. Significantly, manipulation of each of these branches affects longevity in diverse animal models (McIsaac et al., 2016).

As a consequence of these observations, it is plausible to postulate that long-lived humans (like centenarians) significantly delay or in several cases even avoid age-associated diseases because they express and have a specific methionine metabolic phenotype. Up to date no targeted metabolomics analysis investigating differences in the plasma methionine metabolome of exceptionally long-lived humans have been reported. Blood plasma is the major carrier of metabolites in the body (Psychogios et al., 2011). The composition of this biological fluid is well-known, even it is continuous change, reflecting physiological states in health and disease (Burla et al., 2018; Jové et al., 2016). Although metabolomics data interpretation is often challenging and mostly descriptive, it is more than a source of potential biomarkers and metabolomic signatures associated with specific states, such as longevity (Lewis et al., 2018): it also allows the identification of new mechanistic pathways or targets that might lead to healthier and longer

lives. To this end, we have designed a study to detect and quantify a panel of metabolites including 36 different molecular species: a) methionine and its related metabolites, including the intermediates of the transmethylation pathway SAM, SAH and homocysteine; betaine and spermidine as metabolites involved in the regeneration of methionine plasma levels; the intermediates of the transsulfuration pathway cysteine and cystathionine; taurine and glutathione as downstream metabolites of the transsulfuration pathway; and vitamin B6 metabolites pyridoxal, pyridoxal-5'-phosphate and pyridoxamine, as cofactors of the transsulfuration enzymes; b) additional amino acids including 7 non-polar amino acids (alanine, glycine, leucine/isoleucine, phenylalanine, proline, tyrosine and valine), 4 polar uncharged amino acids (asparagine, serine, threonine and tryptophan), 1 polar negatively charged amino acid (glutamate) and 2 polar positively charged amino acids (arginine and histidine); c) TCA cycle metabolites, including pyruvate, citrate, isocitrate, α-ketoglutarate, succinate, fumarate and malate; and d) methionine-derived lipid intermediates such as choline and carnitine. The plasma metabolites profile was determined using a LC-MS/MS platform to systematically define specific phenotypic patterns associated with genotypes of human extreme longevity.

Results

Centenarians have a unique methionine-related metabolites plasma profile

In order to determine whether plasma methionine and its related metabolites concentration differed among adult, aged and centenarian individuals, multivariate statistics were applied. Non-supervised principal component analysis (PCA) suggested a different specific plasma methionine metabolites profile in centenarians (**Figure 2A**), capable to explain 48.7% of sample variability. A hierarchical clustering of the samples represented by a heat map revealed that centenarian's unique plasma profile of methionine-related metabolites was different from those of adults and aged individuals (**Figure 2B**). These results were confirmed by performing a supervised analysis, such as partial least squares discriminant analysis (PLS-DA), which showed that plasma metabolite content is a good model to identify the different groups. The model was trained using 60% of the samples and tested using the remaining 40%, obtaining an accuracy of 0.73 in the classification of the test data (binomial test, p[accuracy>no information ratio] = 0.0005). Permutation tests (1000 repeats) yielded a low $p<0.001$, indicating that none of the distributions formed by the permutated data was better than the observed statistics based on the original data. The discriminating power between groups of the different measured features was ranked by applying the scaled variable importance score (**Figure 2C**), indicating that glutathione, cysteine, homocysteine and cystathionine were the metabolites with higher weight discriminating groups. Specifically, glutathione and cysteine are the metabolites with a highest influence in aged group whereas cysteine, homocysteine and cystathionine defined better adult and centenarians.

Transsulfuration intermediates are increased in plasma from centenarians

The specific changes in methionine and its related metabolites content in plasma from centenarians were evaluated. Globally, methylation and transsulfuration metabolites were increased in plasma from centenarians (**Figure 2D, Supplementary table 2**). Specifically, centenarians have an increased content of SAH, homocysteine, cystathionine and taurine in comparison to adult and aged individuals. SAM and cysteine were also higher in centenarians in comparison with adults. Aged individuals were found to have higher levels of homocysteine and cysteine in comparison to adults. However, homocysteine levels in aged were still lower than those in centenarians. Adults were found to have the lowest plasma levels of homocysteine and cysteine. Methionine and glutathione plasma content remained unchanged among the different age groups, as well as betaine, spermidine and the vitamin B6 intermediate metabolites (**Supplementary figure 1**). Surprisingly, although glutathione presented no significant differences between groups, it had a high impact when defining aged group in multivariate statistics.

Centenarians and aged individuals maintain a similar amino acids plasma profile

Since methionine is a proteinogenic amino acid, we hypothesized the possibility that other amino acids could be also involved in the achievement of centenarian condition. Specifically, we have been able to unambiguously detect 14 additional amino acids apart from cysteine and methionine. In order to determine whether plasma amino acids content differed among adult, aged and centenarian individuals, multivariate statistics were applied using the concentration of 16 plasma amino acids. Non-supervised PCA revealed the existence of an adults-specific plasma

amino acids profile (**Figure 3A**), capable to explain 42% of sample variability. A hierarchical clustering of the samples represented by a heat map revealed that centenarians maintain an aged plasma amino acid profile, and that methionine is associated with longevity (similar content between adult and centenarians) (**Figure 3B**). These results were confirmed by performing a supervised analysis, such as PLS-DA, which showed that plasma metabolite content is a good model to identify the different groups. The model was trained using 60% of the samples and tested using the remaining 40%, obtaining an accuracy of 0.64 in the classification of the test data (binomial test, p[accuracy>no information ratio] = 0.008). Permutation tests (1000 repeats) yielded a low $p<0.001$, indicating that none of the distributions formed by the permutated data was better than the observed statistics based on the original data. The discriminating power between groups of the different measured features was ranked by applying the scaled variable importance score (**Figure 3C**). The results showed that homocysteine and cysteine were the two amino acids with highest weight defining plasma amino acid profile of adult and centenarians, followed by threonine and serine, whereas homocysteine and tyrosine had highest power in defining aged group, followed by glutamate and arginine. In order to discard that the metabolic signature was mainly determined by methionine metabolism metabolites, multivariate statistics were also performed without including the methionine-related amino acids (methionine, homocysteine, cysteine) and similar results were obtained (data not shown).

The specific changes plasma amino acids in centenarians were also evaluated (**Figure 3D-G, Supplementary table 2).** Among the 14 additionally detected amino acids (methionine and cysteine amino acids not included), we have found a specific decrease of tryptophan plasma content in centenarians. Serine, threonine and valine were also decreased in centenarians in comparison to adults. Asparagine, in turn, was increased in adults in comparison to aged and centenarians.

Energy metabolism intermediates are increased in plasma from centenarians

Considering that amino acids can be metabolised into TCA cycle intermediates, we have analysed the plasma changes for TCA cycle metabolites. Specifically, we had been able to unambiguously detect 7 intermediates, including pyruvate, citrate, isocitrate, α-ketoglutarate, succinate, fumarate and malate. In order to determine whether centenarians have a specific plasma profile for TCA cycle intermediates, multivariate statistics were applied using the plasma concentration of the mentioned metabolites. A hierarchical clustering of the samples represented by a heat map revealed that centenarians have a unique plasma TCA cycle intermediates profile (**Figure 4A**), in terms of maintaining increased intermediates plasma content. Furthermore, we have identified a group of aged individuals that clustered together with some centenarians (**Figure 4B**), which might correspond to aged individuals with an optimized energy metabolism and capable to reach the centenarian condition. However, multivariate statistics revealed that TCA metabolites did not discriminate centenarians group. PCA showed no differences between groups (**Supplementary figure 2A**) whereas PLS-DA accuracy for this model was 0.5 and the classification of the test data (binomial test, p[accuracy>no information ratio] = 0.16). The discriminating power between groups of the different measured features was ranked by applying the scaled variable importance score where

succinate, pyruvate and fumarate arose as the TCA metabolites with highest weight defining aged condition (**Supplementary figure 2B**)

The specific changes in plasma intermediates of TCA cycle were also evaluated (**Figure 4C, Supplementary table 2**). Among the 7 detected metabolites, centenarians were found to have the highest plasma content of citrate, α-ketoglutarate, succinate and malate in comparison to adult and aged individuals. Pyruvate and isocitrate were also higher in centenarians in comparison to adults. Aged individuals were found to have higher pyruvate and malate levels, although plasma levels of malate were still lower that those found in centenarians. The lowest plasma content of pyruvate and malate were found in adults. Fumarate plasma content remained unchanged.

Amino acids and TCA cycle intermediates are bidirectionally related: the amino acids carbon skeleton can be used to synthetize TCA cycle intermediates and vice versa (**Figure 5A**). Since plasma amino acids were decreased in centenarians, we have estimated the conversion of specific amino acids into the measured TCA intermediates (**Figure 5B**). In fact, centenarians were found to have increased synthesis of pyruvate from serine and tryptophan, and synthesis of α-ketoglutarate from arginine, glutamate, histidine and proline. The synthesis of pyruvate from alanine, glycine and threonine was higher in centenarians in comparison with adults. Synthesis of pyruvate from serine and threonine was decreased in adults. In addition, positive correlations between pyruvate and serine and alanine were found in centenarians, and between pyruvate and alanine and threonine in adults (**Supplementary figure 3**).

Centenarians plasma metabolome is also related with specific lipid intermediates

Methionine metabolism participates in the biosynthesis of lipid intermediates such as choline and carnitine. Plasma choline levels were higher in centenarians than adults (**Figure 5C**). Carnitine plasma levels, in turn, were increased in aged (**Figure 5C**).

Centenarians maintain network integrity

In addition to identifying changes on individual metabolites content, we have also sought the underlying longevity mechanisms by identifying the metabolomic network integrity through correlation patterns within the different groups of the two main metabolic pathways analysed, methionine metabolism and TCA cycle.

The network plot revealed different hubs (metabolites with multiple interactions) and signalling network for methionine metabolism in plasma for each group (**Figure 6A-F**). Accordingly, centenarians maintain a unique signalling network being cysteine the central hub (**Figure 6A-C**), with a stronger correlation degree in comparison to adult and aged individuals (**Supplementary figure 4**). In adults, we have found an ordered pattern, characterised by correlations within the transmethylation and transsulfuration metabolites separately (**Figure 6D**). Specifically, SAM was negatively correlated with betaine and choline. The sulphur-containing metabolite cystathionine was positively correlated with both homocysteine and pyridoxamine. In aged individuals, no correlations between the transmethylation metabolites were found (**Figure 6E**). Regarding sulphur-containing metabolites, cysteine was positively correlated with cystathionine and glutathione. Pyridoxamine was also positively correlated with glutathione. In both groups, positive correlations between vitamin B12 intermediates pyridoxal and pyridoxamine were also

found. Centenarians, in turn, show a complex but ordered correlation pattern (**Figure 6F**). Accordingly, of biological significance are the correlations found within i) the trans-methylation metabolites (positive correlation of SAM with methionine and SAM); ii) the transsulfuration metabolites (positive correlation of cystathionine with homocysteine, cysteine and pyridoxamine); and iii) sulphur-containing metabolites (positive correlation between cysteine and taurine).

TCA cycle network plot also revealed different plasma signalling network for each group (**Figure 6G-L**). Surprisingly, the highest (**Figure 6 G-I**) and strongest (**Supplementary figure 4**) correlation degree was found in aged individuals, which show a matted signalling network. Positive correlations between fumarate and malate, malate and citrate, and citrate and isocitrate, were found in adults, suggesting the existence of a continuous flux of reactions from fumarate to isocitrate (**Figure 6J**). In aged individuals, citrate was positively correlated with malate, pyruvate and isocitrate (**Figure 6K**). Positive correlation between fumarate and isocitrate was also found. However, this correlation pattern revealed a fragmented network, with a flux of reactions from malate to isocitrate, depending upon pyruvate, and isocitrate to fumarate. Centenarians, in turn, show positive correlations between malate and citrate, citrate and isocitrate, and isocitrate and α-ketoglutarate were also found, suggesting in this case, a continuous flux of reactions from malate to α-ketoglutarate (**Figure 6L**).

Discussion

Transsulfuration is enhanced in centenarians and leads to a unique methionine plasma profile

Human longevity benefits from an organismal reorganization of its whole metabolism. Several intracellular signalling pathways are modulated, but mostly converge in the modulation of a small set of pro-longevity genes (Houtkooper et al., 2010). Consequently, this leads to a specific gene expression pattern (Borrás et al., 2017; Gambini et al., 2016; Inglés et al., 2019; Passtoors et al., 2012) which supports specific proteomics (Lehallier et al., 2019), metabolomics (Cheng et al., 2015; Houtkooper et al., 2010; Lewis et al., 2018) and lipidomics (Jové et al., 2017; Pradas et al., 2019b) profile associated with human longevity. In our study, we have identified that methionine plasma metabolome is associated with exceptional human longevity. Our model revealed that using trans-methylation and transsulfuration metabolites we are able to explain the centenarian condition, being the transsulfuration metabolites cysteine, homocysteine and cystathionine the highest longevity predictors.

The association between methionine and longevity has been deeply studied. Long lived mammals have lower tissue (Pamplona et al., 2005; Portero-Otín et al., 2004; Ruiz et al., 2005) and plasma (Lewis et al., 2018; Viltard et al., 2019) content of methionine, and methionine restriction (MetR) leads to an extended longevity in different experimental models (Ables et al., 2015; Elshorbagy et al., 2010, 2013; Pamplona and Barja, 2006; Tamanna et al., 2018). Methionine is an essential amino acid that is involved in several intracellular processes (**Figure 1**), such as intracellular metabolism and signalling, methylation reactions, maintenance of redox balance, protein synthesis, autophagy, and biosynthesis of polyamines or nucleotides (Sanderson et al., 2019). Likely due to its versatility, and the involvement of these intracellular processes with the determination of animal longevity, we have unfocused solely from methionine and analysed the changes on its related metabolites. Our results revealed that centenarians have higher levels of homocysteine, cystathionine, cysteine and taurine, suggesting an increased transsulfuration directed to increase the plasma levels of taurine, without changing methionine plasma content.

The observed metabolic adaptations associated to human longevity regarding methionine metabolism reveal new insights on inter-individual longevity. It has been previously discussed the existence of factors exerting a “big effect” on longevity determinations, along with factors inducing a “small effect” on longevity (Barja, 2019). Inter-species studies are a powerful source of information to identify mechanism inducing a “big effect” on extended longevity, such as maintaining lower methionine content. These mechanisms determine whether an animal species lives longer than others. However, these mechanisms usually differ from the specific individual metabolic adaptations determining whether a specific individual of a species lives longer than the average, and have a “small effect” on longevity determination. Our study aims to determine the metabolic adaptations leading to human longevity, and the obtained results suggest that although the steady states of plasma methionine decrease with animal longevity, the specific modulations on methionine metabolism, mainly at the transsulfuration pathway, and not methionine content *per se*, determines whether a specimen/individual from one species lives longer than its life expectancy, reaching a longevity condition. In fact, it is well-established that MetR in rodents induces hyperhomocysteinemia (Ables et al., 2015; Elshorbagy et al., 2010, 2013; Tamanna et al., 2018), probably due to an enhanced transsulfuration, as suggested

previously (Vitvitsky et al., 2013). In a recently published study, men that underwent 45 minutes of cycling for 12 weeks showed decreased plasma methionine and increased plasma concentrations of homocysteine, cystathionine, cysteine, glutathione and taurine (Lee et al., 2018), supporting the beneficial effects of an enhanced transsulfuration.

Transsulfuration starts with the metabolic conversion of homocysteine into cystathionine, an enzymatic reaction catalysed by the enzyme CBS, using vitamin B6 as cofactor. According to our hypothesis, we have found that cystathionine is significantly increased in centenarians. Reinforcing this finding, SAM, an allosteric activator of CBS (Jhee and Kruger, 2005), is increased in centenarians and positively correlated with cystathionine. In fact, it has been demonstrated in rodents that injected isotope-labelled methionine is mainly metabolized via the transsulfuration pathway in long living Ames dwarf mouse, along with an enhanced gene expression of methionine adenosyltransferase (MAT), methyltransferases (MTs), betaine-homocysteine methyltransferases (BHMT), adenosylhomocysteinase-like1 (AHCYL) and CBS, but decreased methionine synthase (MS) (Uthus and Brown-Borg, 2006). Furthermore, dietary restriction increases longevity in flies by promoting transsulfuration and CBS activity (Kabil et al., 2011).

Proteins are in continuous turnover and exchanges with the free amino acid pool (EFSA, 2012), such as free methionine, which is essential for the initiation of protein synthesis. Interestingly, methionine plasma levels remained unchanged across the different groups, likely due to its strong regulation. Supporting this idea, plasma methionine levels also remain stable in ageing mice (Jeon et al., 2018). The maintenance of free methionine mainly depends on the transmethylation and the methionine salvage pathway. The transmethylations involves either MS, which requires 5'-methyltetrahydrofolate as a methyl donor; BHMT, which requires betaine as a methyl donor; or the methionine salvage pathway that produces spermidine. Betaine and spermidine plasma levels remained unchanged, and methionine salvage pathway was decreased in centenarians. According to this data, we suggest that although transsulfuration is enhanced, centenarians maintain decreased but sufficient MS activity to maintain methionine plasma levels.

Methylation is needed to modulate gene expression, enzymatic activity and to promote the biosynthesis of several metabolites. It relies upon methyltransferases (MTs), which are the enzymes responsible to donate a methyl group from SAM to DNA, RNA, proteins and lipids, generating SAH. In our model, methylation is associated with human extreme longevity, since plasma content of SAM and SAH is increased. Methylation has been previously positively associated with longevity (Brown-Borg et al., 1996; Hahn et al., 2017; Parkhitko et al., 2019; Tain et al., 2017, 2020). Accordingly, MAT activity was higher in liver of Snell dwarf, and the increased SAM was positively correlated with DNA methylation status (Vitvitsky et al., 2013). PEMT is a methyltransferase that catalyses de biosynthesis of phosphatidylcholine (PC) from phosphatidylethanolamine (PE). The resulting PC can be then hydrolysed via the action of phospholipases to generate choline, constituting the only known endogenous pathway for choline biosynthesis in mammals (Li and Vance, 2008). Choline plasma levels are increased in centenarians, supporting the modulation of lipid metabolism associated to human longevity. Interestingly, liver PEMT activity is inhibited in Alzheimer's disease patients (Selley, 2007).

Globally, the obtained results suggest that centenarians undergo a specific remodulation of the methionine metabolism, being an enhanced transsulfuration and transmethylation two key traits (**Figure 7**). Furthermore, we believe that these two processes are directed to increase the plasma levels of taurine and to modulate the lipidomic profile. Taurine is a cytoprotective β-amino acid with antioxidant properties that has been described to modulate pro-longevity genes (Ito et al., 2014) and its intake is associated with human longevity and cardiovascular health (Yamori et al., 2009). Furthermore, taurine plasma levels are higher in long-lived Dwarf mice than in control mice (Vitvitsky et al., 2013). Adults, in turn, promote the transmethylation and the synthesis of glutathione, an antioxidant compound. In both situations, increased plasma levels of homocysteine, which has been described as a cardiovascular risk factor (Chrysant and Chrysant, 2018), are cleared. Contrarily, the increased homocysteine in aged individuals accumulates, due to the disruption of the transmethylation and transsulfuration metabolism, leading to the cardiovascular comorbidities associated to the ageing process.

Decreased amino acid content in centenarians

Amino acids constitute the building blocks for proteins, the functional biomolecules in our body. However, they can also be found as free metabolites, functioning as signalling molecules or metabolic intermediates. The findings associating methionine metabolism intermediates and human longevity, as well as the strong metabolic inter-connection between amino acids, led us to a challenging question: Is the whole amino acid metabolic profile modulated in longevous individuals? And if it's so, does this modulation affect all the amino acids in the same way, or it occurs through specific and individualized amino acid changes?

Our data revealed that although some amino acid levels are modulated by the ageing process, methionine remains unchanged between adult and centenarians, and plasma cysteine constitutes the most important feature to discern between groups. As previously discussed, this probably might be due to the relevance of the transsulfuration pathway in longevity determination. This centenarian profile is characterised by decreased tryptophan, but also serine, threonine, and valine. It has been reported that tryptophan is needed for the *de novo* NAD+ synthesis, which enhances mitochondrial function and improves health by conserved mechanisms from invertebrates to mammals (Katsyuba et al., 2018). Furthermore, a recent study (Mirisola et al., 2014) demonstrated a promoting aging role for serine, threonine, and valine through the specific activation of Ras/cAMP/PKA, PKH1/2 and Tor/S6K pathways. Consequently, the low content of these amino acids detected in centenarians must be interpreted as a pro-longevity factor by down-regulating the mentioned pathways.

Supporting these results, previous studies in longevity models had already described a global decrease of peptides and amino acids in tissue and plasma (Castro et al., 2013; Davies et al., 2015), along with an increased proteasomal activity and autophagy (Lewis et al., 2018). Furthermore, nutritional interventions in flies (Laye et al., 2015) and humans (Washburn et al., 2019) also led to decreased tissue and plasma amino acid content. On the contrary, some studies associate longevity with increased amino acids (Fuchs et al., 2010; Montoliu et al., 2014).

Energetic metabolism is enhanced in centenarians

Mitochondria has been pointed as a central hub in longevity determination. Decreased reactive oxygen species production (Pamplona and Barja, 2007), quantitative and qualitative

modulations of the electron transport chain complex I (Miwa et al., 2014; Mota-Martorell et al., 2020b; Pamplona and Barja, 2007), decreased membrane unsaturation (Pamplona and Barja, 2007) and lower permeability (Mota-Martorell et al., 2020b; Zhou et al., 2019), and modulation of mitochondrial dynamics (Sharma et al., 2019) represent, among others, structural and functional adaptations leading to a mitochondrial phenotype associated to organismal longevity. The intracellular role of the mitochondria is to provide the cell with ATP obtained either from oxidation of carbohydrate, proteins and fats, although it is also involved in gluconeogenesis, amino acids and one-carbon metabolism, and lipid (Tatsuta et al., 2014) and protein synthesis (Brand, 2014). Due to the previously mentioned structural and functional adaptations, its highly feasible to postulate that mitochondrial metabolism may be also modulated in long-lived individuals.

The TCA cycle occurs in the mitochondrial matrix and constitutes a metabolic epicentre because multiple substrates can feed into it (Martínez-Reyes and Chandel, 2020). The TCA begins with two molecules of acetyl-CoA, generated from fatty acids, amino acids or pyruvate oxidation, that are subsequentially metabolized into different intermediates. During these reactions, GTP and electron donors are generated (e.g., NADH and FADH), that will transfer those electrons to the electron transport chain transporters to subsequentially generate ATP. In our study, we have found that centenarians have a global plasma increase of the TCA cycle intermediates, including citrate, α-ketoglutarate, succinate and malate, suggesting an optimized energetic metabolism. These results are supported by data across experimental models. Gene expression and activity of TCA cycle is enhanced in long-lived yeast mutants (Kamei et al., 2011; Wang et al., 2010). In long-lived rodents, TCA cycle genes are also upregulated (Amador-Noguez et al., 2004), and its function is preserved with ageing (Perron et al., 2000). Data in humans is scant, and revealed higher levels of malate in octogenarians, which were associated with higher cardiovascular risk (Cheng et al., 2015). Accordingly, higher levels of malate were found in aged in comparison with adults, although these levels were still higher in centenarians.

Pyruvate is versatile metabolite generated from glycolysis that can be used to synthetize carbohydrates (gluconeogenesis), acetyl-CoA, oxaloacetate (a TCA cycle intermediate), alanine or lactate. It can enter into the first step of the TCA cycle via its decarboxylation to acetyl-CoA, or its carboxylation to oxaloacetate. Pyruvate plasma levels are increased in centenarians, suggesting a proper glycolysis and TCA cycle activity. The beneficial effects of pyruvate supplementation had been previously reported, including oxidative stress protection (Tauffenberger et al., 2019) and lifespan extension via HIF-1 stabilization (Mishur et al., 2016) in *C. elegans*, as well as increased explorative activity in mice Alzheimer disease models (Koivisto et al., 2016).

Citrate is the first TCA cycle intermediate, and its biosynthesis from acetyl-CoA constitute a limiting reaction of the metabolic pathway. In centenarians, citrate plasma levels are increased, probably due to its enhanced biosynthesis and the decreased estimated aconitase activity, which metabolizes citrate into isocitrate. Supporting this data, serum content of citrate had been previously reported to be higher in centenarians compared to aged individuals (Montoliu et al., 2014). Decreased aconitase is associated with higher odds of living longer than 80 years without cardiovascular diseases (Cheng et al., 2015). When glucose is limited, citrate can be transported to the cytoplasm via the citrate transport protein (CTP), which exchanges mitochondrial citrate

for cytosolic malate (Palmieri et al., 2015). In the cytoplasm, citrate can be broken down into acetyl-CoA and OAA by the ATP citrate lyase (ACLY). The produced acetyl-CoA can be either used for *de novo* lipid biosynthesis or to acetylate proteins and DNA. Lower ACLY activity and histone methylation is associated with longevity in *D. melanogaster* (Peleg et al., 2016). However, genome-wide association studies (GWAS) in humans reported a significant association of citrate plasma content with SLC25A1, which encodes CTP (Kettunen et al., 2012). Altogether these results suggest that retaining citrate in the mitochondria to maintain the TCA cycle is associated to longevity, and with increased plasma citrate, although the molecular mechanisms are unknown.

α-Ketoglutarate is synthetized by the oxidation and decarboxylation of isocitrate via isocitrate dehydrogenase (IDH) or complex II (Cx II). It constitutes a hub of anaplerotic reactions, since it can be synthetized from glutamate via glutamate dehydrogenase, allowing to maintain a proper metabolic activity and ATP generation. In fact, α-ketoglutarate is not only a metabolite, but also a cofactor of multiple dioxygenases that generate succinate as a by-product and are involved in the hypoxic response, histone methylation and inflammation, among others (Loenarz and Schofield, 2008; Martínez-Reyes and Chandel, 2020). The activity of these α-ketoglutarate-dependent dioxygenases is inhibited by a high ratio succinate/α-ketoglutarate or fumarate (Martínez-Reyes and Chandel, 2020). Elevated α-ketoglutarate plasma levels were found in centenarians. According to literature, maintaining elevated α-ketoglutarate would ensure a proper ATP generation, as well as to promote the activity of the α-ketoglutarate-dependent dioxygenases (Martínez-Reyes and Chandel, 2020). Recently it has been associated with longevity, since α-ketoglutarate supplementation increases *C. elegans* longevity by decreasing ATP synthesis and inhibiting TOR (Chin et al., 2014).

Succinate is the substrate of the enzyme succinate dehydrogenase (SDH) or complex II (Cx II), thus its availability is essential for the production of ATP via the mitochondrial electron transport chain. Up to date, it is the only TCA cycle intermediate known to trigger organismal functions, by modulating renin-angiotensin system through its receptors SUCNR1, regulating the immune system and inducing thermogenesis in brown adipocytes (Martínez-Reyes and Chandel, 2020). Succinate plasma levels are increased in centenarians, suggesting a proper maintenance of ATP supply, as well as to maintain a proper immunity. Accordingly, increased succinate was found in worm long-lived models (Fuchs et al., 2010) and in response to MetR in flies (Plummer and Johnson, 2019).

Malate plasma levels were also increased in centenarians. It has been previously suggested that succinate increases due to fumarate accumulation lead to alterations in mitochondrial function (Kerins et al., 2017; Sullivan et al., 2013; Ternette et al., 2013; Zheng et al., 2015). Therefore, it seems that high plasma levels of malate might be an indicator of globally proper mitochondrial function and fumarate clearance.

In some situations, amino acids can be used to synthetize other metabolites, such as glucose or ketone bodies. Specifically, alanine, arginine, asparagine, aspartate, cysteine, glutamate, glutamine, glycine, histidine, methionine, proline, serine and valine are named as glucogenic amino acids, whereas leucine and lysine are ketogenic. Isoleucine, phenylalanine, threonine, tryptophan and tyrosine can be both glucogenic and ketogenic. As it has been mentioned previously, TCA cycle can be feed by amino acids. In fact, the carbon skeleton of several TCA

cycle intermediates can also be used to synthetize amino acids. Accordingly, the obtained results suggest that pyruvate and α-ketoglutarate increases might be, in part, due to its synthesis from amino acids.

Available literature suggests that increased plasma profile of TCA cycle intermediates might be due to modulations on its membrane transporters. INDY (*I'm not dead yet*) is a membrane transporter showing a high affinity for citrate and succinate, but also for α-ketoglutarate and fumarate. Studies on animal models suggest that INDY may account, in part, for extended longevity, occurring with increased plasma levels of the mentioned metabolites (Willmes et al., 2018). INDY mutations in worms (Fei et al., 2004) and fly (Knauf et al., 2002; Rogina and Helfand, 2013) extend lifespan, and are related to dietary restriction phenotypes in mice (Birkenfeld et al., 2011). Consequently, it has raised as a pharmacologic target in longevity (Willmes et al., 2018). However, no studies in human measuring the activity of these specific transporters have been published yet.

Globally, the obtained results suggest that centenarians undergo a metabolic modulation targeted to enhance the TCA cycle activity (**Figure 7**). Glucose metabolism, but also amino acid catabolism, constitute metabolic pathways that fuel the cycle, by maintaining elevated levels of pyruvate and α-ketoglutarate. Furthermore, human longevity is achieved through the maintenance of elevated plasma levels of citrate, α-ketoglutarate and succinate, which might allow a proper energy supply (probably through the Cx I and II of the electron transport chain), histone acetylation and modulation of specific gene expression profile, as well as proper inflammation and immune response.

Network integrity

The interaction between metabolites in large networks, in addition to changes in individual metabolites content, is critical for metabolism function and a source for the generation of new hypothesis about longevity. Networks consist in a set of "nodes" (in this case, metabolites), that are connected through "edges", which are commonly referred as correlations. Therefore, two metabolites that aren't directly connected in a metabolic pathway may nonetheless be connected if their concentrations are correlated with each other (Kim et al., 2016). Network connectivity constitutes a mean of measuring network integrity. Accordingly, loss of network connectivity and non-communicated metabolites leads to cellular homeostasis disruption, as well as mitochondrial dysfunction, genomic instability and proteostasis loss (López-Otín et al., 2013). Our work revealed that centenarians maintain a strongly correlated methionine intermediates, suggesting an improved network integrity, homeostasis and more tightly regulated metabolism. It had been previously demonstrated that longevity is associated with specific correlation networks (Castro et al., 2013), which can be modulated through nutritional interventions such as dietary restriction (DR) (Derous et al., 2016). Globally, lifespan extension during DR occurs along with the strengthening (Laye et al., 2015) or maintenance of network integrity (Derous et al., 2016; Laye et al., 2015; Priebe et al., 2013), even when no changes in mean levels of metabolites are found (Laye et al., 2015). However, for TCA cycle intermediates, the strongest correlation network was found in aged, showing a disordered correlation network. Conversely, it has been suggested that network connectivity often declines with age (Southworth et al., 2009). In this case, increasing or decreasing the correlation degree is not sufficient to define network integrity. Although the performance of correlation matrix provides

new and useful information, it is also important to identify the biological significance of these correlations, and to combine this data with changes in the individual metabolites. Accordingly, we postulate that the higher and stronger correlation pattern found in aged individuals reflects the loss of homeostasis that occurs through the aging process, and the failed efforts of intracellular metabolism to restore it.

Conclusions

In the present work, we define a plasma profile associated to human longevity characterized by an enhanced transsulfuration and TCA cycle intermediates, as well as a reduced specific amino acid content (**Figure 7**). Globally, this metabolic profile might suggest an enhanced energetic metabolism. The connection between transsulfuration and TCA cycle intermediates is through anaplerotic reactions, such as the conversion of cystathionine into succinyl-CoA, and cysteine into pyruvate. Accordingly, methionine supplementation enhanced mitochondrial pyruvate uptake and TCA cycle activity (Tripodi et al., 2018). Furthermore, we suggest that enhanced TCA activity is promoted by the synthesis of its intermediates from amino acids. However, more work is needed to elucidate the organismal functions of the transsulfuration and TCA cycle metabolites and its affinity with its specific transporters, as well as the activity modulation or genetic variants of the enzymes involved in the methionine and energetic metabolism, along with tissue flux measurements in the context of human longevity.

However, our work has some limitations. First, the limited number of measured metabolites leads to uncompleted networks. Although previous data allow us to generate new hypothesis, it should be needed to identify more metabolites in order to define a global network. Specifically, it would be interesting to include intermediate metabolites within the pathways, in order to establish clear associations between methionine metabolism, TCA cycle and amino acids. Second, we have measured a plasma profile, which is dynamic and undergoing continuous changes. It allows us to get a global view of the metabolic processes undergoing in the organisms, but it's also a source of metabolic precursors that are taken by cells to be metabolized. Furthermore, we should keep in mind that metabolism changes within different tissues. And third, the study is performed in a small population from a limited region in Spain. Therefore, the obtained results should be validated in a different and bigger cohort.

Methods

Chemicals

Unless otherwise specified, all reagents were from Sigma-Aldrich, and of the highest purity available.

Sample population

Potential healthy subjects were selected from the population data system of the 11th Health Department of the Valencian Community (Valencia, Spain), which is composed of 29 towns (240,000 inhabitants). The inclusion criteria were to live in the 11th Health Department for at least the last 6 years and to sign the informed consent. The exclusion criterion was to be under statin-therapy or any pharmacological treatment affecting lipid metabolism or to be terminally ill for any reason. We included 18 centenarians (100.8 ± 1.1 years), 21 randomly recruited aged subjects (76.4 ± 0.5 years), and 21 adult individuals (27.9 ± 1.4 years). All experimental procedures were approved by the Committee for Ethics in Clinical Research of the Hospital de la Ribera (Alzira, Valencia, Spain). All subjects or their relatives were fully informed of the aims and scope of the research and signed an informed consent.

Blood collection and plasma isolation

Blood samples were obtained by venipunction in the morning (between 7 and 8 AM) after fasting overnight (8–10 hours) and collected in one vacutainer CPT (Cell Preparation Tube; BD, Franklin Lakes, NJ) containing sodium heparin as the anticoagulant. Plasma fractions were collected after blood sample centrifugation, and immediately frozen in liquid nitrogen, and transferred before 4 hours to a −80°C freezer for storage, to be used later for metabolomic analyses.

Sample processing

Plasma metabolites extraction was performed based on the methodology previously described (Method 1, Cabré et al., 2016). Briefly, 10 µL of plasma were added to 30 µL of cold methanol containing 1 µg/mL of Phe-^{13}C as internal standard and 1µM BHT as antioxidant. Then, samples were incubated at -20°C for 1 hour and centrifuged at 12.000 *g* for 3 minutes at 4°C. Finally, the supernatant was filtrated through a 0.22-µm organic diameter filter (CLS8169, Sigma, Madrid, Spain) and were transferred to vials with glass inserts for further analysis.

Sulphur-containing metabolites were extracted on the bases of the methodology previously described (Method 2, Liu et al., 2017). Briefly, 2 µL of 5 % DTT diluted in methanol (m/v) were added to 10 µL of plasma. The resulting solution was vortexed for 1 minute and allowed to stand at room temperature for 10 minutes. For protein precipitation, 40 µL of acetonitrile containing 0.1 % formic acid (v/v), 0.05 % trifluoroacetic acid (v/v) and 1 µg/mL of Phe-^{13}C as internal standard was added to the sample, and the solution was vortexed for 2 minutes. Then, samples were incubated at room temperature for 15 minutes and centrifuged at 12000 *g* for 3 minutes. Finally, the supernatant was filtrated through a 0.22-µm organic diameter filter (CLS8169, Sigma, Madrid, Spain) and transferred to vials with glass inserts for further analysis.

Analysis conditions

The individual conditions for the detection and quantification of plasma metabolites are listed in **Supplementary table 1 (For details, see Table 6 of this Thesis)**. For non-sulphur-containing metabolites, 2 µL of extracted sample was injected based on the method described (Method 1, Cabré et al., 2016). Chromatographic separation was achieved on a reversed-phase column (Zorbax SB-Aq 2.1 × 50 mm, 1.8 µm particle size, Agilent Technologies, Barcelona, Spain) equipped with a pre-column (Zorba-SB-C8 Rapid Resolution Cartridge, 2.1 × 30 mm, 3.5 µm particle size, Agilent Technologies, Barcelona, Spain) with a column temperature of 60 °C. The flow rate was 0.6 mL/min during 19 minutes. Solvent A was composed of water containing 0.2 % acetic acid (v/v) and solvent B was composed of methanol containing 0.2 % acetic acid (v/v). The gradient started at 2 % of solvent B and increased to 98 % B in 13 minutes and held for 6 minutes. Post-time was established in 5 minutes. Electrospray ionization was performed in both positive and negative ion mode (depending on the target metabolite) using N_2 at a pressure of 50 psi for the nebulizer with a flow of 12 L/min and a temperature of 325 °C, respectively.

For sulphur-containing metabolites, 10 µL of extracted sample was injected based on the method described (Method 2, Liu et al., 2017). Chromatographic separation was achieved on a reversed-phase Supelcosil LC-CN column (Supelco of 4.6 x 250 mm, 5 µm particle size, Sigma, Madrid, Spain) with a column temperature of 30 °C. The flow rate was maintained at 0.5 mL/min during 10 minutes using a mobile phase of 10:90 acetonitrile/water with 0.1 % formic acid (v/v). Electrospray ionization was performed in both positive and negative ion mode (depending on the target metabolite) using N_2 at a pressure of 50 psi for the nebulizer with a flow of 12 L/min and a temperature of 325 °C, respectively.

Data was collected using the MassHunter Data Analysis Software (Agilent Technologies, CA, USA). Samples were decoded and randomized before injection. Metabolite extraction quality controls (plasma samples with internal Phe-^{13}C) were injected every 10 samples. Peak determination and peak area integration were carried out with MassHunter Quantitative Analyses (Agilent Technologies, CA, USA).

Metabolite quantification

Metabolite quantification was performed by constructing standard curves for each metabolite. Serial dilutions of pure standards with internal Phe-^{13}C were prepared and processed following the methods described previously. Peak area normalized by internal Phe-^{13}C, and standard serial dilutions are used to construct the standard curves. Expected plasma concentration of each metabolite is based on the Human Metabolome Database (HMDB, http://www.hmdb.ca).

Equipment

The analysis was performed through liquid chromatography coupled to a hybrid mass spectrometer with electrospray ionization and a triple quadrupole mass analyser. The liquid chromatography system was an ultra-performance liquid chromatography model 1290 coupled to LC-ESI-QqQ-MS/MS model 6420 both from Agilent Technologies (Barcelona, Spain).

Statistics

Prior to statistical analyses, data was pre-treated (auto-scaled). Multivariate statistics were performed using Metaboanalyst software (Chong et al., 2019) (PCA, heatmaps) and caret (Kuhn) package from R (R Core Team, 2020) (PLS-DA). For PLS-DA, models were trained using a random subset of 60% of all the samples and were tested using the remaining 40%. Optimal number of components (1, 2 or 3) was selected according to the accuracy obtained from simple bootstrapping of the training samples. Among them, the model with higher accuracy was chosen. Model performance on test data was evaluated comparing the obtained accuracy with the no information rate accuracy (rate of the largest group) using a one-tailed binomial test. Univariate statistics were performed using GrapPhad Prism (v8.0.1). Pearson correlation, Pearson correlation matrix and network plots were performed using RStudio (v1.1.453). Correlation functions were included in the packages *Hmisc* (Harrel Jr and Dupont, 2020) and *corrplot* (Wei and Simko, 2017), and plotted with *ggplot2* (Wickham, 2016). Network plot were constructed and plotted using the functions included in the package *igraph* (Csardi and Nepusz, 2006).

Conflict of interest

The authors declare no conflict of interest

Funding

We acknowledge funding from the Spanish Ministry of Science, Innovation and Universities (RTI2018-099200-B-I00), and the Generalitat of Catalonia, Agency for Management of University and Research Grants (2017SGR696) and Department of Health (SLT002/16/00250) to R.P., Instituto de Salud Carlos III (CB16/10/00435, CIBERFES), EU-Funded FRAILOMIC Initiative (FP7-HEALTH-2012-Proposal no. 305483-2), ADVANTAGE-724099 (HP-JA) –DIALBFRAIL-LATAM (825546 H2020-SC1-BHC) to J.V., and PCIN-2017-117 of the Ministry of Economy and Competitiveness, the EU Joint Programming Initiative 'A Healthy Diet for a Healthy Life' (JPI HDHL INTIMIC-085) to C.B. This study has been co-financed by FEDER funds from the European Union ("A way to build Europe"). IRBLleida is a CERCA Programme/Generalitat of Catalonia.

Acknowledgements

N.M-M received a predoctoral fellowship from the Generalitat of Catalonia (AGAUR, ref 2018FI_B2_00104). M.J. is a 'Serra Hunter' Fellow. We thank the following members of the Spanish Centenarian Study group for their help in this study: Dr F.J. Tarazona; Dr J.R. Domenech, Dr Carmen Valldecabres, Dr. David Cuesta, Dr Ricardo Bou (Hospital de la Ribera, Alzira). Special thanks go to the nurses: Rosa Carrasco, Maria Jesús Martínez, Miriam Hoya and Alicia Pérez for their excellent care of the people involved in this study.

Author Contributions

J.V. and R.P designed the study. N.M.M., M.J., C.B., I.P., R.B., E.O., J.S., R.C., J.D.G.L. and J.P., performed experimental work. N.M.M, M.J., J.P., and R.P. analysed the data. R.P. supervised the design and data interpretation. The manuscript was written by N.M.M, M.J., C.B., J.V., and R.P. and edited by R.P. All authors discussed the results and commented on the manuscript.

Figures

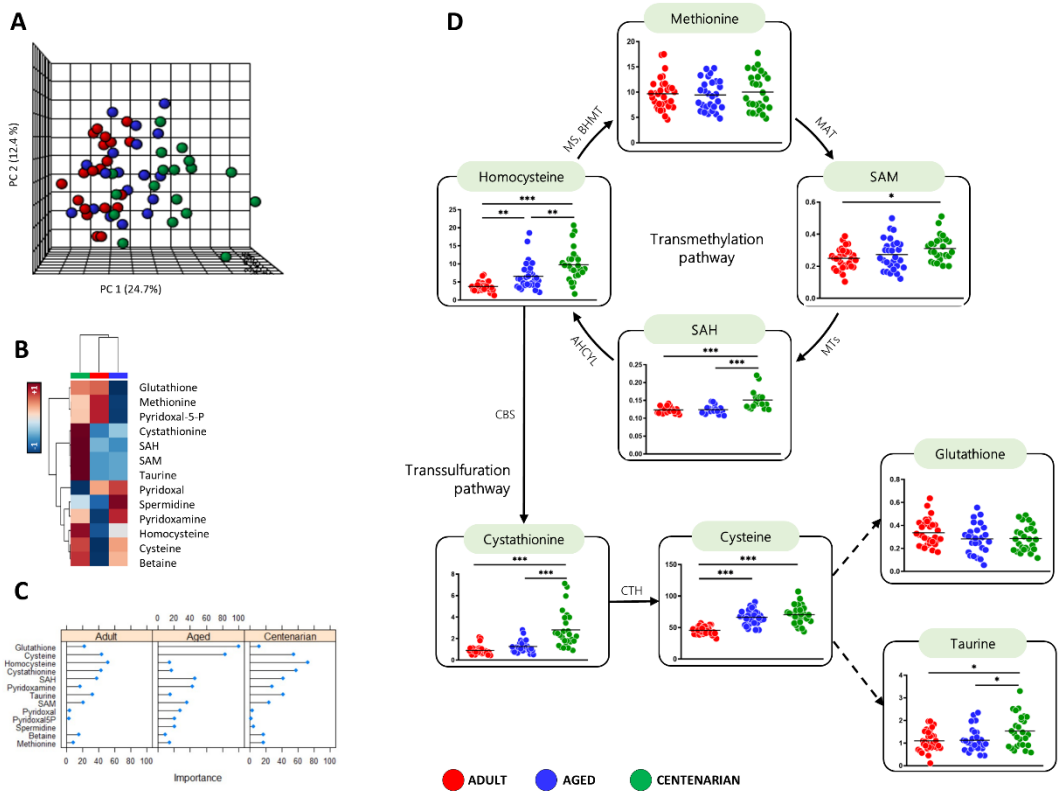

Figure 2. Multivariate statistics reveals a centenarian-specific plasma methionine related metabolites profile. A) Principal component analyses (PCA) representation metabolite content. X: Principal component 1 (PC1); Y: PC2; Z (not shown): PC3, 11.6% (not shown). **B)** Hierarchical clustering of adult, aged and centenarian individuals according to average sample values of metabolite content. **C**) Scaled variable importance of Partial Least Squares Discriminant Analysis (PLS-DA) used for sample classification into each group. **D)** Individual metabolite plasma concentrations reported in µM. Dashed lines refer to reactions in which more than one enzyme is involved. Inter-group differences were measured by one-way ANOVA followed by a post-hoc Tukey multiple test. Minimum signification level was set at $p<0.05$. Enzyme codes refer to: Methionine synthase (MS); Betaine-Homocysteine S-methyltransferase (BHMT); Methyltransferases (MTs); Cystathionine-β-synthase (CBS); Cystathionine-γ-lyase (CTH).

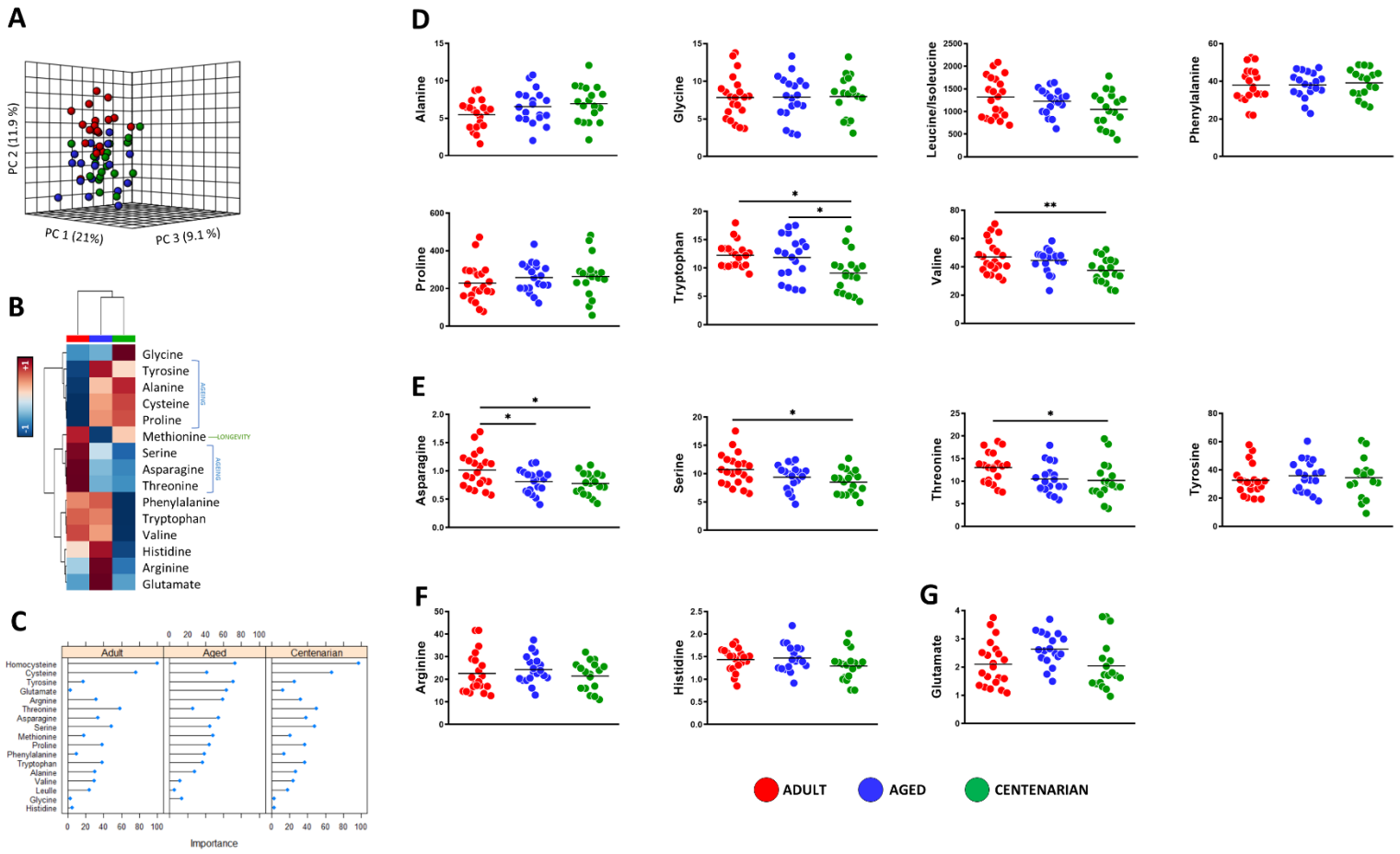

Figure 3. Multivariate statistics reveals an adults-specific plasma amino acid profile. A) PCA representation metabolite content. X: PC1; Y: PC2; Z: PC3. **B)** Hierarchical clustering of adult, aged and centenarian individuals according to average sample values of metabolite content. **C)** Scaled variable importance of PLS-DA used for sample classification into each group. **D-G)** Individual plasma concentration reported in µM of non-polar (**D**), polar uncharged (**E**), negatively charged (**F**) and positively charged (**G**) amino acids. Plasma concentrations for leucine/isoleucine is reported in MS Counts. Inter-group differences were measured by one-way ANOVA followed by a post-hoc Tukey multiple test. Minimum signification level was set at $p<0.05$.

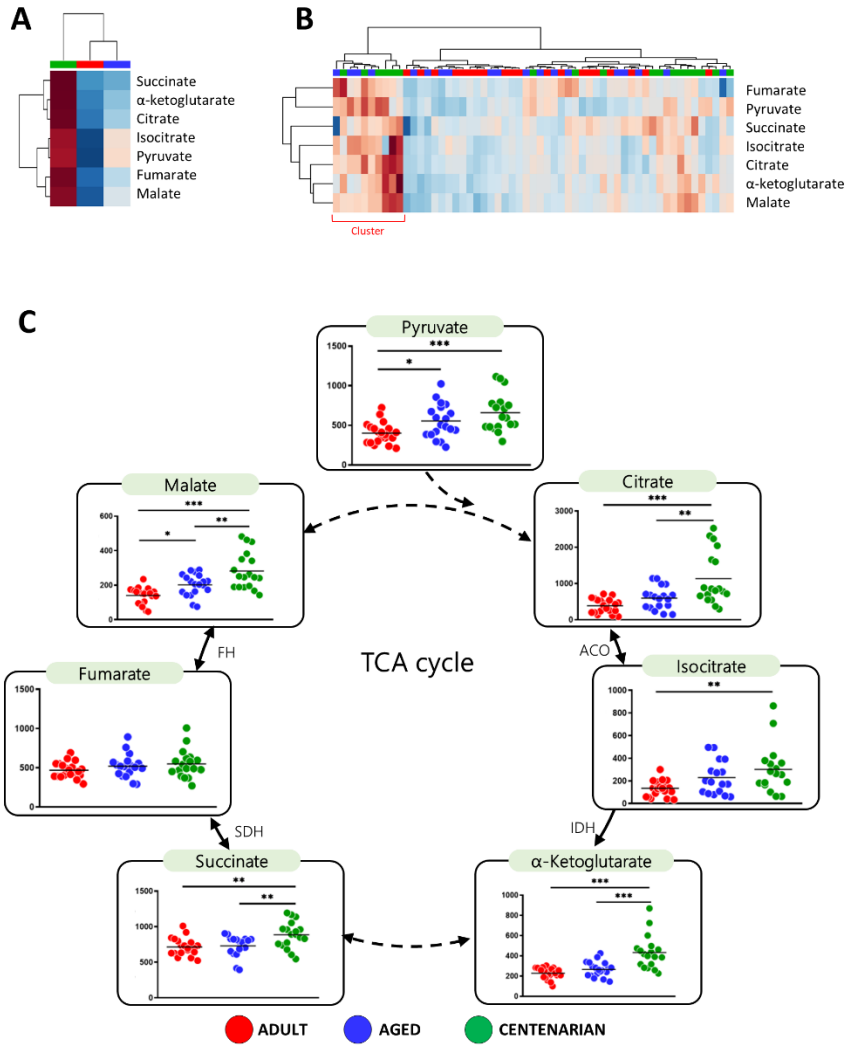

Figure 4. Multivariate statistics reveals a centenarian-specific energetic metabolism plasma profile. A) Hierarchical clustering of adult, aged and centenarian individuals according to average sample values of metabolite content. **B)** Hierarchical clustering of individual samples according to metabolite content. **C)** Individual metabolite plasma concentrations reported in MS Counts. Dashed lines refer to reactions in which more than one enzyme is involved. Inter-group differences were measured by one-way ANOVA followed by a post-hoc Tukey multiple test. Minimum signification level was set at $p<0.05$. Enzyme codes refer to: Aconitase (ACO); Isocitrate dehydrogenase (IDH or Cx I); Succinate dehydrogenase (SDH or Cx II); Fumarate hydratase (FH).

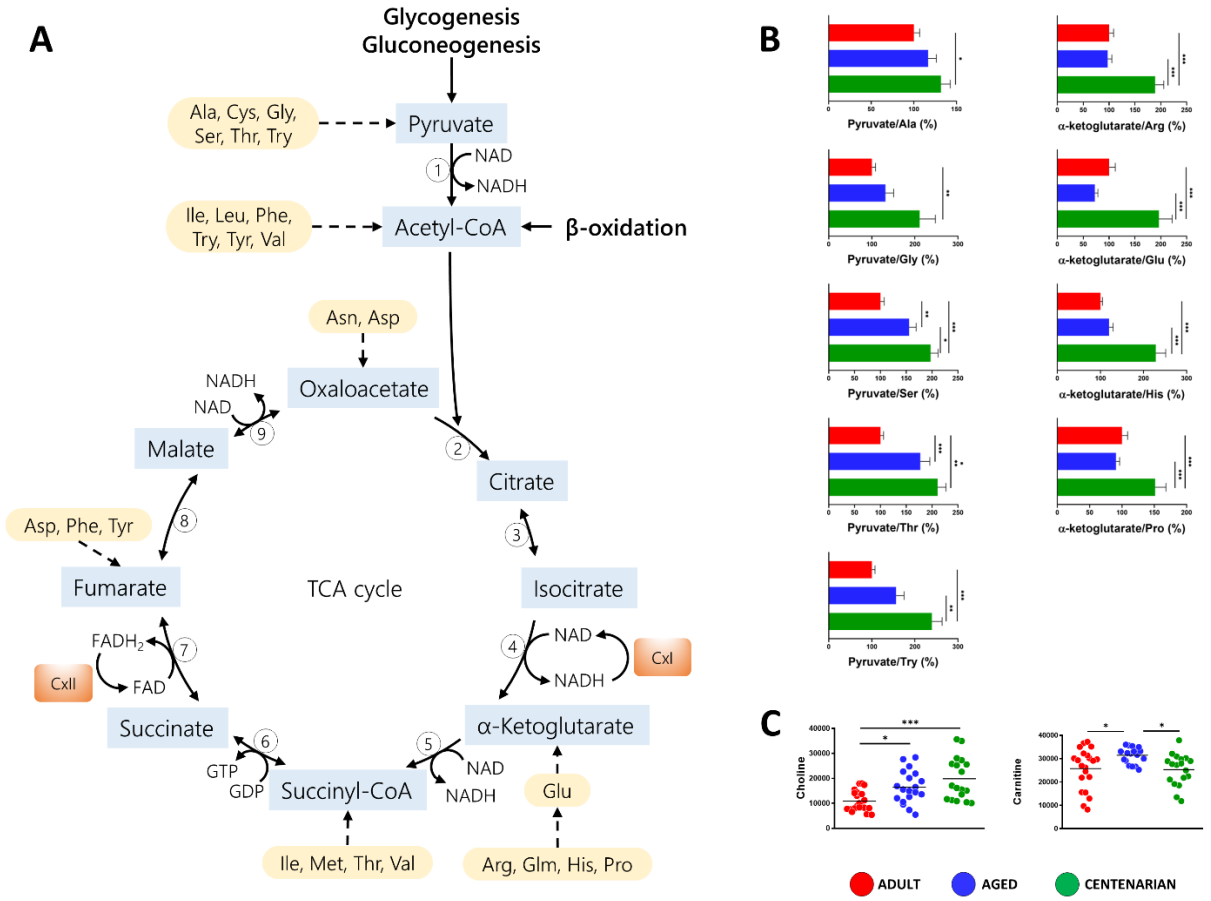

Figure 5. Estimated conversion rate of amino acids into TCA cycle intermediates is enhanced in centenarians. A) Metabolic associations between amino acids and TCA cycle intermediates. Numbers refer to enzymes: **1**, Pyruvate dehydrogenase (PDH); **2**, Citrate synthase (CS); **3**, Aconitase (ACO); **4**, Isocitrate dehydrogenase or Cx I (IDH); **5**, α-ketoglutarate dehydrogenase (OGDH); **6**, Succinyl-CoA synthetase (SCS); **7**; succinate dehydrogenase or Cx II (SDH); **8**, Fumarate hydratase (FH); **9**, Malate dehydrogenase (MDH). **B)** Estimated conversion rate of amino acids into TCA cycle intermediates. **C)** Lipid intermediates plasma concentration. Inter-group differences were measured by one-way ANOVA followed by a post-hoc Tukey multiple test. Minimum signification level was set at $p<0.05$.

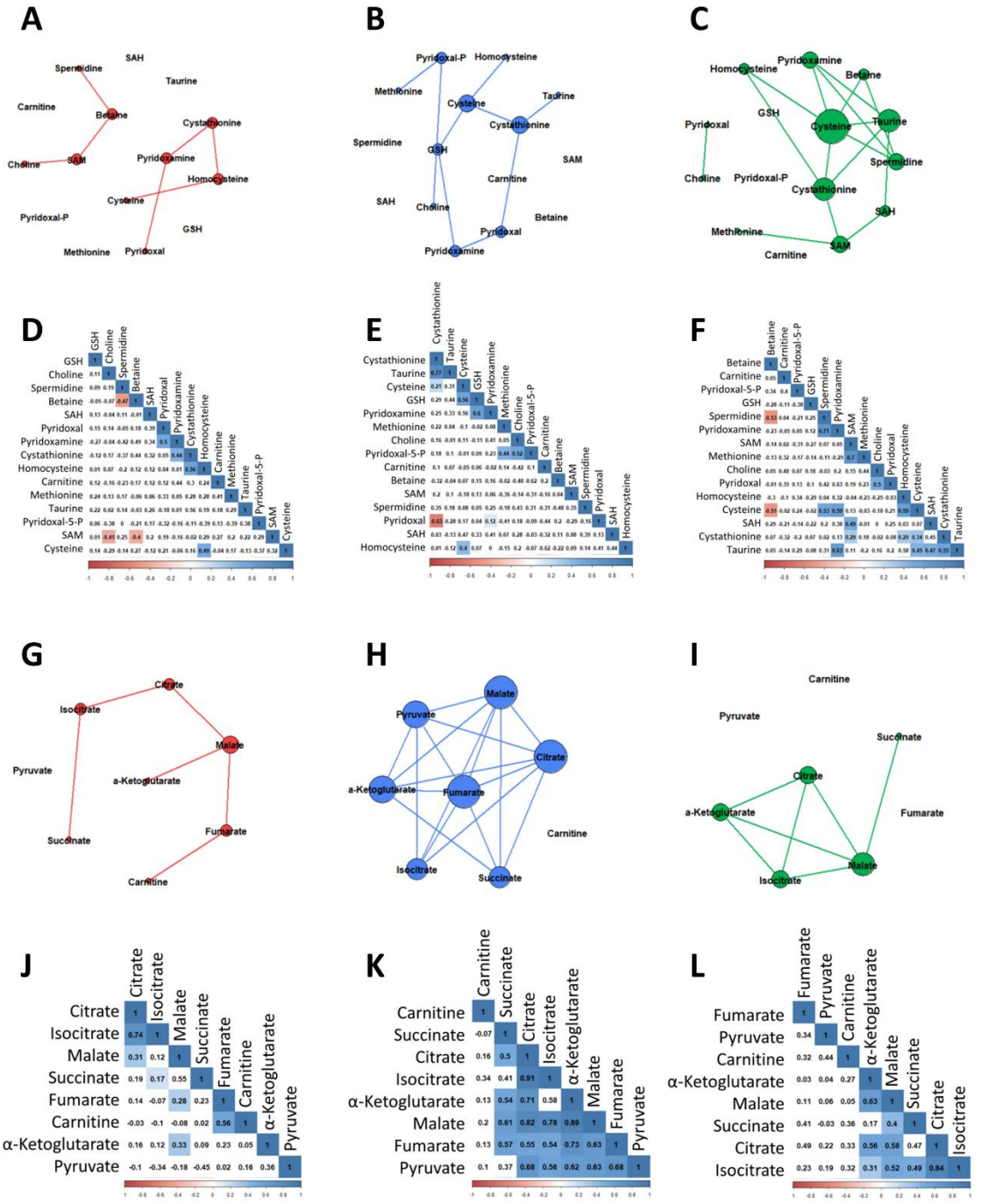

Figure 6. Network integrity of methionine metabolism and TCA cycle in adult, aged and centenarian individuals. Network plot revealing significant and strong correlations (r > 0.65) between methionine metabolites in adults (**A**), aged (**B**) and centenarian (**C**) individuals. Pearson correlation matrix of methionine metabolites in adult (**D**), aged (**E**) and centenarian (**F**) individuals. Network plot revealing significant and strong correlations (r > 0.65) between TCA cycle intermediates in adults (**G**), aged (**H**) and centenarian (**I**) individuals. Pearson correlation matrix of TCA cycle intermediates in adult (**J**), aged (**K**) and centenarian (**L**) individuals. Dot size depends upon hubs.

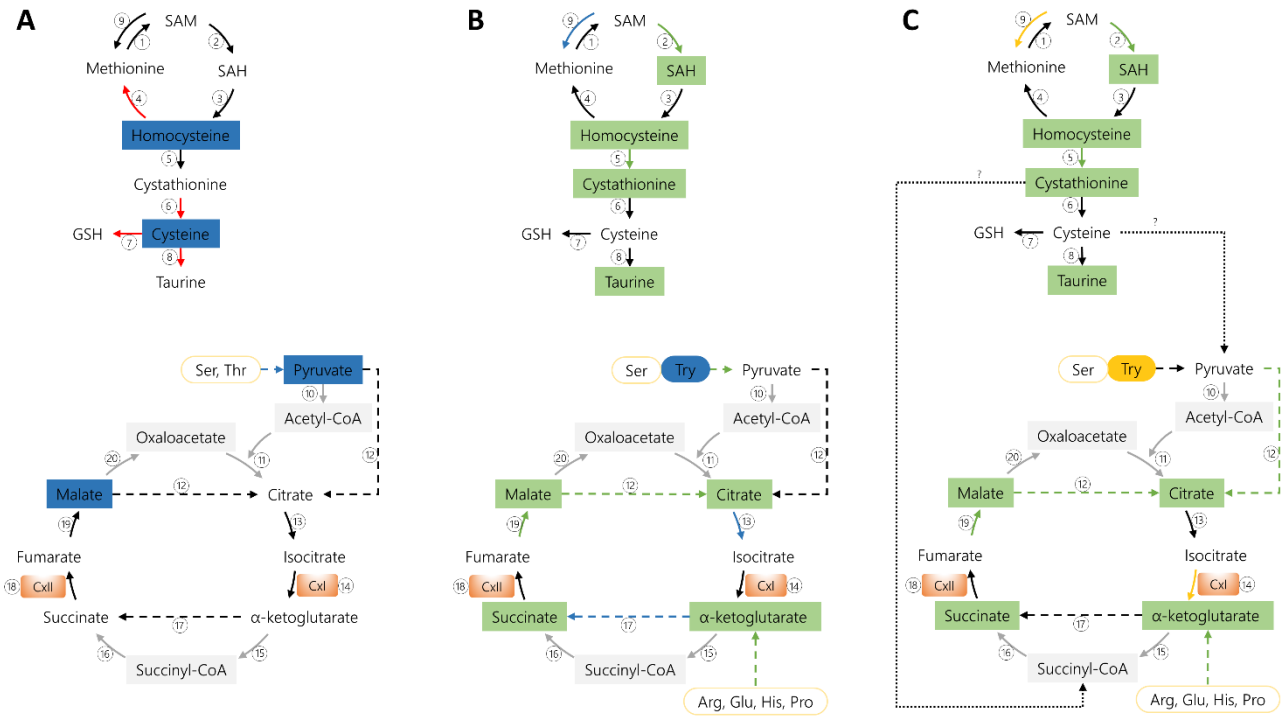

Figure 7. Proposed model for methionine and energetic metabolism plasma profile associated to human longevity. A) Plasma metabolome changes associated to human ageing (*adult vs aged individuals).* **B)** Differential plasma metabolome traits associated to ageing and longevity (*aged vs centenarian individuals*). **C**) Plasma metabolome associated to human longevity (*centenarian vs adult and aged individuals*). Red shaded arrows refer to reactions enhanced in adults. Blue shaded boxes or arrows refer to metabolites or reactions enhanced in aged. Green shaded boxes or arrows refer to metabolites or reactions enhanced in centenarians. Yellow shaded boxes or arrows refer to metabolites or reactions specifically diminished in centenarians (*centenarians vs adult and aged individuals*). Grey shaded boxes or arrows refer to non-detected metabolites or not-estimated reactions. Solid lines refer to enzymatic reactions in which one enzyme is involved. Dashed lines refer to enzymatic reactions in which more than one enzyme is involved (enzyme bypass according to data availability). Dotted black lines refer to hypotheses linking methionine and energetic metabolism. Numbers refer to enzymes or ratios: **1**, Methionine adenosyltansferase Iα/IIα (MAT1A/MAT2A); **2**, Methyltransferases (MTs); **3**, Adenosylhomocysteinase-like 1 (AHCYL); **4**, Methionine synthase (MS); **5**, Cystathionine-β-synthase (CBS); **6**, Cystathionine-γ-lyase (CTH); **7**, Glutathione biosynthesis (ratio glutathione/cysteine); **8**, Taurine biosynthesis (ratio taurine/cysteine); **9**, Methionine salvage pathway (ratio (spermidine+met)/SAM); **10**, Pyruvate dehydrogenase (PDH); **11**, Citrate synthase (CS); **12**, Citrate biosynthesis from malate and pyiruvate (ratio citrate/(malate+pyruvate)); **13**, Aconitase (ACO); **14**, Isocitrate dehydrogenase or Cx I (IDH); **15**, α-ketoglutarate dehydrogenase (OGDH); **16**, Succinyl-CoA synthetase (SCS); **17**, Ratio succinate/a-ketoglutarate; **18**; succinate dehydrogenase or Cx II (SDH); **19**, Fumarate hydratase (FH); **20**, Malate dehydrogenase (MDH)

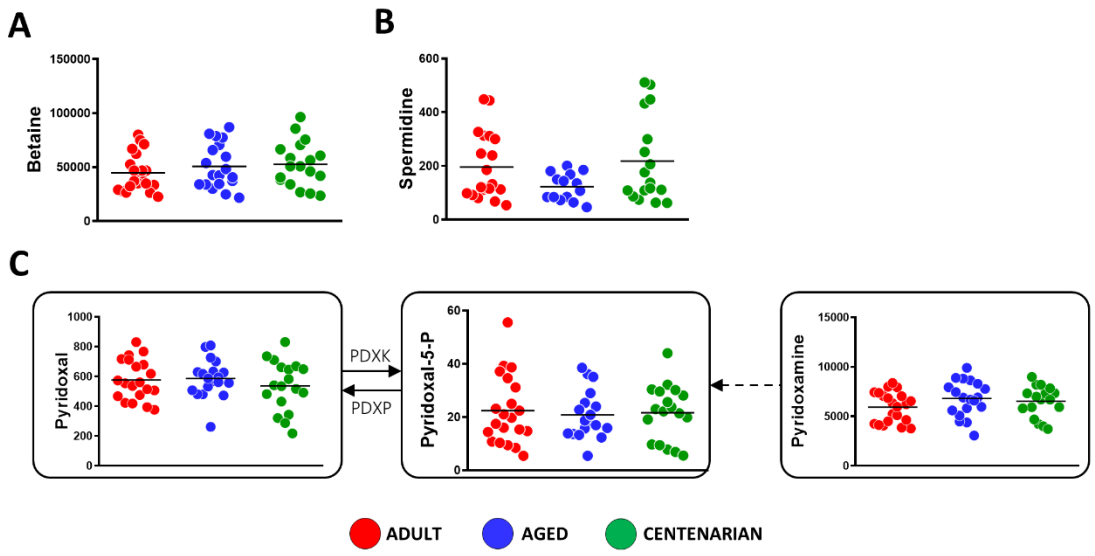

Supplementary figure 1. Betaine (A), Spermidine (B) and vitamin B6 related metabolites (C) plasma content is similar in adult, aged and centenarian individuals. Dashed lines represent reactions in which more than one enzyme is involved. Inter-group differences were measured by one-way ANOVA followed by a post-hoc Tukey multiple test. Minimum signification level was set at $p<0.05$. Enzyme codes refer to: Pyridoxal kinase (PDXK), pyridoxal phosphatase (PDXP)

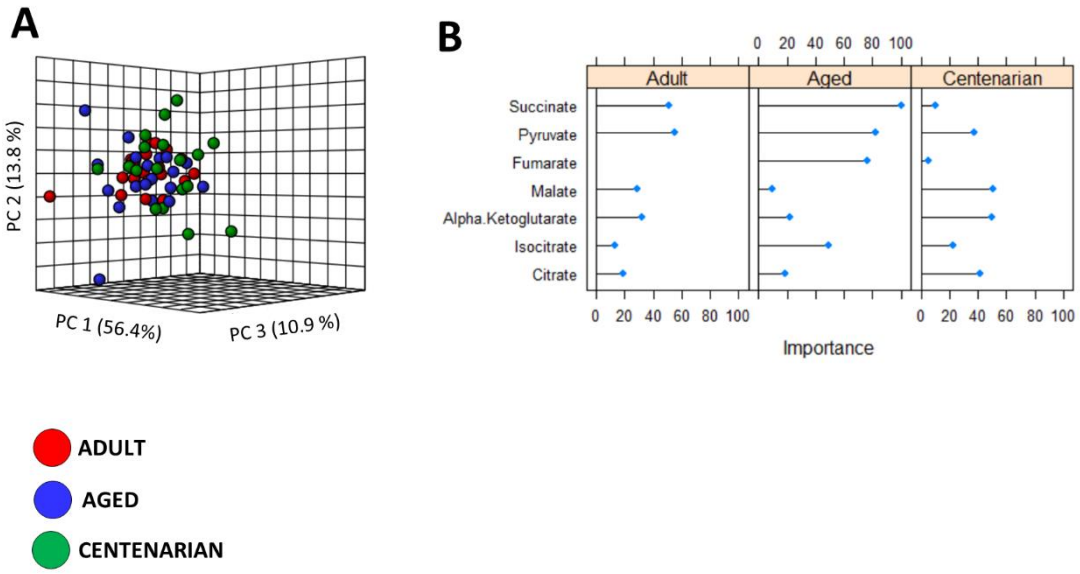

Supplementary figure 2. Multivariate statistics reveals that plasma content of Krebs cycle intermediates is not a good model to identify centenarians. A) Principal component analyses (PCA) representation metabolite content. X: Principal component 1 (PC1); Y: Principal component 2 (PC2); Z: Principal component 3 (PC3). **B)** Scaled variable importance of Partial Least Squares Discrmininant Analysis (PLS-DA) used for sample classification into each group.

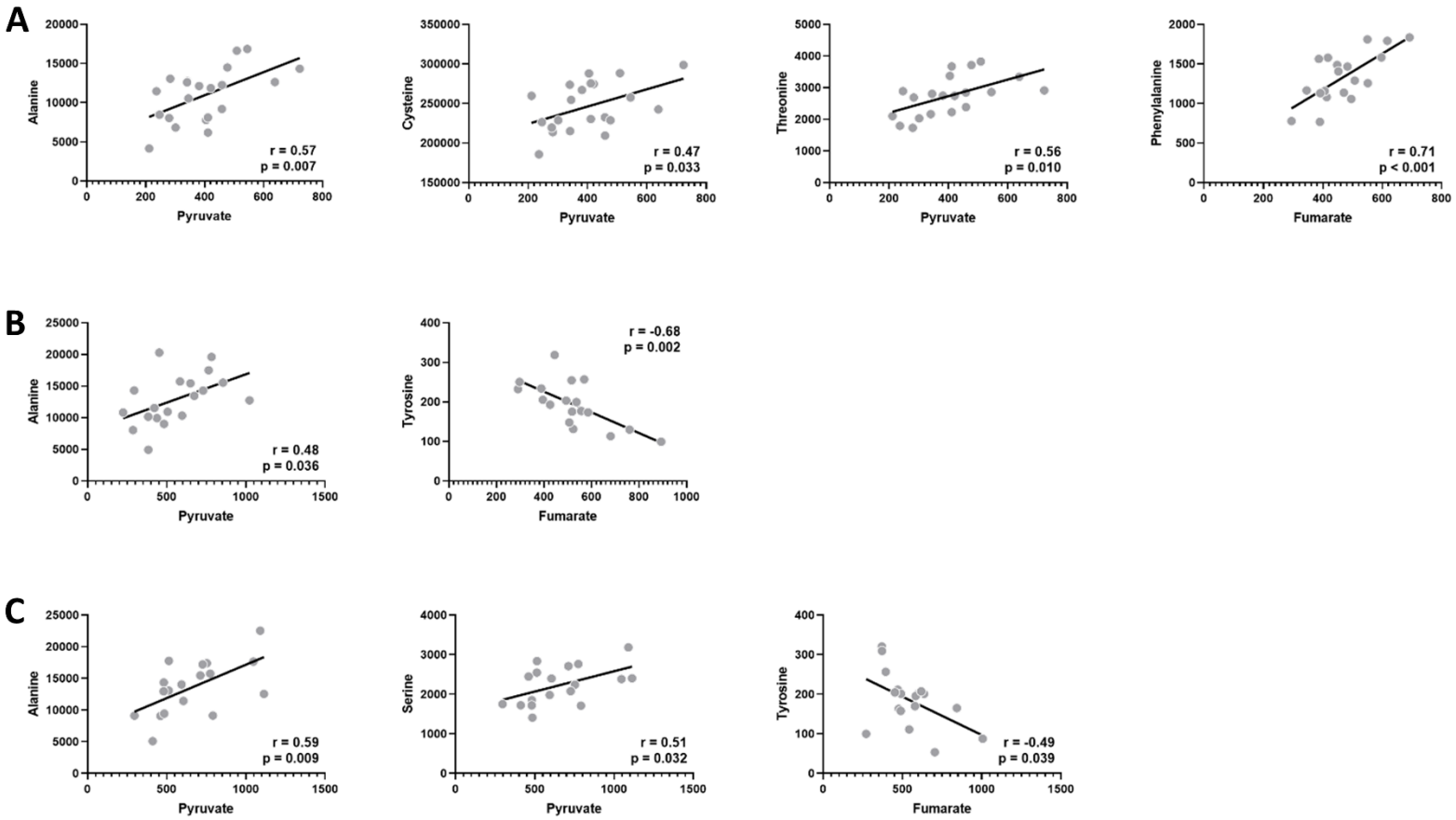

Supplementary figure 3. Correlation between plasma amino acids and TCA cycle intermediates in adult (A), aged (B) and centenarian (C) individuals. Linear regression was applied when significant relationships between metabolites were found. Minimum signification level was set at $p<0.05$.

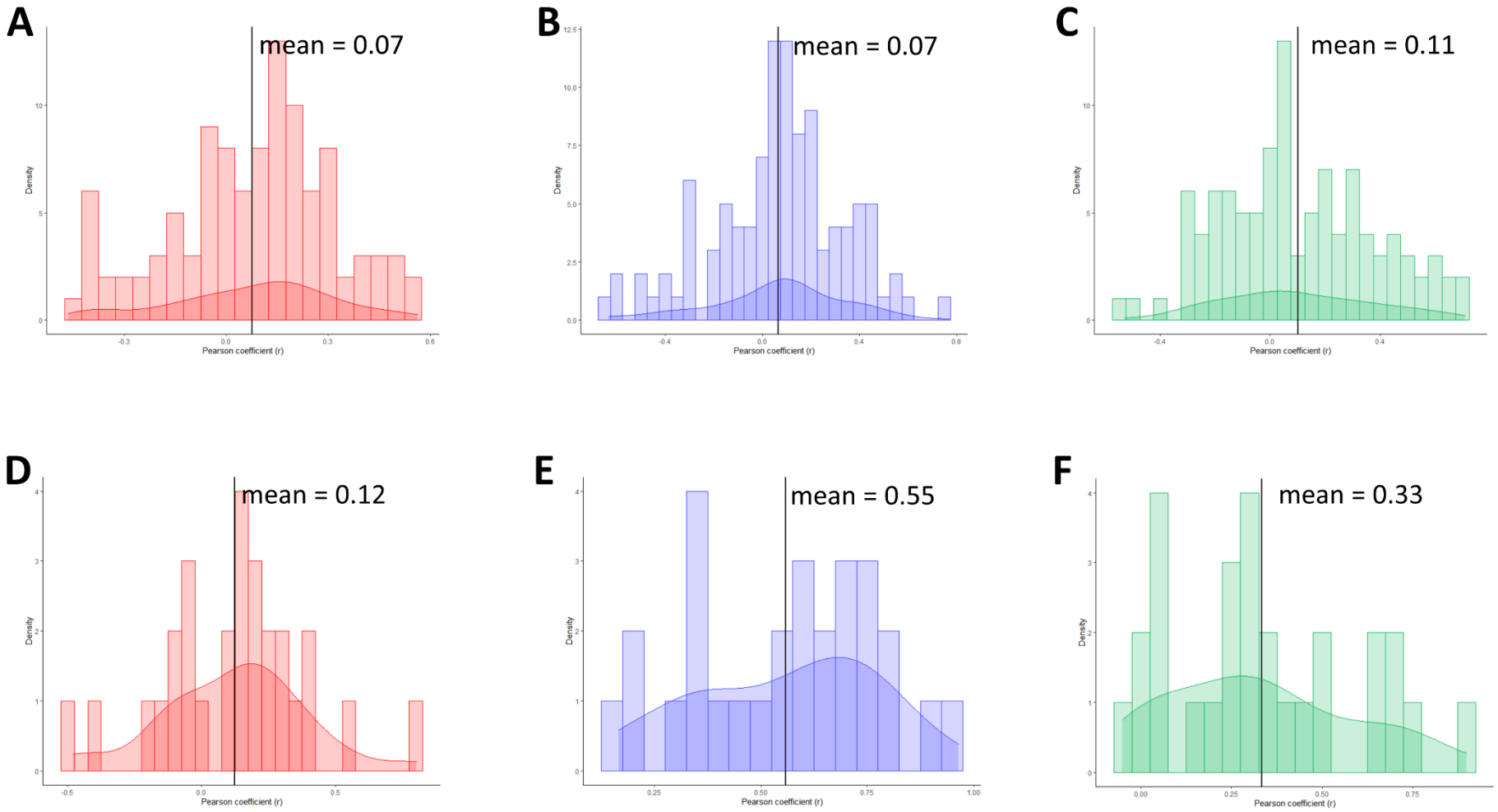

Supplementary figure 4. Pearson coefficient distribution from methionine-related metabolites and TCA cycle intermediates. Correlation coefficients (Pearson r) were obtained from methionine-related metabolites correlation matrix in adults (A), aged (B) and centenarian (C) individuals (Figure 6D-F, respectively), and TCA cycle metabolites correlation matrix in adults (D), aged (E) and centenarian (F) individuals (Figure 6J-L, respectively).

Supplementary Table 2. Plasma metabolite concentration and its differences between groups. Concentration values are reported in µM as mean ± standard error of the mean (SEM) from 18-10 individuals. Inter-group differences were measured by one-way ANOVA followed by a post-hoc Tukey multiple test. Minimum signification level was set at $p<0.05$. [a]Concentration values are reported in MS Counts.

	Descriptive statistics			ANOVA		
	Adult	**Aged**	**Centenarian**	**Adult vs Aged**	**Adult vs Centenarian**	**Centenarian vs Aged**
Amino acids						
Alanine	5.47 ± 0.42	6.56 ± 0.52	6.95 ± 0.57	0.272	0.099	0.847
Asparagine	1.02 ± 0.07	0.81 ± 0.05	0.78 ± 0.05	0.030	0.011	0.913
Arginine	22.63 ± 1.94	24.3 ± 1.40	21.43 ± 1.49	0.751	0.867	0.462
Glutamate	2.10 ± 0.17	2.63 ± 0.14	2.04 ± 0.21	0.079	0.973	0.059
Glycine	7.84 ± 0.63	7.90 ± 0.66	7.97 ± 0.64	0.998	0.990	0.997
Histidine	1.44 ± 0.05	1.47 ± 0.07	1.29 ± 0.08	0.921	0.294	0.170
Leucine/Isoleucine[a]	1319 ± 96.91	1225 ± 63.68	1048 ± 91.52	0.715	0.075	0.336
Phenylalanine	37.99 ± 2.01	38.08 ± 1.57	39.14 ± 1.79	0.999	0.896	0.912
Proline	228.9 ± 21.88	258.4 ± 17.83	263.6 ± 25.69	0.601	0.507	0.986
Serine	10.74 ± 0.61	9.39 ± 0.52	8.51 ± 0.50	0.195	0.016	0.512
Threonine	13.01 ± 0.75	10.48 ± 0.74	10.15 ± 0.95	0.076	0.042	0.957
Tryptophan	12.25 ± 0.49	11.88 ± 0.87	9.10 ± 0.83	0.928	0.010	0.030
Tyrosine	32.61 ± 2.45	35.82 ± 2.54	34.5 ± 3.18	0.677	0.876	0.939
Valine	46.99 ± 2.55	44.42 ± 1.84	37.44 ± 2.08	0.683	0.010	0.084
Methionine metabolism						
Betaine[a]	44650 ± 3787	50731 ± 4728	52708 ± 4873	0.590	0.409	0.949
Cysteine	45.72 ± 1.11	66.35 ± 2.05	70.52 ± 2.80	<0.001	<0.001	0.330
Cystathionine	0.90 ± 0.08	1.27 ± 0.09	2.82 ± 0.33	0.361	<0.001	<0.001
Glutathione	0.34 ± 0.02	0.28 ± 0.02	0.29 ± 0.02	0.194	0.234	0.996
Homocysteine	3.76 ± 0.22	6.60 ± 0.66	9.77 ± 0.86	0.004	<0.001	0.002
Methionine	9.69 ± 0.57	9.46 ± 0.56	10.02 ± 0.71	0.960	0.924	0.802
Pyridoxal[a]	577.3 ± 30.01	587 ± 28.91	536.8 ± 39.64	0.976	0.662	0.540
Pyridoxal-5-P[a]	22.41 ± 2.79	20.88 ± 2.14	21.63 ± 2.46	0.902	0.973	0.978
Pyridoxamine[a]	5944 ± 330.7	6805 ± 410.6	6532 ± 365.7	0.223	0.500	0.866
SAH	0.12 ± 0.00	0.12 ± 0.00	0.15 ± 0.01	0.997	<0.001	<0.001
SAM	0.25 ± 0.01	0.27 ± 0.02	0.31 ± 0.02	0.511	0.016	0.212
Spermidine[a]	195.8 ± 27.7	248.1 ± 53.69	217.5 ± 39.0	0.634	0.928	0.866

Taurine	1.10 ± 0.08	1.13 ± 0.10	1.53 ± 0.14	0.986	0.013	0.023
TCA cycle metabolites						
α-Ketoglutarate[a]	228.2 ± 11.9	267.3 ± 16.86	432.8 ± 38.89	0.481	<0.001	<0.001
Citrate[a]	387 ± 43.58	596.7 ± 73.84	1133 ± 170.4	0.349	<0.001	0.003
Fumarate[a]	468.7 ± 21.1	521.1 ± 35.32	549.4 ± 41.63	0.493	0.193	0.824
Isocitrate[a]	134.4 ± 14.86	229.7 ± 33.41	302.5 ± 51.6	0.120	0.003	0.320
Malate[a]	140.5 ± 10.24	201.6 ± 14.41	282.1 ± 25.03	0.033	<0.001	0.005
Pyruvate[a]	401 ± 28.53	554.5 ± 48.89	658.4 ± 56.19	0.044	<0.001	0.252
Succinate[a]	714.3 ± 27.43	730.1 ± 34.32	885 ± 43.45	0.945	0.003	0.010
Lipid and protein intermediates						
Carnitine[a]	25708 ± 1919	31456 ± 809.2	25278 ± 1585	0.030	0.979	0.024
Choline[a]	10911 ± 888.3	16525 ± 1495	19837 ± 1992	0.022	<0.001	0.274
TMAO[a]	6842 ± 1693	6789 ± 732.1	19242 ± 5136	>0.999	0.016	0.018

Discussion

The description and unravelling of the longevity determinants have been performed based on the use of different experimental designs and animal models (Taormina et al., 2019). In 1935, McCay described for the first time that the reduction of caloric intake in rats extended their longevity (McCay et al., 1935). This protocol, which later was referred to as caloric restriction (CR), was widely used as a nutritional intervention leading to an extended longevity in a vast range of organisms, from yeast to rodents (Pamplona and Barja, 2006, 2007), and to improve health span in macaques (Colman et al., 2009; Mattison et al., 2017) and humans (Flanagan et al., 2020). In the 90s decade, the first long-lived eukaryotic transgenic models were described, opening the era on genetics of aging, and showing changes in the expression of the antioxidant enzyme SOD (Longo et al., 1996; Orr and Sohal, 1994). By that time, studies on long-lived rodents such as Ames dwarf mice (Brown-Borg et al., 1996), cross-species comparative approaches involving animal species of different longevity (Beckman and Ames, 1998), and studies comparing long-lived birds and short-lived rodents with similar body size (Ku and Sohal, 1993) had also begun. Later on, after the discovery of the life span prolonging effect of rapamycin (Harrison et al., 2009), a selective inhibitor of mTORC1 evolved the pharmacologically-induced long-lived models.

The data obtained from these approximations (genetics, nutritional, pharmacological, and comparative) is diverse and complementary, since these models are useful to respond questions regarding longevity. Huge differences exist within species longevity, which is determined by genetic factors inducing a *big effect* on longevity (Barja, 2019). However, variations are found within individuals' longevity of a given specie, which can be bounded in a genetically-determined range of time. In fact, factors inducing a *small effect* on longevity determination are responsible for this inter-individual longevity differences (Barja, 2019). Accordingly, experimental models and approximations to determine longevity-associated factors are grouped into studies aiming to unravel individual or species-longevity determinants. The first group involves the use of longevity-induced models (transgenic, nutritionally or pharmacologically) and exceptionally long-lived individuals of a species, which allow to specifically describe the mechanisms exerting a small effect on longevity. These studies aim to determine *what makes a specimen (of a given species) live longer than the others*. The long-lived specimens represent those that had been able to optimise their inherited, and extend their longevity within a range (which is genetically determined by its species longevity). The intracellular mechanisms exerting a small longevity effect are of great value since they allow to define strategies that can be applied to humans in order to improve their health span. The second group refer to the inter-species studies, in which species of different longevities are compared. These approximations uncover those mechanisms that exert a big effect on longevity determination, since they allow to unravel *why some species live longer than others*. The metabolic adaptations leading to an extended longevity are fixed and genetically determined. However, elucidating how long-lived species have evolved by optimising their metabolisms allows us to understand how longevity is determined.

The present work aimed to describe i) mitochondrial structural adaptations responsible for decreased endogenous damage generation in long-lived species in terms of specific Cx I subunits gene expression and protein content; ii) mitochondrial metabolic adaptations leading to an extended species longevity in terms of metabolic intermediates of methionine, iii) energetic metabolism, and iv) lipid metabolic intermediates; v) proteostasis optimisation in long-lived species in terms of metabolic content of free amino acids; vi) integration of anabolic and

catabolic intracellular signalling pathways in long-lived species in terms of specific mTORC1 elements and its regulators gene expression and protein content; and vii) organismal metabolic adaptations leading to an extended individual longevity in terms of metabolic intermediates of methionine, energetic metabolism and lipid metabolic intermediates.

6.1. FACTORS INVOLVED IN INTER-SPECIES LONGEVITY DETERMINATION

I) DECREASED NDUFV2 CX I SUBUNIT MIGHT BE RESPONSIBLE OF LIMITED ROS PRODUCTION IN LONG-LIVED SPECIES

Mitochondrial Cx I is the main source of ROS production within cells, which is considered to be one of the main determinants of species longevity (Pamplona and Barja, 2007). Low rates of mitochondrial ROS production have been described in many long-lived mammalian and bird species (Barja, 2013; Ku et al., 1993; Pamplona and Barja, 2007), under nutritional and pharmacological pro-longevity interventions such as MetR and rapamycin treatment (Pamplona and Barja, 2006, 2007). The underlying mechanisms responsible for, at least in part, the low mitochondrial ROS production in long-lived species include qualitative and quantitative modulations. A smaller degree of electronic reduction of Cx I under basal conditions (Barja, 2013; Barja and Herrero, 1998) and proper assembly of Cx I (Miwa et al., 2014), as well as lower Cx I content could explain the lower ROS production of those long-lived species (Lambert et al., 2010; Pamplona et al., 2005). Pro-longevity nutritional interventions also decreased Cx I content (Ayala et al., 2007; Gómez et al., 2007; Miwa et al., 2014; Sanchez-Roman et al., 2011; Sanz et al., 2006b), and favoured its assembly (Miwa et al., 2014), concomitantly with a lower mitochondrial ROS production (Ayala et al., 2007; Gómez et al., 2007; Miwa et al., 2014; Sanchez-Roman et al., 2011; Sanz et al., 2006b). Although the site of ROS production within complex I is a matter of controversy, it has been located in the hydrophilic domain (Miwa et al., 2014).

Following a comparative approach, we had been able to define a Cx I phenotype associated with mammalian longevity (Mota-Martorell et al., 2020b). Our results supported the previously described negative correlation between longevity and Cx I content, as decreased expression and protein content of specific Cx I subunits was found in long-lived mammals. Furthermore, we have observed a specific reduction of NDUFS4 and NDUFV2 subunits, which might be involved in Cx I assembly (Budde et al., 2000; Stroud et al., 2016) and limiting ROS production, respectively. Electrons from NADH are transferred to a non-covalently bound FMN located in the hydrophilic Cx I arm. Afterwards, the first FeS cluster from a set of seven (N3, N1b, N4, N5, N6a, N6b and N2) can take two electrons from FMN and transfer them to ubiquinone (Barker et al., 2007). Instead, the highly conserved off-pathway N1a FeS cofactor of NDUFV2 can take one electron from FMN but cannot give it to N3 because the distance from N1a (in subunit NDUFV2, 19.4 Å) to N3 (in subunits NDUFV1, 22.3 Å) is too long compared to the maximum distance for physiological electron transfer between redox centers, 14 Å (Page et al., 1999). N1a is highly susceptible to one electron reduction of oxygen to $O_2^{\cdot-}$ (superoxide radical) due to its very low one electron potential (around -370mV) compared to all the other isopotential FeS clusters (N3 to N6b at around -250 mV). In fact, it has been proposed that N1a can function to prevent excessive ROS production (Sazanov, 2006, 2015). Accordingly, we propose that the low NDUFV2 (and N1a) amount present in long-lived species might serve to limit ROS production. The smaller the NDUFV2 amount, the less the number of electrons transferred from FMN to N1a, and less

would reduce O_2 to $O_2^{\cdot-}$, while more electrons would follow the central path from the flavin to N3 and then the rest of the FeS until N2 (Mota-Martorell et al., 2020b).

II) METABOLISM OF SULPHUR AMINO ACIDS IS INVOLVED IN LONGEVITY DETERMINATION

The plasma metabolomic profile associated to mammalian longevity is modulated by tissue-specific metabolomic profile

Organ, tissue, cell and organelle transcriptomic profile is unique, and respond to specific metabolic needs and functions leading to specific lipidomic and metabolomics profile (Bozek et al., 2017; Cortie et al., 2015; Ma et al., 2015; Pradas et al., 2019a; Sahm et al., 2018a; Seim et al., 2016). Therefore, tissue-specific modulations associated to longevity exist (Ma et al., 2015; Pradas et al., 2019a; Seim et al., 2016). Globally, our data revealed that the metabolome composition of plasma is more stable than that of heart when species with different longevities are compared. Although it could be due to a stronger regulation of plasmatic composition, we believe that its composition is the consequence of the sum of all cell-specific organismal metabolic adaptations.

Accumulation of Met residues in short-lived species might be an organismal adaptation

Longevity is achieved through the reduction of sulphur-containing amino acids, such as Met and Cys. Accordingly, long-lived species have evolved by decreasing the content of encoded Met and Cys in mtDNA (Aledo et al., 2011; Moosmann, 2011), proteins (Aledo et al., 2011; Moosmann, 2011; Portero-Otín et al., 2004; Ruiz et al., 2005) and plasma (Lewis et al., 2018; Viltard et al., 2019). Furthermore, pro-longevity nutritional (McIsaac et al., 2016; Sanz et al., 2006b) and pharmacological interventions (Cabreiro et al., 2013) modulate its content.

The reduced content of sulphur-containing residues in tissue from long-lived species might reflect a protein structural adaptation in long-lived species related to its chemical properties. Sulphur atom location differs in methionine and cysteine side chains, thus affecting its reactivity. Hence, sulphur atoms in Met are located into a sulfide group (R_1-S-R_2), whereas that of Cys are deprotonated into the highly reactive thiolates (R-S^-) under physiological conditions (Netto et al., 2007). Although both sulfide and thiolate can be attacked by ROS, the biological effect of its oxidation are different. Oxidation of Met into MetO can be enzymatically reverted at the low metabolic cost of one NADPH molecule (Levine et al., 1996; Reddy et al., 1994; Stadtman et al., 2005), whereas Cys oxidation can lead to the formation of irreversible and detrimental cross-linking reactions (Aledo et al., 2012; Chung et al., 2013). Consequently, Met has been defined as an anti-oxidant amino acid, whereas cysteine has been proposed to be pro-oxidant (Aledo et al., 2011).

Supporting these data, our study revealed a reduced heart content of methionine and cysteine, along with a reduced plasma content of methionine in long-lived species. Therefore, we propose that modulation of sulphur-containing residues content such as Met in proteins might reflect an organismal adaptation. As it has been discussed previously, we support the fact that since long-lived species have evolved by decreasing mitochondrial content of Cx I (Mota-Martorell et al., 2020b), which might be in part responsible for reduced ROS production, they don't need to protect their proteins from ROS by increasing the content of Met residues. Short-lived species, in turn, have evolved providing their proteins with antioxidant Met residues to protect their tissues from ROS attack (Aledo, 2019; Aledo et al., 2015). Furthermore, we propose that the

reduction of protein content of reactive Cys residues in long-lived species might be a tissue-specific mechanism, since plasma Cys content remained unchanged across mammalian longevity.

Met metabolism, and not only Met, is involved in longevity determination

Sulphur-containing amino acids Met and Cys are metabolically interconnected through the transmethylation and transsulfuration pathways, which are associated with longevity. In fact, the content of Met metabolic intermediates is modified in plasma (Lewis et al., 2018; Viltard et al., 2019) and tissue (Uthus and Brown-Borg, 2006; Vitvitsky et al., 2013) from long-lived rodents, as well as the transcriptomic profile of genes involved in both transmethylation and transsulfuration pathway (Uthus and Brown-Borg, 2006). Besides, a number of studies report genetic interventions in Met-related enzymes modulating longevity (Laschober et al., 2010; McCormick et al., 2015; Ogawa et al., 2016; Parkhitko et al., 2016, 2019). In this line, our data revealed the existence of a species-specific Met profile in plasma and heart. However, plasma Met profile seems to be more species-specific than that of heart, as it is more accurate when identifying animal species as revealed by heat map clusterization patterns. Altogether, our results support that not only Met, but its whole metabolism, involving transmethylation and transsulfuration pathways, is an individual and a species-longevity determinant.

Short-lived species enhance transsulfuration to promote the biosynthesis of metabolites with antioxidant properties

Transsulfuration starts with the conversion of homocysteine into cystathionine via CBS, which has been widely associated with longevity. A growing body of evidence reported that enhanced transsulfuration promotes longevity (Hine et al., 2015; Tyshkovskiy et al., 2019; Uthus and Brown-Borg, 2006; Wang et al., 2019). The injection of isotopically-labelled Met in long-lived Ames dwarf mice revealed an enhanced transsulfuration activity in liver, brain and liver, in comparison to their short-lived counterparts (Uthus and Brown-Borg, 2006). Besides, transsulfuration is enhanced under DR (Wang et al., 2019), and CBS is one of the most commonly upregulated genes among lifespan-extending interventions in mice (Hine et al., 2015; Tyshkovskiy et al., 2019). The longevity extension mechanisms seem to occur through an enhanced CBS activity and hydrogen sulphide H_2S production, which upregulates AMPK and inhibits mTORC1, and its downstream effectors 4EBP1 and S6K (Wang et al., 2019). In this line, exposure to H_2S extends lifespan in worms (Miller and Roth, 2007; Ng et al., 2020). Furthermore, long-lived worms have higher H_2S production which, in part, activate antioxidant signalling pathways and the unfolded protein response (Wei and Kenyon, 2016). Since cystathionine levels are regulated, at least in part, by CBS activity, our data suggest that reduction of cystathionine levels is an organismal metabolic adaptation leading to an extended longevity.

Antioxidant properties had been attributed to H_2S (Hine et al., 2015; Miller and Roth, 2007; Ng et al., 2020; Wei and Kenyon, 2016), as it has been to downstream metabolites of the transsulfuration pathway. Taurine and GSH, which are synthetized from Cys, are defined as antioxidant metabolites (Gould and Pazdro, 2019; Ito et al., 2014), being taurine an autophagy inductor (Kaneko et al., 2018). In humans, Improved cardiovascular health have been associated to taurine intake (Yamori et al., 2009) and reduced systemic oxidative stress after GSH precursors intake (Gould and Pazdro, 2019). Besides, long-lived rodents have evolved by increasing taurine and GSH, along with reducing oxidized GSH (Lewis et al., 2018; Viltard et al.,

2019; Vitvitsky et al., 2013). Conversely, we observed a marked reduction of transsulfuration metabolites (homocysteine, cystathionine and Cys) in tissue from long-lived mammals, but only cystathionine was reduced in plasma. Furthermore, plasma and tissue content of taurine and GSH were also decreased in long-lived species. According to the previous data and the obtained results, we suggest that short-lived species have evolved by enhancing transsulfuration pathway, probably by inducing CBS activity, to promote the biosynthesis of antioxidant molecules and protect their structures from ROS attack and revert oxidative alterations. In the same line, since long-lived species produce less ROS, they don't need to continuously synthetize antioxidants. Supporting our hypothesis, a transcriptomic study involving 33 mammals revealed a negative correlation between cysteine metabolism and longevity, suggesting a reduced cysteine catabolism in long-lived species (Fushan et al., 2015).

III) REDUCED TCA CYCLE INTERMEDIATES IN LONG-LIVED SPECIES MIGHT BE AN INDICATIVE OF AN ENHANCED B-OXIDATION

Mitochondria has been pointed as a central organelle regulating longevity. Reduced ROS production at Cx I (Miwa et al., 2014; Mota-Martorell et al., 2020b; Pamplona and Barja, 2007), membrane unsaturation (Pamplona and Barja, 2007) and permeability (Mota-Martorell et al., 2020b; Zhou et al., 2019), and modulation of mitochondrial dynamics (Sharma et al., 2019), represent some of the mitochondrial structural and functional adaptations leading to organismal longevity. Providing cells with ATP is the central role of mitochondria, although it participates in gluconeogenesis, metabolism of amino acids and one-carbon metabolism, and lipid and protein biosynthesis (Brand, 2014; Tatsuta et al., 2014). Those structural and functional adaptations might be responsible for the specific modulations of mitochondrial metabolism associated with an extended longevity (Faulkes et al., 2019; Heinze et al., 2018; Viltard et al., 2019). In fact, manipulation of longevity-associated genes alters energy metabolism (Yanai et al., 2017).

The TCA cycle occurs within mitochondrial matrix, and constitutes a metabolic epicentre since multiple substrates can feed into it (Martínez-Reyes and Chandel, 2020). Two molecules of acetyl-CoA, generated from fatty acids, amino acids or glucose oxidation enter the cycle and are sequentially metabolized into different intermediates. During these reactions, GTP and electron donors (e.g., NADH and $FADH_2$) are produced, which will feed the mitochondrial ETC. Globally, TCA cycle genes are up-regulated in long-lived mutants (Amador-Noguez et al., 2004; Perron et al., 2000; Wang et al., 2010) and mice subjected to pro-longevity interventions (Tyshkovskiy et al., 2019), suggesting that longevity is associated with an enhanced TCA activity. However, our metabolomics data revealed reduced content of (iso)citrate, fumarate and malate, suggesting a reduction of TCA cycle activity in long-lived species. Supporting our data, an inter-organ transcriptomic study including 33 species of mammals revealed that genes involved in TCA cycle are down-regulated in liver from long-lived species (Fushan et al., 2015).

Succinate is a TCA intermediate that actively participates in the production of ATP via the mitochondrial ETC, since it is the substrate of Cx II. Our data revealed a correlation between succinate and species longevity, being increased in heart but decreased in plasma from long-lived species, suggesting a tissue-specific effect. Previous studies had already reported a tissue increase of succinate in long-lived models (Fuchs et al., 2010) and under nutritional interventions extending lifespan (Plummer and Johnson, 2019; Weckmann et al., 2018). Succinate metabolization through Cx II occurs along with $FADH_2$ oxidation, which derives from fatty acids

β-oxidation (Bezawork-Geleta et al., 2017). Therefore, Cx II constitutes a link between lipid and glucose catabolism, which are mutually exclusive of each other (Randle, 1998). Longevity-associated modulations of mitochondrial metabolism have been described in NMR (Faulkes et al., 2019; Heinze et al., 2018; Viltard et al., 2019). In fact, liver proteomics suggest a longevity shift from mitochondrial respiration to fatty acid oxidation for energy production (Heinze et al., 2018). Most of the electrons feeding the ETC via Cx II flow to Cx III in a forward direction FET, although some can flow in a RET, to ubiquinol and Cx I (Scialò et al., 2017). Although ROS is produced during both FET and RET (Schönfeld et al., 2010), RET-ROS seems to have a signalling role promoting lifespan extension in flies (Scialò et al., 2016). Besides, it has been suggested that succinate accumulation is responsible for RET induction (Chouchani et al., 2014). According to the obtained results and mechanistic underlying RET-ROS production, we suggest that the increased heart content of succinate might be an indicator of an enhanced β-oxidation, rather than TCA cycle induction, found in long-lived species. Accordingly, glucose restriction induces a metabolic reprogramming targeted to decrease glycolysis intermediates and increase succinate (Weckmann et al., 2018). Since β-oxidation influences ETC activity increasing organism fitness (Ramachandran et al., 2019), we propose that by promoting β-oxidation long-lived species are able to by-pass the main source of intracellular ROS production, Cx I.

Up to date, succinate is the only TCA cycle intermediate known to trigger organismal functions. Binding of succinate to its receptor SUCNR1 leads to modulation of renin-angiotensin and immune systems, along with an enhanced thermogenesis. Therefore, it seems that succinate might act as a signalling molecule inducing organismal pro-longevity effects (Martínez-Reyes and Chandel, 2020). Given these data, we propose that plasma succinate is enriched in short-lived species in order to boost the previously described pro-longevity mechanisms.

IV) CHOLINE MIGHT BE ASSOCIATED WITH PROPER LONG-LIVED LIPIDOMIC SIGNATURE

Choline is synthetized from betaine, which is involved in methionine regeneration from homocysteine. Choline, in turn, is the biosynthetic precursor of phosphocholine (PC), which can be metabolised into lysoPC or phosphoserine (PS) by exchanging choline and serine groups (Li and Vance, 2008), or hydrolysed via the action of phospholipases to generate choline, constituting the only known endogenous pathway for choline biosynthesis in mammals (Li and Vance, 2008). PC can be also synthetized from phosphatidylethanolamine (PE) in a reaction coupled to SAM reduction into SAH and catalysed by PE methyltransferase (PEMT). Our data revealed reduced heart and plasma content of choline, which might be involved in determining proper PC profile associated to extended longevity, as previously reported (Pradas et al., 2019a, 2019b). In a similar line, an cross species study comparing the lipid composition across eleven mammalian species revealed the existence of a species-specific diacylclgyceride plasma profile associated to species longevity (Mota-Martorell et al., 2019). As diacylglycerides are biosynthetic precursors of PC through a de novo biosynthetic pathways, these results reinforce the idea that choline is involved in the determination of a proper lipid profile.

V) REDUCED FREE AMINO ACID POOL MIGHT BE INDICATIVE OF PROPER PROTEOSTASIS IN LONG-LIVED SPECIES

Maintenance proteostasis is a hallmark of longevity. This occurs through the specific regulation of anabolic and catabolic processes to ensure protein structure and function. Synthesising more resistant proteins (Pickering et al., 2015a) and maintaining proper proteasomal activity

(Pickering et al., 2015b; Rodriguez et al., 2016) and autophagy (Pride et al., 2015; Rodriguez et al., 2016) to efficiently clear altered and non-functional proteins results in a negative correlation between global protein turnover and species longevity (Swovick et al., 2018). In fact, cross-species studies revealed a down-regulation of genes involved in amino acid catabolism (Fushan et al., 2015) and proteolysis (Ma et al., 2016). Our data revealed a species-specific amino acid tissue profile, marked by a global reduction of free amino acids in long-lived species, which is in good agreement with previous studies performed in long-lived worms (Castro et al., 2013) and NMR (Lewis et al., 2018; Viltard et al., 2019). Besides, we had previously reported that long-lived species maintain a decreased content and phosphorylation pattern compatible with a reduced activity of mTORC1 (Mota-Martorell et al., 2020a), which regulates protein synthesis (Weichhart, 2018). Accordingly, we suggest that the global reduction of tissue free amino acids observed in long-lived species is indicative of a proper proteostasis and might result from mTORC1 inhibition and the subsequent autophagy induction (Bárcena et al., 2019; Khayati et al., 2017; Ruckenstuhl et al., 2014). Supporting this hypothesis, we had also observed in short-lived species, which have higher endogenous damage and altered proteostasis, increased pro-autophagic metabolites, such as taurine and spermidine (Bárcena et al., 2018; Kaneko et al., 2018), to restore protein metabolism.

Plasma amino acid profile was also species-specific, but no consistent pattern within longevity evolution was observed. Contrarily, it has been defined a reduction of plasma amino acid content in NMR (Lewis et al., 2018; Viltard et al., 2019) and after nutritional interventions in humans (Washburn et al., 2019). Therefore, we suggest that longevity extension driven by amino acids is complex, and though the modulation of specific intracellular pathways, as described previously (Edwards et al., 2015).

VI) REDUCED MTORC1 CONTENT AND ACTIVITY AS A KEY MODULATOR OF A LONGEVITY-ASSOCIATED PHENOTYPE

Phenotypic features associated with long-lived animal species seem to be supported by specific cell signalling pathways (Barja, 2019), including the mTOR pathway. mTORC1 plays a central role in the mTOR signalling network, and has been widely associated with animal longevity (Valvezan and Manning, 2019). Rapamycin (Wu et al., 2013a), DR (Kapahi et al., 2004) or downregulation of S6K1 (Selman et al., 2009) leading to direct, upstream or downstream mTOR pathway inhibition respectively, result in an extended longevity in several animal models from yeast to mice (Kapahi et al., 2010; Lushchak et al., 2017; Papadopoli et al., 2019; Weichhart, 2018), whereas mTOR activation shortens longevity (Johnson et al., 2013; Kapahi et al., 2010; Papadopoli et al., 2019). Reduced mRNA content of mTORC1-coding subunits was found in long-lived individuals and its offspring (Passtoors et al., 2013). Our data revealed the existence of a species-specific mTORC1 gene and protein profile, which characterised by a reduced gene expression and protein content of mTORC1 subunits and activators (Mota-Martorell et al., 2020a). Furthermore, we have also identified phosphorylation patterns in mTOR and PRAS40, which is a negative regulator of mTOR activity also constituting mTORC1, that might be consistent with a reduced mTORC1 activity in long-lived species. Supporting our results, long-lived whales with an estimated longevity of 200 years exhibit inhibitory changes at mTORC1 activators (Ma and Gladyshev, 2017).

mTORC1 plays a central role in the mTOR signalling network by integrating a broad diversity of extra- and intracellular signals controlling cell physiology and longevity (Kapahi et al. 2010; Antikainen et al. 2017; Weichhart 2018; Papadopoli et al. 2019; Barja 2019; Valvezan and Manning 2019). Thus, mTORC1 can regulates cell metabolism through a wide range of downstream pathways such as mRNA translation and biosynthesis pathways, mitochondrial function, autophagy and stress response. Therefore, we suggest that given its involvement in longevity determination mTORC1 might be, in part, responsible for the modulation of intracellular species longevity-associated phenotype.

Bidirectional regulation between mTORC1 and mitochondria has been reported (de la Cruz López et al., 2019; Wei et al., 2015). Mitochondrial respiratory activities and expression of ETC complexes I, II and IV are regulated through mTOR/Akt pathway (Goo et al., 2012). In fact, reduced mTORC1 activity correlates with a downregulation of genes encoding ETC proteins and reduced proton leak (Rosario et al., 2019), along with reduced ROS levels (Gredilla et al., 2001; López-Torres et al., 2002; Orr and Sohal, 1994). Besides, Cx I inhibition with metformin leads to mTOR inhibition via Akt, and the subsequent induction of autophagy (Ariaans et al., 2017). Mitochondrial metabolism is also controlled by mTORC1 (Lu et al., 2015; Weichhart, 2018). In cancer cells, mTORC1 triggers an increased glycolytic flux and simultaneously limiting oxidative phosphorylation (Warburg effect) (Weichhart, 2018). However, radiotherapy leads to a metabolic reorganisation in which mTORC1 switches bioenergetic from aerobic glycolysis to oxidative phosphorylation (Lu et al., 2015). Rapamycin or mTORC1 disruption leads to a reduced mitochondrial activity (Ramanathan and Schreiber, 2009; Schieke et al., 2006), although mitochondrial inhibition leads to reduced mTOR activity (Desai et al., 2002). Besides, the TCA intermediate α-ketoglutarate increases lifespan in worm by inhibiting ATP synthase and mTORC1 (Chin et al., 2014). Altogether, these data suggest that decreased mTORC1 content and activity might be responsible for the observed mitochondrial metabolic changes in long-lived species, including a reduced Cx I content and TCA cycle intermediates.

mTORC physically interacts with VDAC1 and the anti-apoptotic protein B-cell lymphoma-extra-large (Bcl-xl) (Ramanathan and Schreiber, 2009). mTORC1 inhibition leads to disruption of VDAC1-Bcl-xl and mTORC1 complex and reduced mitochondrial respiration (Ramanathan and Schreiber, 2009). VDAC1 is a component of the mitochondrial permeability transition pore (mPTP) (Halestrap, 2009; Leanza et al., 2019; Mnatsakanyan et al., 2017, 2019) forming protein found in the outer mitochondrial membrane of all eukaryotes, allowing a direct interaction between mTORC1 and mitochondria (Desai et al., 2002). VDAC1 regulates mPTP opening in response to ROS (Briston et al., 2017; Panel et al., 2018; Rottenberg and Hoek, 2017). Besides, reduced ROS at Cx I (Pamplona and Barja, 2006, 2007) and mPTP (Amigo et al., 2017; Petrosillo et al., 2010) has been described under DR. We suggest that reduced Cx I content, and subsequent limited ROS production found in long-lived species is responsible for the maintenance of proper mitochondrial permeability. Accordingly, increased VDAC leads to increased mPTP permeability and shortened longevity (Zhou et al., 2019). VDAC is essential to maintain mitochondrial ATP through the ETC (Vyssokikh et al., 2020). Altogether, these results suggest that reduced mTORC1 content and activity in long-lived species lead not only to the regulation of mitochondrial metabolism but to its permeability, leading to a decreased ROS production, which is one of the two key traits leading to an extended longevity (Pamplona and Barja, 2007).

Anabolic and catabolic processes are controlled through mTORC1 in response to upstream signals mediated by nutrient availability. Under energy-reach conditions, mTORC1 is activated and drives anabolic cellular processes, such as protein and lipid biosynthesis (Düvel et al., 2010), and supress catabolic processes. Nonetheless, under starving conditions such as nutritional restriction of glucose or amino acids, mTORC1 is inactive and catabolic rather than anabolic pathways are promoted (Laplante and Sabatini, 2009). Accordingly, mTORC1 inhibition during DR promotes autophagy, which clears old and dysfunctional organelles, enhancing longevity (Simonsen et al., 2008). In fact, longevity extension under MetR depends upon autophagy (Bárcena et al., 2019; Ruckenstuhl et al., 2014). Inhibition of mTORC1 also leads to the induction of β-oxidation (Caron et al., 2015). Our results revealed a reduced heart content of amino acids and choline in long-lived species, which might be in accordance with a reduced biosynthesis of proteins and lipids and enhanced catabolism. As we described previously, mTORC1 activity is also regulated by amino acids. Therefore, we suggest that mTORC1 downregulation in long-lived species regulates proper proteostasis and lipid homeostasis, as well as the induction of β-oxidation.

Four major extracellular signals are integrated by mTORC1 (growth factors, energy status, oxygen and amino acids) to regulate all the previously described metabolic processes (Valvezan and Manning, 2019). Reduction of Met intake, rather than DR, is enough to inhibit mTORC1 and promote longevity extension via autophagy induction (Bárcena et al., 2019; Ruckenstuhl et al., 2014). Therefore, it seems that intracellular pathway leading to mTORC1 activation upon amino acid availability might be essential for longevity determination. In fact, we have revealed that mTORC1 inhibition occurs along with reduced content of its activator Arg, Leu and Met in long-lived species. In fact, we have been able to establish positive correlations between mTORC1-longevity associated changes and the methionine metabolism. Accordingly, a study in worms demonstrated that SAMTOR, a regulator of mTOR, detects methionine availability via SAM, and is also involved in longevity extension under DR (Gu et al., 2017b). Besides, mTORC1 also regulates transsulfuration, since its inhibition leads to a reduced gene expression of transsulfuration enzymes CTH and CBS, along with reduced H_2S production (Lyu et al., 2019). Under stress conditions, CTH is translocated to mitochondria, where it induces cysteine metabolization along with H_2S and ATP synthesis. Therefore, it seems that under stress condition, induction of the transsulfuration pathway permits to maintain ATP mitochondrial production (Fu et al., 2012). Available evidence allows to establish a relationship between mitochondrial metabolism, methionine pathways and mTORC1, which is involved in the determination of species longevity.

Altogether, we suggest that mTORC1 reduced activity might be responsible for the longevity associated phenotype described in our work. Therefore, we suggest that long-lived species have evolved by optimising its intracellular metabolism and to bidirectionally coordinate mitochondrial function and mTORC1 to maintain cellular homeostasis and promote longevity.

6.1.1. Dealing with inter-species relationships in longevity determination

Comparative studies across species with different lifespan are a powerful source of information to identify mechanisms linked to extended longevity (Bozek et al., 2017; Ma et al., 2015). However, those studies come up with several technical limitations. Specifically, in terms of protein recognition, the presence of SNPs inducing little sequence or amino acid changes might

alter protein structure, even in highly conserved structure, possibly affecting antibody recognition. Since we lack of methods to improve inter-species antibody reactivity, we have increased the number of repeated measurements up to 7, in order to capture higher inter-individual variability in each specie, and measured gene expression using a very sensible technique in order to confirm those results. However, in some cases we didn't find significant correlations between gene expression and protein content. Although we cannot omit technical issues, the lack of correlation doesn't necessarily invalidate the presented results. Accordingly, it had been reported that mRNA and protein content doesn't need to be necessarily correlated (Maier et al., 2009), even in mammals (Tian et al., 2004). Furthermore, a comparative study has demonstrated an increasing protein divergence with higher evolutionary distance, since expression divergence seems to be more stable (Warnefors and Kaessmann, 2013), which agrees with the obtained data.

Even after dealing with technical issues, inter-species studies have to face that evolutionary relationships don't allow for independence of the data (Cooper et al., 2016). Therefore, it's important to elucidate whether a specific trait correlates with longevity differences, or alternatively, these differences arise because of the data similarity. To overcome this limitation, several longevity cross-species studies in birds (Minias and Podlaszczuk, 2017), bats (Wilkinson and Adams, 2019), primates (Muntané et al., 2018), mammals (Jové et al., 2013; Lindborg et al., 2015) and other vertebrates (Mayne et al., 2019) have applied phylogenetic comparative methods, such as PGLS. In our data, PGLS revealed that *ndufv2, mtor, rptor, fkbp1a* gene expression, VDAC protein content, mTOR^{Ser2448} and PRAS40^{Thr246} phosphorylation, as well as metabolite heart content of methionine, PLP, proline, tyrosine, (iso)citrate, fumarate and plasma metabolite content of pyridoxamine and succinate changes associated with longevity weren't due inter-species relationships. Although robust, the main limitation of the methods for phylogenetic analysis is that they rely on the construction of a phylogenetic tree, which is unknown. Phylogenies are estimated, mainly by aligning homologue gene sequences and using models of mutation to infer most-likely evolutionary histories. However, depending on the genes chosen, how the sequences are aligned and which method is used to infer evolutionary histories we get different phylogenies. And errors in phylogenetic inferences propagate to errors in phylogenetic analyses (Washburne et al., 2018). These limitations arise the need of the development of more robust bioinformatic methodologies for phylogenetic tree inferences.

6.2. METABOLIC DETERMINANTS OF INDIVIDUAL LONGEVITY

As it has been previously discussed, the longevity determinants leading to species longevity include reduced Cx I content and specific subunits (NDUFV2 and NDUFS4), sulphur-containing amino acids, transsulfuration pathway and subsequent biosynthesis of antioxidants, tissue amino acids, TCA cycle intermediates and choline but increased succinate, and reduced content and activity of mTORC1. These molecular adaptations might coincide, or not, with individual determinants of longevity. In fact, although these mechanisms are also involved in promoting individual longevity, they are differently regulated in long-lived individuals, except for plasma amino acid profile, which shows an amino-acid specific plasma regulation.

Longevity extension occurs along with a global modulation of methionine metabolism leading to a reduced content of sulphur-containing metabolites, such as methionine and cysteine. Accordingly, our data revealed that a unique plasma methionine metabolism profile is

associated with the achievement of human extreme longevity, with no changes in methionine plasma content. It has been previously suggested that flux via methionine metabolism is more critical than methionine content itself in longevity determination (Parkhito et al, 2016). Therefore, we suggest that methionine metabolism is a major determinant of species and individual longevity, but not methionine *per se*. Furthermore, increased plasma content of homocysteine, cystathionine and cystathionine suggest an enhanced transsulfuration, as discussed previously. Higher taurine and glutathione plasma content supports the idea that centenarians enhance transsulfuration to induce the biosynthesis of antioxidant compounds, as short-lived species do, to promote its longevity.

Energetic metabolism is also modulated to achieve individual longevity. In fact, it has been reported an increased gene expression and activity of TCA cycle in long-lived models (Amador-Noguez et al., 2004; Kamei et al., 2011; Perron et al., 2000; Wang et al., 2010). Accordingly, we have found an increased plasma content of pyruvate, citrate, isocitrate, α-ketoglutarate, succinate and malate in centenarians. Higher citrate content is associated with longevity (Cheng et al., 2015; Kettunen et al., 2012; Peleg et al., 2016) and increased plasma levels had already been found in centenarians compared to aged individuals (Montoliu et al., 2014). Higher succinate has also been described in long-lived animal models (Fuchs et al., 2010; Plummer and Johnson, 2019). Nutritional supplementation of pyruvate and α-ketoglutarate leads to an extended lifespan (Chin et al., 2014; Mishur et al., 2016). The molecular mechanisms linking these metabolic intermediates and longevity are diverse, and include oxidative stress protection (Tauffenberger et al., 2019), HIF-1α stabilization (Mishur et al., 2016), mTOR inhibition (Chin et al., 2014) and immunity maintenance (Martínez-Reyes and Chandel, 2020). Accordingly, we suggest that the achievement of individual longevity occurs through the induction of energetic metabolism and multiple metabolic pathways as a consequence of the increased plasma content of TCA cycle intermediates. In fact, the increased energetic demands could be interpreted as a response to the metabolic cost of the continuous maintenance of the biosynthesis of antioxidant molecules and signalling pathways.

Lipid metabolism, and therefore lipidomic profile, is also modulated to achieve a higher longevity (Gonzalez-Covarrubias et al., 2013; Jové et al., 2013). Accordingly, choline was increased in plasma from centenarians. Choline is the metabolic precursor of PC, LysoPC and PS, but it also promotes lipid oxidation (Shen et al., 2020). Besides, centenarians have an increased content of plasmatic ether lipids containing alkyl groups derived from PC (Pradas et al., 2019b), which confers them an increased resistant to oxidation. Altogether, these results support the role of choline in maintaining a long-lived lipidomics profile.

6.3. Factors determining inter-species and inter-individual longevity

Longevity achievement occurs through a complex metabolic modulation, and involve factors that are genetically determined leading to species longevity (**Figure 24A**) as well as modulating factors responsible for the achievement of individual longevity (**Figure 24B**). By following an inter-species and inter-individual approaches, we had been able to describe a long-lived associated phenotype in both mammals and humans. Methionine metabolism, transsulfuration, TCA cycle and succinate are factors involved in species and individual longevity determination, but are oppositely regulated. In fact, reduced metabolic activity is associated with species longevity, whereas individual longevity is achieved by enhancing intracellular metabolism.

Besides, methionine *per se* is only involved the determination of species longevity, although its reduced content in long-lived species seems to be an organismal optimisation affecting all tissues. Nonetheless, reduced cysteine content and energetic metabolic shifts associated with animal longevity seem to vary within tissues. Globally, we suggest that these structural and energetic modulations, along with Cx I regulations leading to limited ROS production associated with longevity, might be globally orchestrated by specific signalling pathways, such as mTORC1.

However, our work has some limitations. First, the limited number of measured metabolites leads to incomplete networks. Although previous data allow us to generate new hypothesis, it should be needed to identify more metabolites in order to define a global network. Specifically, it would be interesting to include intermediate metabolites within the pathways, in order to establish clear associations between methionine metabolism, TCA cycle and amino acids. Second, we have only tracked changes in two tissues, and since evidence suggest the existence of tissue-specific modulations, it would be interesting to evaluate specific longevity modulation in specific tissue metabolism. Third, the comparative approach involves a limited number of mammals and specimens. To obtain a more accurate view of longevity determinants of animal species, it would be interesting to increase both the number of species and specimens, as well as to include non-mammalian species such as birds. Fourth, a small population from a limited region in Spain is used for the evaluation of human extreme longevity determinants. Therefore, the obtained results should be validated in different and bigger cohorts

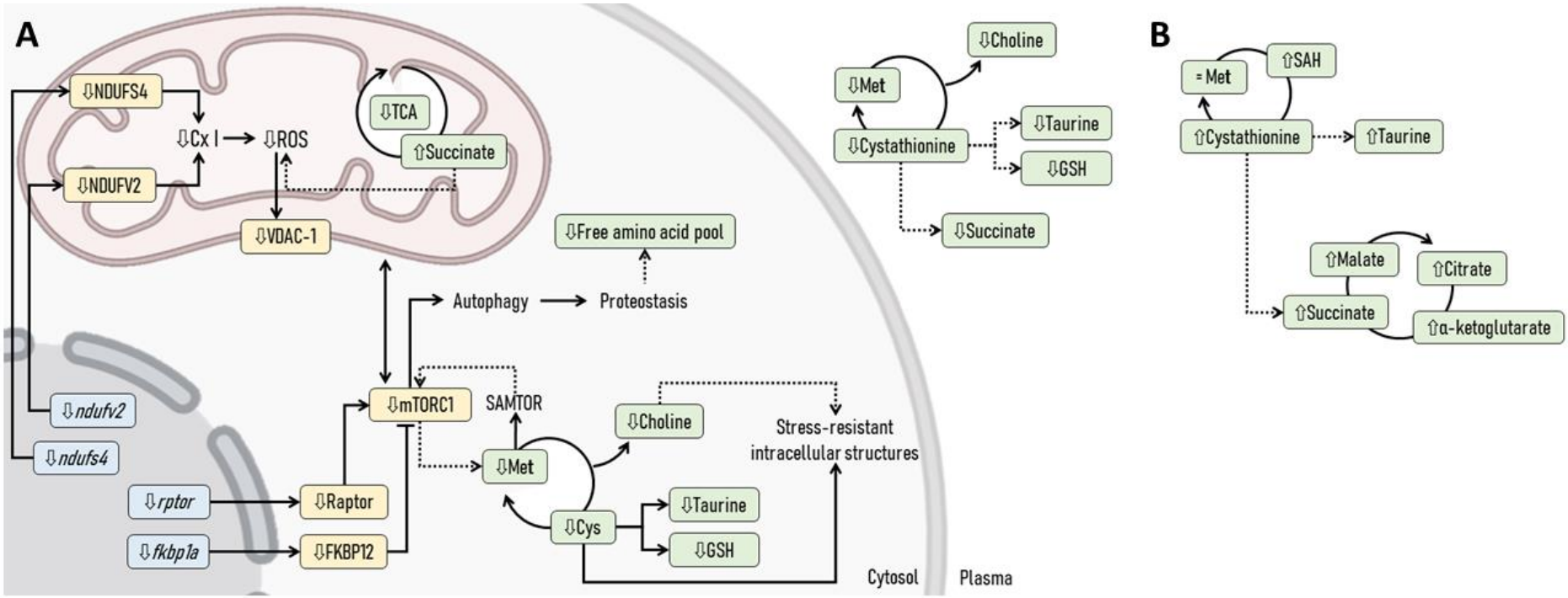

Figure 24. Determinants of species longevity (A) and human extreme longevity (B). A) Long-lived species have evolved by decreasing the rate of intracellular ROS production and synthetizing stress-resistant molecules. Accordingly, we have observed that long-lived species maintain a lowered content of NDUFV2 and NDUFS4 Cx I subunits, which might be associated with limited ROS production. Maintaining proper mitochondrial permeability, in terms of VDAC protein content, could also be responsible for the decreased ROS generation and thus associated to a higher longevity. Aside of mitochondrial structure optimization, the metabolic pathways occurring within the matrix might also be regulated in a longevity context. In fact, we have observed that long-lived species maintain a lower content of TCA cycle intermediates, except for increased succinate. Hence, we propose that this might be an indicative of a limited glucose oxidation. Based on metabolomics data, we propose that β-oxidation could be favored, to promote the feeding of electrons through Cx II, and by-passing Cx I. Furthermore, the reduced content of Met metabolic intermediates, and the reduced free amino acid pools, might be indicative of the biosynthesis of stress-resistant lipids and proteins. Besides, the lowered biosynthesis of sulphur-containing metabolites with antioxidant properties is interpreted as an expression of the long-lived species resistance to oxidative stress. We propose that lowered mTORC1 content and activity is responsible for this longevity-associated tissue phenotype. Little changes in plasma composition are found when comparing species of different longevities. In fact, plasma composition of sulphur-containing metabolites was similar to that of tissue, although succinate was lowered. we found a reduced content of sulphur-containing metabolites and antioxidants, as well as lowered succinate. **B)** Plasma determinants of human extreme longevity are similar to that of short-lived species, in terms of increased content of sulphur-containing intermediates and TCA cycle intermediates, including succinate. We propose that enhancement of energetic metabolism is necessary to cope with the metabolic cost of maintaining the activity of antioxidant defenses. Results obtained in this thesis are in colored boxes, representing metabolomics (green), proteomics (yellow) or transcriptomics (blue) data. Dashed lines are hypothesis based on thesis results

Conclusions

1. Long-lived species have evolved by decreasing the content of NDUFV2 and NDUFS4 Cx I subunits, which might be associated with the limited ROS production described in long-lived species.
2. Increased content of the mPTP component VDAC-1 in short-lived species might be associated to a higher mitochondrial permeability and, at least in part, responsible for its shortened longevity.
3. Higher Met content and transsulfuration metabolites are species-specific traits associated with longevity, which might lead to an increased biosynthesis of sulphur-containing metabolites with antioxidant properties in short-lived species, aimed to overcome the effects of its increased basal ROS production compared to long-lived ones.
4. The decreased content of amino acids found in post-mitotic tissue from long-lived species might respond to an improved proteostasis, whereas the diverse regulation of plasma amino acids might be in response to its organismal functions as signalling molecules.
5. The increased content of TCA cycle intermediates in post-mitotic tissue from short-lived species might be aimed to supply the energetic demand to maintain antioxidant systems and associated with a higher metabolic activity leading to an increased ROS production at Cx I.
6. The higher content of succinate found in post-mitotic tissue from long-lived species might be an indicative of a metabolic adaptation to promote Cx II activity and by-pass Cx I ROS production.
7. The lower content of the lipid precursor choline in longevous species might be associated with the achievement of a proper longevity-associated lipid profile.
8. The unique centenarian-specific Met metabolism plasma profile suggested that increasing the content of Met-related metabolites, instead of Met *per se*, is determinant to achieve a higher longevity within a specie.
9. The lack of an amino acid pattern associated to a centenarian condition suggest that its plasmatic composition is strongly regulated in order to maintain proper organismal functions.
10. Centenarians maintain a higher content of TCA cycle intermediates that might be compatible with an enhanced energetic metabolism to maintain the activity and biosynthesis of antioxidant molecules and signalling pathways, and associated with the achievement of a higher longevity within a specie.
11. mTORC1 species-specific protein content and gene expression profile is associated with longevity, being lowered protein content and gene expression, along with a phosphorylation pattern compatible with a lower activity, hallmarks of increased species longevity.
12. The basal lowered mTORC1 activity in long-lived species is associated with a decreased content of its regulators FKBP12, and the amino acids Arg and Met.
13. Species longevity occurs through a global intracellular reorganization affecting mitochondrial structure and metabolism, leading to a lower ROS production, reduced sulphur-containing metabolites, amino acids and energetic intermediates that might be regulated by evolutionary conserved intracellular metabolic regulators such as mTORC1.
14. The metabolic adaptations leading to a higher longevity within a specie do not always correlate with those leading to a higher species longevity, since maintaining lower

content of Met and energetic intermediates is associated with species longevity although an enhanced transsulfuration and energetic metabolism leads to an increased individual longevity within a species.

References

Ables, G.P., Ouattara, A., Hampton, T.G., Cooke, D., Perodin, F., Augie, I., and Orentreich, D.S. (2015). Dietary Methionine Restriction in Mice Elicits an Adaptive Cardiovascular Response to Hyperhomocysteinemia. Sci. Rep. *5*, 8886.

Aledo, J.C. (2019). Methionine in proteins: The Cinderella of the proteinogenic amino acids. Protein Sci. *28*, 1785–1796.

Aledo, J.C., Li, Y., de Magalhães, J.P., Ruíz-Camacho, M., and Pérez-Claros, J.A. (2011). Mitochondrially encoded methionine is inversely related to longevity in mammals. Aging Cell *10*, 198–207.

Aledo, J.C., Valverde, H., and de Magalhães, J.P. (2012). Mutational Bias Plays an Important Role in Shaping Longevity-Related Amino Acid Content in Mammalian mtDNA-Encoded Proteins. J. Mol. Evol. *74*, 332–341.

Aledo, J.C., Cantón, F.R., and Veredas, F.J. (2015). Sulphur Atoms from Methionines Interacting with Aromatic Residues Are Less Prone to Oxidation. Sci. Rep. *5*, 16955.

Amador-Noguez, D., Yagi, K., Venable, S., and Darlington, G. (2004). Gene expression profile of long-lived Ames dwarf mice and Little mice. Aging Cell *3*, 423–441.

Amigo, I., Menezes-Filho, S.L., Luévano-Martínez, L.A., Chausse, B., and Kowaltowski, A.J. (2017). Caloric restriction increases brain mitochondrial calcium retention capacity and protects against excitotoxicity. Aging Cell *16*, 73–81.

Antikainen, H., Driscoll, M., Haspel, G., and Dobrowolski, R. (2017). TOR-mediated regulation of metabolism in aging. Aging Cell *16*, 1219–1233.

Ariaans, G., Jalving, M., Vries, E.G.E. de, and Jong, S. de (2017). Anti-tumor effects of everolimus and metformin are complementary and glucose-dependent in breast cancer cells. BMC Cancer *17*, 232.

Austad, S.N., and Fischer, K.E. (1991). Mammalian Aging, Metabolism, and Ecology: Evidence From the Bats and Marsupials. J. Gerontol. *46*, B47–B53.

Ayala, V., Naudí, A., Sanz, A., Caro, P., Portero-Otín, M., Barja, G., and Pamplona, R. (2007). Dietary Protein Restriction Decreases Oxidative Protein Damage, Peroxidizability Index, and Mitochondrial Complex I Content in Rat Liver. Journals Gerontol. Ser. A Biol. Sci. Med. Sci. *62*, 352–360.

Aylett, C.H.S., Sauer, E., Imseng, S., Boehringer, D., Hall, M.N., Ban, N., and Maier, T. (2016). Architecture of human mTOR complex 1. Science (80-.). *351*, 48–52.

Bárcena, C., Quirós, P.M., Durand, S., Mayoral, P., Rodríguez, F., Caravia, X.M., Mariño, G., Garabaya, C., Fernández-García, M.T., Kroemer, G., et al. (2018). Methionine Restriction Extends Lifespan in Progeroid Mice and Alters Lipid and Bile Acid Metabolism. Cell Rep. *24*, 2392–2403.

Bárcena, C., López-Otín, C., and Kroemer, G. (2019). Methionine restriction for improving progeria: another autophagy-inducing anti-aging strategy? Autophagy *15*, 558–559.

Barja, G. (1998). Mitochondrial free radical production and aging in mammals and birds. Ann. N. Y. Acad. Sci. *854*, 224–238.

Barja, G. (2004). Aging in vertebrates, and the effect of caloric restriction: a mitochondrial free radical production-DNA damage mechanism? Biol. Rev. *79*, 235–251.

Barja, G. (2007). Mitochondrial Oxygen Consumption and Reactive Oxygen Species Production are Independently Modulated: Implications for Aging Studies. Rejuvenation Res. *10*, 215–224.

Barja, G. (2008). The gene cluster hypothesis of aging and longevity. Biogerontology *9*, 57–66.

Barja, G. (2010). Longevity and Evolution (New York, USA: Nova Science Publishers, Inc.).

Barja, G. (2013). Updating the Mitochondrial Free Radical Theory of Aging: An Integrated View, Key Aspects, and Confounding Concepts. Antioxid. Redox Signal. *19*, 1420–1445.

Barja, G. (2019). Towards a unified mechanistic theory of aging. Exp. Gerontol. *124*, 110627.

Barja, G., and Herrero, A. (1998). Localization at complex I and mechanism of the higher free radical production of brain nonsynaptic mitochondria in the short-lived rat than in the longevous pigeon. J. Bioenerg. Biomembr. *30*, 235–243.

Barja, G., Cadenas, S., Rojas, C., Pérez-Campo, R., and López-Torres, M. (1994). Low mitochondrial free radical production per unit O2 consumption can explain the simultaneous presence of high longevity and high aerobic metabolic rate in birds. Free Radic. Res. *21*, 317–327.

Barker, C.D., Reda, T., and Hirst, J. (2007). The Flavoprotein Subcomplex of Complex I (NADH:Ubiquinone Oxidoreductase) from Bovine Heart Mitochondria: Insights into the Mechanisms of NADH Oxidation and NAD + Reduction from Protein Film Voltammetry †. Biochemistry *46*, 3454–3464.

Bechinger, B. (2001). Membrane insertion and orientation of polyalanine peptides: a (15)N solid-state NMR spectroscopy investigation. Biophys. J. *81*, 2251–2256.

Beckman, K.B., and Ames, B.N. (1998). The Free Radical Theory of Aging Matures. Physiol. Rev. *78*, 547–581.

Bender, A., Hajieva, P., and Moosmann, B. (2008). Adaptive antioxidant methionine accumulation in respiratory chain complexes explains the use of a deviant genetic code in mitochondria. Proc. Natl. Acad. Sci. *105*, 16496–16501.

Bezawork-Geleta, A., Rohlena, J., Dong, L., Pacak, K., and Neuzil, J. (2017). Mitochondrial Complex II: At the Crossroads. Trends Biochem. Sci. *42*, 312–325.

Birkenfeld, A.L., Lee, H.-Y., Guebre-Egziabher, F., Alves, T.C., Jurczak, M.J., Jornayvaz, F.R., Zhang, D., Hsiao, J.J., Martin-Montalvo, A., Fischer-Rosinsky, A., et al. (2011). Deletion of the Mammalian INDY Homolog Mimics Aspects of Dietary Restriction and Protects against Adiposity and Insulin Resistance in Mice. Cell Metab. *14*, 184–195.

Bjelland, S. (2003). Mutagenicity, toxicity and repair of DNA base damage induced by oxidation. Mutat. Res. Mol. Mech. Mutagen. *531*, 37–80.

Blinova, K., Levine, R.L., Boja, E.S., Griffiths, G.L., Shi, Z.-D., Ruddy, B., and Balaban, R.S. (2008). Mitochondrial NADH Fluorescence Is Enhanced by Complex I Binding. Biochemistry *47*, 9636–9645.

Bolisetty, S., and Jaimes, E.A. (2013). Mitochondria and reactive oxygen species: physiology and pathophysiology. Int. J. Mol. Sci. *14*, 6306–6344.

Borrás, C., Serna, E., Gambini, J., Inglés, M., and Vina, J. (2017). Centenarians maintain miRNA biogenesis pathway while it is impaired in octogenarians. Mech. Ageing Dev. *168*, 54–57.

Bowles, J.T. (1998). The evolution of aging: a new approach to an old problem of biology. Med. Hypotheses *51*, 179–221.

Bozek, K., Khrameeva, E.E., Reznick, J., Omerbašić, D., Bennett, N.C., Lewin, G.R., Azpurua, J., Gorbunova, V., Seluanov, A., Regnard, P., et al. (2017). Lipidome determinants of maximal

lifespan in mammals. Sci. Rep. *7*, 1–5.

Brand, M.D. (2014). The role of mitochondria in longevity and healthspan. Longev. Heal. *3*, 7.

Brand, M.D. (2016). Mitochondrial generation of superoxide and hydrogen peroxide as the source of mitochondrial redox signaling. Free Radic. Biol. Med. *100*, 14–31.

Bridges, H.R., Bill, E., and Hirst, J. (2012). Mössbauer Spectroscopy on Respiratory Complex I: The Iron–Sulfur Cluster Ensemble in the NADH-Reduced Enzyme Is Partially Oxidized. Biochemistry *51*, 149–158.

Briston, T., Roberts, M., Lewis, S., Powney, B., Staddon, J.M., Szabadkai, G., and Duchen, M.R. (2017). Mitochondrial permeability transition pore: Sensitivity to opening and mechanistic dependence on substrate availability. Sci. Rep. *7*, 1–13.

Brosnan, J.T., and Brosnan, M.E. (2006). The Sulfur-Containing Amino Acids: An Overview. J. Nutr. *136*, 1636S-1640S.

Brown-Borg, H.M., Borg, K.E., Meliska, C.J., and Bartke, A. (1996). Dwarf mice and the ageing process. Nature *384*, 33–33.

Budde, S.M.S., van den Heuvel, L.P.W.J., Janssen, A.J., Smeets, R.J.P., Buskens, C.A.F., DeMeirleir, L., Van Coster, R., Baethmann, M., Voit, T., Trijbels, J.M.F., et al. (2000). Combined Enzymatic Complex I and III Deficiency Associated with Mutations in the Nuclear Encoded NDUFS4 Gene. Biochem. Biophys. Res. Commun. *275*, 63–68.

Bulterijs, S., Hull, R.S., Björk, V.C.E., and Roy, A.G. (2015). It is time to classify biological aging as a disease. Front. Genet. *6*.

Bunn, H., and Higgins, P. (1981). Reaction of monosaccharides with proteins: possible evolutionary significance. Science (80-.). *213*, 222–224.

Burks, S., Raymick, J., Robinson, B., Hanig, J., and Sarkar, S. (2019). Neuroprotective effects of acetyl-l-carnitine (ALC) in a chronic MPTP-induced Parkinson's disease mouse model: Endothelial and microglial effects. Neurosci. Lett. *703*, 86–95.

Burla, B., Arita, M., Arita, M., Bendt, A.K., Cazenave-Gassiot, A., Dennis, E.A., Ekroos, K., Han, X., Ikeda, K., Liebisch, G., et al. (2018). MS-based lipidomics of human blood plasma: a community-initiated position paper to develop accepted guidelines. J. Lipid Res. *59*, 2001–2017.

Butler, J.A., Ventura, N., Johnson, T.E., and Rea, S.L. (2010). Long-lived mitochondrial (Mit) mutants of Caenorhabditis elegans utilize a novel metabolism. FASEB J. *24*, 4977–4988.

Butler, P.G., Wanamaker, A.D., Scourse, J.D., Richardson, C.A., and Reynolds, D.J. (2013). Variability of marine climate on the North Icelandic Shelf in a 1357-year proxy archive based on growth increments in the bivalve Arctica islandica. Palaeogeogr. Palaeoclimatol. Palaeoecol. *373*, 141–151.

Cabré, R., Jové, M., Naudí, A., Ayala, V., Piñol-Ripoll, G., Gil-Villar, M.P., Dominguez-Gonzalez, M., Obis, È., Berdun, R., Mota-Martorell, N., et al. (2016). Specific Metabolomics Adaptations Define a Differential Regional Vulnerability in the Adult Human Cerebral Cortex. Front. Mol. Neurosci. *9*, 138.

Cabreiro, F., Au, C., Leung, K.-Y., Vergara-Irigaray, N., Cochemé, H.M., Noori, T., Weinkove, D., Schuster, E., Greene, N.D.E., and Gems, D. (2013). Metformin Retards Aging in C. elegans by Altering Microbial Folate and Methionine Metabolism. Cell *153*, 228–239.

Cadenas, E., and Davies, K.J.A. (2000). Mitochondrial free radical generation, oxidative stress,

and aging11This article is dedicated to the memory of our dear friend, colleague, and mentor Lars Ernster (1920–1998), in gratitude for all he gave to us. Free Radic. Biol. Med. *29*, 222–230.

Calabrese, V., Cornelius, C., Dinkova-Kostova, A.T., Iavicoli, I., Di Paola, R., Koverech, A., Cuzzocrea, S., Rizzarelli, E., and Calabrese, E.J. (2012). Cellular stress responses, hormetic phytochemicals and vitagenes in aging and longevity. Biochim. Biophys. Acta - Mol. Basis Dis. *1822*, 753–783.

Caraveo, G., Soste, M., Cappelleti, V., Fanning, S., van Rossum, D.B., Whitesell, L., Huang, Y., Chung, C.Y., Baru, V., Zaichick, S., et al. (2017). FKBP12 contributes to α-synuclein toxicity by regulating the calcineurin-dependent phosphoproteome. Proc. Natl. Acad. Sci. *114*, 311–322.

Cardona, T. (2019). Thinking twice about the evolution of photosynthesis. Open Biol. *9*, 180246.

Caron, A., Richard, D., and Laplante, M. (2015). The roles of mTOR complexes in lipid metabolism. Annu. Rev. Nutr. *35*, 321–348.

Carroll, J., Fearnley, I.M., Shannon, R.J., Hirst, J., and Walker, J.E. (2003). Analysis of the Subunit Composition of Complex I from Bovine Heart Mitochondria. Mol. Cell. Proteomics *2*, 117–126.

Carroll, J., Fearnley, I.M., Skehel, J.M., Shannon, R.J., Hirst, J., and Walker, J.E. (2006). Bovine Complex I Is a Complex of 45 Different Subunits. J. Biol. Chem. *281*, 32724–32727.

Castro, C., Krumsiek, J., Lehrbach, N.J., Murfitt, S.A., Miska, E.A., and Griffin, J.L. (2013). A study of Caenorhabditis elegans DAF-2 mutants by metabolomics and differential correlation networks. Mol. Biosyst. *9*, 1632.

Chao, L.H., and Avruch, J. (2019). Cryo-EM insight into the structure of MTOR complex 1 and its interactions with Rheb and substrates. F1000Research *8*, 14.

Chellappa, K., Brinkman, J.A., Mukherjee, S., Morrison, M., Alotaibi, M.I., Carbajal, K.A., Alhadeff, A.L., Perron, I.J., Yao, R., Purdy, C.S., et al. (2019). Hypothalamic mTORC2 is essential for metabolic health and longevity. Aging Cell *18*.

Chen, A., Raule, N., Chomyn, A., and Attardi, G. (2012). Decreased Reactive Oxygen Species Production in Cells with Mitochondrial Haplogroups Associated with Longevity. PLoS One *7*, e46473.

Cheng, S., Larson, M.G., McCabe, E.L., Murabito, J.M., Rhee, E.P., Ho, J.E., Jacques, P.F., Ghorbani, A., Magnusson, M., Souza, A.L., et al. (2015). Distinct metabolomic signatures are associated with longevity in humans. Nat. Commun. *6*, 6791.

Chiang, G.G., and Abraham, R.T. (2005). Phosphorylation of mammalian target of rapamycin (mTOR) at Ser-2448 is mediated by p70S6 kinase. J. Biol. Chem. *280*, 25485–25490.

Chin, R.M., Fu, X., Pai, M.Y., Vergnes, L., Hwang, H., Deng, G., Diep, S., Lomenick, B., Meli, V.S., Monsalve, G.C., et al. (2014). The metabolite α-ketoglutarate extends lifespan by inhibiting ATP synthase and TOR. Nature *510*, 397–401.

Chong, J., Wishart, D.S., and Xia, J. (2019). Using MetaboAnalyst 4.0 for comprehensive and integrative metabolomics data analysis. Curr. Protoc. Bioinforma. *68*.

Chouchani, E.T., Pell, V.R., Gaude, E., Aksentijević, D., Sundier, S.Y., Robb, E.L., Logan, A., Nadtochiy, S.M., Ord, E.N.J., Smith, A.C., et al. (2014). Ischaemic accumulation of succinate controls reperfusion injury through mitochondrial ROS. Nature *515*, 431–435.

Chowdhury, B., and Garai, G. (2017). A review on multiple sequence alignment from the perspective of genetic algorithm. Genomics *109*, 419–431.

Chrysant, S.G., and Chrysant, G.S. (2018). The current status of homocysteine as a risk factor for cardiovascular disease: a mini review. Expert Rev. Cardiovasc. Ther. *16*, 559–565.

Chung, H.S., Wang, S.-B., Venkatraman, V., Murray, C.I., and Van Eyk, J.E. (2013). Cysteine Oxidative Posttranslational Modifications. Circ. Res. *112*, 382–392.

Clarkson, A.N., Liu, H., Pearson, L., Kapoor, M., Harrison, J.C., Sammut, I.A., Jackson, D.M., and Appleton, I. (2004). Neuroprotective effects of spermine following hypoxia-ischemia-induced brain damage: A mechanistic study. FASEB J. *18*, 1114–1116.

Collino, S., Montoliu, I., Martin, F.P.J., Scherer, M., Mari, D., Salvioli, S., Bucci, L., Ostan, R., Monti, D., Biagi, E., et al. (2013). Metabolic Signatures of Extreme Longevity in Northern Italian Centenarians Reveal a Complex Remodeling of Lipids, Amino Acids, and Gut Microbiota Metabolism. PLoS One *8*, 1–12.

Colman, R.J., Anderson, R.M., Johnson, S.C., Kastman, E.K., Kosmatka, K.J., Beasley, T.M., Allison, D.B., Cruzen, C., Simmons, H.A., Kemnitz, J.W., et al. (2009). Caloric Restriction Delays Disease Onset and Mortality in Rhesus Monkeys. Science (80-.). *325*, 201–204.

Cooper, N., Thomas, G.H., and FitzJohn, R.G. (2016). Shedding light on the 'dark side' of phylogenetic comparative methods. Methods Ecol. Evol. *7*, 693–699.

Cortie, C.H., Hulbert, A.J., Hancock, S.E., Mitchell, T.W., McAndrew, D., and Else, P.L. (2015). Of mice, pigs and humans: An analysis of mitochondrial phospholipids from mammals with very different maximal lifespans. Exp. Gerontol. *70*, 135–143.

Csardi, G., and Nepusz, T. (2006). The igraph software package for complex network research. InterJournal *Complex Sy*, 1695.

Cunningham, J.T., Rodgers, J.T., Arlow, D.H., Vazquez, F., Mootha, V.K., and Puigserver, P. (2007). mTOR controls mitochondrial oxidative function through a YY1–PGC-1α transcriptional complex. Nature *450*, 736–740.

Davies, M.J. (2016). Protein oxidation and peroxidation. Biochem. J. *473*, 805–825.

Davies, S.K., Bundy, J.G., and Leroi, A.M. (2015). Metabolic Youth in Middle Age: Predicting Aging in Caenorhabditis elegans Using Metabolomics. J. Proteome Res. *14*, 4603–4609.

Derous, D., Mitchell, S., Green, C., Wang, Y., Han, J., Chen, L., Promislow, D., Lusseau, D., Speakman, J., and Douglas, A. (2016). The effects of graded levels of calorie restriction: VII. Topological rearrangement of hypothalamic aging networks. Aging (Albany. NY). *8*, 917–931.

Desai, B.N., Myers, B.R., and Schreiber, S.L. (2002). FKBP12-rapamycin-associated protein associates with mitochondria and senses osmotic stress via mitochondrial dysfunction. Proc. Natl. Acad. Sci. *99*, 4319–4324.

Deweerdt, S. (2012). Comparative biology: Looking for a master switch. Nature *492*, S10–S11.

Dibble, C.C., and Cantley, L.C. (2015). Regulation of mTORC1 by PI3K signaling. Trends Cell Biol. *25*, 545–555.

Dieffenbach, C.W., Lowe, T.M., and Dveksler, G.S. (1993). General concepts for PCR primer design. PCR Methods Appl. *3*, S30-7.

Dorn, G.W. (2013). Mitochondrial dynamics in heart disease. Biochim. Biophys. Acta - Mol. Cell Res. *1833*, 233–241.

Düvel, K., Yecies, J.L., Menon, S., Raman, P., Lipovsky, A.I., Souza, A.L., Triantafellow, E., Ma, Q., Gorski, R., Cleaver, S., et al. (2010). Activation of a metabolic gene regulatory network

downstream of mTOR complex 1. Mol. Cell *39*, 171–183.

Edwards, C., Canfield, J., Copes, N., Brito, A., Rehan, M., Lipps, D., Brunquell, J., Westerheide, S.D., and Bradshaw, P.C. (2015). Mechanisms of amino acid-mediated lifespan extension in Caenorhabditis elegans. BMC Genet. *16*, 8.

EFSA (2012). Scientific Opinion on Dietary Reference Values for protein. EFSA J. *10*, 2557.

Eisenberg, T., Abdellatif, M., Schroeder, S., Primessnig, U., Stekovic, S., Pendl, T., Harger, A., Schipke, J., Zimmermann, A., Schmidt, A., et al. (2016). Cardioprotection and lifespan extension by the natural polyamine spermidine. Nat. Med. *22*, 1428–1438.

Elshorbagy, A.K., Valdivia-Garcia, M., Refsum, H., Smith, A.D., Mattocks, D.A.L., and Perrone, C.E. (2010). Sulfur amino acids in methionine-restricted rats: Hyperhomocysteinemia. Nutrition *26*, 1201–1204.

Elshorbagy, A.K., Valdivia-Garcia, M., Mattocks, D.A.L., Plummer, J.D., Orentreich, D.S., Orentreich, N., Refsum, H., and Perrone, C.E. (2013). Effect of taurine and N-acetylcysteine on methionine restriction-mediated adiposity resistance. Metabolism *62*, 509–517.

Elurbe, D.M., and Huynen, M.A. (2016). The origin of the supernumerary subunits and assembly factors of complex I: A treasure trove of pathway evolution. Biochim. Biophys. Acta - Bioenerg. *1857*, 971–979.

Embley, T.M., and Martin, W. (2006). Eukaryotic evolution, changes and challenges. Nature *440*, 623–630.

Evans, C., Bogan, K.L., Song, P., Burant, C.F., Kennedy, R.T., and Brenner, C. (2010). NAD+ metabolite levels as a function of vitamins and calorie restriction: evidence for different mechanisms of longevity. BMC Chem. Biol. *10*, 2.

Falkowski, P.G., and Godfrey, L. V (2008a). Electrons, life and the evolution of Earth's oxygen cycle. Philos. Trans. R. Soc. B Biol. Sci. *363*, 2705–2716.

Falkowski, P.G., and Godfrey, L. V (2008b). Electrons, life and the evolution of Earth's oxygen cycle. Philos. Trans. R. Soc. B Biol. Sci. *363*, 2705–2716.

Fan, K., and Wang, W. (2003). What is the Minimum Number of Letters Required to Fold a Protein? J. Mol. Biol. *328*, 921–926.

Faulkes, C.G., Eykyn, T.R., and Aksentijevic, D. (2019). Cardiac metabolomic profile of the naked mole-rat—glycogen to the rescue. Biol. Lett. *15*.

Fei, Y.-J., Liu, J.-C., Inoue, K., Zhuang, L., Miyake, K., Miyauchi, S., and Ganapathy, V. (2004). Relevance of NAC-2, an Na+-coupled citrate transporter, to life span, body size and fat content in Caenorhabditis elegans. Biochem. J. *379*, 191–198.

Fiedorczuk, K., and Sazanov, L.A. (2018). Mammalian Mitochondrial Complex I Structure and Disease-Causing Mutations. Trends Cell Biol. *28*, 835–867.

Fiedorczuk, K., Letts, J.A., Degliesposti, G., Kaszuba, K., Skehel, M., and Sazanov, L.A. (2016). Atomic structure of the entire mammalian mitochondrial complex I. Nature *538*, 406–410.

Figueiredo, V.C., Markworth, J.F., and Cameron-Smith, D. (2017). Considerations on mTOR regulation at serine 2448: implications for muscle metabolism studies. Cell. Mol. Life Sci. *74*, 2537–2545.

Flanagan, E.W., Most, J., Mey, J.T., and Redman, L.M. (2020). Calorie Restriction and Aging in Humans. Annu. Rev. Nutr. *40*, 105–133.

Fontana, L., Partridge, L., and Longo, V.D. (2010). Extending healthy life span--From yeast to humans. Science (80-.). *328*, 321–326.

Fredslund, J., Schauser, L., Madsen, L.H., Sandal, N., and Stougaard, J. (2005). PriFi: using a multiple alignment of related sequences to find primers for amplification of homologs. Nucleic Acids Res. *33*, 516–520.

Fu, C., Hickey, M., Morrison, M., McCarter, R., and Han, E.-S. (2006). Tissue specific and non-specific changes in gene expression by aging and by early stage CR. Mech. Ageing Dev. *127*, 905–916.

Fu, M., Zhang, W., Wu, L., Yang, G., Li, H., and Wang, R. (2012). Hydrogen sulfide (H2S) metabolism in mitochondria and its regulatory role in energy production. Proc. Natl. Acad. Sci. *109*, 2943–2948.

Fuchs, S., Bundy, J.G., Davies, S.K., Viney, J.M., Swire, J.S., and Leroi, A.M. (2010). A metabolic signature of long life in Caenorhabditis elegans. BMC Biol. *8*, 14.

Fushan, A.A., Turanov, A.A., Lee, S.-G., Kim, E.B., Lobanov, A. V., Yim, S.H., Buffenstein, R., Lee, S.-R., Chang, K.-T., Rhee, H., et al. (2015). Gene expression defines natural changes in mammalian lifespan. Aging Cell *14*, 352–365.

Gambini, J., Gimeno-Mallench, L., Inglés, M., Olaso, G., Abdelaziz, K.M., Avellana, J.A., Belenguer, Á., Cruz, R., Mas-Bargues, C., Borras, C., et al. (2016). Identificación de polimorfismos de nucleótido simple en centenarios. Rev. Esp. Geriatr. Gerontol. *51*, 146–149.

García-Cañaveras, J.C., Donato, M.T., Castell, J. V., and Lahoz, A. (2012). Targeted profiling of circulating and hepatic bile acids in human, mouse, and rat using a UPLC-MRM-MS-validated method. J. Lipid Res. *53*, 2231–2241.

Genova, M.L., Ventura, B., Giuliano, G., Bovina, C., Formiggini, G., Parenti Castelli, G., and Lenaz, G. (2001). The site of production of superoxide radical in mitochondrial Complex I is not a bound ubisemiquinone but presumably iron-sulfur cluster N2. FEBS Lett. *505*, 364–368.

Gnandt, E., Dörner, K., Strampraad, M.F.J., de Vries, S., and Friedrich, T. (2016). The multitude of iron–sulfur clusters in respiratory complex I. Biochim. Biophys. Acta - Bioenerg. *1857*, 1068–1072.

Gomez, A., Gomez, J., Torres, M.L., Naudí, A., Mota-Martorell, N., Pamplona, R., and Barja, G. (2015). Cysteine dietary supplementation reverses the decrease in mitochondrial ROS production at complex I induced by methionine restriction. J. Bioenerg. Biomembr. *47*, 199–208.

Gómez, J., Caro, P., Naudí, A., Portero-Otín, M., Pamplona, R., and Barja, G. (2007). Effect of 8.5% and 25% caloric restriction on mitochondrial free radical production and oxidative stress in rat liver. Biogerontology *8*, 555–566.

Gonzalez-Covarrubias, V., Beekman, M., Uh, H.-W., Dane, A., Troost, J., Paliukhovich, I., van der Kloet, F.M., Houwing-Duistermaat, J., Vreeken, R.J., Hankemeier, T., et al. (2013). Lipidomics of familial longevity. Aging Cell *12*, 426–434.

Goo, C.K., Lim, H.Y., Ho, Q.S., Too, H.-P., Clement, M.-V., and Wong, K.P. (2012). PTEN/Akt Signaling Controls Mitochondrial Respiratory Capacity through 4E-BP1. PLoS One *7*, e45806.

Gordon, A.H., Martin, A.J.P., and Synge, R.L.M. (1943). Partition chromatography in the study of protein constituents. Biochem. J. *37*, 79–86.

Gould, R.L., and Pazdro, R. (2019). Impact of Supplementary Amino Acids, Micronutrients, and Overall Diet on Glutathione Homeostasis. Nutrients *11*, 1056.

Granold, M., Hajieva, P., Toşa, M.I., Irimie, F.-D., and Moosmann, B. (2018). Modern diversification of the amino acid repertoire driven by oxygen. Proc. Natl. Acad. Sci. *115*, 41–46.

Gredilla, R., Sanz, A., Lopez-Torres, M., and Barja, G. (2001). Caloric restriction decreases mitochondrial free radical generation at complex I and lowers oxidative damage to mitochondrial DNA in the rat heart. FASEB J. *15*, 1589–1591.

van der Greef, J., van Wietmarschen, H., van Ommen, B., and Verheij, E. (2013). Looking back into the future: 30 years of metabolomics at TNO. Mass Spectrom. Rev. *32*, 399–415.

Grivennikova, V.G., and Vinogradov, A.D. (2006). Generation of superoxide by the mitochondrial Complex I. Biochim. Biophys. Acta - Bioenerg. *1757*, 553–561.

Gu, X., Orozco, J.M., Saxton, R.A., Condon, K.J., Liu, G.Y., Krawczyk, P.A., Scaria, S.M., Harper, J.W., Gygi, S.P., and Sabatini, D.M. (2017a). SAMTOR is an S-adenosylmethionine sensor for the mTORC1 pathway. Science (80-.). *358*, 813–818.

Gu, X., Orozco, J.M., Saxton, R.A., Condon, K.J., Liu, G.Y., Krawczyk, P.A., Scaria, S.M., Harper, J.W., Gygi, S.P., and Sabatini, D.M. (2017b). SAMTOR is an S -adenosylmethionine sensor for the mTORC1 pathway. Science (80-.). *358*, 813–818.

Guarente, L., and Kenyon, C. (2000). Genetic pathways that regulate ageing in model organisms. Nature *408*, 255–262.

Gubina, N., Naudi, A., Stefanatos, R., Jove, M., Scialo, F., Fernandez-Ayala, D.J., Rantapero, T., Yurkevych, I., Portero-Otin, M., Nykter, M., et al. (2019). Essential Physiological Differences Characterize Short- and Long-Lived Strains of Drosophila melanogaster. Journals Gerontol. Ser. A *74*, 1835–1843.

Guénebaut, V., Schlitt, A., Weiss, H., Leonard, K., and Friedrich, T. (1998). Consistent structure between bacterial and mitochondrial NADH:ubiquinone oxidoreductase (complex I). J. Mol. Biol. *276*, 105–112.

Hahn, O., Grönke, S., Stubbs, T.M., Ficz, G., Hendrich, O., Krueger, F., Andrews, S., Zhang, Q., Wakelam, M.J., Beyer, A., et al. (2017). Dietary restriction protects from age-associated DNA methylation and induces epigenetic reprogramming of lipid metabolism. Genome Biol. *18*, 56.

Halestrap, A.P. (2009). What is the mitochondrial permeability transition pore? J. Mol. Cell. Cardiol. *46*, 821–831.

Halliwell, B. (1999). Antioxidant defence mechanisms: From the beginning to the end (of the beginning). Free Radic. Res. *31*, 261–272.

Halliwell, B., and Gutteridge, J.M.C. (2007). Free radicals in biology and medicine (UK: Oxford University Press).

Harman, D. (1972). The Biologic Clock: The Mitochondria? J. Am. Geriatr. Soc. *20*, 145–147.

Harrel Jr, F.E., and Dupont, C. (2020). Harrell Miscellaneous.

Harrison, D.E., Strong, R., Sharp, Z.D., Nelson, J.F., Astle, C.M., Flurkey, K., Nadon, N.L., Wilkinson, J.E., Frenkel, K., Carter, C.S., et al. (2009). Rapamycin fed late in life extends lifespan in genetically heterogeneous mice. Nature *460*, 392–395.

Heinze, I., Bens, M., Calzia, E., Holtze, S., Dakhovnik, O., Sahm, A., Kirkpatrick, J.M., Szafranski, K., Romanov, N., Sama, S.N., et al. (2018). Species comparison of liver proteomes reveals links to naked mole-rat longevity and human aging. BMC Biol. *16*, 82.

Herrero, A., and Barja, G. (1997). Sites and mechanisms responsible for the low rate of free

radical production of heart mitochondria in the long-lived pigeon. Mech. Ageing Dev. *98*, 95–111.

Herrero, A., and Barja, G. (1998). H2O2 production of heart mitochondria and aging rate are slower in canaries and parakeets than in mice: sites of free radical generation and mechanisms involved. Mech. Ageing Dev. *103*, 133–146.

Herrero, A., and Barja, G. (2000). Localization of the site of oxygen radical generation inside the complex I of heart and nonsynaptic brain mammalian mitochondria. J. Bioenerg. Biomembr. *32*, 609–615.

Herrmann, J.M., and Riemer, J. (2010). The Intermembrane Space of Mitochondria. Antioxid. Redox Signal. *13*, 1341–1358.

Hindson, B.J., Ness, K.D., Masquelier, D.A., Belgrader, P., Heredia, N.J., Makarewicz, A.J., Bright, I.J., Lucero, M.Y., Hiddessen, A.L., Legler, T.C., et al. (2011). High-throughput droplet digital PCR system for absolute quantitation of DNA copy number. Anal. Chem. *83*, 8604–8610.

Hindson, C.M., Chevillet, J.R., Briggs, H.A., Gallichotte, E.N., Ruf, I.K., Hindson, B.J., Vessella, R.L., and Tewari, M. (2013). Absolute quantification by droplet digital PCR versus analog real-time PCR. Nat. Methods *10*, 1003–1005.

Hine, C., Harputlugil, E., Zhang, Y., Ruckenstuhl, C., Lee, B.C., Brace, L., Longchamp, A., Treviño-Villarreal, J.H., Mejia, P., Ozaki, C.K., et al. (2015). Endogenous Hydrogen Sulfide Production Is Essential for Dietary Restriction Benefits. Cell *160*, 132–144.

Hoeffer, C.A., Tang, W., Wong, H., Santillan, A., Patterson, R.J., Martinez, L.A., Tejada-Simon, M. V., Paylor, R., Hamilton, S.L., and Klann, E. (2008). Removal of FKBP12 enhances mTOR-Raptor interactions, LTP, memory, and perseverative/repetitive behavior. Neuron *60*, 832–845.

Hoffman, J.M., Lyu, Y., Pletcher, S.D., and Promislow, D.E.L. (2017). Proteomics and metabolomics in ageing research: from biomarkers to systems biology. Essays Biochem. *61*, 379–388.

Hoffman, J.M., Poonawalla, A., Icyuz, M., Swindell, W.R., Wilson, L., Barnes, S., and Sun, L.Y. (2020). Transcriptomic and metabolomic profiling of long-lived growth hormone releasing hormone knock-out mice: Evidence for altered mitochondrial function and amino acid metabolism. Aging (Albany. NY). *12*, 3473–3485.

Holman, R.T. (1954). Autoxidation of fats and related substances. Prog. Chem. Fats Other Lipids *2*, 51–98.

Hou, Y.-C.C., Yu, H.-C., Martin, R., Cirulli, E.T., Schenker-Ahmed, N.M., Hicks, M., Cohen, I. V., Jönsson, T.J., Heister, R., Napier, L., et al. (2020). Precision medicine integrating whole-genome sequencing, comprehensive metabolomics, and advanced imaging. Proc. Natl. Acad. Sci. *117*, 3053–3062.

Houtkooper, R.H., Williams, R.W., and Auwerx, J. (2010). Metabolic Networks of Longevity. Cell *142*, 9–14.

Hulbert, A.J., Pamplona, R., Buffenstein, R., and Buttemer, W.A. (2007). Life and Death: Metabolic Rate, Membrane Composition, and Life Span of Animals. Physiol. Rev. *87*, 1175–1213.

Hunter, D.R., and Haworth, R.A. (1979). The Ca2+-induced membrane transition in mitochondria. Arch. Biochem. Biophys. *195*, 453–459.

Inglés, M., Mas-Bargues, C., Berna-Erro, A., Matheu, A., Sanchís, P., Avellana, J.-A., Borrás, C., and Viña, J. (2019). Centenarians Overexpress Pluripotency-Related Genes. Journals Gerontol.

Ser. A *74*, 1391–1395.

Ito, T., Yoshikawa, N., Inui, T., Miyazaki, N., Schaffer, S.W., and Azuma, J. (2014). Tissue Depletion of Taurine Accelerates Skeletal Muscle Senescence and Leads to Early Death in Mice. PLoS One *9*, e107409.

Jarvis, R.M., and Goodacre, R. (2005). Genetic algorithm optimization for pre-processing and variable selection of spectroscopic data. Bioinformatics *21*, 860–868.

Jeon, J.S., Oh, J.-J., Kwak, H.C., Yun, H., Kim, H.C., Kim, Y.-M., Oh, S.J., and Kim, S.K. (2018). Age-related changes in sulfur amino acid metabolism in male C57BL/6 mice. Biomol. Ther. (Seoul). *26*, 167–174.

Jhee, K.-H., and Kruger, W.D. (2005). The Role of Cystathionine β-Synthase in Homocysteine Metabolism. Antioxid. Redox Signal. *7*, 813–822.

Johnson, S.C., Rabinovitch, P.S., and Kaeberlein, M. (2013). mTOR is a key modulator of ageing and age-related disease. Nature *493*, 338–345.

Jones, O.R., Scheuerlein, A., Salguero-Gómez, R., Camarda, C.G., Schaible, R., Casper, B.B., Dahlgren, J.P., Ehrlén, J., García, M.B., Menges, E.S., et al. (2014). Diversity of ageing across the tree of life. Nature *505*, 169–173.

Jones, T.E., Ribas de Pouplana, L., and Alexander, R.W. (2013). Evidence for Late Resolution of the AUX Codon Box in Evolution. J. Biol. Chem. *288*, 19625–19632.

Jové, M., Naudí, A., Aledo, J.C., Cabré, R., Ayala, V., Portero-Otín, M., Barja, G., and Pamplona, R. (2013). Plasma long-chain free fatty acids predict mammalian longevity. Sci. Rep. *3*, 3346.

Jové, M., Naudí, A., Ramírez-Núñez, O., Portero-Otín, M., Selman, C., Withers, D.J., and Pamplona, R. (2014). Caloric restriction reveals a metabolomic and lipidomic signature in liver of male mice. Aging Cell *13*, 828–837.

Jové, M., Maté, I., Naudí, A., Mota-Martorell, N., Portero-Otín, M., De La Fuente, M., and Pamplona, R. (2016). Human Aging Is a Metabolome-related Matter of Gender. Journals Gerontol. - Ser. A Biol. Sci. Med. Sci. *71*.

Jové, M., Naudí, A., Gambini, J., Borras, C., Cabré, R., Portero-Otín, M., Viña, J., and Pamplona, R. (2017). A Stress-Resistant Lipidomic Signature Confers Extreme Longevity to Humans. Journals Gerontol. Ser. A Biol. Sci. Med. Sci. *72*, 30–37.

Kabil, H., Kabil, O., Banerjee, R., Harshman, L.G., and Pletcher, S.D. (2011). Increased transsulfuration mediates longevity and dietary restriction in Drosophila. Proc. Natl. Acad. Sci. *108*, 16831–16836.

Kamei, Y., Tamura, T., Yoshida, R., Ohta, S., Fukusaki, E., and Mukai, Y. (2011). GABA metabolism pathway genes, UGA1 and GAD1, regulate replicative lifespan in Saccharomyces cerevisiae. Biochem. Biophys. Res. Commun. *407*, 185–190.

Kaneko, H., Kobayashi, M., Mizunoe, Y., Yoshida, M., Yasukawa, H., Hoshino, S., Itagawa, R., Furuichi, T., Okita, N., Sudo, Y., et al. (2018). Taurine is an amino acid with the ability to activate autophagy in adipocytes. Amino Acids *50*, 527–535.

Kapahi, P., Zid, B.M., Harper, T., Koslover, D., Sapin, V., and Benzer, S. (2004). Regulation of Lifespan in Drosophila by Modulation of Genes in the TOR Signaling Pathway. Curr. Biol. *14*, 885–890.

Kapahi, P., Chen, D., Rogers, A.N., Katewa, S.D., Li, P.W.-L., Thomas, E.L., and Kockel, L. (2010).

With TOR, less is more: A key role for the conserved nutrient-sensing TOR pathway in aging. Cell Metab. *11*, 453–465.

Karunadharma, P.P., Basisty, N., Chiao, Y.A., Dai, D.-F., Drake, R., Levy, N., Koh, W.J., Emond, M.J., Kruse, S., Marcinek, D., et al. (2015). Respiratory chain protein turnover rates in mice are highly heterogeneous but strikingly conserved across tissues, ages, and treatments. FASEB J. *29*, 3582–3592.

Katsyuba, E., Mottis, A., Zietak, M., De Franco, F., van der Velpen, V., Gariani, K., Ryu, D., Cialabrini, L., Matilainen, O., Liscio, P., et al. (2018). De novo NAD+ synthesis enhances mitochondrial function and improves health. Nature *563*, 354–359.

Kenyon, C.J. (2010). The genetics of ageing. Nature *464*, 504–512.

Kerins, M.J., Vashisht, A.A., Liang, B.X.-T., Duckworth, S.J., Praslicka, B.J., Wohlschlegel, J.A., and Ooi, A. (2017). Fumarate Mediates a Chronic Proliferative Signal in Fumarate Hydratase-Inactivated Cancer Cells by Increasing Transcription and Translation of Ferritin Genes. Mol. Cell. Biol. *37*.

Kettunen, J., Tukiainen, T., Sarin, A.-P., Ortega-Alonso, A., Tikkanen, E., Lyytikäinen, L.-P., Kangas, A.J., Soininen, P., Würtz, P., Silander, K., et al. (2012). Genome-wide association study identifies multiple loci influencing human serum metabolite levels. Nat. Genet. *44*, 269–276.

Khayati, K., Antikainen, H., Bonder, E.M., Weber, G.F., Kruger, W.D., Jakubowski, H., and Dobrowolski, R. (2017). The amino acid metabolite homocysteine activates mTORC1 to inhibit autophagy and form abnormal proteins in human neurons and mice. FASEB J. *31*, 598–609.

Kim, E.B., Fang, X., Fushan, A.A., Huang, Z., Lobanov, A. V., Han, L., Marino, S.M., Sun, X., Turanov, A.A., Yang, P., et al. (2011). Genome sequencing reveals insights into physiology and longevity of the naked mole rat. Nature *479*, 223–227.

Kim, G., Weiss, S.J., and Levine, R.L. (2014). Methionine oxidation and reduction in proteins. Biochim. Biophys. Acta - Gen. Subj. *1840*, 901–905.

Kim, S.J., Kim, S.H., Kim, J.H., Hwang, S., and Yoo, H.J. (2016). Understanding Metabolomics in Biomedical Research. Endocrinol. Metab. *31*, 7.

Knauf, F., Rogina, B., Jiang, Z., Aronson, P.S., and Helfand, S.L. (2002). Functional characterization and immunolocalization of the transporter encoded by the life-extending gene Indy. Proc. Natl. Acad. Sci. *99*, 14315–14319.

Koivisto, H., Leinonen, H., Puurula, M., Hafez, H.S., Barrera, G.A., Stridh, M.H., Waagepetersen, H.S., Tiainen, M., Soininen, P., Zilberter, Y., et al. (2016). Chronic Pyruvate Supplementation Increases Exploratory Activity and Brain Energy Reserves in Young and Middle-Aged Mice. Front. Aging Neurosci. *8*.

Koopman, W.J.H., Nijtmans, L.G.J., Dieteren, C.E.J., Roestenberg, P., Valsecchi, F., Smeitink, J.A.M., and Willems, P.H.G.M. (2010). Mammalian Mitochondrial Complex I: Biogenesis, Regulation, and Reactive Oxygen Species Generation. Antioxid. Redox Signal. *12*, 1431–1470.

Ku, H.-H., and Sohal, R.S. (1993). Comparison of mitochondrial pro-oxidant generation and anti-oxidant defenses between rat and pigeon: possible basis of variation in longevity and metabolic potential. Mech. Ageing Dev. *72*, 67–76.

Ku, H.H., Brunk, U.T., and Sohal, R.S. (1993). Relationship between mitochondrial superoxide and hydrogen peroxide production and longevity of mammalian species. Free Radic. Biol. Med. *15*, 621–627.

Kühlbrandt, W. (2015). Structure and function of mitochondrial membrane protein complexes. BMC Biol. *13*, 89.

Kuhn, M. Classification and Regression Training [R package caret version 6.0-86].

Kumar, S., Stecher, G., Suleski, M., and Hedges, S.B. (2017). TimeTree: A Resource for Timelines, Timetrees, and Divergence Times. Mol. Biol. Evol. *34*, 1812–1819.

Kunath, S., and Moosmann, B. (2020). What is the rate-limiting step towards aging? Chemical reaction kinetics might reconcile contradictory observations in experimental aging research. GeroScience *42*, 857–866.

Kushnareva, Y., Murphy, A.N., and Andreyev, A. (2002). Complex I-mediated reactive oxygen species generation: modulation by cytochrome c and NAD(P)+ oxidation–reduction state. Biochem. J. *368*, 545–553.

de la Cruz López, K.G., Toledo Guzmán, M.E., Sánchez, E.O., and García Carrancá, A. (2019). mTORC1 as a Regulator of Mitochondrial Functions and a Therapeutic Target in Cancer. Front. Oncol. *9*.

van der Laan, M., Horvath, S.E., and Pfanner, N. (2016). Mitochondrial contact site and cristae organizing system. Curr. Opin. Cell Biol. *41*, 33–42.

Lambert, A.J., Buckingham, J.A., Boysen, H.M., and Brand, M.D. (2010). Low complex I content explains the low hydrogen peroxide production rate of heart mitochondria from the long-lived pigeon, Columba livia. Aging Cell *9*, 78–91.

Lane, N., and Martin, W. (2010). The energetics of genome complexity. Nature *467*, 929–934.

Laplante, M., and Sabatini, D.M. (2009). mTOR signaling at a glance. J. Cell Sci. *122*, 3589–3594.

Laschober, G.T., Ruli, D., Hofer, E., Muck, C., Carmona-Gutierrez, D., Ring, J., Hutter, E., Ruckenstuhl, C., Micutkova, L., Brunauer, R., et al. (2010). Identification of evolutionarily conserved genetic regulators of cellular aging. Aging Cell *9*, 1084–1097.

Laye, M.J., Tran, V., Jones, D.P., Kapahi, P., and Promislow, D.E.L. (2015). The effects of age and dietary restriction on the tissue-specific metabolome of Drosophila. Aging Cell *14*, 797–808.

Leanza, L., Checchetto, V., Biasutto, L., Rossa, A., Costa, R., Bachmann, M., Zoratti, M., and Szabo, I. (2019). Pharmacological modulation of mitochondrial ion channels. Br. J. Pharmacol. *176*, 4258–4283.

Lee, S., Olsen, T., Vinknes, K., Refsum, H., Gulseth, H., Birkeland, K., and Drevon, C. (2018). Plasma Sulphur-Containing Amino Acids, Physical Exercise and Insulin Sensitivity in Overweight Dysglycemic and Normal Weight Normoglycemic Men. Nutrients *11*, 10.

Lehallier, B., Gate, D., Schaum, N., Nanasi, T., Lee, S.E., Yousef, H., Moran Losada, P., Berdnik, D., Keller, A., Verghese, J., et al. (2019). Undulating changes in human plasma proteome profiles across the lifespan. Nat. Med. *25*, 1843–1850.

Levine, R.L., Mosoni, L., Berlett, B.S., and Stadtman, E.R. (1996). Methionine residues as endogenous antioxidants in proteins. Proc. Natl. Acad. Sci. *93*, 15036–15040.

Lewis, K.N., Rubinstein, N.D., and Buffenstein, R. (2018). A window into extreme longevity; the circulating metabolomic signature of the naked mole-rat, a mammal that shows negligible senescence. GeroScience *40*, 105–121.

Li, X., and Yan, X. (2019). Sensors for the mTORC1 pathway regulated by amino acids. J. Zhejiang Univ. B *20*, 699–712.

Li, Z., and Vance, D.E. (2008). Thematic Review Series: Glycerolipids. Phosphatidylcholine and choline homeostasis. J. Lipid Res. *49*, 1187–1194.

Li, X., Fang, P., Mai, J., Choi, E.T., Wang, H., and Yang, X. (2013). Targeting mitochondrial reactive oxygen species as novel therapy for inflammatory diseases and cancers. J. Hematol. Oncol. *6*, 19.

Libertini, G. (1988). An adaptive theory of the increasing mortality with increasing chronological age in populations in the wild. J. Theor. Biol. *132*, 145–162.

Lim, J.M., Kim, G., and Levine, R.L. (2019). Methionine in Proteins: It's Not Just for Protein Initiation Anymore. Neurochem. Res. *44*, 247–257.

Lindborg, C.M., Propert, K.J., and Pignolo, R.J. (2015). Conservation of pro-longevity genes among mammals. Mech. Ageing Dev. *146–148*, 23–27.

Liu, C.C., and Schultz, P.G. (2010). Adding New Chemistries to the Genetic Code. Annu. Rev. Biochem. *79*, 413–444.

Liu, Y., Song, D., Xu, B., Li, H., Dai, X., and Chen, B. (2017). Development of a matrix-based candidate reference material of total homocysteine in human serum. Anal. Bioanal. Chem. *409*, 3329–3335.

Loenarz, C., and Schofield, C.J. (2008). Expanding chemical biology of 2-oxoglutarate oxygenases. Nat. Chem. Biol. *4*, 152–156.

Lombard, J., López-García, P., and Moreira, D. (2012). The early evolution of lipid membranes and the three domains of life. Nat. Rev. Microbiol. *10*, 507–515.

Longo, L.M., and Blaber, M. (2012). Protein design at the interface of the pre-biotic and biotic worlds. Arch. Biochem. Biophys. *526*, 16–21.

Longo, V.D., Gralla, E.B., and Valentine, J.S. (1996). Superoxide Dismutase Activity Is Essential for Stationary Phase Survival in Saccharomyces cerevisiae. J. Biol. Chem. *271*, 12275–12280.

Longo, V.D., Mitteldorf, J., and Skulachev, V.P. (2005). Programmed and altruistic ageing. Nat. Rev. Genet. *6*, 866–872.

Longo, V.D., Antebi, A., Bartke, A., Barzilai, N., Brown-Borg, H.M., Caruso, C., Curiel, T.J., de Cabo, R., Franceschi, C., Gems, D., et al. (2015). Interventions to slow aging in humans: Are we ready? Aging Cell *14*, 497–510.

Lopez-Fabuel, I., Le Douce, J., Logan, A., James, A.M., Bonvento, G., Murphy, M.P., Almeida, A., and Bolaños, J.P. (2016). Complex I assembly into supercomplexes determines differential mitochondrial ROS production in neurons and astrocytes. Proc. Natl. Acad. Sci. *113*, 13063–13068.

López-Otín, C., Blasco, M.A., Partridge, L., Serrano, M., and Kroemer, G. (2013). The hallmarks of aging. Cell *153*, 1194–1217.

López-Torres, M., Gredilla, R., Sanz, A., and Barja, G. (2002). Influence of aging and long-term caloric restriction on oxygen radical generation and oxidative DNA damage in rat liver mitochondria. Free Radic. Biol. Med. *32*, 882–889.

Lu, C.-L., Qin, L., Liu, H.-C., Candas, D., Fan, M., and Li, J.J. (2015). Tumor Cells Switch to Mitochondrial Oxidative Phosphorylation under Radiation via mTOR-Mediated Hexokinase II Inhibition - A Warburg-Reversing Effect. PLoS One *10*, e0121046.

Luo, S., and Levine, R.L. (2009). Methionine in proteins defends against oxidative stress. FASEB

J. *23*, 464–472.

Lushchak, O., Strilbytska, O., Piskovatska, V., Storey, K.B., Koliada, A., and Vaiserman, A. (2017). The role of the TOR pathway in mediating the link between nutrition and longevity. Mech. Ageing Dev. *164*, 127–138.

Lyons, T.W., Reinhard, C.T., and Planavsky, N.J. (2014). The rise of oxygen in Earth's early ocean and atmosphere. Nature *506*, 307–315.

Lyu, Z., Gao, X., Wang, W., Dang, J., Yang, L., Yan, M., Ali, S.A., Liu, Y., Liu, B., Yu, M., et al. (2019). mTORC1-Sch9 regulates hydrogen sulfide production through the transsulfuration pathway. Aging (Albany. NY). *11*, 8418–8432.

Ma, S., and Gladyshev, V.N. (2017). Molecular signatures of longevity: Insights from cross-species comparative studies. Semin. Cell Dev. Biol. *70*, 190–203.

Ma, S., Yim, S.H., Lee, S.-G., Kim, E.B., Lee, S.-R., Chang, K.-T., Buffenstein, R., Lewis, K.N., Park, T.J., Miller, R.A., et al. (2015). Organization of the mammalian metabolome according to organ function, lineage specialization and longevity. Cell Metab. *22*, 332–343.

Ma, S., Upneja, A., Galecki, A., Tsai, Y.-M., Burant, C.F., Raskind, S., Zhang, Q., Zhang, Z.D., Seluanov, A., Gorbunova, V., et al. (2016). Cell culture-based profiling across mammals reveals DNA repair and metabolism as determinants of species longevity. Elife *5*, 1–25.

Madamanchi, N.R., and Runge, M.S. (2007). Mitochondrial Dysfunction in Atherosclerosis. Circ. Res. *100*, 460–473.

Maddocks, O.D.K., Labuschagne, C.F., Adams, P.D., and Vousden, K.H. (2016). Serine Metabolism Supports the Methionine Cycle and DNA/RNA Methylation through De Novo ATP Synthesis in Cancer Cells. Mol. Cell *61*, 210–221.

Maier, T., Güell, M., and Serrano, L. (2009). Correlation of mRNA and protein in complex biological samples. FEBS Lett. *583*, 3966–3973.

Mailloux, R.J., and Harper, M.-E. (2012a). Mitochondrial proticity and ROS signaling: lessons from the uncoupling proteins. Trends Endocrinol. Metab. *23*, 451–458.

Mailloux, R.J., and Harper, M.-E. (2012b). Mitochondrial proticity and ROS signaling: lessons from the uncoupling proteins. Trends Endocrinol. Metab. *23*, 451–458.

Majtan, T., Pey, A.L., Fernández, R., Fernández, J.A., Martínez-Cruz, L.A., and Kraus, J.P. (2014). Domain Organization, Catalysis and Regulation of Eukaryotic Cystathionine Beta-Synthases. PLoS One *9*, e105290.

Maranzana, E., Barbero, G., Falasca, A.I., Lenaz, G., and Genova, M.L. (2013). Mitochondrial Respiratory Supercomplex Association Limits Production of Reactive Oxygen Species from Complex I. Antioxid. Redox Signal. *19*, 1469–1480.

Marino, S.M., and Gladyshev, V.N. (2010). Cysteine Function Governs Its Conservation and Degeneration and Restricts Its Utilization on Protein Surfaces. J. Mol. Biol. *404*, 902–916.

Marino, S.M., and Gladyshev, V.N. (2012). Analysis and functional prediction of reactive cysteine residues. J. Biol. Chem. *287*, 4419–4425.

Martin, W., and Russell, M.J. (2003). On the origins of cells: a hypothesis for the evolutionary transitions from abiotic geochemistry to chemoautotrophic prokaryotes, and from prokaryotes to nucleated cells. Philos. Trans. R. Soc. London. Ser. B Biol. Sci. *358*, 59–85.

Martin, F.-P.J., Spanier, B., Collino, S., Montoliu, I., Kolmeder, C., Giesbertz, P., Affolter, M.,

Kussmann, M., Daniel, H., Kochhar, S., et al. (2011). Metabotyping of Caenorhabditis elegans and their Culture Media Revealed Unique Metabolic Phenotypes Associated to Amino Acid Deficiency and Insulin-Like Signaling. J. Proteome Res. *10*, 990–1003.

Martínez-Cisuelo, V., Gómez, J., García-Junceda, I., Naudí, A., Cabré, R., Mota-Martorell, N., López-Torres, M., González-Sánchez, M., Pamplona, R., and Barja, G. (2016). Rapamycin reverses age-related increases in mitochondrial ROS production at complex I, oxidative stress, accumulation of mtDNA fragments inside nuclear DNA, and lipofuscin level, and increases autophagy, in the liver of middle-aged mice. Exp. Gerontol. *83*, 130–138.

Martínez-Reyes, I., and Chandel, N.S. (2020). Mitochondrial TCA cycle metabolites control physiology and disease. Nat. Commun. *11*, 102.

Mattison, J.A., Colman, R.J., Beasley, T.M., Allison, D.B., Kemnitz, J.W., Roth, G.S., Ingram, D.K., Weindruch, R., de Cabo, R., and Anderson, R.M. (2017). Caloric restriction improves health and survival of rhesus monkeys. Nat. Commun. *8*, 14063.

Mayne, B., Berry, O., Davies, C., Farley, J., and Jarman, S. (2019). A genomic predictor of lifespan in vertebrates. Sci. Rep. *9*, 17866.

McCay, C.M., Crowell, M.F., and Maynard, L.A. (1935). The effect of retarded growth upon the length of life span and upon the ultimate body size. 1935. Nutrition *5*, 155–171; discussion 172.

McCord, J.M. (2000). The evolution of free radicals and oxidative stress. Am. J. Med. *108*, 652–659.

McCormick, M.A., Delaney, J.R., Tsuchiya, M., Tsuchiyama, S., Shemorry, A., Sim, S., Chou, A.C.-Z., Ahmed, U., Carr, D., Murakami, C.J., et al. (2015). A Comprehensive Analysis of Replicative Lifespan in 4,698 Single-Gene Deletion Strains Uncovers Conserved Mechanisms of Aging. Cell Metab. *22*, 895–906.

McIsaac, R.S., Lewis, K.N., Gibney, P.A., and Buffenstein, R. (2016). From yeast to human: exploring the comparative biology of methionine restriction in extending eukaryotic life span. Ann. N. Y. Acad. Sci. *1363*, 155–170.

Miller, D.L., and Roth, M.B. (2007). Hydrogen sulfide increases thermotolerance and lifespan in Caenorhabditis elegans. Proc. Natl. Acad. Sci. *104*, 20618–20622.

Minias, P., and Podlaszczuk, P. (2017). Longevity is associated with relative brain size in birds. Ecol. Evol. *7*, 3558–3566.

Miquel, J., Economos, A.C., Fleming, J., and Johnson, J.E. (1980). Mitochondrial role in cell aging. Exp. Gerontol. *15*, 575–591.

Mirisola, M.G., Taormina, G., Fabrizio, P., Wei, M., Hu, J., and Longo, V.D. (2014). Serine- and Threonine/Valine-Dependent Activation of PDK and Tor Orthologs Converge on Sch9 to Promote Aging. PLoS Genet. *10*, e1004113.

Mishur, R.J., Khan, M., Munkácsy, E., Sharma, L., Bokov, A., Beam, H., Radetskaya, O., Borror, M., Lane, R., Bai, Y., et al. (2016). Mitochondrial metabolites extend lifespan. Aging Cell *15*, 336–348.

Mitteldorf, J. (2016). Aging is a group-selected adaptation: theory, evidence, and medical implications (Boca Ratón, FL: CRC Press).

Mitteldorf, J. (2018). Can aging be programmed? Biochem. *83*, 1524–1533.

Miwa, S., Jow, H., Baty, K., Johnson, A., Czapiewski, R., Saretzki, G., Treumann, A., and Von

Zglinicki, T. (2014). Low abundance of the matrix arm of complex I in mitochondria predicts longevity in mice. Nat. Commun. *5*, 1–12.

Mnatsakanyan, N., Beutner, G., Porter, G.A., Alavian, K.N., and Jonas, E.A. (2017). Physiological roles of the mitochondrial permeability transition pore. J. Bioenerg. Biomembr. *49*, 13–25.

Mnatsakanyan, N., Llaguno, M.C., Yang, Y., Yan, Y., Weber, J., Sigworth, F.J., and Jonas, E.A. (2019). A mitochondrial megachannel resides in monomeric F1FO ATP synthase. Nat. Commun. *10*, 5823.

Montoliu, I., Scherer, M., Beguelin, F., DaSilva, L., Mari, D., Salvioli, S., Martin, F.-P.J., Capri, M., Bucci, L., Ostan, R., et al. (2014). Serum profiling of healthy aging identifies phospho- and sphingolipid species as markers of human longevity. Aging (Albany. NY). *6*, 9–25.

Moosmann, B. (2011). Respiratory chain cysteine and methionine usage indicate a causal role for thiyl radicals in aging. Exp. Gerontol. *46*, 164–169.

Moosmann, B., and Behl, C. (2008). Mitochondrially encoded cysteine predicts animal lifespan. Aging Cell *7*, 32–46.

Moosmann, B., Schindeldecker, M., and Hajieva, P. (2020). Cysteine, glutathione and a new genetic code: biochemical adaptations of the primordial cells that spread into open water and survived biospheric oxygenation. Biol. Chem. *401*, 213–231.

Morgenstern, B., Prohaska, S.J., Pöhler, D., and Stadler, P.F. (2006). Multiple sequence alignment with user-defined anchor points. Algorithms Mol. Biol. *1*, 1–12.

Mosharov, E., Cranford, M.R., and Banerjee, R. (2000). The Quantitatively Important Relationship between Homocysteine Metabolism and Glutathione Synthesis by the Transsulfuration Pathway and Its Regulation by Redox Changes †. Biochemistry *39*, 13005–13011.

Mota-Martorell, N., Pradas, I., Jové, M., Naudí, A., and Pamplona, R. (2019). Biosíntesis de novo de glicerofosfolípidos y longevidad. Rev. Esp. Geriatr. Gerontol. *54*, 88–93.

Mota-Martorell, N., Jove, M., Pradas, I., Berdún, R., Sanchez, I., Naudi, A., Gari, E., Barja, G., and Pamplona, R. (2020a). Gene expression and regulatory factors of the mechanistic target of rapamycin (mTOR) complex 1 predict mammalian longevity. GeroScience.

Mota-Martorell, N., Jové, M., Pradas, I., Sanchez, I., Gómez, J., Naudí, A., Barja, G., and Pamplona, R. (2020b). Low abundance of NDUFV2 and NDUFS4 subunits of the hydrophilic complex I domain and VDAC1 predicts mammalian longevity. Redox Biol.

Mouchiroud, L., Molin, L., Kasturi, P., Triba, M.N., Dumas, M.E., Wilson, M.C., Halestrap, A.P., Roussel, D., Masse, I., Dallière, N., et al. (2011). Pyruvate imbalance mediates metabolic reprogramming and mimics lifespan extension by dietary restriction in Caenorhabditis elegans. Aging Cell *10*, 39–54.

Mulder, D.W., Shepard, E.M., Meuser, J.E., Joshi, N., King, P.W., Posewitz, M.C., Broderick, J.B., and Peters, J.W. (2011). Insights into [FeFe]-Hydrogenase Structure, Mechanism, and Maturation. Structure *19*, 1038–1052.

Muntané, G., Farré, X., Rodríguez, J.A., Pegueroles, C., Hughes, D.A., de Magalhães, J.P., Gabaldón, T., and Navarro, A. (2018). Biological processes modulating longevity across primates: A phylogenetic genome-phenome analysis. Mol. Biol. Evol. *35*, 1990–2004.

Murphy, E., and Steenbergen, C. (2008). Mechanisms Underlying Acute Protection From Cardiac Ischemia-Reperfusion Injury. Physiol. Rev. *88*, 581–609.

Nascimento, E.B.M., Snel, M., Guigas, B., van der Zon, G.C.M., Kriek, J., Maassen, J.A., Jazet, I.M., Diamant, M., and Ouwens, D.M. (2010). Phosphorylation of PRAS40 on Thr246 by PKB/AKT facilitates efficient phosphorylation of Ser183 by mTORC1. Cell. Signal. *22*, 961–967.

Naudí, A., Jové, M., Ayala, V., Portero-Otín, M., Barja, G., and Pamplona, R. (2013). Membrane lipid unsaturation as physiological adaptation to animal longevity. Front. Physiol. *4*, 372.

Netto, L.E.S., de Oliveira, M.A., Monteiro, G., Demasi, A.P.D., Cussiol, J.R.R., Discola, K.F., Demasi, M., Silva, G.M., Alves, S.V., Faria, V.G., et al. (2007). Reactive cysteine in proteins: Protein folding, antioxidant defense, redox signaling and more. Comp. Biochem. Physiol. Part C Toxicol. Pharmacol. *146*, 180–193.

Ng, L.T., Ng, L.F., Tang, R.M.Y., Barardo, D., Halliwell, B., Moore, P.K., and Gruber, J. (2020). Lifespan and healthspan benefits of exogenous H2S in C. elegans are independent from effects downstream of eat-2 mutation. Npj Aging Mech. Dis. *6*, 6.

Nicholson, J.K., Lindon, J.C., and Holmes, E. (1999). "Metabonomics": understanding the metabolic responses of living systems to pathophysiological stimuli via multivariate statistical analysis of biological NMR spectroscopic data. Xenobiotica *29*, 1181–1189.

Ogawa, T., Tsubakiyama, R., Kanai, M., Koyama, T., Fujii, T., Iefuji, H., Soga, T., Kume, K., Miyakawa, T., Hirata, D., et al. (2016). Stimulating S -adenosyl-l-methionine synthesis extends lifespan via activation of AMPK. Proc. Natl. Acad. Sci. *113*, 11913–11918.

Orme, D., Freckleton, R., Thomas, G., Petzoldt, T., Fritz, S., Isaac, N., and Pearse, W. (2018). Comparative Analyses of Phylogenetics and Evolution in R.

Orr, W., and Sohal, R. (1994). Extension of life-span by overexpression of superoxide dismutase and catalase in Drosophila melanogaster. Science (80-.). *263*, 1128–1130.

Page, C.C., Moser, C.C., Chen, X., and Dutton, P.L. (1999). Natural engineering principles of electron tunnelling in biological oxidation–reduction. Nature *402*, 47–52.

Palmieri, E.M., Spera, I., Menga, A., Infantino, V., Porcelli, V., Iacobazzi, V., Pierri, C.L., Hooper, D.C., Palmieri, F., and Castegna, A. (2015). Acetylation of human mitochondrial citrate carrier modulates mitochondrial citrate/malate exchange activity to sustain NADPH production during macrophage activation. Biochim. Biophys. Acta - Bioenerg. *1847*, 729–738.

Pamplona, R. (2011). Mitochondrial DNA Damage and Animal Longevity: Insights from Comparative Studies. J. Aging Res. *2011*, 1–9.

Pamplona, R., and Barja, G. (2006). Mitochondrial oxidative stress, aging and caloric restriction: The protein and methionine connection. Biochim. Biophys. Acta - Bioenerg. *1757*, 496–508.

Pamplona, R., and Barja, G. (2007). Highly resistant macromolecular components and low rate of generation of endogenous damage: Two key traits of longevity. Ageing Res. Rev. *6*, 189–210.

Pamplona, R., and Barja, G. (2011). An evolutionary comparative scan for longevity-related oxidative stress resistance mechanisms in homeotherms. Biogerontology *12*, 409–435.

Pamplona, R., and Costantini, D. (2011). Molecular and structural antioxidant defenses against oxidative stress in animals. Am. J. Physiol. Integr. Comp. Physiol. *301*, R843–R863.

Pamplona, R., Barja, G., and Portero-Otín, M. (2002). Membrane fatty acid unsaturation, protection against oxidative stress and maximum life span. Ann. N. Y. Acad. Sci. *959*, 475–490.

Pamplona, R., Portero-Otín, M., Sanz, A., Ayala, V., Vasileva, E., and Barja, G. (2005). Protein and lipid oxidative damage and complex I content are lower in the brain of budgerigar and canaries

than in mice. Relation to aging rate. Age (Omaha). *27*, 267–280.

Pan, H., and Finkel, T. (2017). Key proteins and pathways that regulate lifespan. J. Biol. Chem. *292*, 6452–6460.

Panel, M., Ghaleb, B., and Morin, D. (2018). Mitochondria and aging: A role for the mitochondrial transition pore? Aging Cell *17*, e12793.

Papa, S., De Rasmo, D., Scacco, S., Signorile, A., Technikova-Dobrova, Z., Palmisano, G., Sardanelli, A.M., Papa, F., Panelli, D., Scaringi, R., et al. (2008). Mammalian complex I: A regulable and vulnerable pacemaker in mitochondrial respiratory function. Biochim. Biophys. Acta - Bioenerg. *1777*, 719–728.

Papadopoli, D., Boulay, K., Kazak, L., Pollak, M., Mallette, F., Topisirovic, I., and Hulea, L. (2019). mTOR as a central regulator of lifespan and aging. F1000Research *8*, 998.

Parkhitko, A.A., Binari, R., Zhang, N., Asara, J.M., Demontis, F., and Perrimon, N. (2016). Tissue-specific down-regulation of S-adenosyl-homocysteine via suppression of dAhcyL1/dAhcyL2 extends health span and life span in Drosophila. Genes Dev. *30*, 1409–1422.

Parkhitko, A.A., Jouandin, P., Mohr, S.E., and Perrimon, N. (2019). Methionine metabolism and methyltransferases in the regulation of aging and lifespan extension across species. Aging Cell *18*.

Passtoors, W.M., Boer, J.M., Goeman, J.J., van den Akker, E.B., Deelen, J., Zwaan, B.J., Scarborough, A., van der Breggen, R., Vossen, R.H.A.M., Houwing-Duistermaat, J.J., et al. (2012). Transcriptional Profiling of Human Familial Longevity Indicates a Role for ASF1A and IL7R. PLoS One *7*, e27759.

Passtoors, W.M., Beekman, M., Deelen, J., van der Breggen, R., Maier, A.B., Guigas, B., Derhovanessian, E., van Heemst, D., de Craen, A.J.M., Gunn, D.A., et al. (2013). Gene expression analysis of mTOR pathway: association with human longevity. Aging Cell *12*, 24–31.

Patil, N., Tailhades, J., Hughes, R., Separovic, F., Wade, J., and Hossain, M. (2015). Cellular Disulfide Bond Formation in Bioactive Peptides and Proteins. Int. J. Mol. Sci. *16*, 1791–1805.

Patti, G.J., Yanes, O., and Siuzdak, G. (2012). Metabolomics: the apogee of the omics trilogy. Nat. Rev. Mol. Cell Biol. *13*, 263–269.

Patti, G.J., Tautenhahn, R., Johannsen, D., Kalisiak, E., Ravussin, E., Brüning, J.C., Dillin, A., and Siuzdak, G. (2014). Meta-analysis of global metabolomic data identifies metabolites associated with life-span extension. Metabolomics *10*, 737–743.

Peleg, S., Feller, C., Forne, I., Schiller, E., Sévin, D.C., Schauer, T., Regnard, C., Straub, T., Prestel, M., Klima, C., et al. (2016). Life span extension by targeting a link between metabolism and histone acetylation in Drosophila. EMBO Rep. *17*, 455–469.

Perez-Campo, R., López-Torres, M., Cadenas, S., Rojas, C., and Barja, G. (1998). The rate of free radical production as a determinant of the rate of aging: evidence from the comparative approach. J. Comp. Physiol. B Biochem. Syst. Environ. Physiol. *168*, 149–158.

Perron, J.T., Tyson, R.L., and Sutherland, G.R. (2000). Maintenance of tricarboxylic acid cycle kinetics in Brown–Norway Fischer 344 rats may translate to longevity. Neurosci. Lett. *281*, 91–94.

Petrosillo, G., Moro, N., Paradies, V., Ruggiero, F.M., and Paradies, G. (2010). Increased susceptibility to Ca 2+ -induced permeability transition and to cytochrome c release in rat heart mitochondria with aging: effect of melatonin. J. Pineal Res. *48*, 340–346.

Pickering, A.M., Lehr, M., Kohler, W.J., Han, M.L., and Miller, R.A. (2015a). Fibroblasts From Longer-Lived Species of Primates, Rodents, Bats, Carnivores, and Birds Resist Protein Damage. Journals Gerontol. Ser. A *70*, 791–799.

Pickering, A.M., Lehr, M., and Miller, R.A. (2015b). Lifespan of mice and primates correlates with immunoproteasome expression. J. Clin. Invest. *125*, 2059–2068.

Pietrocola, F., Galluzzi, L., Bravo-San Pedro, J.M., Madeo, F., and Kroemer, G. (2015). Acetyl Coenzyme A: A Central Metabolite and Second Messenger. Cell Metab. *21*, 805–821.

Pinheiro, L.B., Coleman, V.A., Hindson, C.M., Herrmann, J., Hindson, B.J., Bhat, S., and Emslie, K.R. (2012). Evaluation of a droplet digital polymerase chain reaction format for DNA copy number quantification. Anal. Chem. *84*, 1003–1011.

Plummer, J.D., and Johnson, J.E. (2019). Extension of Cellular Lifespan by Methionine Restriction Involves Alterations in Central Carbon Metabolism and Is Mitophagy-Dependent. Front. Cell Dev. Biol. *7*.

Porcelli, A.M., Ghelli, A., Zanna, C., Pinton, P., Rizzuto, R., and Rugolo, M. (2005). pH difference across the outer mitochondrial membrane measured with a green fluorescent protein mutant. Biochem. Biophys. Res. Commun. *326*, 799–804.

Portero-Otín, M., Requena, J.R., Bellmunt, M.J., Ayala, V., and Pamplona, R. (2004). Protein nonenzymatic modifications and proteasome activity in skeletal muscle from the short-lived rat and long-lived pigeon. Exp. Gerontol. *39*, 1527–1535.

Pradas, I., Jové, M., Cabré, R., Ayala, V., Mota-Martorell, N., and Pamplona, R. (2019a). Effects of Aging and Methionine Restriction on Rat Kidney Metabolome. Metabolites *9*, 280.

Pradas, I., Jové, M., Huynh, K., Puig, J., Ingles, M., Borras, C., Viña, J., Meikle, P.J., and Pamplona, R. (2019b). Exceptional human longevity is associated with a specific plasma phenotype of ether lipids. Redox Biol. *21*, 101127.

Prasai, K. (2017). Regulation of mitochondrial structure and function by protein import: A current review. Pathophysiology *24*, 107–122.

Pride, H., Yu, Z., Sunchu, B., Mochnick, J., Coles, A., Zhang, Y., Buffenstein, R., Hornsby, P.J., Austad, S.N., and Pérez, V.I. (2015). Long-lived species have improved proteostasis compared to phylogenetically-related shorter-lived species. Biochem. Biophys. Res. Commun. *457*, 669–675.

Priebe, S., Menzel, U., Zarse, K., Groth, M., Platzer, M., Ristow, M., and Guthke, R. (2013). Extension of life span by impaired glucose metabolism in Caenorhabditis elegans is accompanied by structural rearrangements of the transcriptomic network. PLoS One *8*, e77776.

Psychogios, N., Hau, D.D., Peng, J., Guo, A.C., Mandal, R., Bouatra, S., Sinelnikov, I., Krishnamurthy, R., Eisner, R., Gautam, B., et al. (2011). The Human Serum Metabolome. PLoS One *6*, e16957.

Qi, W., Li, J., Chain, C.Y., Pasquevich, G.A., Pasquevich, A.F., and Cowan, J.A. (2012). Glutathione complexed Fe-S centers. J. Am. Chem. Soc. *134*, 10745–10748.

Quinlan, C.L., Treberg, J.R., Perevoshchikova, I. V., Orr, A.L., and Brand, M.D. (2012). Native rates of superoxide production from multiple sites in isolated mitochondria measured using endogenous reporters. Free Radic. Biol. Med. *53*, 1807–1817.

R Core Team (2020). R: The R Project for Statistical Computing.

Ramachandran, P. V, Savini, M., Folick, A.K., Hu, K., Masand, R., Graham, B.H., and Wang, M.C.

(2019). Lysosomal Signaling Promotes Longevity by Adjusting Mitochondrial Activity. Dev. Cell *48*, 685-696.e5.

Ramanathan, A., and Schreiber, S.L. (2009). Direct control of mitochondrial function by mTOR. Proc. Natl. Acad. Sci. *106*, 22229–22232.

Ramsay, R.R. (2019). Electron carriers and energy conservation in mitochondrial respiration. ChemTexts *5*, 9.

Randle, P.J. (1998). Regulatory interactions between lipids and carbohydrates: the glucose fatty acid cycle after 35 years. Diabetes / Metab. Rev. *14*, 263–283.

Rattray, N.J.W., Trivedi, D.K., Xu, Y., Chandola, T., Johnson, C.H., Marshall, A.D., Mekli, K., Rattray, Z., Tampubolon, G., Vanhoutte, B., et al. (2019). Metabolic dysregulation in vitamin E and carnitine shuttle energy mechanisms associate with human frailty. Nat. Commun. *10*, 5027.

Reddy, V.Y., Desorchers, P.E., Pizzo, S. V, Gonias, S.L., Sahakian, J.A., Levine, R.L., and Weiss, S.J. (1994). Oxidative dissociation of human alpha 2-macroglobulin tetramers into dysfunctional dimers. J. Biol. Chem. *269*, 4683–4691.

Reid, K.S.C., Lindley, P.F., and Thornton, J.M. (1985). Sulphur-aromatic interactions in proteins. FEBS Lett. *190*, 209–213.

Rhee, H.J., Kim, E.-J., and Lee, J.K. (2007). Physiological polyamines: simple primordial stress molecules. J. Cell. Mol. Med. *11*, 685–703.

Rich, P.R., and Maréchal, A. (2010). The mitochondrial respiratory chain. Essays Biochem. *47*, 1–23.

Roberts, L.D., Souza, A.L., Gerszten, R.E., and Clish, C.B. (2012). Targeted Metabolomics. Curr. Protoc. Mol. Biol. *98*, 30.2.1-30.2.24.

Rodriguez, K.A., Valentine, J.M., Kramer, D.A., Gelfond, J.A., Kristan, D.M., Nevo, E., and Buffenstein, R. (2016). Determinants of rodent longevity in the chaperone-protein degradation network. Cell Stress Chaperones *21*, 453–466.

Rogina, B., and Helfand, S.L. (2013). Indy Mutations and Drosophila Longevity. Front. Genet. *4*.

Röhrig, F., and Schulze, A. (2016). The multifaceted roles of fatty acid synthesis in cancer. Nat. Rev. Cancer *16*, 732–749.

Rosario, F.J., Gupta, M.B., Myatt, L., Powell, T.L., Glenn, J.P., Cox, L., and Jansson, T. (2019). Mechanistic Target of Rapamycin Complex 1 Promotes the Expression of Genes Encoding Electron Transport Chain Proteins and Stimulates Oxidative Phosphorylation in Primary Human Trophoblast Cells by Regulating Mitochondrial Biogenesis. Sci. Rep. *9*, 246.

Rottenberg, H., and Hoek, J.B. (2017). The path from mitochondrial ROS to aging runs through the mitochondrial permeability transition pore. Aging Cell *16*, 943–955.

Roux, J., Privman, E., Moretti, S., Daub, J.T., Robinson-Rechavi, M., and Keller, L. (2014). Patterns of positive selection in seven ant genomes. Mol. Biol. Evol. *31*, 1661–1685.

Ruckenstuhl, C., Netzberger, C., Entfellner, I., Carmona-Gutierrez, D., Kickenweiz, T., Stekovic, S., Gleixner, C., Schmid, C., Klug, L., Sorgo, A.G., et al. (2014). Lifespan Extension by Methionine Restriction Requires Autophagy-Dependent Vacuolar Acidification. PLoS Genet. *10*, e1004347.

Ruiz, M.C., Ayala, V., Portero-Otín, M., Requena, J.R., Barja, G., and Pamplona, R. (2005). Protein methionine content and MDA-lysine adducts are inversely related to maximum life span in the heart of mammals. Mech. Ageing Dev. *126*, 1106–1114.

Sahm, A., Bens, M., Platzer, M., and Cellerino, A. (2017). Parallel evolution of genes controlling mitonuclear balance in short-lived annual fishes. Aging Cell *16*, 488–496.

Sahm, A., Bens, M., Szafranski, K., Holtze, S., Groth, M., Görlach, M., Calkhoven, C., Müller, C., Schwab, M., Kraus, J., et al. (2018a). Long-lived rodents reveal signatures of positive selection in genes associated with lifespan. PLOS Genet. *14*, e1007272.

Sahm, A., Bens, M., Henning, Y., Vole, C., Groth, M., Schwab, M., Hoffmann, S., Platzer, M., Szafranski, K., and Dammann, P. (2018b). Higher gene expression stability during aging in long-lived giant mole-rats than in short-lived rats. Aging (Albany. NY). *10*, 3938–3956.

Salvioli, S., Capri, M., Santoro, A., Raule, N., Sevini, F., Lukas, S., Lanzarini, C., Monti, D., Passarino, G., Rose, G., et al. (2008). The impact of mitochondrial DNA on human lifespan: A view from studies on centenarians. Biotechnol. J. *3*, 740–749.

Samuels, D.C. (2005). Life span is related to the free energy of mitochondrial DNA. Mech. Ageing Dev. *126*, 1123–1129.

Sancak, Y., Thoreen, C.C., Peterson, T.R., Lindquist, R.A., Kang, S.A., Spooner, E., Carr, S.A., and Sabatini, D.M. (2007). PRAS40 is an insulin-regulated inhibitor of the mTORC1 protein kinase. Mol. Cell *25*, 903–915.

Sánchez-Caballero, L., Guerrero-Castillo, S., and Nijtmans, L. (2016a). Unraveling the complexity of mitochondrial complex I assembly: A dynamic process. Biochim. Biophys. Acta - Bioenerg. *1857*, 980–990.

Sánchez-Caballero, L., Guerrero-Castillo, S., and Nijtmans, L. (2016b). Unraveling the complexity of mitochondrial complex I assembly: A dynamic process. Biochim. Biophys. Acta - Bioenerg. *1857*, 980–990.

Sanchez-Roman, I., and Barja, G. (2013). Regulation of longevity and oxidative stress by nutritional interventions: Role of methionine restriction. Exp. Gerontol. *48*, 1030–1042.

Sanchez-Roman, I., Gomez, A., Gomez, J., Suarez, H., Sanchez, C., Naudí, A., Ayala, V., Portero-Otín, M., Lopez-Torres, M., Pamplona, R., et al. (2011). Forty percent methionine restriction lowers DNA methylation, complex I ROS generation, and oxidative damage to mtDNA and mitochondrial proteins in rat heart. J. Bioenerg. Biomembr. *43*, 699–708.

Sanderson, S.M., Gao, X., Dai, Z., and Locasale, J.W. (2019). Methionine metabolism in health and cancer: a nexus of diet and precision medicine. Nat. Rev. Cancer *19*, 625–637.

Sanz, A., Pamplona, R., and Barja, G. (2006a). Is the Mitochondrial Free Radical Theory of Aging Intact? Antioxid. Redox Signal. *8*, 582–599.

Sanz, A., Caro, P., Ayala, V., Portero-Otín, M., Pamplona, R., and Barja, G. (2006b). Methionine restriction decreases mitochondrial oxygen radical generation and leak as well as oxidative damage to mitochondrial DNA and proteins. FASEB J. *20*, 1064–1073.

Saxton, R.A., and Sabatini, D.M. (2017). mTOR Signaling in Growth, Metabolism, and Disease. Cell *168*, 960–976.

Sazanov, L.A. (2006). Structure of the Hydrophilic Domain of Respiratory Complex I from Thermus thermophilus. Science (80-.). *311*, 1430–1436.

Sazanov, L.A. (2015). A giant molecular proton pump: structure and mechanism of respiratory complex I. Nat. Rev. Mol. Cell Biol. *16*, 375–388.

Sazanov, L.A., Carroll, J., Holt, P., Toime, L., and Fearnley, I.M. (2003). A Role for Native Lipids in

the Stabilization and Two-dimensional Crystallization of the Escherichia coli NADH-Ubiquinone Oxidoreductase (Complex I). J. Biol. Chem. *278*, 19483–19491.

Sbodio, J.I., Snyder, S.H., and Paul, B.D. (2019). Regulators of the transsulfuration pathway. Br. J. Pharmacol. *176*, 583–593.

Schieke, S.M., Phillips, D., McCoy, J.P., Aponte, A.M., Shen, R.-F., Balaban, R.S., and Finkel, T. (2006). The mammalian target of rapamycin (mTOR) pathway regulates mitochondrial oxygen consumption and oxidative capacity. J. Biol. Chem. *281*, 27643–27652.

Schindeldecker, M., and Moosmann, B. (2015). Protein-borne methionine residues as structural antioxidants in mitochondria. Amino Acids *47*, 1421–1432.

Schöneich, C. (2005). Methionine oxidation by reactive oxygen species: reaction mechanisms and relevance to Alzheimer's disease. Biochim. Biophys. Acta - Proteins Proteomics *1703*, 111–119.

Schönfeld, P., Więckowski, M.R., Lebiedzińska, M., and Wojtczak, L. (2010). Mitochondrial fatty acid oxidation and oxidative stress: Lack of reverse electron transfer-associated production of reactive oxygen species. Biochim. Biophys. Acta - Bioenerg. *1797*, 929–938.

Schultz, B.E., and Chan, S.I. (2001). Structures and proton-pumping strategies of mitochondrial respiratory enzymes. Annu. Rev. Biophys. Biomol. Struct. *30*, 23–65.

Scialò, F., Sriram, A., Fernández-Ayala, D., Gubina, N., Lõhmus, M., Nelson, G., Logan, A., Cooper, H.M., Navas, P., Enríquez, J.A., et al. (2016). Mitochondrial ROS Produced via Reverse Electron Transport Extend Animal Lifespan. Cell Metab. *23*, 725–734.

Scialò, F., Fernández-Ayala, D.J., and Sanz, A. (2017). Role of Mitochondrial Reverse Electron Transport in ROS Signaling: Potential Roles in Health and Disease. Front. Physiol. *8*.

Seim, I., Ma, S., Zhou, X., Gerashchenko, M. V., Lee, S.-G., Suydam, R., George, J.C., Bickham, J.W., and Gladyshev, V.N. (2014). The transcriptome of the bowhead whale Balaena mysticetus reveals adaptations of the longest-lived mammal. Aging (Albany. NY). *6*, 879–899.

Seim, I., Ma, S., and Gladyshev, V.N. (2016). Gene expression signatures of human cell and tissue longevity. Npj Aging Mech. Dis. *2*, 16014.

Selley, M.L. (2007). A metabolic link between S-adenosylhomocysteine and polyunsaturated fatty acid metabolism in Alzheimer's disease. Neurobiol. Aging *28*, 1834–1839.

Selman, C., Tullet, J.M.A., Wieser, D., Irvine, E., Lingard, S.J., Choudhury, A.I., Claret, M., Al-Qassab, H., Carmignac, D., Ramadani, F., et al. (2009). Ribosomal protein S6 Kinase 1 signaling regulates mammalian life span. Science (80-.). *326*, 140–144.

Sena, L.A., and Chandel, N.S. (2012a). Physiological roles of mitochondrial reactive oxygen species. Mol. Cell *48*, 158–167.

Sena, L.A., and Chandel, N.S. (2012b). Physiological roles of mitochondrial reactive oxygen species. Mol. Cell *48*, 158–167.

Sharma, A., Smith, H.J., Yao, P., and Mair, W.B. (2019). Causal roles of mitochondrial dynamics in longevity and healthy aging. EMBO Rep. *20*.

Shen, J., Sun, B., Yu, C., Cao, Y., Cai, C., and Yao, J. (2020). Choline and methionine regulate lipid metabolism via the AMPK signaling pathway in hepatocytes exposed to high concentrations of nonesterified fatty acids. J. Cell. Biochem. *121*, 3667–3678.

Shen, Y.-Y., Liang, L., Zhu, Z.-H., Zhou, W.-P., Irwin, D.M., and Zhang, Y.-P. (2010). Adaptive

evolution of energy metabolism genes and the origin of flight in bats. Proc. Natl. Acad. Sci. *107*, 8666–8671.

Simonsen, A., Cumming, R.C., Brech, A., Isakson, P., Schubert, D.R., and Finley, K.D. (2008). Promoting basal levels of autophagy in the nervous system enhances longevity and oxidant resistance in adult Drosophila. Autophagy *4*, 176–184.

Singh, P.P., Demmitt, B.A., Nath, R.D., and Brunet, A. (2019). The henetics of aging: A vertebrate perspective. Cell *177*, 200–220.

Sivanesan, S., Taylor, A., Zhang, J., and Bakovic, M. (2018). Betaine and Choline Improve Lipid Homeostasis in Obesity by Participation in Mitochondrial Oxidative Demethylation. Front. Nutr. *5*.

Skulachev, V.P. (1997). Aging is a specific biological function rather than the result of a disorder in complex living systems: biochemical evidence in support of Weismann's hypothesis. Biochemistry. (Mosc). *62*, 1191–1195.

Sousa, F.L., Thiergart, T., Landan, G., Nelson-Sathi, S., Pereira, I.A.C., Allen, J.F., Lane, N., and Martin, W.F. (2013). Early bioenergetic evolution. Philos. Trans. R. Soc. B Biol. Sci. *368*, 20130088.

Southworth, L.K., Owen, A.B., and Kim, S.K. (2009). Aging mice show a decreasing correlation of gene expression within genetic modules. PLoS Genet. *5*, e1000776.

Speakman, J.R. (2005). Body size, energy metabolism and lifespan. J. Exp. Biol. *208*, 1717–1730.

Spinelli, J.B., and Haigis, M.C. (2018). The multifaceted contributions of mitochondria to cellular metabolism. Nat. Cell Biol. *20*, 745–754.

Stadtman, E.R., Moskovitz, J., and Levine, R.L. (2003). Oxidation of Methionine Residues of Proteins: Biological Consequences. Antioxid. Redox Signal. *5*, 577–582.

Stadtman, E.R., Van Remmen, H., Richardson, A., Wehr, N.B., and Levine, R.L. (2005). Methionine oxidation and aging. Biochim. Biophys. Acta - Proteins Proteomics *1703*, 135–140.

Stroud, D.A., Formosa, L.E., Wijeyeratne, X.W., Nguyen, T.N., and Ryan, M.T. (2013). Gene Knockout Using Transcription Activator-like Effector Nucleases (TALENs) Reveals That Human NDUFA9 Protein Is Essential for Stabilizing the Junction between Membrane and Matrix Arms of Complex I. J. Biol. Chem. *288*, 1685–1690.

Stroud, D.A., Surgenor, E.E., Formosa, L.E., Reljic, B., Frazier, A.E., Dibley, M.G., Osellame, L.D., Stait, T., Beilharz, T.H., Thorburn, D.R., et al. (2016). Accessory subunits are integral for assembly and function of human mitochondrial complex I. Nature *538*, 123–126.

Suarez-Diez, M., Adam, J., Adamski, J., Chasapi, S.A., Luchinat, C., Peters, A., Prehn, C., Santucci, C., Spyridonidis, A., Spyroulias, G.A., et al. (2017). Plasma and Serum Metabolite Association Networks: Comparability within and between Studies Using NMR and MS Profiling. J. Proteome Res. *16*, 2547–2559.

Sullivan, L.B., Martinez-Garcia, E., Nguyen, H., Mullen, A.R., Dufour, E., Sudarshan, S., Licht, J.D., Deberardinis, R.J., and Chandel, N.S. (2013). The Proto-oncometabolite Fumarate Binds Glutathione to Amplify ROS-Dependent Signaling. Mol. Cell *51*, 236–248.

Swovick, K., Welle, K.A., Hryhorenko, J.R., Seluanov, A., Gorbunova, V., and Ghaemmaghami, S. (2018). Cross-species Comparison of Proteome Turnover Kinetics. Mol. Cell. Proteomics *17*, 580–591.

Szekely, P., Korem, Y., Moran, U., Mayo, A., and Alon, U. (2015). The Mass-Longevity Triangle: Pareto Optimality and the Geometry of Life-History Trait Space. PLOS Comput. Biol. *11*, e1004524.

Tacutu, R., Craig, T., Budovsky, A., Wuttke, D., Lehmann, G., Taranukha, D., Costa, J., Fraifeld, V.E., and de Magalhães, J.P. (2013). Human Ageing Genomic Resources: integrated databases and tools for the biology and genetics of ageing. Nucleic Acids Res. *41*, D1027-33.

Tain, L.S., Sehlke, R., Jain, C., Chokkalingam, M., Nagaraj, N., Essers, P., Rassner, M., Grönke, S., Froelich, J., Dieterich, C., et al. (2017). A proteomic atlas of insulin signalling reveals tissue-specific mechanisms of longevity assurance. Mol. Syst. Biol. *13*, 939.

Tain, L.S., Jain, C., Nespital, T., Froehlich, J., Hinze, Y., Grönke, S., and Partridge, L. (2020). Longevity in response to lowered insulin signaling requires glycine N-methyltransferase-dependent spermidine production. Aging Cell *19*.

Tamanna, N., Mayengbam, S., House, J.D., and Treberg, J.R. (2018). Methionine restriction leads to hyperhomocysteinemia and alters hepatic H2S production capacity in Fischer-344 rats. Mech. Ageing Dev. *176*, 9–18.

Tanaka, M., Gong, J.-S., Zhang, J., Yamada, Y., Borgeld, H.-J., and Yagi, K. (2000). Mitochondrial genotype associated with longevity and its inhibitory effect on mutagenesis. Mech. Ageing Dev. *116*, 65–76.

Taormina, G., Ferrante, F., Vieni, S., Grassi, N., Russo, A., and Mirisola, M.G. (2019). Longevity: Lesson from Model Organisms. Genes (Basel). *10*, 518.

Tatsuta, T., Scharwey, M., and Langer, T. (2014). Mitochondrial lipid trafficking. Trends Cell Biol. *24*, 44–52.

Tauffenberger, A., Fiumelli, H., Almustafa, S., and Magistretti, P.J. (2019). Lactate and pyruvate promote oxidative stress resistance through hormetic ROS signaling. Cell Death Dis. *10*, 653.

Ternette, N., Yang, M., Laroyia, M., Kitagawa, M., O'Flaherty, L., Wolhulter, K., Igarashi, K., Saito, K., Kato, K., Fischer, R., et al. (2013). Inhibition of Mitochondrial Aconitase by Succination in Fumarate Hydratase Deficiency. Cell Rep. *3*, 689–700.

Tian, Q., Stepaniants, S.B., Mao, M., Weng, L., Feetham, M.C., Doyle, M.J., Yi, E.C., Dai, H., Thorsson, V., Eng, J., et al. (2004). Integrated Genomic and Proteomic Analyses of Gene Expression in Mammalian Cells. Mol. Cell. Proteomics *3*, 960–969.

Trifonov, E.. (2000). Consensus temporal order of amino acids and evolution of the triplet code. Gene *261*, 139–151.

Trifonov, E.N. (2009). The origin of the genetic code and of the earliest oligopeptides. Res. Microbiol. *160*, 481–486.

Tripodi, F., Castoldi, A., Nicastro, R., Reghellin, V., Lombardi, L., Airoldi, C., Falletta, E., Maffioli, E., Scarcia, P., Palmieri, L., et al. (2018). Methionine supplementation stimulates mitochondrial respiration. Biochim. Biophys. Acta - Mol. Cell Res. *1865*, 1901–1913.

Tyshkovskiy, A., Bozaykut, P., Borodinova, A.A., Gerashchenko, M. V., Ables, G.P., Garratt, M., Khaitovich, P., Clish, C.B., Miller, R.A., and Gladyshev, V.N. (2019). Identification and application of gene expression signatures associated with lifespan extension. Cell Metab. *30*, 573-593.e8.

Untergasser, A., Cutcutache, I., Koressaar, T., Ye, J., Faircloth, B.C., Remm, M., and Rozen, S.G. (2012). Primer3-new capabilities and interfaces. Nucleic Acids Res. *40*, 1–12.

Uthus, E.O., and Brown-Borg, H.M. (2006). Methionine flux to transsulfuration is enhanced in the long living Ames dwarf mouse. Mech. Ageing Dev. *127*, 444–450.

Valley, C.C., Cembran, A., Perlmutter, J.D., Lewis, A.K., Labello, N.P., Gao, J., and Sachs, J.N. (2012). The Methionine-aromatic Motif Plays a Unique Role in Stabilizing Protein Structure. J. Biol. Chem. *287*, 34979–34991.

Valvezan, A.J., and Manning, B.D. (2019). Molecular logic of mTORC1 signalling as a metabolic rheostat. Nat. Metab. *1*, 321–333.

Viltard, M., Durand, S., Pérez-Lanzón, M., Aprahamian, F., Lefevre, D., Leroy, C., Madeo, F., Kroemer, G., and Friedlander, G. (2019). The metabolomic signature of extreme longevity: naked mole rats versus mice. Aging (Albany. NY). *11*, 4783–4800.

Vinothkumar, K.R., Zhu, J., and Hirst, J. (2014). Architecture of mammalian respiratory complex I. Nature *515*, 80–84.

Vitvitsky, V., Martinov, M., Ataullakhanov, F., Miller, R.A., and Banerjee, R. (2013). Sulfur-based redox alterations in long-lived Snell dwarf mice. Mech. Ageing Dev. *134*, 321–330.

Vyssokikh, M.Y., Holtze, S., Averina, O.A., Lyamzaev, K.G., Panteleeva, A.A., Marey, M. V., Zinovkin, R.A., Severin, F.F., Skulachev, M. V., Fasel, N., et al. (2020). Mild depolarization of the inner mitochondrial membrane is a crucial component of an anti-aging program. Proc. Natl. Acad. Sci. *117*, 6491–6501.

Wächtershäuser, G. (2008). Iron-Sulfur World. In Wiley Encyclopedia of Chemical Biology, (Hoboken, NJ, USA: John Wiley & Sons, Inc.), p.

Walsh, C.T., Tu, B.P., and Tang, Y. (2018). Eight Kinetically Stable but Thermodynamically Activated Molecules that Power Cell Metabolism. Chem. Rev. *118*, 1460–1494.

Walters, R.O., Arias, E., Diaz, A., Burgos, E.S., Guan, F., Tiano, S., Mao, K., Green, C.L., Qiu, Y., Shah, H., et al. (2018). Sarcosine Is Uniquely Modulated by Aging and Dietary Restriction in Rodents and Humans. Cell Rep. *25*, 663-676.e6.

Wang, J., Jiang, J.C., and Jazwinski, S.M. (2010). Gene regulatory changes in yeast during life extension by nutrient limitation. Exp. Gerontol. *45*, 621–631.

Wang, S.-Y., Wang, W.-J., Liu, J.-Q., Song, Y.-H., Li, P., Sun, X.-F., Cai, G.-Y., and Chen, X.-M. (2019). Methionine restriction delays senescence and suppresses the senescence-associated secretory phenotype in the kidney through endogenous hydrogen sulfide. Cell Cycle *18*, 1573–1587.

Warnefors, M., and Kaessmann, H. (2013). Evolution of the Correlation between Expression Divergence and Protein Divergence in Mammals. Genome Biol. Evol. *5*, 1324–1335.

Washburn, R., Cox, J., Muhlestein, J., May, H., Carlquist, J., Le, V., Anderson, J., and Horne, B. (2019). Pilot Study of Novel Intermittent Fasting Effects on Metabolomic and Trimethylamine N-oxide Changes During 24-hour Water-Only Fasting in the FEELGOOD Trial. Nutrients *11*, 246.

Washburne, A.D., Morton, J.T., Sanders, J., McDonald, D., Zhu, Q., Oliverio, A.M., and Knight, R. (2018). Methods for phylogenetic analysis of microbiome data. Nat. Microbiol. *3*, 652–661.

Weckmann, K., Diefenthäler, P., Baeken, M.W., Yusifli, K., Turck, C.W., Asara, J.M., Behl, C., and Hajieva, P. (2018). Metabolomics profiling reveals differential adaptation of major energy metabolism pathways associated with autophagy upon oxygen and glucose reduction. Sci. Rep. *8*, 2337.

Wei, T., and Simko, V. (2017). R package “corrplot”: Visualization of a Correlation Matrix.

Wei, Y., and Kenyon, C. (2016). Roles for ROS and hydrogen sulfide in the longevity response to germline loss in Caenorhabditis elegans. Proc. Natl. Acad. Sci. *113*, E2832–E2841.

Wei, Y., Zhang, Y.-J., Cai, Y., and Xu, M.-H. (2015). The role of mitochondria in mTOR-regulated longevity. Biol. Rev. *90*, 167–181.

Weichhart, T. (2018). mTOR as regulator of lifespan, aging, and cellular senescence: A mini-review. Gerontology *64*, 127–134.

Westermann, B. (2010). Mitochondrial fusion and fission in cell life and death. Nat. Rev. Mol. Cell Biol. *11*, 872–884.

Wickham, H. (2016). ggplot2: Elegant Graphics for Data Analysis (Cham: Springer International Publishing).

Wilkinson, G.S., and Adams, D.M. (2019). Recurrent evolution of extreme longevity in bats. Biol. Lett. *15*, 20180860.

Willmes, D.M., Kurzbach, A., Henke, C., Schumann, T., Zahn, G., Heifetz, A., Jordan, J., Helfand, S.L., and Birkenfeld, A.L. (2018). The longevity gene INDY (I ’m N ot D ead Y et) in metabolic control: Potential as pharmacological target. Pharmacol. Ther. *185*, 1–11.

Winterbourn, C.C., and Metodiewa, D. (1999). Reactivity of biologically important thiol compounds with superoxide and hydrogen peroxide. Free Radic. Biol. Med. *27*, 322–328.

Wirth, C., Brandt, U., Hunte, C., and Zickermann, V. (2016). Structure and function of mitochondrial complex I. Biochim. Biophys. Acta - Bioenerg. *1857*, 902–914.

Wong, H.-S., Dighe, P.A., Mezera, V., Monternier, P.-A., and Brand, M.D. (2017). Production of superoxide and hydrogen peroxide from specific mitochondrial sites under different bioenergetic conditions. J. Biol. Chem. *292*, 16804–16809.

Wu, J.J., Liu, J., Chen, E.B., Wang, J.J., Cao, L., Narayan, N., Fergusson, M.M., Rovira, I.I., Allen, M., Springer, D.A., et al. (2013a). Increased mammalian lifespan and a segmental and tissue-specific slowing of aging after genetic reduction of mTOR expression. Cell Rep. *4*, 913–920.

Wu, Z., Song, L., Liu, S.Q., and Huang, D. (2013b). Independent and Additive Effects of Glutamic Acid and Methionine on Yeast Longevity. PLoS One *8*, e79319.

Wunderlich, B., Leirer, C., Idzko, A.-L., Keyser, U.F., Wixforth, A., Myles, V.M., Heimburg, T., and Schneider, M.F. (2009). Phase-State Dependent Current Fluctuations in Pure Lipid Membranes. Biophys. J. *96*, 4592–4597.

Xu, J., Bian, X., Liu, Y., Hong, L., Teng, T., Sun, Y., and Xu, Z. (2017). Adenosine A 2 receptor activation ameliorates mitochondrial oxidative stress upon reperfusion through the posttranslational modification of NDUFV2 subunit of complex I in the heart. Free Radic. Biol. Med. *106*, 208–218.

Yamori, Y., Liu, L., Mori, M., Sagara, M., Murakami, S., Nara, Y., and Mizushima, S. (2009). Taurine as the Nutritional Factor for the Longevity of the Japanese Revealed by a World-Wide Epidemiological Survey. pp. 13–25.

Yanai, H., Budovsky, A., Barzilay, T., Tacutu, R., and Fraifeld, V.E. (2017). Wide-scale comparative analysis of longevity genes and interventions. Aging Cell *16*, 1267–1275.

Yang, H., Chen, X., Liu, M., and Xu, Y. (2018). The structure of mTOR complexes at a glance. Precis. Cancer Med. *1*, 7–7.

Zauhar, R.J., Colbert, C.L., Morgan, R.S., and Welsh, W.J. (2000). Evidence for a strong sulfur-

aromatic interaction derived from crystallographic data. Biopolymers *53*, 233–248.

Zhang, H., Gong, G., Wang, P., Zhang, Z., Kolwicz, S.C., Rabinovitch, P.S., Tian, R., and Wang, W. (2018). Heart specific knockout of Ndufs4 ameliorates ischemia reperfusion injury. J. Mol. Cell. Cardiol. *123*, 38–45.

Zhang, W., Zhang, S., Yan, P., Ren, J., Song, M., Li, J., Lei, J., Pan, H., Wang, S., Ma, X., et al. (2020). A single-cell transcriptomic landscape of primate arterial aging. Nat. Commun. *11*, 2202.

Zheng, L., Cardaci, S., Jerby, L., MacKenzie, E.D., Sciacovelli, M., Johnson, T.I., Gaude, E., King, A., Leach, J.D.G., Edrada-Ebel, R., et al. (2015). Fumarate induces redox-dependent senescence by modifying glutathione metabolism. Nat. Commun. *6*, 6001.

Zhou, B., Kreuzer, J., Kumsta, C., Wu, L., Kamer, K.J., Cedillo, L., Zhang, Y., Li, S., Kacergis, M.C., Webster, C.M., et al. (2019). Mitochondrial Permeability Uncouples Elevated Autophagy and Lifespan Extension. Cell *177*, 299-314.e16.

Zhu, J., Vinothkumar, K.R., and Hirst, J. (2016). Structure of mammalian respiratory complex I. Nature *536*, 354–358.

Zickermann, V., Wirth, C., Nasiri, H., Siegmund, K., Schwalbe, H., Hunte, C., and Brandt, U. (2015a). Mechanistic insight from the crystal structure of mitochondrial complex I. Science (80-.). *347*, 44–49.

Zickermann, V., Wirth, C., Nasiri, H., Siegmund, K., Schwalbe, H., Hunte, C., and Brandt, U. (2015b). Mechanistic insight from the crystal structure of mitochondrial complex I. Science (80-.). *347*, 44–49.